Biomimetic polymeric membranes for water treatment

Habel, Joachim Erich Otto; Hélix-Nielsen, Claus; Almdal, Kristoffer; Højer Nielsen, Kent ; Ogbonna, Anayo; Geschke, Oliver

Publication date:
2015

Document Version
Publisher's PDF, also known as Version of record

AQUAPORIN

Technical University of Denmark

DTU

Biomimetic polymeric membranes for water treatment

Joachim Habel

DTU Environment
Department of Environmental Engineering

PhD Thesis
November 2015

Biomimetic polymeric membranes for water treatment

Joachim Habel

PhD Thesis
November 2015

DTU Environment
Department of Environmental Engineering
Technical University of Denmark

Joachim Habel

Biomimetic polymeric membranes for water treatment

PhD Thesis, November 2015

Address: DTU Environment
Department of Environmental Engineering
Technical University of Denmark
Miljoevej, building 113
2800 Kgs. Lyngby
Denmark

Phone reception: +45 4525 1600
Fax: +45 4593 2850

Homepage: http://www.env.dtu.dk
E-mail: info@env.dtu.dk

Printed by: GraphicCo
November 2015

Cover: Torben Dolin

Preface

This thesis presents the outcome of an Industrial PhD project carried out experimentally at the Department of Micro- and Nanotechnology at the Technical University of Denmark (DTU Nanotech) in the period of September 2012 to November 2013, at Aquaporin A/S in the period of November 2013 to September 2015 with a secondment at the University of Twente in the period of January 2015 to March 2015. The project was carried out administratively at the Department of Physics (September 2012 to April 2014) and the Department of Environmental Engineering (DTU Environment) (May 2014 - September 2015). The project was supervised by Professor Claus Hélix-Nielsen (DTU Environment) as academic main supervisor and Professor Kristoffer Almdal (DTU Nanotech) as the academic co-supervisor throughout the whole project, as well as several industrial co-supervisors from Aquaporin A/S over certain periods of the project - Kent Højer Nielsen (September 2012 to March 2014), Anayo Ogbonna (April 2014 to February 2015) and Oliver Geschke (March 2015 to September 2015).

The project was funded by an Industrial PhD grant from Innovation Fund Denmark.

There are four papers integrated in the thesis. They are listed on the next pages, as well as the integration of the paper in the thesis, a small description of the paper and my contribution to the paper.

In this online version of the thesis, Paper 1 is included, where Paper 2-4 are not included but can be obtained from electronic article databases e.g. via www.orbit.dtu.dk or on request from DTU Environment, Technical University of Denmark, Miljøvej, Building 113, 2800 Kgs. Lyngby, Denmark, info@env.dtu.dk.

1. Original paper: **Joachim Habel**, Michael Hansen, Nanna Larsen, Søren Kynde, Søren Roi Midtgaard, Grethe Vestergaard Jensen, Julie Bomholt, Anayo Ogbonna, Kristoffer Almdal, Alexander Schulz, and Claus Hélix-Nielsen, *Aquaporin-based biomimetic polymeric membranes: approaches and challenges.* Membranes, 5 (3) **2015**, 307-351 [1]

Integration in the thesis: Modified chapters of the paper in subchapter 1.3, 1.5 and chapter 2, 6

This article investigates the interplay and characterization possibilities of the major components of aquaporin-based biomimetic polymeric membranes (ABPMs): Aquaporins (AQPs), block copolymers and polymer membranes. The interplay of AQPs and block copolymers was reviewed and experimental data to a variety of characterization methods like Freeze-fracture transmission electron microscopy (FF-TEM), stopped-flow light scattering (SFLS), Small-angle x-ray scattering (SAXS) and fluorescence correlation spectroscopy (FCS). This was followed by a state of the art review of the interplay of all three components, as well as recent efforts to optimize their interplay. Characterization methods were described with a main focus of describing the embedment of proteopolymersomes in a polyamide matrix of polyhedral oligomeric silsesquioxane and trimesoyl chloride in a non-supported film or supported on microfiltration polyethersulfone. The non-supported film was characterized using fouier-transformed infrared spectroscopy (FTIR), scanning electron microscopy (SEM) and a novel microfluidic approach, the supported film was characterized using FTIR, SEM and standard forward osmosis flux and rejection tests. ABPMs have a the potential for a groundbreaking change in membrane technology.

My contribution:

- I designed the research
- I performed all FF-TEM, SFLS experiments as well as the production of all non-supported and supported AL
- I performed all data analysis except SAXS/SANS
- I wrote the manuscript

2. Accepted Manuscript: **Joachim Habel**, Anayo Ogbonna, Nanna Larsen, Solène Cherré, Søren Kynde, Søren Roi Midtgaard Koji Kinoshita, Simon Krabbe, Grethe Vestergaard Jensen, Kristoffer Almdal, Claus Hélix-Nielsen, *Selecting analytical tools for characterization of polymersomes in aqueous solution*, accepted at RSC Advances

Integration in the thesis: Manuscript in chapter 5, accepted manuscript in RSC style in subchapter 8.3

This compares numerous characterization methods for polymersomes in aqueous solution. The main focus is comparing analyzed polymersome size distributions obtained from electron-based visualization methods, scattering-based methods and other methods. Polymerosme bilayer properties like thickness, lamellarity, stretching and bending moduli, polarity and zetapotential are compared as well. 17 methods in total are investigated, including: DLS, nanoparticle tracking analysis, SAXS, small-angle neutron scattering, SFLS, TEM, negative-staining-TEM (NS-TEM), Cryo-TEM, FF-TEM, SEM, Cryo-FF-SEM, confocal laser scanning microscopy, generalized polarization microscopy (GPM), atomic force microscopy, micropipette aspiration and laser doppler electrophoresis (LDE).

My contribution:

- I designed the research
- I performed all FF-TEM, NS-TEM, TEM and GPM experiments and partly SFLS experiments
- I performed all data analysis except size analysis on half of the FF-TEM samples
- I wrote the manuscript

3. Submitted manuscript: **Joachim Habel**, Anayo Ogbonna, Nanna Larsen, Lars Schulte, Kristoffer Almdal, Claus Hélix-Nielsen, *How molecular internal-geometric parameters affect PB-PEO polymersome size in aqueous solution*

Integration in the thesis: Manuscript in chapter 3

This article investigates the influence of molecular parameters on the diameter of polymersomes, based on polybutadiene polyethylene oxide (PB-PEO) in aqueous buffer. The chosen parameters are molecular weight (M_n) and hydrophilic volume ratio (f) that are thought be to highly relevant parameters for assembly behavior of polymers. The influence of the preparation method was minimized by chosing equal handling and avoiding modifications that could potentially influence the polymersome diameter, like dilution or centrifugation. Polymersomes of 14 polymers with different M_n and f were analyzed with dynamic light scattering (DLS) and FF-TEM. Both analysis techniques revealed highly polydisperse samples with slightly increasing diameter with increasing M_n and f. Polydispersity was increased with decreasing M_n and high f.

My contribution:

- I designed the research
- I performed all FF-TEM experiments
- I performed all data analysis except size analysis on half of the FF-TEM samples
- I wrote the manuscript

4. Submitted manuscript: **Joachim Habel**, Anayo Ogbonna, Nanna Larsen, Simon Krabbe, Kristoffer Almdal, Claus Hélix-Nielsen, *Towards biocompatible polymersome production*

Integration in the thesis: Manuscript in chapter 4

This article addresses a biocompatible polymersome formation processes for future integration of biomolecules. To achieve that goal, two formation methods are compared; solvent evaporation using mild organic solvents and detergent-mediated film rehydration on PB-PEO-based polymersomes in aqueous buffer. Polymersomes, prepared with the first method, appeared to have stiffer and but also less leaky membranes, probably due to shorter formation time. Additionally, polymersomes of higher molecular weight polymers (> 4000g/mol) prepared by SE increased significantly in diameter at concentrations above 10mg/ml in aqueous solution. Two biocompatible polymersome modification methods were compared afterwards; detergent removal us-ing dialysis and biobeads, while changing time and temperature in oder to study the influence of these methods on polymer rearrangement and bilayer conformation and when detergent is removed from the bilayer. At 4°C, both modification methods have similar response to harsh treatment with excess of detergent and applying 95°C combined with NaCl. The optimal combination seems to be be dialysis at RT for three days. These findings show the dependence of polymersomes as a separate systems on biocompatible formation processes.

My contribution:

- I designed the research
- I performed all FF-TEM experiments
- I performed all data analysis except size analysis on half of the FF-TEM samples
- I wrote the manuscript

Acknowledgements

This work would never be possible without a big bunch of great help from a big bunch of great people.
First, I want to thank my main supervisor Claus Hélix-Nielsen. He gave me the unique opportunity to realize my ideas in a PhD project by putting them into a realistic frame. During the project, he always had an open ear and the sixth sense for sensing when it's time to change direction before risking a dead-end. He always asked me first what fits best for me instead of letting me know what would fit him best. Also out of business we had discussions about the most noble alcoholic beverages.
I had a big bunch of co-supervisors. Here, I want to first thank Anayo Ogbonna for his extraordinary flood of ambition that was able to enlighten me as well. He always tried to support as his best with correcting and discussing my work over two years of my PhD.
Thanks to Kristoffer Almdal, my supervisor from DTU Nanotech, whose expertise in all around polymers, biophysics and basics behind all characterization methods was a high value in all discussions and communications.
Finally thanks to Kent Højer Nielsen for being a helpful supervisor during my first year of the PhD and Oliver Geschke for being a helpful supervisor during my last half year.

From Aquaporin A/S I want to thank especially Nanna Larsen and Simon Krabbe for their excellent help with all different kinds of experiments, without I would not have been able to publish any paper.
Great thanks to Sylvie Braekevelt, Yun Shi and Michael Abildgren for a huge bunch of valuable discussions out of the box (and inside working time).
I want to thank Karen Gerstandt for "who-is-who" introducing me to the "holy membrane community" that enabled me to see people on conferences with educated eyes.
Thanks to Julie Bomholt for sharing the "good and evil" of being an Industrial PhD and good advice concerning the freakiness of aquaporins.
Also general thanks to the whole formulation group (Karen, Julie, Boqian Wu, Dana Tværtemos, Fadoua Sbai and Bo Heinemann) for great discussions about the magical world of aquaporins, detergents, polymers and lipids, as well as to Dorte Kristine Schou and Maiken Micheelsen for their great help in and outside of the lab.
Thanks to Leah Hines for all administrative help and trying her best to fill out hieroglyphic VISA formulas.
Thanks to all other Aquaporin members for the great atmosphere I really hope to enjoy after my PhD as well.

From DTU Nanotech side, special thanks goes to Lars Schulte, the “good wizard” of the polymer lab, who just needed to touch something to make it polymerize well (for me the opposite was true). His advice and small tipps helped me through long periods of frustration and darkness of mind.
Thanks to Simon Levinsen, Andriy Dorokhin and Maja Lind-Nielsen for being good lab bodies and always willing to help out in trouble.
Thanks to Lotte Nielsen for helping me in the lab, Ole Kristoffersen for the administrative help, Anne Hektor for help with NMR analysis and Hans Nordlund Hansen for reparing and producing tons of glasswear for my experiments.

From DTU Miljø side thanks to my group members Niada Bajraktari, Mathias Gruber and Elizabeth Wood for help and advice, Vincent Maklawe Essonanawe Edjabou and Hans-Jørgen Albrechtsen for the nice introduction, Tove Larsen for valuable talks and Torben Dolin for help with poster printing.
From DTU Fysik side thanks to Jane Hvolbæk-Nielsen for good advice, Thorsen Kjær and Sardar Bilal Alam for interesting discussion during the physics course and Jytte Findinge Mikkelsen and Helle Wedel Wellejus for administrative help.
From University of Twente thanks for Michiel Raaijmakers, Evelien Maaskant and Kristianne Tempelmann for lab assistance and supervision regarding interfacial polymerization and characterization, Krzysztof Trzaskus, Joris de Groot and Harmen Zwijnenberg for assistance in water separation testing, Wojciech Ogieglo and Rian Ruhl for many valuable discussions, Cindy Huiskes for lab instructions, Frank Morssinkhoff and Susanna van Rijn for administrative and technical help and finally Nieck Benes for good supervision and suggestions during my 3-months-stay abroad in Enschede.
Great thanks to the CFIM group for the opportunity to perform freeze fracture and TEM observation, in particular Klaus Qvortrup for the opportunity to use his facility and to Ramon Liebrechts, Zhila Nikrozi and Laure Plantard for practical help.
Thanks also to Fabrice Rose and Yang Hwan Yun for their help in ultracentrifugation at KU SUND.
Thanks to Grete Jensen for being a great organizer of the SAXS project, Søren Roi Midtgaard for practical help and Søren Kynde for doing the calculations.
A big thanks goes also to Koji Kinoshiba for spending a whole day with me on the micropipet aspiration experiments at Syddanske Universitet in Odense.

I also want to thank Manuel Pinelo for his outstanding Membrane technology course for introducing me to the world of membranes, Ole Mouritsen for giving me the opportunity to learn to know a lot of other PhDs in biophysics over whole Danmark and to Paul Santner, Henrike Sasse-Middelhoff, Maria Lindkvist, Lars Jørgensen and Gunnar Olsen for their nice company during that course.

Great thanks also to Manish Kumar, my supervisor during my master studies, who introduced me to Claus and Aquaporin A/S. He greatly introduced me as well in the whole field of biomimetic membranes and what it means to be a scientist. We worked together at Harvard Medical School, where I probably spent more time in the lab than in any other place but it was worth it. Sadly, there was no opportunity of another collaboration during this PhD but hopefully in the future I will be able to do work together again.
Thanks as well to Wolfgang Meier for the opportunity to sneak in the field and start working with polymersomes.
Special thanks to Fabian Itel, my "Word" supervisor, for all the valuable discussions about proteopolymerosomes and related methods that enriched my research.
Thanks as well to Mohamed Chami for valuable comments on freeze fracture and Daniela Pirner for great discussions on polymer synthesis.
This PhD was funded by the Danish ministry of higher education and science.

I want to thank all my friends from the IA sprog language school, from DTU Nanotech, my ex-band Capeli and of course all friends and relatives from Germany and Switzerland for your support.
Thanks to my parents Annemarie and Dieter for giving me the opportunity to exist and to study what I chose, far away from their field of study and to my sisters Dorothea, Simone and Viktoria and my brother Raphael for asking me questions about my field that I was never able to answer but that broadened my horizon.
Finally the greatest thanks to my girlfriend Solène, the sunshine of my life day and night, for being there, for taking care and giving me a reason to move on or slow down if necessary. You are the best that ever happened to me.

If you would line-up all senseless citations on the first pages of PhD theses on a row, you could span a line from Earth to the moon.[*]

I. Romny

[*] provided that the gaps in between are big enough.

Summary

This project is about the interplay of the three major components of aquaporin based biomimetic polymeric membranes (ABPMs): Aquaporins (AQPs), amphiphilic block copolymers, serving as a vesicular matrix for the hydrophobic AQP exterior (proteopolymersomes) and a polymeric membrane as embedment for the proteopolymersomes and mechanical support. To reach maximal functionality of ABPMs, the interplay of each component needs to be optimized. The optimization of AQPs and amphiphilic block copolymers was investigated by mixing bacterial Aquaporin Z (AqpZ) with polybutadiene polyethylene oxide (PB-PEO) diblock copolymers, where molecular weight (M_n) and hydrophilic volume ratio (f) were systematically varied to study the effect of incorporation efficiency on these molecular parameters. The incorporation was characterized using freeze fracture transmission electron microscopy (FF-TEM), fluorescence correlation spectroscopy (FCS), small-angle x-ray and neutron scattering (SAXS/SANS), stopped-flow light scattering (SFLS) and Sodium dodecyl sulphate polyacrylamide gel electrophoresis (SDS-PAGE). Polymersomes as separate systems were further characterized on their molecular parameters, on formation and analysis methods. The interplay of proteopolymersomes and polymeric mesh support (in this case polyethersulfone, PES) was examined via integration of proteopolymersomes in an active layer (AL) formed by interfacial polymerisation between a linker molecule in aqueous phase and another in organic phase on top of the PES. The resulting thin-film composite (TFC) membrane was analyzed via cross-flow forward osmosis (FO), scanning electron microscopy (SEM), fourier-transformed infrared spectroscopy (FTIR), as well as in the non-supported form over FTIR and a specialized microfluidic visualization approach.

Where no clear differences between proteopolymersomes and polymersomes could be obtained within FF-TEM, SAXS showed that the incorporation of AQPs in a polymersome bilayer changed its property to a more smooth and well-defined shape, as well as a to a shift to more vesicular structures, as compared to coexisting micellar structures in the case of polymersomes. FCS revealed a protein-to-vesicle-ratio of 2.78, when AQP10 was incorporated in polymersome of a low M_n PB-PEO polymer.

With regard to the molecular parameters of the polymersomes, FF-TEM and DLS revealed that the size and polydispersity of polymersomes is expressed in three main regions of M_n and f: Low M_n/high f (mixed sizes/polydisperse), low f (small size/monodisperse) and high M_n/high f (large size/monodisperse). This could be related to a less determined free energy function for polymersome formation with several minima for the first region. With regard to polymersome formation, polymersomes formed with detergent-mediated film dehydration (FR) were found to be less brittle than the ones formed by solvent evap-

oration (SE). This was revealed by SFLS, where a higher signal was obtained for FR prepared polymersomes and by DLS. The brittleness of SE prepared polymersomes was significantly increased from polymers of 3.75 kg/mol M_n and lower as compared to to 3.8 kg/mol and higher, where it was slightly increased above polymer concentrations of 5 mg/ml. FR prepared polymersomes were furthermore modified using biobead removal and dialysis at varying temperature and time. No difference in polymersome size and configuration was obtained between any of the variations. With regard to polymersome analysis, 17 different analysis techniques were used to obtain polymersome size, lamellarity, bilayer thickness or surface charge. Novel methods like atomic force microscopy and nanoparticle tracking analysis turned out to give reliable information on polymersome size like known techniques such as Cryo-TEM. Cryo-TEM gave as well reliable information about lamellarity, SAXS/SANS about bilayer thickness.

SEM, FTIR and microfluidic experiments on the interaction between all three components of ABPMs revealed that (proteo)polymersomes could be integrated successfully in the AL for the one AL linker couple (polyhedral oligomeric silsesquioxane, POSS and trimesoyl chloride, TMC) where for the other couple (polyethyleneimine, PEI and cyanuric chloride, CC), the AL was almost not formed in presence of the proteopolymersomes. The modest membrane performance of all membranes revealed however defects in the AL, which could be due to the micrometer sized pores of PES.

ABPMs could provide a smart solution to one of the worlds greatest challenges in the next decades: the scarcity of clean water and sanitation access.

Dansk sammenfatning

Dette projekt handler om samspillet mellem de tre hovedkomponenter i aquaporin baserede biometriske polymere membraner (ABPMs): Aquaporiner (AQPs), amfifile blokcopolymerer, som fungerer som en vesikulær matrix for AQPs vandafvisende ydre (proteopolymersomer) og en polymer membran til indkapsling af proteopolymersomerne og mekanisk support. For at opnå maksimal funktionalitet af ABPMs skal interaktionen mellem de enkelte komponenter optimeres. Optimeringen af AQPs og de amfifile blokcopolymerer er blevet undersøgt, idet det det bakterielle Aquaporin Z (AqpZ) blev blandet med polybutadien polyethylenoxid (PB-PEO) diblok copolymerer. Molekylvægt (M_n) og hydrofile volumen forhold (f) af PB-PEO blev systematisk varieret for at studere disse molekylære parametres effekt på inkorporeringseffektiviteten. Inkorporeringen blev karakteriseret med freeze fracture transmissionselektronmikroskopi (FF-TEM), fluorescens korrelationsspektroskopi (FCS), små vinkel Røntgen- eller neutronspredning (SAXS/SANS), stopped-flow lys spredning (SFLS) og natrium dodecylsulfat polyacrylamid gel elektroforese (SDS-PAGE). Derudover blev polymersomer som separate systemer karakteriseret med hensyn til deres molekylare parameter, fremstillingsmetoder og analysemetoder. Interaktionen mellem proteopolymersomer og det polymere supportnet (i dette tilfælde polyethersulfon, PES) blev undersøgt gennem proteopolymersomers integration i et aktiv lag (AL) som danner ved interfase polymerisation mellem et linker molekyle i vandfase og et andet indeholdt i en organiske fase på overfladen af PES. Den resulterende tyndfilm kompositmembran (TFC) blev karakteriseret i cross-flow osmose (FO), skanningelektronmikroskopi (SEM), fourier-transform infrarød spektroskopi (FTIR) både for kompositten i den fristående form og en specialiseret mikrofluid metode.

Hvor der var ikke noget klar forskel mellem proteopolymersomer og polymersomer i FF-TEM, viste SAXS at indkapsling af AQPs i polymersom dobbeltlaget ændrer deres egenskaber til en mere glat og veldefineret form, og derudover til flere vesikulære strukturer, i sammenligning med coeksisterende micellære stukturer i tilfældet af polymersomer. FCS opnåede en protein-per-vesikel-forhold på 2,78, når AQP10 blev indkapslet i polymersomer af en lav M_n PB-PEO polymer.

Med hensyn til molekulare parameter af polymersomer viste FF-TEM og DLS at størrelse og polydispersitet af polymersomer falder i tre hovedregioner af M_n og f: Lav M_n/høj f (blanded størrelser/polydispers), lav f (mindre størrelse/monodisperse) og høj M_n/høj f (stor størrelse/monodisperse). Det kan være i overensstemmelse med en mindre definerede fri energi funktion for polymersom dannelse med flere minima for den første region. Med hensyn til polymersom dannelse var polymersomer som blev dannet ved detergent medierede film rehydrering (FR) mindre skør end dem som blev dannede ved

solvent fordamping (SE). Det blev vist med SFLS, hvor der var et stærkere signal for FR dannede polymersomer og med DLS. Skørhed af SE dannede polymersomer var signifikant højere for polymerer med 3,75 kg/mol M_n og lavere i sammenligning med 3,8 kg/mol og højere, hvor den var lidt større for polymer koncentrationer over 5 mg/ml. FR dannede polymersomer blev derudover modificerede ved anvendelse af biobead removal og dialyse med varierende temperature og tid. Der var ikke nogle forskel i polymersom størrelse og konfiguration opnået mellem hver variation. Med hensyn til polymersom analyse blev 17 forskellige analysemetoder anvendt for at måle polymersom størrelse, lamellaritet, dobbeltlag tykkelse eller ledning af overfladen. Nye metoder som atomart kraftmikroskopi (AFM) og nanopartikel tracking analyse gav pålidelige informationer om polymersom størrelse lige som kendte metoder som Cryo-TEM. Cryo-TEM gav også pålidelige information om lamellaritet, SAXS/SANS om bilage tykkelse.

SEM, FTIR og mikrofluidik eksperimenten om sammenspillet mellem alle tre komponenter af ABPMs viste at (proteo)polymersomer kan integreres med succes i AL for det ene linker par (polyhedrale oligomeriske silsesquioksaner, POSS og trimesoyl klorid, TMC), hvor i det tilfælde af det andet par (polyethylenimid, PEI og cyanurisk klorid, CC), dannede det AL sig næsten ikke når der var proteopolymersomer med. Den beskedne membraneffekt i alle membraner viste dog af der var defekter i AL, som kunne skyldes mikrometer porer i PES.

ABPMs kan udgøre en smart løsning på en af verdens største udfordringer i de næste årtier: manglen på adgang til rent vand og sanitet.

Contents

Abbreviations / Nomenclature

7-ADCA - 7-aminodesacetoxycephalosporanic acid
A - Pure water permeability coefficient
A_0 - Initial polymersome surface before micropipette aspiration
A4F - Asymmetrical flow field-flow fractionation
ABPM - Aquaporin-based biomimetic polymeric membrane
ABLM - Aquaporin-based biomimetic lipidic membrane
AFM - Atomic force microscopy
AL - Active layer
APM - Auto painted chamber
AQP - Aquaporin
AqpZ - Aquaporin Z
AU - Arbitrary units
B - Salt permeability coefficient
Bd - Butadiene
BR - Bacteriorhodopsin
BSA - Bovine serum albumin
n-BuLi - *n*-Butyl lithium
n-Bu_2Mg - *n*-Dibutylmagnesium
$c_{F,m}$ - Salt concentration on feed side
$c_{D,m}$ - Salt concentration on draw side
$c_{P,wt}$ - Polymer weight concentration
CA - Cellulose acetate
CTA - Cellulose triacetate
CaH_2 - Calcium hydride
CcO - Cytochrome c oxidase
CGMD - Coarse grain molecular dynamics
cmc - Critical micelle concentration
CNT - Carbon nanotube
CC - Cyanuric chloride
CLSM - Confocal laser scanning microscopy
CP - Concentration polarization
Cr - Planar shape with protein crystals
CYMAL - 5-cyclohexyl-1-pentyl-β-D-maltoside
d - Particle diameter (chapter 2) / scattering point distance (chapter 5)
D_L - Lateral diffusion coefficient

d_P - Polymersome diameter
$\langle d_P \rangle$ - Mean value of polymersome diameter
DCA - Dichloroacetamide
DIB - Droplet interface bilayer
DLS - Dynamic light scattering
DMA - Dimethacrylate
DOPC - 1,2-dioleoyl-*sn*-glycero-3-phosphocholine
DOPE - 1,2-dioleoyl-sn-glycero-3-phosphoethanolamine
DPD - Dissipative particle dynamics
DPhPC - 1,2-diphytanoyl-*sn*-glycero-3-phosphocholine
DTNB - 5,5'-dithiobis-2-nitrobenzoic acid
DTU - Danish Technical University
E_{bend} - Bilayer bending energy
E_{disk} - Bilayer line energy
ECP - External concentration polarization
ELF - Enzyme-labelled fluorescence
EM - Electron microscopy
EMIM-TFSI - 1-ethyl-3-methylimidazolium-bis-(trifluoro-methylsulfonyl)imide
EO - Ethylene oxide
EPR - Electron paramagnetic resonance
ESEM - Environmental scanning electron microscopy
ESRF - European Synchrotron Radiation Facility
ETFE - Ethylene tetra-fluorethylene
f - Hydrophilic volume ratio
f_w - Hydrophilic weight ratio
FCM - Flow cytometry
FCS - Fluorescence correlation spectroscopy
FF - Freeze fracture
FhuA - Ferric hydroxamate uptake protein
FI - Functional incorporation
FO - Forward osmosis
FR - Film rehydration
FRM II - Forschungs-Neutronenquelle Heinz-Maier-Leibniz
FTIR - Fourier-transformed infrared spectroscopy
FTLA - Finite track length adjustment
GFP - Green fluorescent protein
GlpF - Glycerol facilitator

GP - Generalized polarization
GPM - Generalized polarization microscopy
GUV - Giant unilamellar vesicle
H-bond - Hydrogen bond
HF - Hollow fibre
HPLC - High performance liquid chromatography
HTI - Hydration Technology Innovations
I - Light scattering intensity
ICP - Internal concentration polarization
IP - Intrinsic protein
ITO - Indium tin oxide
J_s - Reverse salt flux
J_v - Water flux
k - Rate constant of initial rise in stopped-flow light scattering curve
K_a - Elastic-area compressibility modulus
k_c - Bending elasticity modulus
k_{app} - Apparent first-order-reaction rate constant
L_p - Length of membrane protein
LamB - Phage lambda receptor
Laurdan - 6-lauroyl-2-(dimethylamino)naphthalene
LbL - Layer-by-layer deposition
LDE - Laser doppler electrophoresis
LMH - Liters per square meter per hour
M_h - Weight-averaged molecular weight of the hydrophobic polymer within block copolymer
M_n - Number-averaged molecular weight
$M_{n,Polymer}$ - Number-averaged molecular weight of certain polymer within block copolymer
M_w - Molecular weight for proteins / weight-averaged molecular weight for polymers
MAq - Mixing in aqueous phase
Mc - Micellar shape
mPAR - molar protein-to-amphiphile-ratio
MD - Molecular dynamics
MF - Microfiltration
MIP - Major intrinsic protein
MloK1 - Potassium channel from Mesorhizobium loti
MOr - Mixing in organic phase

MPD - m-phenylene diamine
MPEG - Methyl polyethyleneglycol
MWCO - Molecular weight cut-off
$N_{Monomer}$ - Monomer block length in block copolymer / degree of polymerization
NA - Not announced
NAD - β-nicotinamide adenine dinucleotide
NADH - Hydrogenated β-nicotinamide adenine dinucleotide
ND - Not determined
NF - Nanofiltration
NIBS - Non-invasive back scattering
NMR - Nuclear magnetic resonance
NNLS - Non-negatively constrained least squares
NPA - Asparagine-proline-alanine
NS - Negative staining
NTA - Nanoparticle tracking analysis
NtAQP1 - Tobacco plasma membrane intrinsic protein 1
NtPIP2;1 - Tobacco plasma membrane intrinsic protein 2
NTU - Nanyang Technological University
NUS - National University of Singapore
GlpF - Glycerol facilitator
OG - n-Octyl-β-D-Glucopyranoside
OGST - OG stress treatment
OmpF - Outer membrane protein F
OmpG - Outer membrane protein G
P - Planar shape
P_f - Vesicle bilayer permeability
P2VP - Poly-2-vinyl pyridine
P4MVP - Poly-4-vinyl methylpyridine iodide
P4VP - Poly-4-vinyl pyridine iodide
PA - Polyamide
PAA - Polyacrylic acid
PAH - Polyallylamine hydrochloride
PAI - Polyamide imide
PAN - Polyacrylonitrile
PAO - Pressure assisted osmosis
PB - Polybutadiene
PBI - Polybenzimidazole

PBMA - Polybutyl methacrylate
PBO - Polybutylene oxide
PBR - Polymer film rehydration
PBzMA - Polybenzyl methacrylate
PCM - Phase contrast microscopy
PCTE - Polycarbonate track-etched
PDA - Polydopamine
PDI_M - Polydispersity index of polymer
$PDI_{M,Polymer}$ - Polydispersity index of certain polymer within block copolymer
PDI_{DLS} - Polydispersity index of the polymersome diameter at DLS analysis
PDMS - Polydimethylsiloxane
PDPA - Polydiisopropylaminoethyl methacrylate
PEE - Polyethylethylene
PEG - Polyethylene glycol
PEI - Polyethyleneimine
PEO - Polyethylene oxide
PEOXA - Polyethyloxazoline
PES - Polyethersulfone
PFR - Polymer film rehydration
PGC - Palmitoyl glycol chitosan
PGM - Polyglycerol monomethacrylate
PGMA - Polyglycerol monomethacrylate
PGME - Phenylglycine methyl ester
PHEMA - Polyhydroxyethyl methacrylate
PHPMA - Polyhydroxypropyl methacrylate
PI - Polyisoprene
PIAT - Poly-L-isocyanoalanine(2-thiophen-3-yl-ethyl) amide
PIB - Polyisobutylene
PLA - Polylactic acid
PMOXA - Polymethyloxazoline
PMPC - Polymethacryl oyloxyethylphophorylcholine
PPFR - Protein/polymer film rehydration
PPO - Polypropylene oxide
POSS - Polyhedral oligomeric silsesquioxane
PR - Proteorhodopsin
PRO - Pressure retarded osmosis
PS - Polystyrene

PSf - Polysulfone
PSS - sulfonated polysulfone
PVA - Polyvinyl alcohol
PVL - Polyvalerolactone
PVP - Polyvinylpyrrolidone
q - X-ray and neutron scattering vector
QCM-D - Quartz crystal microbalance with dissipation
R_P - Outer polymersome radius
RC - Reaction centre
RO - Reverse osmosis
RT - Room temperature
s_P - Width of polymersome interface
S - Structural parameter of membrane (chapter 1.4) / Shape (Table 2) / Vesicle surface area (chapter 3-5)
SANS - Small-angle neutron scattering
SAXS - Small-angle x-ray scattering
SDL - Size detection limit
SDS-PAGE - Sodium dodecyl sulphate polyacrylamide gel electrophoresis
SDU - University of Southern Denmark
SE - Solvent evaporation
SEC - Size exclusion chromatography
SF - Selectivity filter
SEM - Scanning electron microscopy
SFLS - Stopped-flow light scattering
SI - Solvent injection
SIADH - Syndrome of inappropriate anti-diuretic hormone
SLS - Static light scattering
SMTC - Singapore Membrane Technology Center
SoPIP2;1 - Spinach plasma membrane intrinsic protein 2;1
STED - Stimulated emission depletion microscopy
STM - Scanning tunneling microscopy
t_s - Support layer thickness
t_P - Thickness of the hydrophobic core of polymersomes
tBuP4 - 1-*tert*-Butyl-4,4,4-tris(dimethylamino)-2,2-bis[tris(dimethylamino)phosphoranylidenamino]-2λ^5,4λ^5-catenadi(phosphazene)
TEM - Transmission electron microscopy
TFC - Thin film composite

THF - Tetrahydrofuran
TMB - 3,3,5,5-tetramethyl-benzidine
TMC - Trimesoyl chloride
TRPS - Tunable resistive pulse sensing
TSST - Temperature / NaCl stress treatment
UF - Ultrafiltration
UV - Ultraviolet
V - Vesicular shape
V_0 - Vesicle volume before osmotic shock at stopped-flow light scattering
V_{DLS} - Variation coefficient of polymersome size at DLS analysis
V_{FF-TEM} - Variation coefficient of polymersome size at FF-TEM analysis
V_w - Molar volume of water (18 cm^3/mol)
WAXS - Wide-angle x-ray scattering
XIP - uncategorized X intrinsic protein
Z_D - Intensity-weighted hydrodynamic diameter at DLS analysis
α - Fractional surface area change of polymersomes
δ - Distribution width of the polymersome diameter at DLS analysis
Δ_{osm} - Difference in osmolarity
ΔA - Polymersomes surface area change
ΔP - Applied operational pressure
$\Delta\pi$ - Osmotic pressure
$\Delta\pi_m$ - Effective osmotic pressure across the active membrane layer
ϵ - Support layer porosity
γ - Bilayer line tension
κ - Bilayer bending modulus
λ - Wavelength
σ - Standard deviation of polymersome diameter at FF-TEM analysis
τ - Support layer tortuosity (chapter 1.4) / isotropic tension change of the polymersome surface (chapter 5)
τ_c - Rupture tension
θ - X-ray or neutron scattering angle

Thesis outline

Given the fact that 70% of the earth is covered with water and a human body is made of almost 70%, it seems strange that the greatest challenges of human population on earth will be the lack of water. It is however not the water itself that is lacking. Drinkable water requires a few minerals, where the mineral NaCl should not exceed 10 mg/ml [2] - which is the case for 95% of all water on earth - and there should of course be no traces of arsen or boron. Water in the pharmaceutical or semiconductor industry needs to be completely demineralized, where water for fertilizing requires enrichment in nitrogen and phosphor. Actually there is a lack of water in a desired state.

To get water from an undesired state to an desired one, the simplest solution is to just transport it from a zone with undesired features to a zone with desired features - without transporting anything else. For this selective transport, a selective barrier, called membrane, is required. The membranes of cells achieve the desired water transport through molecular water channel proteins, called aquaporins (AQPs). Only water molecules are transported through AQP channels, whereas everything else, including protons, are excluded [3]. This transport works since billions of years with a water transport rate about three billion molecules per second [4], without membrane fouling or channel clogging.

Industrial water separation membranes are on the other side much better in fouling and clogging, whereas the exclusion on other molecules than water is still difficult to achieve. The most selective membrane based on reverse osmosis (RO) have reasonable NaCl rejection of 99%, however molecules like boron are only rejected by 97%, which is not sufficient to achieve drinking quality [5].

To combine the well-established and perfectly optimized technologies (nature) with recently upcoming and rarely developed technologies (human-made industrial membranes) it needs some thinking out of the box. The Danish cleantech company Aquaporin A/S from Copenhagen, went several steps out of the box to come to different approaches of possible combination of both technologies, thereby creating a biomimetic membrane - meaning a synthetic membrane that mimics nature by the integration of AQPs. Their first approach was an auto painted chamber (APM), where AQPs are supposed to be embedded in a lipid bilayer sheet that was painted over a micropore-size scaffold [6], followed by liquid membranes, where they should sit in the interfaces of lipid coated water drops in an emulsion (droplet interface bilayers, DIB) [7] and finally to polymer membrane sheets, where AQPs were integrated in a thin active layer (AL) made of polyamide (PA) on top of a porous support [8].

The PhD project is adressing this last approach. The biomimetic membrane here contains of two main components: the natural component, aquaporins, and the synthetic compo-

nent, a polymeric mesh membrane sheet. AQPs need to be in amphiphilic environment, thus, a third component is needed, which can be natural (lipids) or synthetic (amphiphilic block copolymers). For this project, the block copolymers were chosen, as far as they have several advantages over lipids that will be described in details later in chapter 1.2. Some amphiphilic block copolymers assemble spontaneously to hollow spheres (polymersomes, as an analogue to liposomes, lipid based hollow spheres) [9], which can be seen as simplified cells. Despite their simplicity, AQPs could be integrated functionally in such systems [10].

0.1 Aim

The main goal of this PhD project is to perfect the interplay of each component of a AQP-based biomimetic polymeric membranes (ABPMs, polymeric due to the block copolymers not to the polymer membrane). The project can be subdivided into three steps: optimization of the interplay of aquaporins and block copolymers by variation the molecular parameters of the block copolymers; optimization of the same interplay by variation of the mixing process and optimization of the interplay of proteopolymersomes (polymersomes with AQPs incorporated in the bilayer) with the polymer membrane by variation of the PA-layer formation. The steps are visualized in Figure 1. The AQP used is the bacterial Aquaporin Z (AqpZ), the polymer membrane used is polyethersulfone (PES) and the chemistry of the (di)block copolymers that remain the same during the whole project as well, is polybutadiene polyethylene oxide (PB-PEO). For the first step, (number-averaged) molecular weight (M_n) and volume ratio of the hydrophilic blocks to the whole polymer (f) will be varied systematically and examined for their ability to incorporate a maximal amount of AQPs. The incorporation efficiency will be characterized using flourescence correlation spectroscopy (FCS), freeze fracture transmission electron microscopy (FF-TEM), small-angle x-ray scattering (SAXS) and stopped-flow light scattering (SFLS). Further details to characterization methods are described in chapter 2. The step includes the variation of AQP and block copolymer mixing (film rehydration, FR and SE) and detergent removal (dialysis and biobeads). Details to the methods can also be found in chapter 2. AQPs from the stock solution are first embedded in detergent that needs to be removed due to its destablization of proteopolymersomes. The characterization will be the same as described before. Finally, proteopolymersome embedment on a polymer membrane will be optimized by varying the AL linker molecules in aqueous and organic phase and characterize the resulting membrane using scanning electron microscopy (SEM), fourier-transformed infrared-spectroscopy (FTIR) and cross-flow flux and rejection test in forward osmosis (FO) mode.

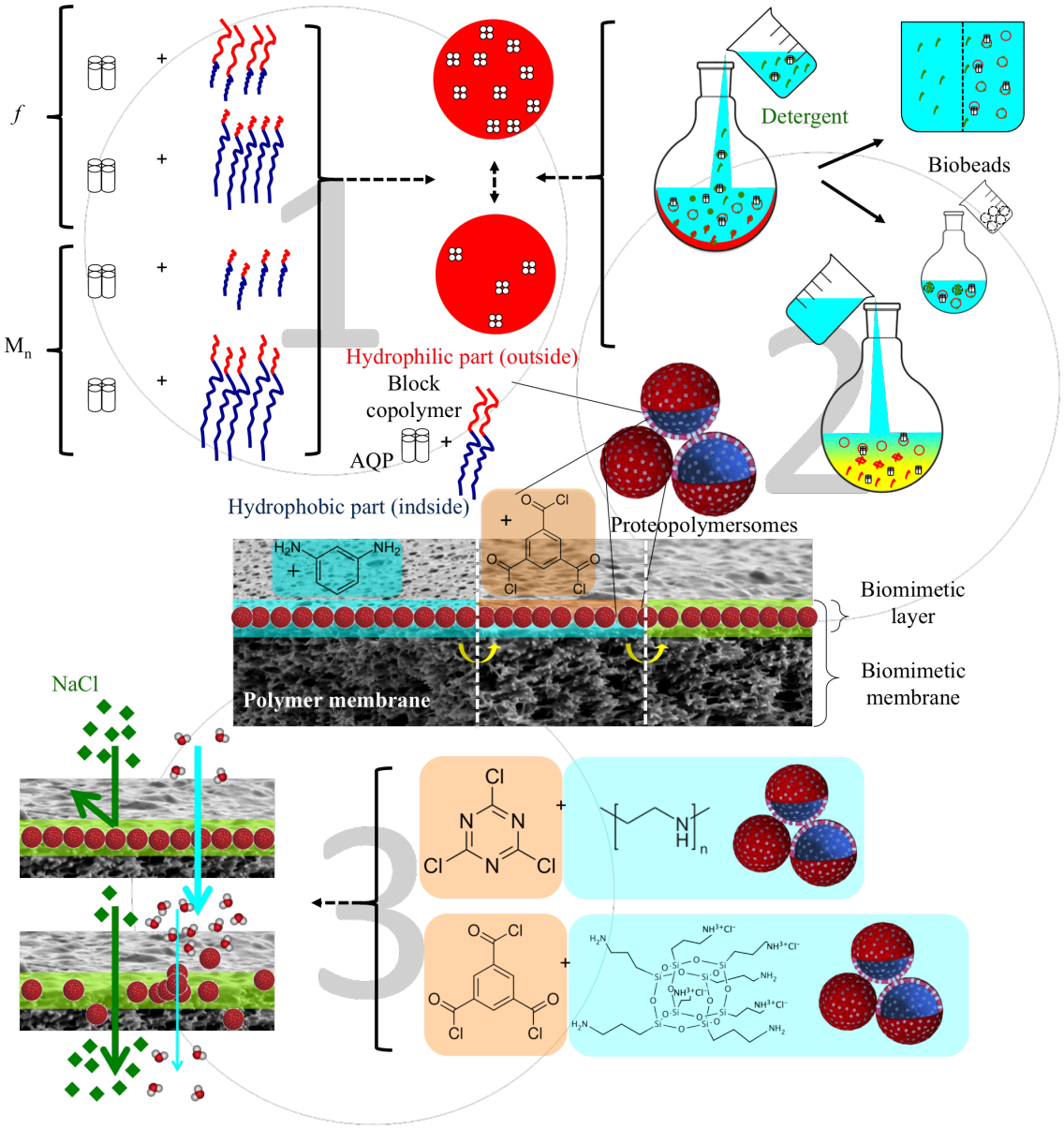

Figure 1: Schematic guidelines through the PhD project, focussing on the three major components of ABPMs: AQPs, block copolymers as their matrix molecules and a polymer membrane for mechanical support. The first examination (1) will be on the interplay of AQPs and block copolymers, where the molecular parameters of the latter are varied systematically, followed by the interplay of AQPs and block copolymers with regard to their mixing (2) and finally the integration of proteopolymersomes (hollow spheres of block copolymer self-assembly with AQPs in the bilayer) in the polymer membrane (3). Characterization methods and interplay optimization criteria are shown as well.

0.2 Thesis structure & reader instruction

The PhD thesis is structure according to these steps mentioned before. Each ABPM component, separately and in interplay among each other, will be introduced in the introduction chapter 1, where main aspects of membrane technology will be discussed in the polymer membrane chapter 1.4 as well. The experimental part starts with the interplay of AQPs and block copolymers due to variation of the molecular parameters and the mixing varation in chapter 2. Further research on polymersomes alone resulted in three publications that can be found in chapter 3-5. Chapter 6 concludes with the experiments on the final interplay between proteopolymersomes and the polymer membrane. An appendix is attached with details on the synthesis of the PB-PEO polymers with varied M_n and f that was done prior to the experiments of chapter 2. If a paper is published, the published versions can be found as well in the appendix.

If the reader is interested in the experiments performed, he/she is recommended to read chapter 2-6 as they are experimental chapters. Chapter 3-5 are complete submitted manuscripts, whereas chapter 2 and 6 are partly submitted and published, whereas other parts have not been submitted. If the reader is a biologist or a biochemist, chapter 1.1, 1.3, 1.5, 2 and 6 are recommended for reading as they contain information and experiments with AQPs. If the reader is a polymer physicist, chapter 1.2, 3-5 are recommended for reading, especially chapter 3 as it has a strong focus on polymer(some) physics. If the reader is a polymer chemist, the appendix 8.1 are recommended for reading as it contains detailed information about polymer synthesis and synthesis optimization steps. If the reader is a membrane specialist, chapter 1.4, 1.5 and 6 are recommended for reading as they have information and experiments with industrial membranes.

There are several state-of-the-art information, as well as graphical and tabular summaries to the following fields: Membrane protein-block copolymer interactions (chapter 1.3), biomimetic membranes (chapter 1.5), polymersome formation and modification methods (introduction of chapter 4 and polymersome analysis techniques (introduction of chapter 5).

1 Introduction

The introduction is structured as follows: First, AQPs are introduced, including genetical and crystallographic information, their most relevant regions for water transport and selectivity and underlying mechanisms. Some extra information is added on AqpZ which is mainly used in this project. The AQP-introduction is followed by an introduction to block copolymers with a major focus on polymersomes and the PB-PEO chemistry, used in this project followed by a comparison to lipids in terms of properties. Then, AQP incorporation into block copolymers is introduced, with a broader perspective to other membrane proteins. This is followed by an introduction to polymer membranes and membrane technology with a major focus on forward osmosis. Finally the introduction concludes with an overview over biomimetic membrane designs, including their history, development, state-of-the-art and alternative novel membrane technologies.

1.1 Aquaporins

AQPs, channel shaped membrane proteins with a molecular weight (M_w) of 26-35 kDa [3], play a major regulatory role in transmembrane water transport. They are essential for cell volume regulation, energy metabolism and have minor roles in degradation and phosphorylation processes [3, 11, 12]. It has been proven by mutation experiments that disfunction of AQPs is a direct cause of kidney-related diseases like the syndrome of inappropriate anti-diuretic hormone (SIADH) or nephrogenic diabetes. Further major roles has been proposed in diseases related to the eye (cataract), brain (cerebral edema, epileptic seizure), pancreas (pancreatic insufficiency & diabetes) and cancer (angiogenesis and tumor edema) [3, 13].
Several research groups found water permeabilities in renal tubules, red cells and secretory glands that exceeded by rate of simple water diffusion through lipid bilayers by a factor of 50, whereas the activation energy (E_a) remains the same [3, 14, 15]. The enhanced permeability was caused by proteins, which was proven by mercury inhibition experiments [15]. Peter Agre and coworkers achieved the final proof of the existence of AQP in frog oocyte experiments [10], which has been awarded with a Nobel prize in 2003 [14].

Today, it is known that AQPs are one of the two functional subgroups of major intrinsic proteins (MIPs), a group with more than 1700 proteins. AQPs are evolutionary originated in AqpZ of E.coli. All AQPs (except AQP11+12) share two highly conserved asparagine-proline-alanine (NPA) motifs, whose role will be described later. The other subgroup is

aquaglyceroporins (GLPs). Their main difference are five side chains around the NPA motif. Where AQPs are only permeable to water, GLPs have an additional asparigine after the second NPA motif. The channel diameter is therefore larger, enabling the transport of larger molecules than water like H_2O_2, glycerol, urea, ammonia, lactic acid or metalloids [3]) as well as to gases like CO_2, NH_3 or nitric oxide (NO) [3, 16]. Their origin is from Glycerol facilitator GlpF. AQP11 and AQP12 have only one NPA motif and therefore called superAQPs (due to super-gene family with low homology to all other AQPs [3]).

All known organisms have AQPs. Bacteria and archae have one kind of AQP and one of GLP [3]. Humans have 13 MIPs, some of them highly expressed in certain organs: the AQPs AQP0 (in the eye lens), 1, 2 (kidney), 4 (brain), 5 (testes, lungs and thyroid), 6 (kidneys) and 8 (digestive tract), 11, 12 (pancreas) and the GLPs AQP3, 7, 9 (blood) and 10 [3, 11]. Plants share several groups of intrinsic proteins (IPs) that have their origin in AQP (plasma, tonoplast, hybrid, small basic, NOD26-like and uncategorized X-IPs) or GLP (GlpF-like IPs) [3].

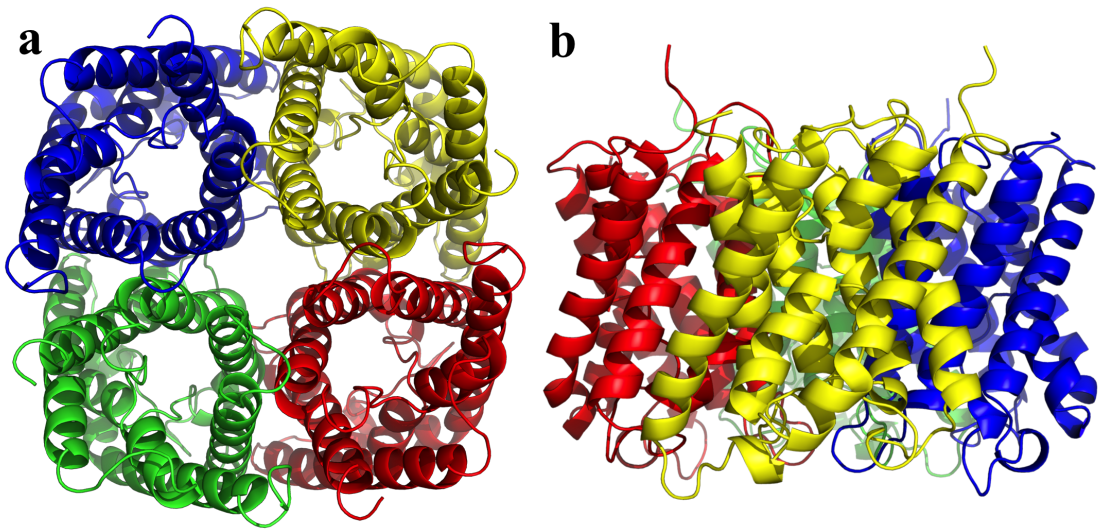

Figure 2: Ribbon representation of the tertiary structure of general AQP tetramer from (a) top view (left) and (b) side view (right). Every momomer (blue, green, yellow and red) functions as a water selective channel. With friendly permission from Mathias Gruber.

AQPs consist of four functional monomer channels (see Figure 2). Every channel has six membrane-spanning domains that can be seen as similar three-domain-twins, shown in Figure 3a+c. They are linked via five loops A-E, whose lengths are mainly determining AQP families like prokaryotic and eukaryotic AQPs, whereas loop E and B contain a short helix [14, 17].

Another essential characteristic to differentiate between AQPs are the two NPA motifs mentioned before, located on both short helices on loop B and E. They are thought to play a major role in AQP's low E_a transport of water molecules and proton exclusion. They are linked within a head-to-tail contact between both proline rings and alanines as well as within a hydrogen bond (H-bond) between both asparigines. These contacts form the typical hourglass shape of the AQP's pore [18, 19]. Asparagine is the major side chain for cation repulsion and protein stabilization as shown by point mutations [20].

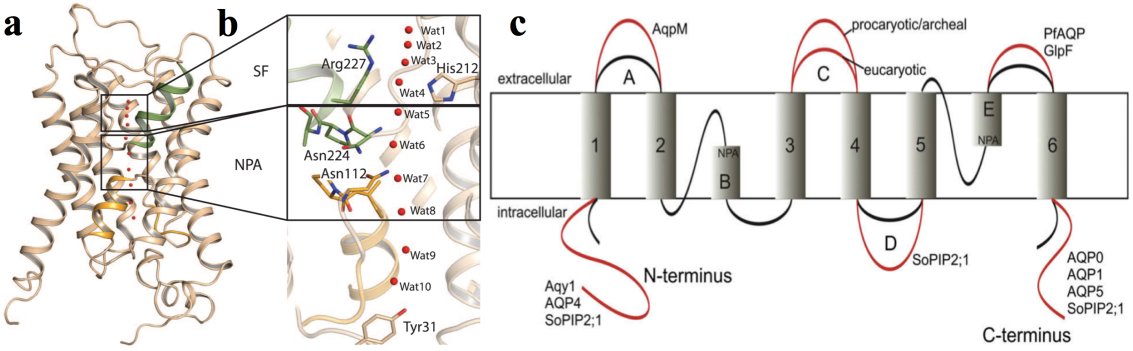

Figure 3: (a) Ribbon representation and (c) schematic sketch of tertiary structure of general AQP monomer/channel. Every AQP channel contains a highly conserved NPA region and a so-called selectivity filter (SF) region (b). The NPA residues are located on the B (yellow) and the E (green) loop [21]. The domain, formed by helices 1-3, is equal the one of helices 4-6. The characteristic hourglass shape is a result of the binding of the NPA motifs of loop B and E that also forms a helix. Varieties in AQPs appear mainly in form of loop lengths [17].

Selective substrate permeability is thought to be ensured via another highly conserved region, called the ar/R region or selectivity filter (SF, Figure 3b). The SF is the narrowest point of the channel with less than 4 Å diameter (AqpZ: 3.0 Å, GlpF: 4.0 Å, AQP1: 3.5 Å) [19]. It is formed by hydrophilic residues, an aromatic histidine at helix 5, an arginine at short helix E and the carbonyl of a threonin (for AqpZ, cysteine for AQP1) that are opposing the hydrophobic phenylalanin at helix 2 [19], [22]. Their selectivity is based on size exclusion, proton exclusion by the positively charged residues Arg and His, anion exclusion by a Arg-induced negatively charged carbonyl backbone [23] and hydrophilicity for repulsion of ammonium, as shown by point-mutation [22], x-ray crystallography studies [19] and molecular dynamics (MD) simulation [24]. While the NPA region is responsible for alkali cation exclusion, the SF only excludes protons. The NPA motif is thought to exist in primordial AQPs, where the SF was adapted later for enabling proton exclusion [25].

A strong discrepancy between the high water permeation rate of AQP while excluding protons at the same time led to long lasting debates. One would logically assume that at high permeation rate, there has to be high densities of water molecules in the channel.

However the distance between water molecules at least at one part of the channel has to be more than 3.5 Å so that they cannot form H-bonds with each other. H-bonds enable the formation of a proton wire that again enable protons to be transported through the pore via "hopping" via H-bonds between water molecules, also called Grotthuß mechanism [14, 26].

Several models have been proposed to address this contrast of having lots of water molecules passing the channel and still providing a distance between each molecule, long enough to break up the proton wire. The most prominent one try to explain the contrast within the amine groups of the Asp residues of both the NPA regions that build out H-bonds with the oxygen of the passing water molecule. Consequently, the hydrogen atoms of the water molecule are oriented perpendicular to the channel axis and thus too far to form H-bonds with neighbour water molecules. The permeation rate is not thought to be affected by that reorientation [3]. Other scientists think that the short α-helices containing the NPA motifs are generating a macrodipole that builds an electrostatic barrier for protons and other cations, where the H-bond breaking is more a secondary effect and more pronounced at the SF [13, 27–29]. Removal of charge at the SF residues resulted in proton conductance [22]. A third one assumes the high packing of H-bond-building side chains at the SF to discrimate water from other small molecules [21].

Previous models excluded the role of NPA or SF and state desolvation effects as the main proton barrier [30]. Others suggest the passing of water molecules in pairs and so preventing the building of H-bonds [3].

Even today, the true mechanism remains unclear, although the vast majority believes in the involvement of the NPA motif and the SF [3].

This study will focus on AqpZ, as the first component of ABPMs. AqpZ, shown in Figure 4, is tightly packed and more hydrophobic than other AQPs [31]. The permeability of AqpZ ($13*10^{-14}$ $cm^3s^{-1}subunit^{-1}$)[10] is the highest among AQPs, only exceeded by AQP4 ($24*10^{-14}$ $cm^3s^{-1}subunit^{-1}$)[32]. Where E.coli AqpZ (used in this study) is only permeable to water, AqpZ of cyanobacteria also has CO_2 permeability [33]. AqpZ has 28-38% identity with plant and mammalian AQPs, however its terminal helices are significantly shorter. Furthermore, it is more resistant to proteases, mild detergents like SDS (no unfolding in 1% SDS) and insensitive to mercury because it lacks a cysteine in the mercury sensitive region [31, 34]. At 4° C, AqpZ can be stored for six months without becoming inactive [31].The lateral stability is enabled by H-bonds and salt bridges that are facing diagonally through the hourglass structure, as shown by AFM experiments [35]. The tetrameric stability is mainly enabled within a cysteine residue, Cys20. Mutants of that residue appeared in monomers [31]. Higher amounts of aromatic residues in the interface between monomers, compared to GlpF, are thought as well to stabilize the tetrameric

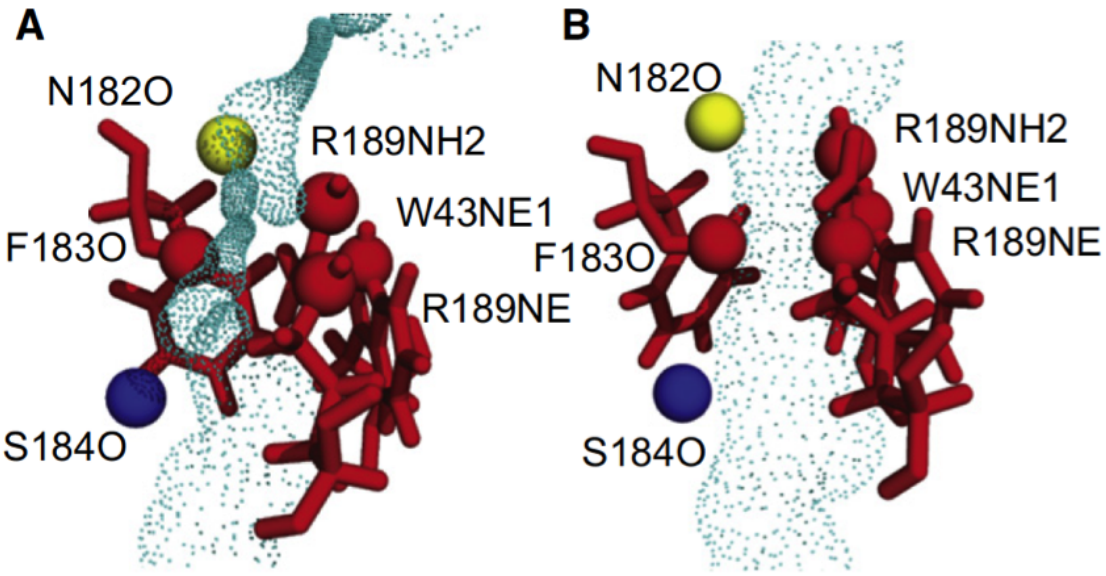

Figure 4: Closed (A) and open (B) conformation of AqpZ as a HOLE representation. All relevant residues for the gate mechanism are coloured in red. After the first gate, represented with the arginine residue R189, the phenylalanine residue F1830 and the tryptophan residue W43NE1 appear as a stacked ring, and so act as a second gate [24].

form in denaturing conditions [19]. Further stabilization at denaturing conditions is enabled within an high presence of glycine residues in the transmembrane segment, allowing short interhelix distances with bond energies of 2.5-3.0 kcal/mol. [19] Stabilization and channel performance are relatively independent from the surrounding lipids in cell membranes with the exception of cardiolipin [36]. On the other hand, AqpZ stabilizes the lipid membranes against surface tension [37]. AqpZ is pH insensitive in a range of $4.5 \leq \text{pH} \leq 7.5$ [38], whereas below pH 4, the pore of AqpZ closes reversibly [39], [24]. The mechanism behind that gating is related to the imidazole ring of the histidine residue of the SF. There are two nitrogens at this ring that can be protonated, whereas one of them facing the inside of the pore. Below pH 4, the protonation of the pore facing nitrogen is preferred. The proton builds an H-bond with the guanidinium group of an opposing arginine residue, inducing a conformation change of arginine [23]. As a result, the arginine residue is facing inside the pore, minimizing its radius to less than 1 Å. Consequently four times less water molecules can pass the channel [38]. This function is thought to be essential for bacterial survival at hypo osmotic shocks [26, 40]. AqpZ plays furthermore a role in cell volume regulation, cell growth and division of bacteria [34, 40]. The common production of AqpZ is achieved by over-expression in E.coli, however with only low yields of 15 mg/ml. Recent studies could enhance the yield to 350-500 mg/ml by cell-free approaches using fusion vectors at the N-terminus for enhanced expression, supplemented with liposomes and detergents [41].

1.2 Block copolymers

Block copolymers are polymers with two or more homopolymer chains, also called blocks, that are linked by covalent binding [42]. The only block copolymers that are capable of mimicking a cell bilayer and thus incorporating membrane proteins are amphiphilic diblock and triblock copolymers. Amphiphilic block copolymers requires a block of least one hydrophilic and a block of at least one hydrophobic polymer subunit. Where cell-like bilayer forming diblock copolymers can only exhibit one conformation AB (hydrophobic-hydrophilic), triblock copolymers can adopt an ABA conformation (hydrophilic-hydrophobic-hydrophilic) or a ABC conformation (hydrophilic-hydrophobic-different hydrophilic).

In polar environment, amphiphilic block copolymers assemble to a monolayer that can form three main shapes (micelles, cylinders and bilayer sheets), depending on the interfacial curvature of the monolayer [43] that is directly linked to the ratio between the hydrophilic block and the hydrophobic block (see Figure 5). Similar to lipids, a hydrophilic weight ratio (f_{mol}) of 0.35±0.1 results in a self-assembly to bilayer sheets, 0.35 to 0.5 results in cylinder shape and above 0.45 micelles are forming, where the borders are overlapping and structures can coexist. Below 0.25, inverted structures are formed [9].

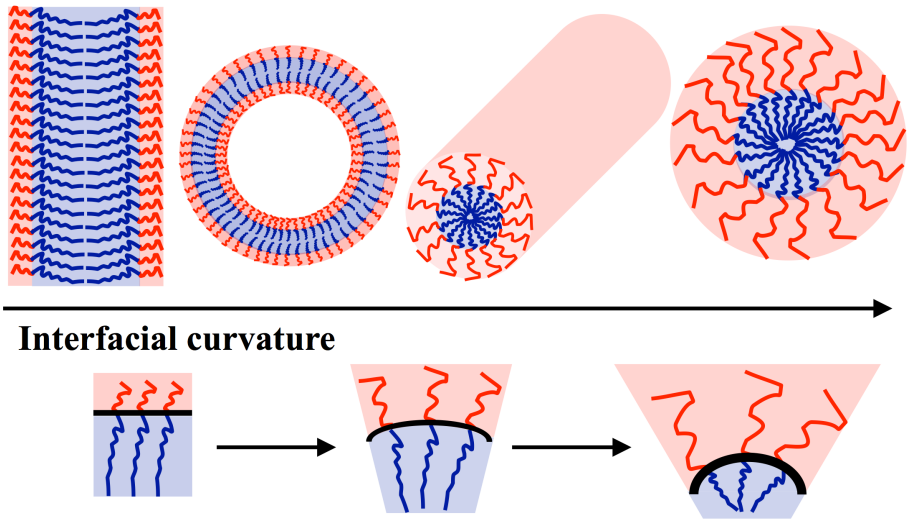

Figure 5: Sketch of occuring self-assembly morphologies with increasing interfacial curvature with schematic sketch of the curvature and the hydrophilic and hydrophobic block proportions below. At zero curvature, block copolymers are assembled to plane bilayer sheets, where they turn into vesicles or polymersomes, cylinder and micelles.

Where there are approaches to incorporate membrane proteins in planar bilayer sheets, the most promising approach goes the natural way over cell-like closed vesicular bilayer

structures, hereafter stated as polymersomes. Polymersomes is an analogue to liposomes, lipid-based vesicular structures that are used since the 50's as a simplified version of a cell. Polymersome formation occurs via two mechanism: closure of planar bilayer sheets and nucleation with nucleus growth [44]. The closure of bilayer sheet happens, when the closure energy is energetically preferable compared to the surface tension of the planar sheet [43]. From a thermodynamical point of view, the polymersome diameter d_P can therefore be seen as the product of the balance between bending energy and rim energy of the planar sheet. However, formation method-based factors play a larger role in the diameter and polydispersity of polymersomes. In chapter 3, the effect of polymer chemistry on d_P and polydispersity are discussed in detail.

Polymersomes were first introduced by Eisenberg and coworkers in the late 90's [45], 30 years after the invention of liposomes from Bangham [46]. They dialyzed polystyrene-polyacrylic acid (PS-PAA) in organic solvents against water in order to get PS-PAA to precipitate to the aqueous phase in vesicular form. The earliest block copolymers that assembled directly in water were polymer-peptid-hybrids like PS-poly(isocyano-alanine-alanine), where the first stable polymersomes in water were achieved by the Bates group around 2000, using PB-PEO (chemical structure in Figure 6a), respectively the hydrogenated homologue of PB, polyethylethylene (PEE-PEO) [9, 47, 48]. Nowadays there are plenty of polymer chemistries known that are able to form polymersomes (a list can be found in [49]). They form polymersomes in the M_w range of 1 to 20 kg/mol, thus exceeding lipids from a factor 1.5 to 30 [9, 50]. The most prominent ones for membrane protein incorporation remain PB-PEO and a ABA triblock copolymer based on polymethyloxazoline-polydimethylsiloxane-polymethyloxazoline (PMOXA-PDMS-PMOXA, see Figure 6b), where the last one is especially interesting for drug delivery applications, as far as it remains in its shape in the dry state, whereas PB-PEO mostly appear in collapsed form when brought out of water [51]. PB-PEO, used for this study, will be described in the last section of this subchapter.
Even though amphiphilic block copolymers like PB-PEO form polymersome spontaneously in water there are several formation methods for polymersome with the main objective to control size, polydispersity and lamellarity, meaning the occurrence of several concentric polymersomes that are encapsulated in each other. Methods are either solvent-mediated or complete solvent-free. In the first methods, the organic solvent, the block copolymer is dissolved in, is exchanged with water, whether by mixing or adding of organic solvent droplets to water. Solvent free methods, remove the organic solvent first and rehydrate the dry block copolymer with water, whether as bulk or as a film. To fine-tune size or lamellarity, the formed polymersomes are extruded through polycarbonate

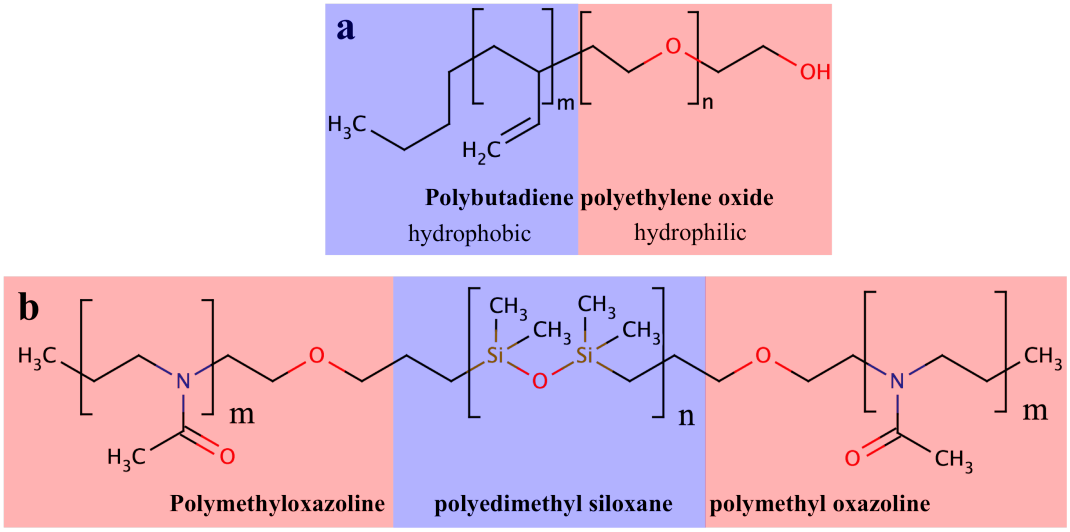

Figure 6: Chemical sketch of a) PB-PEO and b) PMOXA-PDMS-PMOXA.

track-etched (PCTE) membranes with a defined pore size, or sonicated, where for further organic solvent removal, they are dialyzed [52]. A summary and detailed discussion about formation and further processing steps is given in a paper in chapter 4.
Polymersomes and other morphologies are usually characterized by in-depth techniques like TEM or SAXS. The main fast technique for polymersome analysis is dynamic light scattering (DLS). It is however not recommended for highly polydisperse polymersomes, as far as the underlying algorithm is strongly biased towards larger particles. Recently upcoming methods like nanoparticle tracking analysis (NTA) or atomic force microscopy (AFM) could provide alternative methods to the drawbacks of the convenient one like flawed distributions or vacuum conditions. Further details about polymersome analysis will be discussed in chapter 5.

When in comes to their use in industrial membranes, polymersomes need to provide high stability and low permeability to water and other molecules. Compared to liposomes, polymersomes provide various advantages like higher polydispersity, easy chemical tuning and better flexibility [53]. They are more thermodynamically stable due to strong hydration and repulsion of hydrophilic chains and entropy of the hydrophobic coils, whereas liposomes are easily oxidized. Their bilayer is more flexible than lipid membranes because the greater length give more possibilities of conformal arrangements [53]. Bending and stretching elastic moduli are about 4 times higher, the surface viscosity of polymersomes is exceeding the one from liposomes by a factor of 1500 and a factor of 100 for the interfacial coupling constant that determines the strength of the coupling between single molecules in a vesicle. Polymersomes can remain stable in temperatures over 100°C,

whereas liposomes break down above 40°C. All values are liste in Table 1. Rupture tension, voltage and robustness are as well significantly higher [54]. The most values are based on PB-PEO polymersomes [55].

Table 1: Stability parameter of polymersomes and liposomes.

Property	Polymersomes	Liposomes	References
Thermodynamic stability	stable	not stable	[56, 57]
Bending elasticity modulus k_c [kT]	42±5	10	[55]
Elastic-area compressibility modulus K_a [mN/m]	470±15	100	[55]
Surface viscosity [mN*s/m]	$1.5*10^{-3}$	10^{-6}	[55]
Interfacial coupling constant [N*s/m^3]	$1.3*10^7 \pm 0.6*10^7$	10^5-10^6	[55]
Thermal stability	>100°C	until 40°C	[58]
Rupture tension τ_c [pN/nm]	23.3±6.6	9	[54]
Rupture voltage [V]	5.5±2.7	1.1	[54]
Robustness [V*pN/nm]	140±108	9.9	[54]
Membrane thickness [nm]	3-40	3-4	[53, 59]
Vesicle bilayer permeability P_f [μm/s]	0.7-190	10-150	[10, 50, 60]
Lateral diffusion coefficient D_L [μm^2/s]	0.002-6	4-12.5	[58, 61]
Membrane viscosity [Pa*s]	0.03-0.08	0.03-0.08	[61]
M_w [kg/mol]	1-35	0.5-0.7	[50, 62]

For their use in water separation applications, permeability of the polymer bilayer to water and other solutes are crucial aspects to be aware of. Permeability and bilayer fluidity decreases with increasing M_w, linearly related to bilayer thickness, shown in Figure 7. Thus, polymersomes of small M_w polymers (1.05 kg/mol) can even exhibit higher water permeability than liposomes (190 μm/s compared to 10-150 μm/s [50]), where they exhibit only 2.5 μm/s for polymersomes of 4 kg/mol M_w polymers [47] or 0.7 μm/s for polymersomes of 11 kg/mol M_w polymers [10]. For water, permeability decreases by a factor of 5 with each 10 further hydrophobic subunits [60]. The strongly correlated lateral diffusivity of the bilayer (mobility of the polymers within the bilayer) decreases with M_w following a power law of the lateral diffusion coefficient D_L to the M_w of the hydrophobic blocks M_h of $D_L \sim M_h^{-1.25}$ [61]. Additionally to the increasing hydrophobic barrier length for water with increasing M_h, the chains can entangle or interdigitate, which result in even higher hydrophobic density and lower water permeability. The permeability can be increased by UV illumination [63] or CO_2 addition [64] for certain polymer chemistries. Furthermore, PB-PEO polymersome membranes exhibited a low permeability for dichloroacetamide (DCA, 0.002-0.01 μm/s) and PS-PAA are almost proton-impermeable (3.5*10−9-$3.5*10^{-5}$ μm/s). Similarly small permeabilities were obtained for the permeation of PEO and polyvinyl alcohol (PVA) through poly-2-vinyl-pyridine (P2VP)-PEO polymersomes independent of pH and temperature (0.2-6 molecules/s for PEO and 0.003-0.02 molecules/s for PVA) [65]. The permeation of 5,5'-

dithiobis-2-nitrobenzoic acid (DTNB) through polybutylene oxide (PBO)-PEO bilayer is highly pH dependent, which is also linked to the decreased hydrophobicity of PBO [66]. From a theoretical point of view, a small permeating molecule has a decreasing solubility with increasing chain length of the polymer matrix for permeation, which is in best agreement with observations in experiments [60].

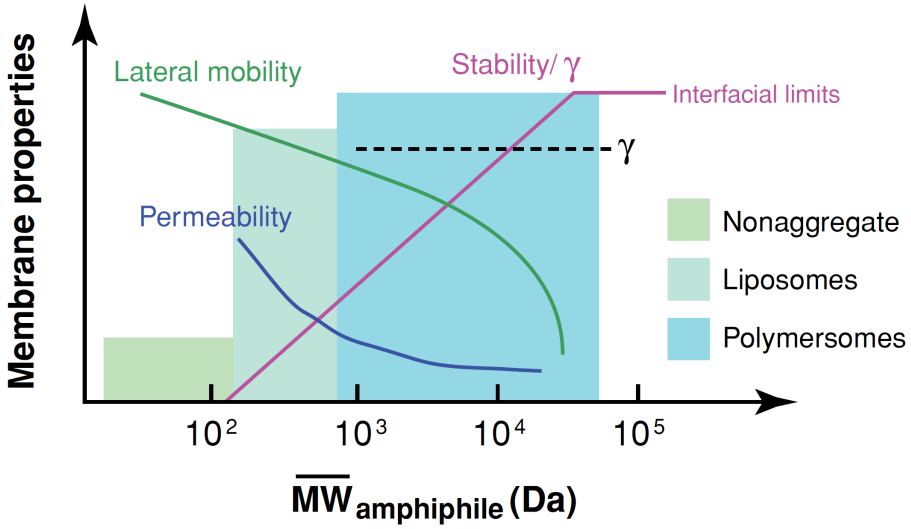

Figure 7: Diagram of M_w dependent parameters vs M_w for polymersomes and liposomes. Where stability linearly increases to a M_w independent maximum and lateral mobility linearly decrease until $5*10^4$ Da, permeability exhibits a more exponential decrease behavior. Surface tension γ appears to be independent of M_w [48].

This study focus on PB-PEO. PB-PEO was originally found as a stable alternative to commercially available polypropylene oxide-PEO (PPO-PEO) that is used as emulsifier, wetting agent or detergent [42]. However, PPO exhibits only weakly hydrophobicity at low temperatures and polymersomes only last for a few hours [67]. PB and PEE are a strongly hydrophobic alternatives that are at the same time chemically related to biocompatible polyprenyl chains, which can be found in dolichol, a ubiquitous component of animal and plant membranes [9, 68]. PEO (or Polyethylene glycol PEG) is the most well-known hydrophilic non-toxic polymer used in numerous applications [69]. PB-PEO is the polymer chemistry with the lowest M_w block copolymers ever studied and therefore probably with properties most closely to lipids [70].

PB-PEO is synthesized via anionic polymerization, where the polymer itself acts as the active species that perform the polymerization after activation by an initiator, which is advantageous to other polymerization methods in terms of preventing termination reactions, high conversion and narrow polydispersity index (PDI_M, defined as defined as weight-average molecular weight M_w divided by number-averaged molecular weight M_w/M_n)

[71]. There is a one-step-approach [72] and a two-step-approach [70] (see Figure 8). The latter polymerizes butadiene (Bd) and ethylene oxide (EO) separately, where the PB is precipitated and redissolved again [70]. The first has both polymerization in one solution, where the initiator of the Bd polymerization, which would otherwise bind to the active EO end and hinder EO polymerization, is shielded by a highly steric base [72]. Discussions in detail, especially to the one-step-approach can be found in the appendix chapter 8.1.

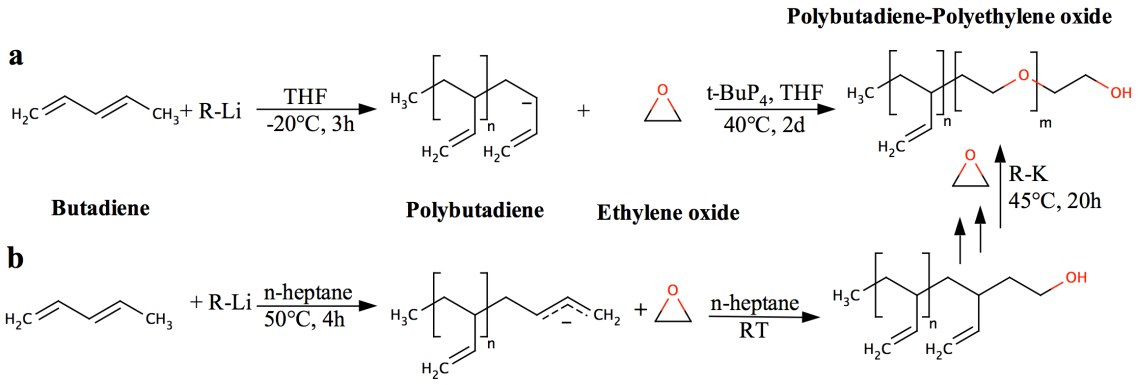

Figure 8: Chemical sketch of PB-PEO synthesis, where the one-step-approach (a) includes a steric base ($tBuP_4$) that hinders binding of the first initiator to the reactive EO-end and the two-step-approach (b) reintroduce the PB after precipitation for EO polymerization with slight modifications from the original methods [70, 72]. Details are described in the appendix chapter 8.1.

Apart from membrane protein incorporation that will be discussed in the coming chapter 1.3, PB-PEO polymersomes showed good encapsulation efficiency for proteins like bovine hemoglobin [73], drugs like Paclitaxel [74] and ionic liquids like 1-ethyl-3-methylimidazolium bis(trifluoromethylsulfonyl)imide (EMIM-TFSI) [75]. A pH gradient in their interior has been kept stable for several weeks [76]. They can furthermore be biotinylated and thus attached via biotin-avidin-bonding to avidin-coated surfaces or cells [48]. When functionalized with guanidine, PB-PEO polymerosmes are capable of being uptaken by cells via endocytosis, without toxic side-effects [77]. Sulphur-functionalized PB-PEO is furthermore capable of forming a lipid like film on a gold surface, however superior to lipid films with regard to resistance against rinsing, drying, rehydration or gaseous environment and higher flexibility in thickness tuning [78].

1.3 Interplay of AQPs & block copolymers

This subchapter has been published in [1]

Although most work on membrane protein incorporation has been performed with lipids as host matrix components (first proteoliposomes publication appeared in 1971 [79]), polymer-based incorporation has gained considerable interest since the first proteopolymersomes publication appeared in 2000 [80]. The early work focused on incorporation of membrane-spanning proteins including ATPases and bacteriorhodopsin (BR) into PMOXA-PDMS-PMOXA triblock copolymer bilayers in planar [81] or vesicular form [82–84].

It is intriguing that membrane proteins can be incorporated functionally in polymeric bilayers (e.g. based on PMOXA-PDMS-PMOXA) that can be up to 10 times thicker than their lipidic counterparts [10]. In fact proteopolymersomes have been observed with protein densities that exceed proteoliposomes by far [50].
A theoretical approach has been established for general membrane protein incorporation into amphiphilic structures. In this approach, the membrane protein incorporation efficiency depends on the its hydrophobicity and its coupling to the host membrane, which is directly related to hydrophobic mismatch. To minimize the mismatch, the host membrane has to deform to match the hydrophobic length of the transmembrane segment of the membrane protein about 3-4 nm. The alternative mode of adaption, a host membrane-induced membrane protein deformation is unlikely as far as the compressibility of membrane proteins is generally one to two orders of magnitude higher than lipids [85]. For polymers, the compression-expansion modulus is assumed to rise linearly with increasing M_w, in which chain compression is favorable over chain stretching. This linear increase is consistent with the notion that the hydrophobic mismatch energy can be balanced with a decrease in stretching energy in the polymer chains around the incorporated membrane protein [86]. Srinivas and Discher found by using coarse-grain simulations that flexible hydrophobic chains can allow protein incorporation, even when the hydrophobic mismatch between membrane protein and hydrophobic interior of the chain region is greater than 22% [87, 88] (Figure 9). Thus, membrane proteins can be incorporated more effectively if the hydrophobic chains are flexible [86]. Because flexible chains may however block the channel, no functionality of proteopolymersomes might be observed, even if the membrane protein has been incorporated functionally [87]. Moreover, high polydispersity can as well lead to a higher incorporation efficiency because the shorter chains can gather around the membrane protein and compensate for the hydrophobic mismatch.

The good incorporation observed with PMOXA-PDMS-PMOXA could therefore also be attributed to their significantly high PDI_M. In contrast, for natural lipid environment, the annual lipids around the incorporated protein can be selected in part by affinity to the protein surface and lateral diffusion [89]. The effect of hydrophobic mismatch is significant for ATPases, co-transporter proteins and ion channels [85], whereas for AQPs the effect appear smaller – likely because the protein itself is structurally more rigid [90].

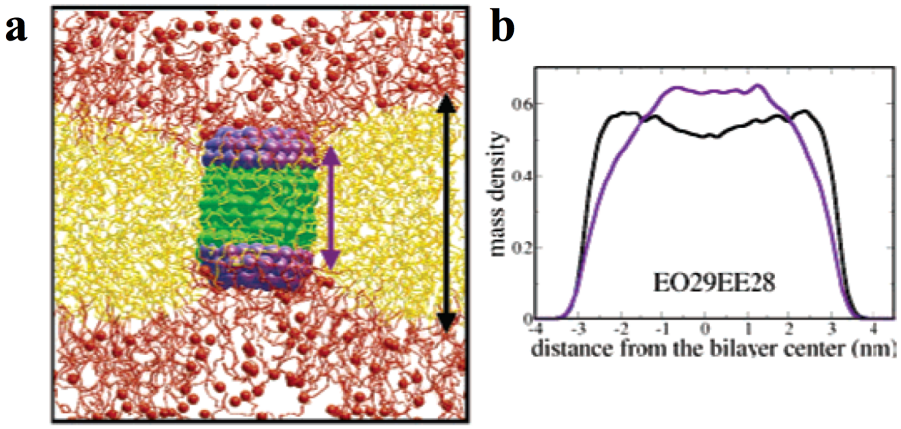

Figure 9: (a) Coarse grain simulation of OmpF as a model membrane protein into a PEE-PEO bilayer. The hydrophobic interior of OmpF is labeled green, where the hydrophilic exterior is violet. PEE chains are marked in yellow and PEO chains in red. If the bilayer is thicker than OmpF, the flexible PEE chains can be compressed around OmpF in order to minimize the hydrophobic mismatch. (b) Compressibility within the mass density to (a). The long PEO chains are blocking the OmpF channel leading to misfunctional proteobilayer even though OmpF itself may be functional [87].

The first incorporation of AQPs in polymer bilayer was done in 2004 by Stoenescu and coworkers [91]. They incorporated AQP0 that is derived from the mammalian eye-lens, in polymersomes of three different block architectures (ABA, ABC, CBA, where A stands for PMOXA, B for PDMS and C for PEO). The block configuration dictates the orientation of the incorporated AQP0. Where ABA had 50% of incorporated AQP0 with an orientation similar to that observed in liposomes, CBA had only 20% and ABC 80%, as evidenced by antibody labeling. In all cases, incorporation is achieved by adding AQP0 in detergent during the polymersome formation and removing the non-incorporated protein by size exclusion chromatography (SEC) [91].

The first demonstration of functional AQP incorporation was presented by Kumar in 2007 who incorporated bacterial AqpZ from E.coli in PMOXA-PDMS-PMOXA polymersomes [10] and proved their functionality within SFLS. SFLS is a common permeability characterization method, in which the polymersome shrinkage due to a response to osmolarity change is monitored over time by light scattering. Incorporation of AqpZ led to 800 times

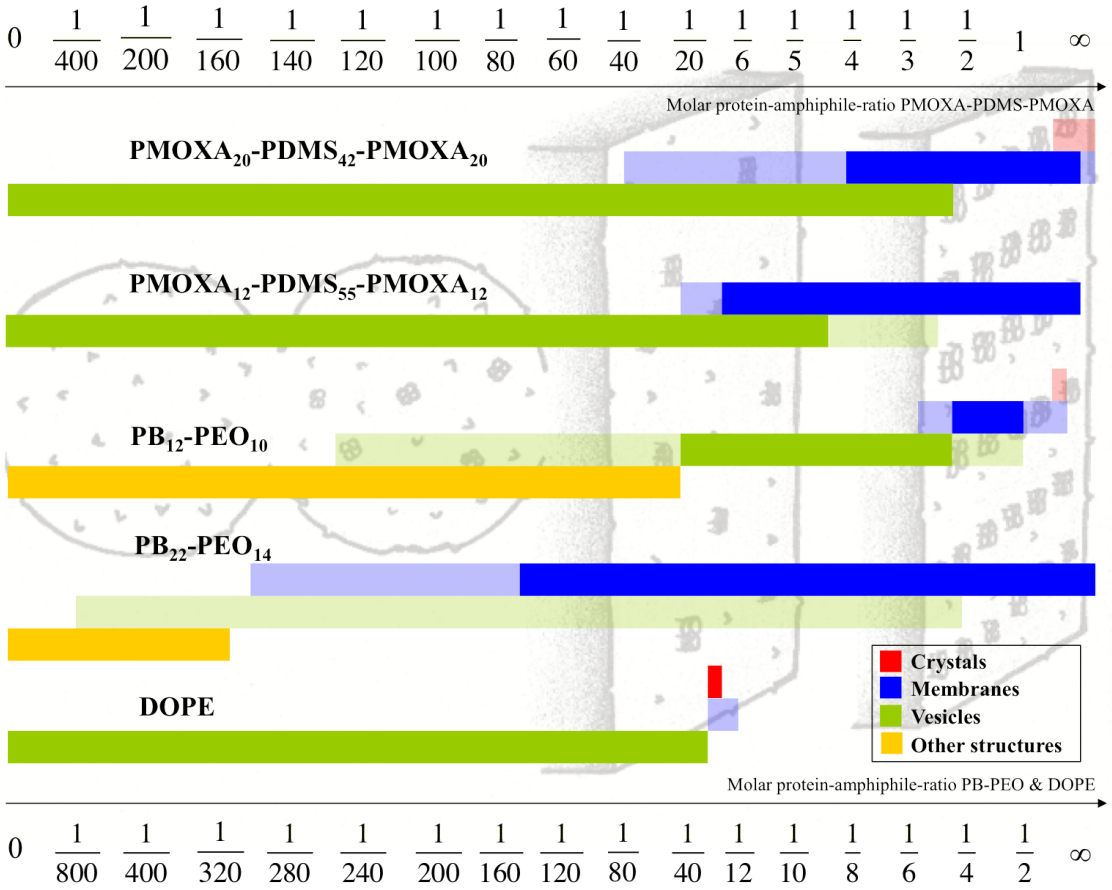

Figure 10: Schematic drawing of aggregate morphologies as a function of mPAR. PB_{12}-PEO_{10} undergoes four transitions. Surprisingly, the vesicle shape remained at significantly higher densities at block copolymers, compared to a standard lipid like 1,2-dioleoyl-sn-glycero-3-phosphoethanolamine (DOPE). The mPAR of the one-molecule-bilayer-forming ABA triblock copolymers was divided by 2 enabling direct comparison with the PB-PEO diblock copolymers and DOPE, both forming bilayers. The morphologies in full color are the main morphologies, pale colors denote coexisting morphologies. Adapted from [96]. Background image with friendly permission from Viktoria Habel.

higher osmotic response of proteopolymersomes compared to empty polymersomes and showed that the activation energy, meaning the barrier for water to pass through the AqpZ, was comparable to that of AQP reconstituted in proteoliposomes and frog oocytes. The molar protein-to-amphiphile-ratio (mPAR) for optimal AqpZ performance in the triblock copolymer system was found to be 1:50 which would correspond to 1:100 in a (diblock- or lipid) bilayer system [10]. The high density reconstitution of AQP is further exempilfied by the formation of 2D AQP crystals to achieve structural (crystallographic) information about AQP - analogous to what has been done with lipid based 2D AQP crystals [92]. For this purpose, a monolayer of nickel-functionalized PB-PEO is accumulated at the water-interface, where in the aqueous solution, mixed micelles of detergent, histidine-tagged

AqpZ and PDMS-PMOXA-PDMS were present [93]. The nickel affinity to the histidine binds the AqpZ to the PB-PEO layer [94], facilitating a high packing of AqpZ in this layer. After removing the detergent via biobeads and the PB-PEO via imidazole, densely packed AqpZ PMOXA-PDMS-PMOXA crystals were left, unfortunately not of sufficient quality to obtain any structural information [26, 95].

2D crystals can in fact used to investigate the influence of AQP on polymer self-assembly in general. AQP0 is known to easily form 2D crystals due to its natural occurrence in stacks in the eye lens [97]. The findings here were that AQP0 dictates the self-assembling behavior of both polymers in a reciprocal way to the hydrophilic volume ratio f. With increasing mPAR, the interfacial curvature decreases and polymersomes turn into membrane sheets and partly crystals (see Figure 10 and 11). In the case of PB-PEO, formation of polymersomes only occurred by adding AQP0, whereas without AQP0 only cylindrical structures are observed. The highest measured packing densities of functional AQPs into vesicular structures are observed at PB-PEO polymersomes with an mPAR of 1:15, which is significantly higher than what has been achieved in proteoliposomes or frog oocytes. Although not all AQP0 protein was incorporated, the 7-fold increase in osmotic response is consistent with a high-packing density given the relatively low permeability of AQP0 [98]. In this case incorporation was done via mixing detergent-solubilized polymers with detergent-solubilized AQP0 and subsequently dialyzing out the detergent [50, 99].

With respect to fabrication of biomimetic membranes for technological purposes the first protein incorporation approaches from 2009-2011 were mainly lipid based [100, 101], but also planar polymeric membranes have been demonstrated with functional incorporation of gramicidin A [102]. These efforts were pioneered by the Danish company Aquaporin A/S. Their later achievements in fabricating biomimetic membrane will be discussed in the next subchapter, as well as the work coming out of the groups at the Singapore Membrane Technology Center (SMTC) at Nanyang Technological University (NTU) and the National University of Singapore (NUS).

Table 2 summarizes all experimental membrane protein (and peptide) incorporations in block copolymer membranes, including polymer chemistry and stochiometry, PDI_M, M_n, f, the incorporated membrane protein, the transport cargo (e.g. water for AQP), if there was functional incorporation, mPAR, the shape of the polymer self-assembled structure, how polymer and membrane protein were mixed and how the function incorporation was measured. M_n (which can be quantified using NMR) is related to M_w as $PDI_M = M_w/M_n$. The table excludes those incorporation studies which do not involve block copolymer-protein interactions, such as cell-free expression systems [103–105], encapsulation in hydrophobic interior [84], nanopores [106, 107], non-amphiphilic polymers [108] and hydrogel approaches [109, 110]. With this limitation, the table shows that most results

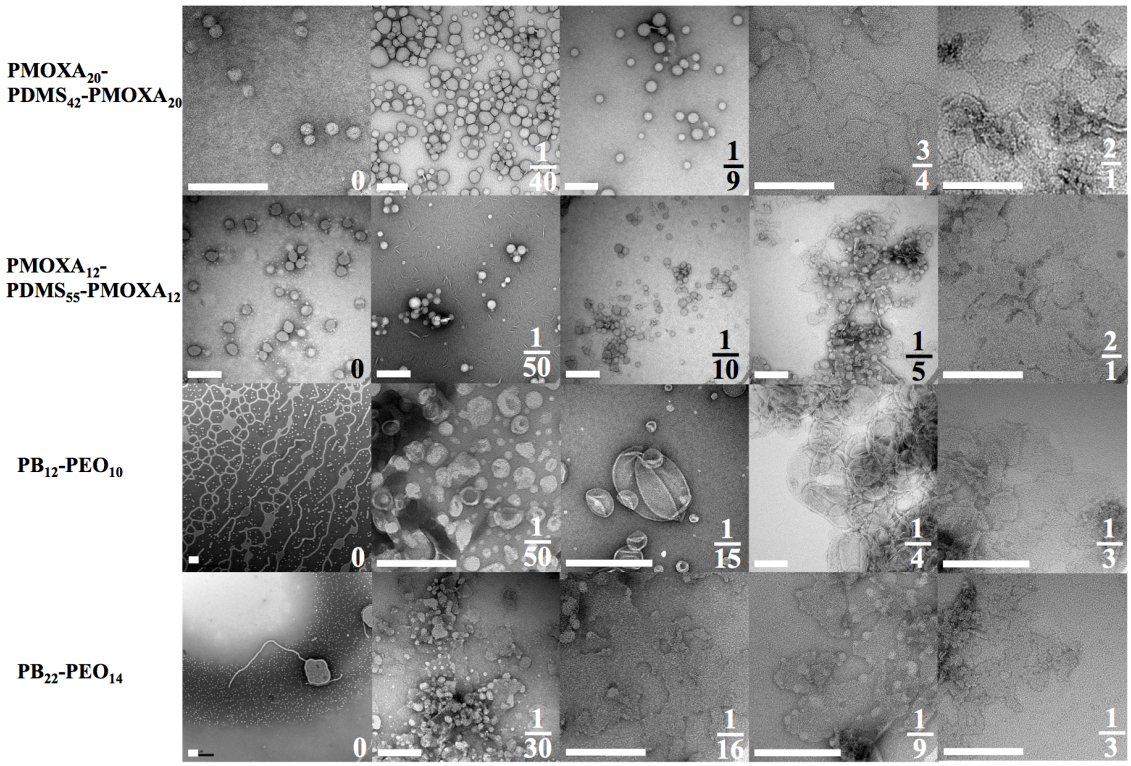

Figure 11: TEM images of aggregate morphologies as a function mPAR. Where the PMOXA-PDMS-PMOXA copolymers self-assemble to vesicles, PB-PEO forms network- and sperm-like structures and only after incorporation of AQP0 vesicular structures are observed. Scale bar is 200 nm. Adapted from [99].

were published by Wolfgang Meier and coworkers using on PMOXA-PDMS-PMOXA triblock copolymers.

Figure 12 presents an overview of membrane protein incorporation into polymers with a known M_n and f. Each black dot represents one polymer. The connected box shows the polymer chemistry, the incorporated membrane protein family, the self-assembled morphology (vesicular or planar), the incorporation method, the PDI_M of the polymer (not of the polymersomes), the mPAR and if the incorporation was functional or not, respectively not measured. If there are several sketches in the box, several different experiments has been performed on the polymer. If there are two crossing circles respectively two close lines, two different mPARs were investigated, where all other parameters remained the same. If there are three crossing circles, three or more mPARs were investigated. In the case of varying another parameter than mPAR (incorporation method, polymer chemistry, incorporated membrane protein etc.) a new sketch is drawn. Generally polymers capable of functional incorporation have an f between 0.2 and 0.35 and M_n was in between 2 and 12 kg/mol. Compared with PB-PEO, PMOXA-PDMS-PMOXA has a far broader PDI_M [9], its bilayer is highly water impermeable [10] and they do not collapse in dried

Table 2: Overview of studies of membrane protein incorporation into amphiphilic block copolymers. Most studies are done with the porin OmpF, followed by AqpZ. For explanations please refer to the list of abbreviations.

Polymer	M_n	PDI_M	f	Membrane protein	Transport cargo	FI?	mPAR	S	Incorporation method	Main FI measurement	References
$PMOXA_{13}$-$PDMS_{23}$-$PMOXA_{13}$	3.9	NA	0.53	NADH reductase	e^-	X	1:3300	V	MAq, biobeads & SEC	Cargo → Reduction of MP → EPR signal	[112]
$PMOXA_{13}$-$PDMS_{33}$-$PMOXA_{13}$	4.7	NA	0.44	Alamethicin		X	1:590	P	MAq	Current change	[113]
$PMOXA_{13}$-$PDMS_{33}$-$PMOXA_{13}$	4.7	NA	0.44	Hemolysin		X	1:110 000 000	P	MAq	Current change	[113]
$PMOXA_{13}$-$PDMS_{33}$-$PMOXA_{13}$	4.7	NA	0.44	OmpG		X	1:33 000 000	P	MAq	Current change	[113]
$PMOXA_{20}$-$PDMS_{41}$-$PMOXA_{20}$	6.4	1.61	0.49	NtAQP1	CO_2	X	1:360	P	MOr	Cargo → Reaction inside vesicle → pH change	[16]
$PMOXA_{20}$-$PDMS_{41}$-$PMOXA_{20}$	6.4	1.61	0.49	NtPIP2:1	CO_2	X	1:360	P	MOr	Cargo → Reaction inside vesicle → pH change	[16]
$PMOXA_{20}$-$PDMS_{41}$-$PMOXA_{20}$	6.5	< 1.2	0.51	AQP0	H_2O	ND	10:1-1:1	Cr	MAq & dialysis		[50]
$PMOXA_{20}$-$PDMS_{41}$-$PMOXA_{20}$	6.5	< 1.2	0.51	AQP0	H_2O	ND	10:1-1:50	P	MAq & dialysis		[50]
$PMOXA_{20}$-$PDMS_{41}$-$PMOXA_{20}$	6.5	< 1.2	0.51	AQP0	H_2O	-	1:2.5 - 0	V	MAq & dialysis	Vesicle size change	[50]
$PMOXA_{12}$-$PDMS_{54}$-$PMOXA_{12}$/ $PMOXA_{19}$-$PDMS_{74}$-$PMOXA_{19}$	6.0 8.7	1.01 1.46	0.2 0.23	AqpZ	H_2O	X	1:100-1:1600	V	MAq & biobeads	Vesicle size change	[114, 115]
$PMOXA_{12}$-$PDMS_{54}$-$PMOXA_{12}$	6.0	1.01	0.30	AqpZ	H_2O	X	1:50-1:400	V	MAq & biobeads	Vesicle size change	[116, 117]
$PMOXA_{12}$-$PDMS_{54}$-$PMOXA_{12}$	6.0	1.01	0.30	Hemolysin		-	1:83 000 000	P	MAq	Current change	[113]
$PMOXA_{20}$-$PDMS_{54}$-$PMOXA_{20}$	7.4	NA	0.42	TsX	Nucleosides	X	1:450	V	MOr, SI & SEC	Cargo → Encapsulated enzyme activity → Color change	[118]
$PMOXA_8$-$PDMS_{55}$-$PMOXA_8$	5.4	NA	0.22	AqpZ	H_2O	X	1:3500	V	PFR, biobeads & SEC	Vesicle size change	[119]
$PMOXA_{12}$-$PDMS_{55}$-$PMOXA_{12}$	6.1	1.64	0.30	OmpF	ELF97	X	1:1200	V	MAq & SEC	Cargo → Precipitation inside vesicle → Color change	[120]
$PMOXA_{12}$-$PDMS_{55}$-$PMOXA_{12}$	6.1	1.64	0.30	OmpF	Acridine orange	X	1:9 100 000	V	PPFR & SEC	Cargo release → Color change	[121]
$PMOXA_{12}$-$PDMS_{55}$-$PMOXA_{12}$	6.1	1.64	0.30	OmpF	Paraquat. Pyocyanin	X	1:640	V	MAq & dialysis	No cargo → No detoxication of encapsulated enzyme → cell death	[122, 123]
$PMOXA_{12}$-$PDMS_{55}$-$PMOXA_{12}$	6.1	1.64	0.33	AQP0	H_2O	ND	10:1-1:25	P	MAq & dialysis		[50]
$PMOXA_{12}$-$PDMS_{55}$-$PMOXA_{12}$	6.1	1.64	0.33	AQP0	H_2O	-	1:3 - 0	V	MAq & dialysis	Vesicle size change	[50]
$PMOXA_{12}$-$PDMS_{55}$-$PMOXA_{12}$	6.1	1.64	0.33	AqpZ	H_2O	ND	1:4	Cr. V	MAq & biobeads		[26]
$PMOXA_7$-$PDMS_{60}$-$PMOXA_7$	5.6	NA	0.19	Gramicidin A	Monovalent cations	X	1:81 000	P	MOr	Current change	[102]
$PMOXA_8$-$PDMS_{60}$-$PMOXA_8$	5.8	NA	0.21	AqpZ	H_2O	X	1:3800	V	PFR, biobeads & SEC	Vesicle size change	[119]
$PMOXA_{13}$-$PDMS_{62}$-$PMOXA_{13}$	6.8	1.47	0.29	NADH reductase	e^-	X	1:1900	V	MAq, biobeads & SEC	Cargo → Reduction of MP → EPR signal	[112]
$PMOXA_{15}$-$PDMS_{62}$-$PMOXA_{15}$	7.1	1.50	0.32	NADH reductase	e^-	X	1:1800	V	MAq, biobeads & SEC	Cargo → Reduction of MP → EPR signal	[112]
$PMOXA_{12}$-$PDMS_{65}$-$PMOXA_{12}$	6.9	1.67	0.27	MloK1	Potassium	X	1:390	P	MAq & biobeads	Current change	[124]

Continued on next page

Table 2 – *Continued from previous page*

Polymer	M_n	PDI_M	f	Membrane protein	Transport cargo	FI?	mPAR	S	Incorporation method	Main FI measurement	References
$PMOXA_{15}$-$PDMS_{68}$-$PMOXA_{15}$	7.6	NA	0.30	LamB	Maltohexaose	X	NA	P	MAq	Current change at varying cargo concentrations	[125]
$PMOXA_{15}$-$PDMS_{68}$-$PMOXA_{15}$	7.6	NA	0.30	OmpF	Actylthiocholine	X	1:10000	V	PFR	Cargo → Encapsulated enzyme activity → Color change	[125]
$PMOXA_{15}$-$PDMS_{68}$-$PMOXA_{15}$	7.6	1.20	0.30	AqpZ	H_2O	X	1:10-1:1000	V	PFR & biobeads	Vesicle size change	[126]
$PMOXA_{15}$-$PDMS_{68}$-$PMOXA_{15}$	7.6	1.20	0.30	Hemolysin		-	1:66 000 000	P	MAq	Current change	[113]
$PMOXA_{21}$-$PDMS_{69}$-$PMOXA_{21}$	8.7	2.00	0.37	NADH reductase	e^-	X	1:1500	V	MAq, biobeads & SEC	Cargo → Reduction of MP → EPR signal	[112]
$PMOXA_{16}$-$PDMS_{72}$-$PMOXA_{16}$	8.0	1.17	0.30	OmpF	Enone	X	1:220	V	PPFR & dialysis	Cargo → Encapsulated enzyme activity → Color change	[127]
PMOXA-PDMS-PMOXA	8.8	NA	NA	OmpF	ELF97	X	1:50	V	MAq & SEC	Cargo → Precipitation inside vesicle → Color change	[128]
$PMOXA_{32}$-$PDMS_{72}$-$PMOXA_{32}$	10.7	1.83	0.47	OmpF	7-ADCA. PGME	X	NA	V	PFR & dialysis	Cargo → Encapsulated enzyme activity → Bacterial death	[129]
$PMOXA_{11}$-$PDMS_{73}$-$PMOXA_{11}$	7.2	1.70	0.22	LamB	DNA	X	1:390	V	MOr, SI & SEC	Fluorescence-labelled cargo	[130]
$PMOXA_{11}$-$PDMS_{73}$-$PMOXA_{11}$	7.2	1.70	0.22	OmpF	Nucleosides	X	1:10, 1:100	V	PPFR & SEC	Cargo → Encapsulated enzyme activity → Color change	[131]
$PMOXA_{11}$-$PDMS_{73}$-$PMOXA_{11}$	7.2	1.70	0.22	TsX	Nucleosides	X	1:10, 1:100	V	PPFR & SEC	Cargo → Encapsulated enzyme activity → Color change	[131]
$PMOXA_{11}$-$PDMS_{73}$-$PMOXA_{11}$/ Lipids	7.2	1.70	0.22	LamB	DNA	X	NA	P	MAq		[130]
$PMOXA_{21}$-$PDMS_{73}$-$PMOXA_{21}$	9.0	1.70	0.36	Alamethicin	Calcium	X	1:24	V	MAq	Cargo precipitation inside vesicle	[132, 133]
$PMOXA_{21}$-$PDMS_{73}$-$PMOXA_{21}$	9.0	1.70	0.36	FhuA	Sulphorhodamine B	X	1:6 000 000	V	MOr, SI & SEC	Cargo → Quenching inside vesicle → Color change	[134–136]
$PMOXA_{21}$-$PDMS_{73}$-$PMOXA_{21}$	9.0	1.70	0.36	FhuA	TMB	X	1:4500. 1:3 600 000	V	MAq & biobeads / MOr, SI & SEC	Cargo → Encapsulated enzyme activity → Color change	[134, 135, 137]
$PMOXA_{21}$-$PDMS_{73}$-$PMOXA_{21}$	9.0	1.70	0.36	FhuA		ND	3000:1	P	MAq		[135]
$PMOXA_{21}$-$PDMS_{73}$-$PMOXA_{21}$	9.0	1.70	0.36	FhuA	NAD	-	NA	V	MAq	Cargo → Encapsulated enzyme activity → Absorbance change of cargo	[136]
$PMOXA_{21}$-$PDMS_{73}$-$PMOXA_{21}$	9.0	1.70	0.36	FhuA	DNA	-	NA	V	MOr, SI & SEC	Fluorescence-labelled cargo	[136]
$PMOXA_{21}$-$PDMS_{73}$-$PMOXA_{21}$	9.0	1.70	0.36	LamB	Sugar	X	NA	P	MAq	Current change at varying cargo concentration	[138]
$PMOXA_{21}$-$PDMS_{73}$-$PMOXA_{21}$	9.0	1.70	0.36	OmpF	e^-	X	NA	P	MAq	Current change	[138]

Continued on next page

Table 2 – *Continued from previous page*

Polymer	M_n	PDI_M	f	Membrane protein	Transport cargo	FI?	mPAR	S	Incorporation method	Main FI measurement	References
$PMOXA_{21}$-$PDMS_{73}$-$PMOXA_{21}$	9.0	1.70	0.36	OmpF	Ampicillin	X	1:1000	V	MOr & SEC	Cargo → Hydrolysis inside vesicle → Color change	[80, 139]
$PMOXA_{20}$-$PDMS_{75}$-$PMOXA_{20}$	9.0	1.46	0.34	AqpZ	H_2O	X	1:25, 1:50, 1:200	V	PFR & biobeads	Vesicle size change	[140]
$PMOXA_{11}$-$PDMS_{76}$-$PMOXA_{11}$	7.8	1.48	0.25	BR	H^+	X	NA	V/Mc	MOr & SI	pH change	[141, 142]
$PMOXA_{11}$-$PDMS_{76}$-$PMOXA_{11}$	7.8	1.48	0.25	BR & ATPase	H^+	X	1:180	V	MOr & dialysis	pH change & bioluminescence assay	[83]
$PMOXA_{11}$-$PDMS_{76}$-$PMOXA_{11}$	7.8	1.48	0.25	BR & ATPase	H^+	X	1:20	V	PBR & dialysis	pH change	[143–145]
$PMOXA_6$-$PDMS_{90}$-$PMOXA_6$	9.5	NA	0.12	OmpF	L-ascorbic acid, CO, $Na_2S_2O_4$, $ONOO^-$	X	1:1300	V	PFR, dialysis & SEC	Cargo → Absorbance change of encapsulated protein	[146]
$PMOXA_{21}$-$PDMS_{97}$-$PMOXA_{21}$	9.0	1.70	0.30	Hemaglutinin		X	1:3800	V	MAq & biobeads	MP → Fusion with fluorescence-labelled liposomes	[137]
$PMOXA_9$-$PDMS_{106}$-$PMOXA_9$	9.4	1.38	0.14	NADH reductase	e^-	X	1:1400	V	MAq, biobeads & SEC	Cargo → Reduction of MP → EPR signal	[112]
$PMOXA_{13}$-$PDMS_{110}$-$PMOXA_{13}$	10.4	1.44	0.19	NADH reductase	e^-	X	1:1200	V	MAq, biobeads & SEC	Cargo → Reduction of MP → EPR signal	[112]
$PMOXA_{14}$-$PDMS_{110}$-$PMOXA_{14}$	10.5	1.36	0.20	NADH reductase	e^-	X	1:1200	V	MAq, biobeads & SEC	Cargo → Reduction of MP → EPR signal	[112]
$PMOXA_{15}$-$PDMS_{110}$-$PMOXA_{15}$	10.7	1.62	0.21	AqpZ	H_2O	X	1:25-1:500	V	PFR & SEC	Vesicle size change	[10, 26]
$PMOXA_{15}$-$PDMS_{110}$-$PMOXA_{15}$/ Lipids	10.7	1.62	0.21	OmpF		ND	NA	P	MAq		[147]
PMOXA-PDMS-PMOXA	20.0	NA	NA	FhuA	Calcein	X	1:2 700 000	V	MOr, SI & SEC	Cargo release → Color change	[148]
$PMOXA_{65}$-$PDMS_{165}$-$PMOXA_{65}$	23.3	1.63	0.44	NADH reductase	e^-	X	1:550	V	MAq, biobeads & SEC	Cargo → Reduction of MP → EPR signal	[112]
PMOXA-PDMS-PMOXA	NA	NA	NA	BR	H^+	X	NA	P	MAq	pH change	[149, 150]
PMOXA-PDMS-PMOXA	NA	NA	NA	BR & CcO	H^+ & e^-	X	NA	V	MOr, SI & SEC	Current & pH change	[150, 151]
PMOXA-PDMS-PMOXA	NA	NA	NA	CcO	e^-	X	NA	P	MOr, SI & SEC	Current change	[149, 150]
PMOXA-PDMS-PMOXA	NA	NA	NA	OmpF	H^+	X	NA	P	MAq	Current change	[152]
$PMOXA_{110}$-$PDMS_{40}$-PEO_{25}	13.4	NA	0.75	AQP0	H_2O	ND	1:200	V	MOr, SI & SEC		[91]
PEO_{45}-$PDMS_{40}$-$PMOXA_{67}$	10.6	NA	0.68	AQP0	H_2O	ND	1:200	V	MOr, SI & SEC		[91]
MPEG-PVL	6.5	¡ 1.2	0.00	Polymyxin B	Calcein	X	1:2	V	MAq	Cargo release → Color change	[136]
P2VP-PEO	NA	NA	NA	FhuA	NAD	-	NA	V	MOr, SI & SEC	Cargo → Enzyme reaction inside vesicle → Absorbance change of cargo	[136]
PB_{12}-PEO_{10}	1.1	1.09	0.32	AQP0	H_2O	X	1:5-1:250	V	MAq & dialysis	Vesicle size change	[50]
PB_{12}-PEO_{10}	1.1	1.09	0.32	AQP0	H_2O	ND	1:1.3	Cr	MAq & dialysis		[50]
PB_{12}-PEO_{10}	1.1	1.09	0.32	AQP0	H_2O	ND	1:1-1:10	P	MAq & dialysis		[50]
PB_{12}-PEO_{10}	1.1	1.09	0.32	AqpZ	H_2O	X	1:50-1:1000	V	MAq & dialysis	Vesicle size change	[153]
PB_{12}-PEO_{10}	1.1	1.09	0.32	BR	H^+	X	1:500	V	MAq & biobeads	pH change	[154]
PB_{12}-PEO_{10}	1.1	1.09	0.32	SoPIP2;1	H_2O	-	1:200	V	MAq & biobeads	Vesicle size change	[153]

Continued on next page

Table 2 – *Continued from previous page*

Polymer	M_n	PDI_M	f	Membrane protein	Transport cargo	FI?	mPAR	S	Incorporation method	Main FI measurement	References
PB_{12}-PEO_{10}	1.1	NA	0.34	Hemolysin	Calcein	X	1:33 000	V	MAq & dialysis	Cargo release → Color change	[155]
PB_{22}-PEO_{14}	1.8	1.17	0.28	AQP0	H_2O	ND	2:1-1:300	P	MAq & dialysis		[50]
PB_{22}-PEO_{23}	2.2	1.09	0.39	AqpZ	H_2O	X	1:15-1:200	V	MAq & dialysis	Vesicle size change	[153]
PB_{22}-PEO_{23}	2.2	1.09	0.39	SoPIP2;1	H_2O	-	1:15, 1:200	V	MAq & dialysis	Vesicle size change	[153]
PB_{29}-PEO_{16}	2.3	1.00	0.25	AQP10	H_2O	-	1:990	V	PFR & SE	Vesicle size change	-
PB_{35}-PEO_{14}	2.5	1.09	0.19	AqpZ	H_2O	-	1:15	V	MAq & dialysis	Vesicle size change	[153]
PB_{35}-PEO_{14}	2.5	1.09	0.19	SoPIP2;1	H_2O	-	1:15	V	MAq & dialysis	Vesicle size change	[153]
PB_{43}-PEO_{32}	3.7	1.03	0.31	AQP10	H_2O	X	1:600	V	PFR & SE	Vesicle size change	[156]
PB_{46}-PEO_{30}	3.8	1.04	0.28	AqpZ	H_2O	-	1:50,1:100,1:200	V	MAq & dialysis	Vesicle size change	[153]
PB_{46}-PEO_{32}	3.9	1.00	0.30	AQP10	H_2O	-	1:580	V	PFR & SE	Vesicle size change	-
PB_{52}-PEO_{29}	4.1	< 1.1	0.25	Hemolysin	e^-	X	NA	P	MAq	Current change	[157]
PB_{52}-PEO_{29}	4.1	< 1.1	0.25	Polymyxin B		X	NA	P	MAq	Current change	[158]
PB_{52}-PEO_{29}-LA	4.1	< 1.1	0.25	Hemolysin	e^-	X	NA	P	MAq	Current change	[157]
PB_{52}-PEO_{29}-LA	4.1	< 1.1	0.25	Polymyxin B		X	NA	P	MAq	Current change	[158]
PB_{92}-PEO_{78}	8.4	1.08	0.34	AQP10	H_2O	-	1:270	V	PFR & SE	Vesicle size change	-
PB_{125}-PEO_{80}	8.9	< 1.1	0.28	Alamethicin	Calcein	-	1:2-1:8	V	MAq	Cargo release → Color change	[159]
$PHEMA_{25}$-$PBMA_{25}$-$PHEMA_{25}$	14.3	1.30	0.83	AqpZ		-	NA	P	MAq & biobeads	Current change	[160]
$PHEMA_{25}$-$PBMA_{25}$-$PHEMA_{25}$	14.3	1.30	0.83	Hemolysin		X	NA	P	MAq	Current change	[160]
$PHEMA_{25}$-$PBMA_{25}$-$PHEMA_{25}$	14.3	1.30	0.83	OmpF		-	1:70	P	MAq & biobeads	Current change	[160]
PEE_{37}-PEO_{40}	3.9	< 1.1	0.39	Alamethicin	Calcein	X	1:2-1:8	V	MAq	Cargo release → Color change	[159]
PPO_{34}-PGM_{14}	6.5	1.30	0.66	Strepatividin-BSA		ND	1:5, 1:15, 1:50	V	PPFR		[161]
PI_{93}-PEO_{87}	10.2	1.00	0.31	FhuA	TMB	X	1:6700. 1:5 300 000	V	MOr, SI & SEC	Cargo → Encapsulated enzyme activity → Color change	[136]
PEO_{136}-PIB_{18}-PEO_{136}	8.0	1.86	0.90	Cecropin A	Calcein	X	1:30	V	MAq & SEC	Cargo release → Color change	[162]
$P4MVP_{21}$-PS_{26}-$P4MVP_{21}$	13.1	NA	0.80	PR		X	1:10	V	MAq & precipitation	Absorbance change in membrane protein	[163]
$P4MVP_{21}$-PS_{38}-$P4MVP_{21}$	14.3	1.19	0.74	PR		X	1:10	V	MAq & precipitation	Absorbance change in membrane protein	[163]
$P4MVP_{29}$-PS_{42}-$P4MVP_{29}$	18.7	NA	0.78	PR		X	1:10	V	MAq & precipitation	Absorbance change in membrane protein	[163]
$P4MVP_{22}$-PB_{28}-$P4MVP_{22}$	15.0	NA	0.92	PR		ND	1:10	V	MAq & precipitation		[164]
$P4MVP_{22}$-PB_{28}-$P4MVP_{22}$	15.0	NA	0.92	RC	e^-	X	1:25	V	MAq & precipitation	Cargo → Reduction of MP → EPR signal	[165]
$P4VP_{22}$-PB_{28}-$P4VP_{22}$	7.1	NA	0.82	PR		ND	1:10	V	MAq & precipitation		[164]
$P4MVP_{29}$-PB_{56}-$P4MVP_{29}$	17.4	1.08	0.81	RC	e^-	X	1:25	V	MAq & precipitation	Cargo → Reduction of MP → EPR signal	[165]
$P4MVP_{18}$-PB_{93}-$P4MVP_{18}$	13.9	1.06	0.62	PR		ND	1:10	V	MAq & precipitation		[164]

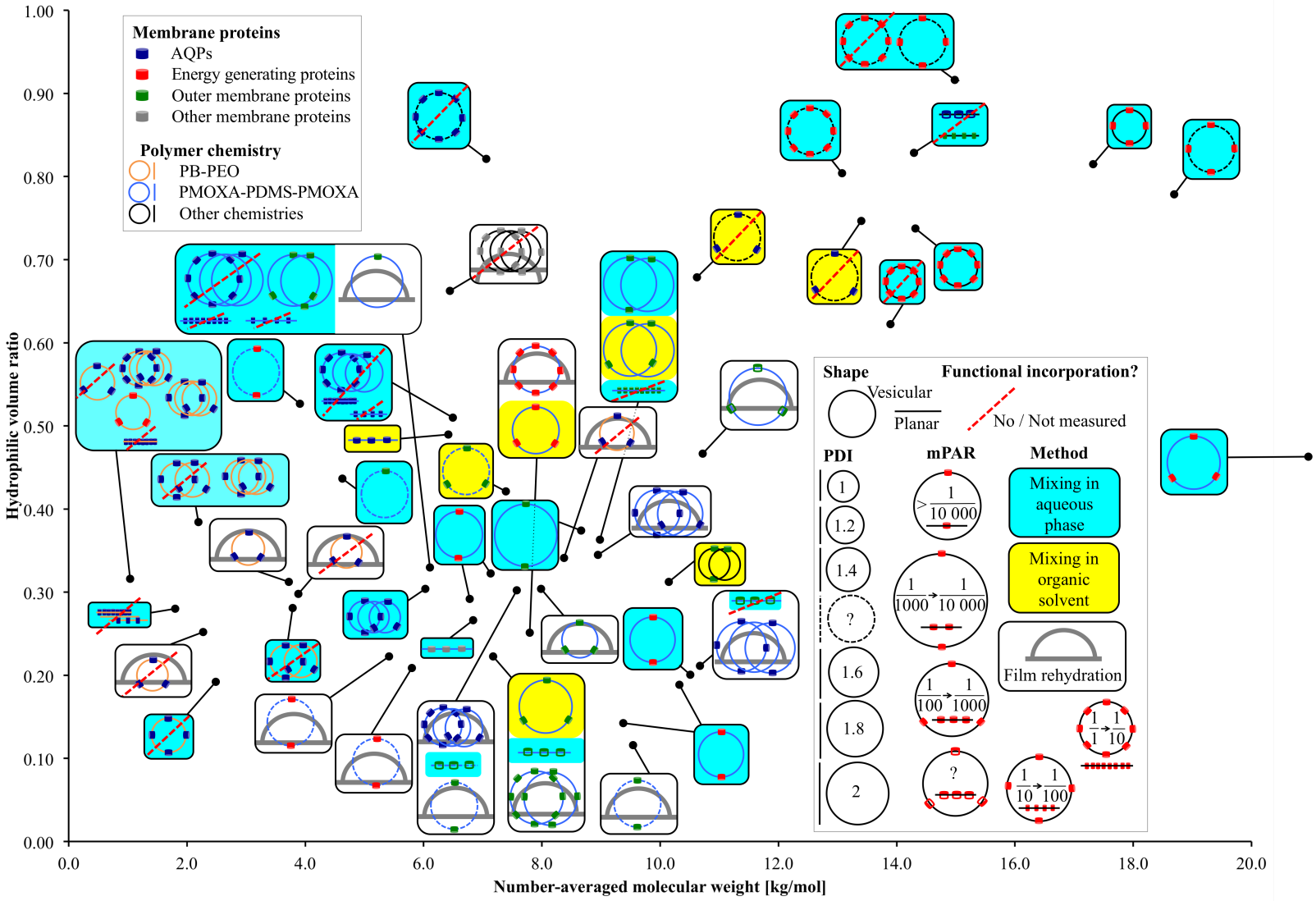

Figure 12: Overview of relevant parameters for membrane protein incorporation into amphiphilic block copolymers.

form [51]. PB-PEO is more lipid-like as far it collapses easier and has higher water permeability [50]. The polymers that did not achieve functional AQP incorporation were mainly PB-PEO polymers with small M_n and PDI_M. Energy generating (BR, cytochrome c oxidase, CcO; NADH reductase, ATPase, reaction centre, RC; proteorhodopsin, PR) and outer membrane proteins (OmpF, OmpG, Ferric hydroxamate uptake protein, FhuA; TsX) were incorporated mainly into PMOXA-PDMS-PMOXA polymers, but outer membrane proteins also has been incorporated in more exotic chemistries in an f range where one would not expect vesicular structures. The great majority of functional incorporation trials were performed with vesicular structures, where mixing was done in aqueous phase. Generally at smaller PDI_M values no functional membrane proteins can be incorporated, which is in agreement with the findings from Pata et al. [86]. A wide range of mPARs have been used with no optimal ratios detected. However, mPARs are based on the initial or nominal concentrations of membrane proteins and polymers and the final mPAR after incorporation may be different [111].

1.4 Polymer membranes

Polymers membranes are the most common used material in membrane technology, due to superior performance and higher economic efficiency compared to liquid, ceramic or metal membranes [166]. The first polymeric membrane was developed in 1865 from Fick and coworkers made of nitrocellulose [167]. Until the 1960's all polymeric membrane related achievements were more research-based until the development of the first asymmetric membrane by Loeb and Sourirajan that had a 10 times higher flux than any other membranes of that time [168]. Since then, membrane technology shifted to industrial scale and product development. The next milestone was achieved with the invention of the AL, a thin top-layer made of two aromatic linkers that forming an PA layer via interfacial polymerization. These PA (or thin film composite, TFC) membranes had another significant increase in salt rejection at similar flux [168].

To provide efficient liquid or gas separation, thousands of square meters membrane area are required. Thus, there are several ways for packing them efficiently in so-called modules. In the earliest design, plate & frame, membrane sheets are layered between spacers, where the whole stack is framed of two end plates. The feed solution, the membranes are "fed" with for separation, is forced across the membrane surface, where it enters a permeate channel in the module center after it passes through the membrane, shown in Figure 13a. Another possibility is to wound the membrane, enveloped between spacers, in a spiral around a central perforated tube for the permeate, placed inside a tubular pressure vessel (Spiral wound module, Figure 13b). The feed is flowing in parallel to the permeate

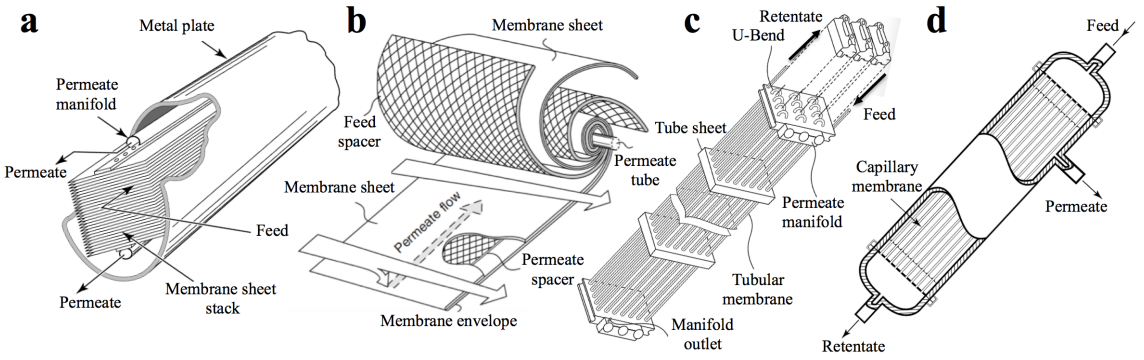

Figure 13: Schematic drawings of four membrane module types: a) Plate & frame, b) Spiral wound, c) tubular and d) hollow fibre (HF). Plate & frame module consists of stacked membrane-spacer-sheets, the feed solution has to pass through, where in the spiral wound module it needs to pass through a spiral wounded membrane-spacer-envelope. The tubular module presses the feed through manifolded tubular membranes from the tubule interior to the outside. This is also possible in the capillary membrane / HF module with much smaller diameter, but the flow direction can be as well converted [168].

tube, where it is pressed through several membrane envelopes until reaching the permeate tube. Polymer membranes can also be produced in tubular forms. In the tubular module, several tubes of diameter between half and several cm in diameter are packed inside a larger tube, often manifolded in series. The feed is introduced to the interior of the tubes and permeating outside the tube, reversely to the spiral wound (Figure 13c). Tubular membranes with diameter around 50 μm are called capillary or hollow fibre (HF) membranes. They are packed in higher numbers than tubular membranes, where the permeate direction can be as well inside the fibre to the outside but also vice versa, shown in Figure 13d. There are large membrane areas packed in one HF module. Where spiral wound and HF modules are commonly used, the use of plate & frame and tubular modules are restricted to niche applications due to their high cost [168].

Depending on the size dimension of their separation material, polymer membranes are divided into four pressure-driven operations, sorted after decreasing diameter: conventional filtration, microfiltration (MF), ultrafiltration (UF), nanofiltration (NF) and RO, shown in Figure 14. In the water separation field, each category has a main target. Where conventional filtration filters mainly macromolecular particles, MF focusses on bacteria, UF on separating proteins, NF on sugar molecules and the main task of RO is desalination. Conventional filtration, MF and UF rarely need pressure for achieving reasonable fluxes. RO on the other side needs operating pressures up to 100 bar [167]. From an economical point of view, RO has the far highest market with 10 times higher installed capacity than any other membrane operations. NF has moderate operational pressure [168].

The separation mechanism of the first three is based on simple size exclusion (pore-flow

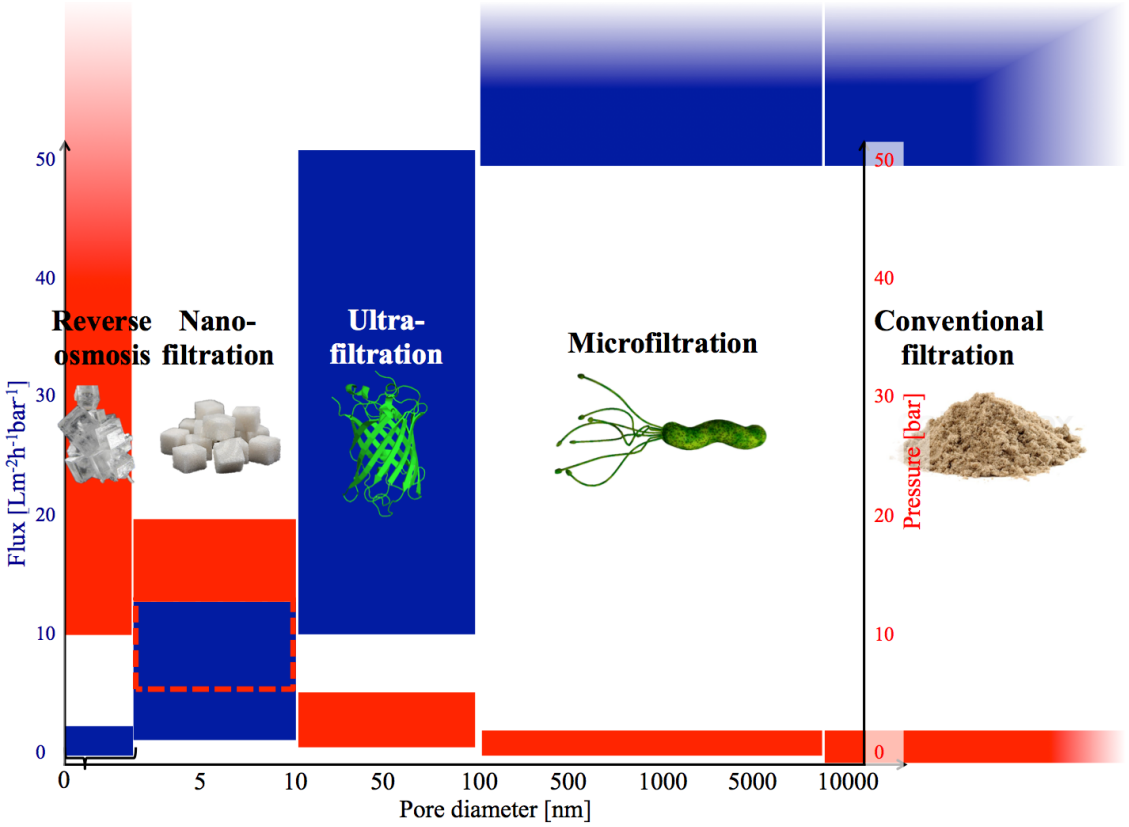

Figure 14: Schematic diagram of pressure-driven membrane operations, characterized by membrane pore size (labeled black), flux (labeled red) and operational pressure (labeled blue). Flux is given in $Lm^{-2}h^{-1}bar^{-1}$. Each operation has a specific target, visualized below the name, which is salt for reverse osmosis (RO), sugar for nanofiltration (NF), proteins for ultrafiltration (UF), bacteria for microfiltration (MF) and macro particles like sand for conventional filtration. Pressure is significantly increased towards operations with smaller pore size, whereas flux (per bar) is decreasing.

model). RO has a complete different underlying mechanism for its separation. This mechanism can be described using the solution-diffusion model. Diffusion is based on random thermal motion of nanoscopic particles (atoms, molecules) in gas or liquid solutions. If a particle concentration is unequally distributed, statistically more particles move from higher concentrated to lower concentrated region than vice versa. This results in a concentration distribution equilibrium over the whole region. The same principle applies when a semipermeable membrane is separating two compartments of different (permeate) particle concentration. Statistically more permeate molecules are passing the membrane towards the region of lower particle concentration. Note that in the case of desalination this is the salt solution side, because the concentration of the permeating water molecules is smaller there. This kind of diffusion process is called osmosis. In contrast to the pore-flow model, the separation does not depend on size but on the different solubility of permeate and retentate in the membrane material. The separation process during NF is a

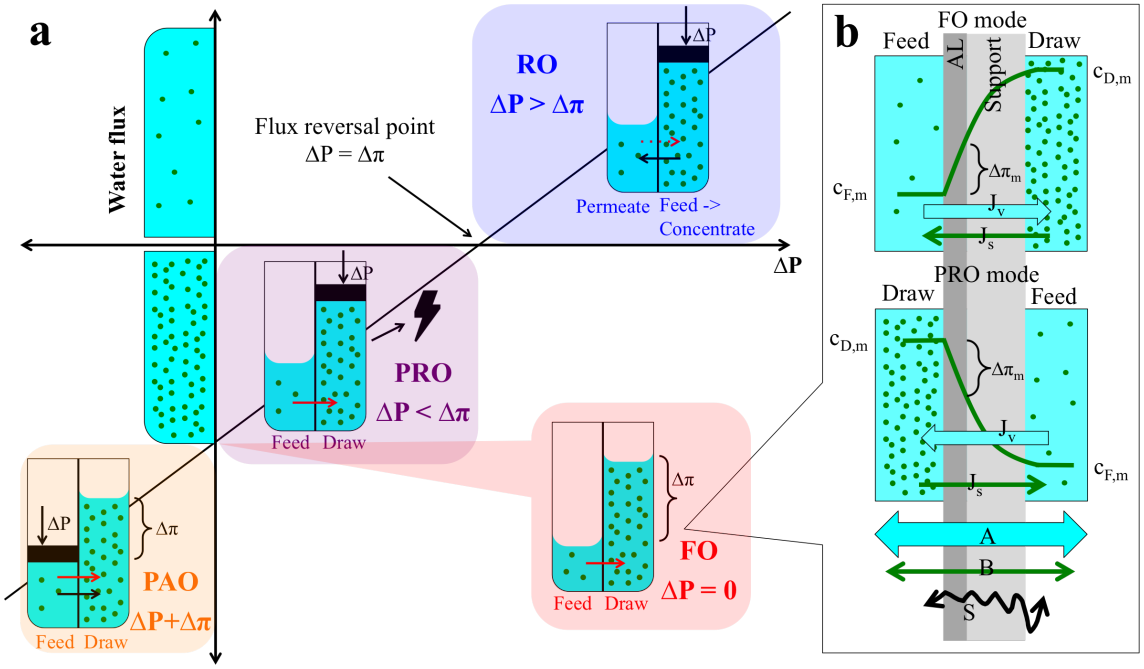

Figure 15: a) Schematic diagram of all osmotic operations, characterized by the direction of the water flux (black arrow) and the balance of applied (ΔP) and osmotic pressure ($\Delta\pi$). Where in RO ΔP has to overcome $\Delta\pi$ and the water flux is directed against the osmotic gradient (full and dotted red arrow), Pressure retarded osmosis (PRO) utilizes $\Delta\pi$ for power generation and in pressure-assisted osmosis (PAO) both pressures are facing the same direction. The feed side is the concentrated side at RO, whereas for all other operations, a draw solution is fed by the diluted feed side. b) Schematic sketch of operation modes of asymmetric FO membranes and membrane characterization parameters. FO and PRO mode describes which side the active layer (AL) of the membrane is facing. $c_{F,m}$ and $c_{D,m}$ is the salt (or other draw solute) concentration in feed and draw, $\Delta\pi_m$ is the effective osmotic pressure across the AL, J_v the water flux and J_s the reverse salt flux through the membrane, A the pure water and B the pure salt permeability coefficient of the membrane. S is the structural parameter of the membrane.

combination of both models [168].

RO requires immense pressure because the water is pressed to the region of high water concentration, thus reverse to the osmotic gradient. A new emerging operation, FO, utilizes the osmotic gradient for water separation. As far as FO is the main technology, ABPMs will be used for, FO will be discussed a little more in detail. FO membranes separate material of the same size as RO membranes. Both are asymmetric, they have a porous support for mechanic stability and a thin (200 nm diameter) AL for their selectivity. It is not shown in Figure 14 as far as no pressure is applied. Recent FO membranes can however exhibit competitive water fluxes of 30-40 $Lm^{-2}h^{-1}$ [169]. Due to the lack of applied pressure, fouling is far less relevant than in pressure-driven operations, the equipment is simple, membrane support less crucial and high rejections for various contaminants can be achieved. However, as pressure-driven operations, it struggles from concentration po-

larization (CP) [170]. CP is an accumulation of retentate or permeate inside the membrane (internal CP, ICP, see Figure 15b) or at its surface (external CP, ECP) that reduces the flux significantly. The FO terminology is reverse to RO. The feed side is the retentate-diluted side where the draw side is the retentate-concentrated side, the permeate is "drawn" over. Together with FO, other pressure-mediated operations emerged, like pressure retarded osmosis (PRO) [171] or pressure assisted osmosis (PAO) [172]. PRO uses the osmotic pressure to generate energy, whereas PAO applies an additional pressure at the feed side to increase the membrane flux. All osmotic operations are shown in Figure 15a.
Apart from permeate (in this case water) flux J_v and rejection, respectively reverse salt flux J_s, which are also related to external factors, the performance of FO polymer membranes can be described via intrinsic membrane parameters: the pure water permeability coefficient A, the salt permeability coefficient B that describes the salt transport through the AL of a membrane and the structural parameter S, quantifying the length scale of mass transport though the membrane support layer [173]. For FO membranes, the relationship between the measurable fluxes and A or B is given by $J_v = A\Delta\pi_m$, where $\Delta\pi_m$ is the effective osmotic pressure difference across the AL. B can be set in relation to J_s by the equation $J_s = B(c_{D,m} - c_{F,m})$, where $c_{D,m}$ and $c_{F,m}$ are the salt concentration on draw and feed side. S is calculated by $S = t_s\tau/\epsilon$ where t_s is the thickness, τ the tortuosity and ϵ the porosity of the support layer. τ is a measure how twisted the interior of the support layer is. For FO membranes, A is in the range of 1-5 $\mathrm{Lm^{-2}h^{-1}bar^{-1}}$ (the determination is pressure-driven), B between 0.2 and 2 $\mathrm{Lm^{-2}h^{-1}}$ and S between 300 and 1500 μm [173]. All parameters are shown in Figure 15b.

FO can be used as well in the most module forms described before. A reversed spirale wound module has been developed, where the diluted feed side is introduced from the central tube [170]. There are plenty of academic groups in FO research with 150 publications in 2013 [174]. Elimelech and coworkers covers all general aspects of FO [173, 175, 176], the McCutcheon lab from University of Connecticut [177–179] and the Chung lab in NUS [180–182] are focussing on FO membrane modifications, the Cath group from Colorado School of mines is targeting FO applications and upscaling [183–185]. SMTC from NTU has the main focus on HF FO [186–188] and biomimetic FO membranes [189–191]. On the industrial side, there are companies that sell single FO membranes or modules like HTI [192], Aquaporin A/S [193], Porifera [194], Oasys Water [195], CSM [196], Toyobo [197] or whole plants like Modern Water [198] or CDM Smith [199]. HTI is the only company though that worked on FO membranes since more than a decade.
A crucial aspect of FO is the design of a suitable draw solution. An ideal draw solution should contain an osmolyte that generates a high osmotic pressure and can be easily re-

moved from water. Some companies only focus on the draw solution design, like Trevi Systems [200] or Forward water technologies [201]. Even though there are potentially easy removable osmolytes, to finally end up with pure water, the highest potential in FO could be the simple exchange of water from a compartment where it is in undesired excess to one where it is required. Thus, hybrid systems, like the combining of seawater or wastewater as the feed solution and a concentrated fertilizer as draw are promising applications [202]. Other niche applications in desalination and waste water treatment are realized [169]. Further applications are liquid food concentration, pharmaceutical applications, point-of-use drinking water and biofuel generation [203].

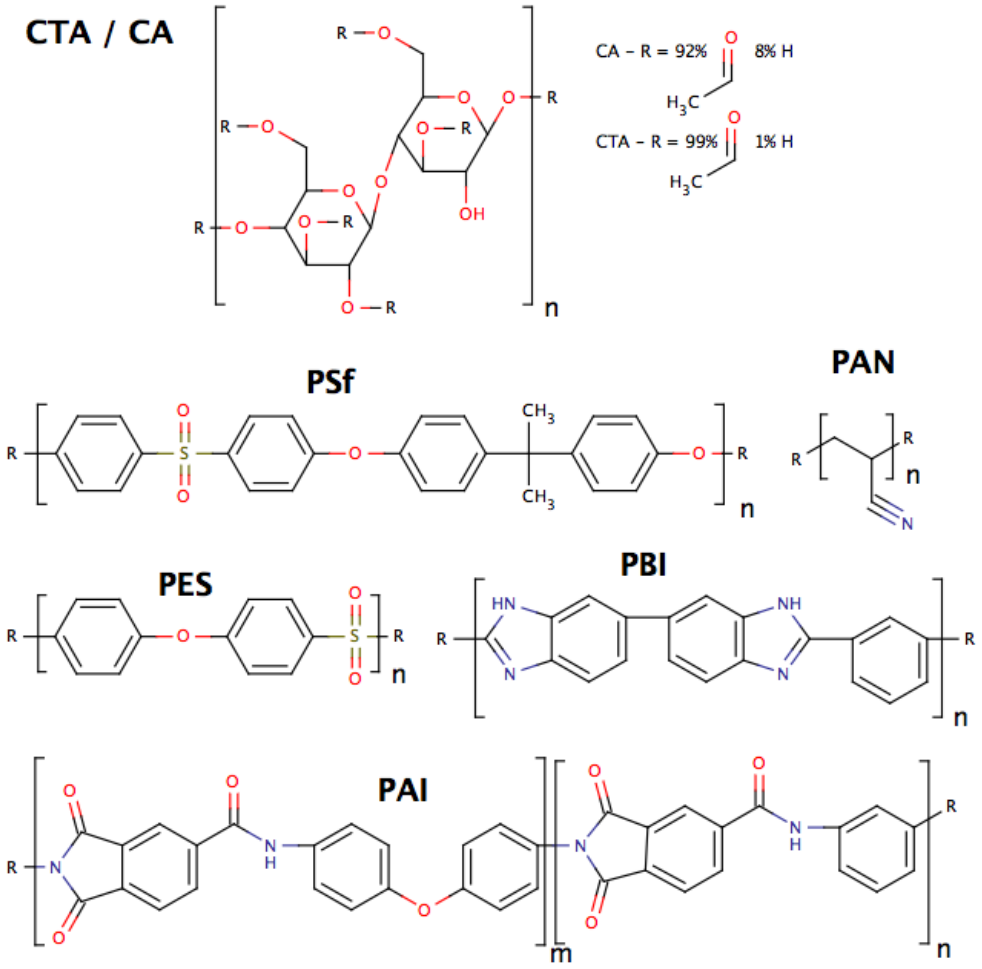

Figure 16: Chemical sketches of all relevant polymer chemistries as material for FO membranes. Cellulose acetate (CA) and cellulose triacetate (CTA) have been used extensively for decades. Polysulfone (PSf) and polyethersulfone (PES) are common materials for RO, UF and MF membranes. Polyacrylonitrile (PAN), polybenzimidazole (PBI) and polyamide amide (PAI) have been recently discovered for FO purposes.

Polymer membranes for FO should ideally have a dense, ultrathin AL, followed by a porous support that also should be as thin as possible to minimize ICP and a general hydrophilicity for high flux and low fouling [174].
The first FO polymer membrane material was cellulose acetate (CA), a synthetic cellulose ester produced by heating cellulose with acetic anhydride. In CA, 92% of all hydroxyl groups of cellulose are acetylated, which is increased to 99% for cellulose triacetate (CTA). The big advantage of CA and CTA is their hydrophilicity, which is higher at lower acetylation [204]. They have also high resistance to chlorine treatment, mineral and fatty oils. However their major drawback of a narrow pH tolerance and insufficient mechanical stability makes them unsuitable for many applications [174].
Polysulfone (PSf) and PES (used in this study), the most common used polymer membrane materials for water treatment, are synthetic polymers with aryl-sulfonyl-aryl-groups, respectively aryl ether groups [205]. Both chemistries are quite hydrophobic, but provide good chemical and mechanical resistance due to high glass transition temperatures (PSf: 190°C, PES 230°C) [167]. PES enables furthermore good pore size control, low oligomer content and a possibility for high porosity. PES is UV-sensitive and can thus be functionalized via UV treatment. The most common fabricated PES is Ultrason E6020P and Radel A-100 with an M_w of 58 kg/mol and 15 kg/mol respectively [206].
PSf has an additional dimethylgroup, thus it is slightly more hydrophobic, less flexible but also better in mechanical resistance [207]. Sulfonation or blending with hydrophilic additives like PEO or polyvinylpyrrolidone (PVP) has been investigated with the main disadvantage of lower fluxes [208].
Polyacrylonitrile (PAN) has recently been used as a promising candidate for FO membranes due to its higher hydrophilicity compared to PSf and PES with equal good resistance against chemical, thermal and solvent influences. PAN is mainly employed for RO and UF [208].
Another heterocyclic polymer, polybenzimidazole (PBI), usually employed in RO and NF, has recently been used for HF FO membranes [209]. Additionally to excellent chemical and thermal stability, it rarely change its physical properties at when heated to 250°C for longer time periods [204]. The heterocyclic imidazole ring enables inter- and intramolecular H-bonding between PBI molecules, thus PBI self-charges in aqueous environment, because the benzene ring delocalizes a proton of the imidazole group [209]. Consequently, hydrophilicity and tolerance on a broad range of pH and organic solvents is enhanced. Poor mechanical strength however reduces its potential for self-supported membranes [210].
Another possible material for HF membranes is polyamide imide (PAI), distributed from Solvay under the trade name Torlon 4000T. This resin is mainly used as additive and

for compounding with other polymers. Outstanding mechanical, thermal and oxidative performance under extreme conditions and chemical, wear and creep resistance make it desirable for HF [204, 211]. Equal to PBI, PAI has an imidazole ring, thus it shares the same properties arising from the inter- and intramolecular H-bond formation. Recently, the amine group was allowed to react with polyethyleneimine (PEI) resulting in positively charged membranes with better salt rejection [210]. All polymers are shown in Figure 16.

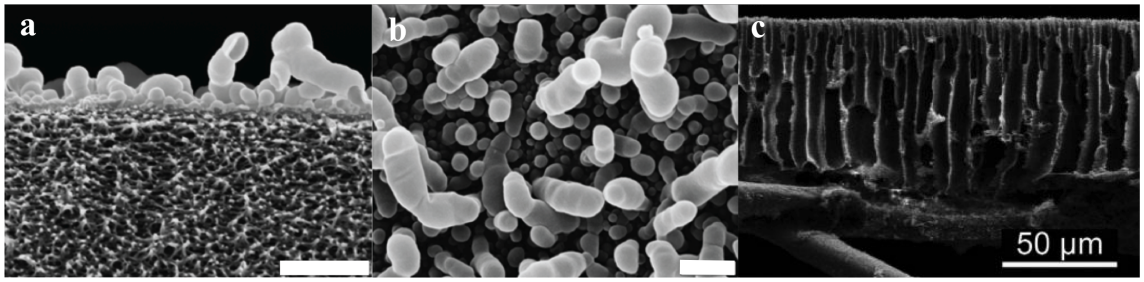

Figure 17: SEM micrographs of a standard AL, made of m-phenylenediamine (MPD) and trimesoyl chloride (TMC) in a) profile view and b) top view [204] and c) an asymmetric fingerlike porous FO membrane with dense toplayer for optimal AL embedment [212]. Scale bar in a+b is 500 nm.

Polymer membrane flat sheets are mainly synthesized using the immersion precipitation technique. The polymer, dissolved in a proper solvent, is cast on a support and immersed in a coagulation bath, which contains a nonsolvent. Due to the exchange of solvent and nonsolvent, the polymer precipitates out. Membrane structure is a result of phase separation and mass transfer [167].

Nearly all FO polymer membranes nowadays, have an AL (see Figure 17a + b). More details on AL and its synthesis by interfacial polymerization are given in chapter 6. To place an AL on a polymer membrane, the surface has to be dense. Dense membrane interior however decrease flux and increase ICP. Therefore, a modified immersion precipitation was developed from the Elimelech lab involving two solvents with different solvent outflux to obtain a membrane with a dense toplayer and a highly porous fingerlike support structure below [212] (Figure 17c). Other possible polymer membrane modifications are placing electrolyte layer of different charge on top of the membrane, called layer-by-layer deposition (LbL) [213] or increasing the mechanical strength within electrospun nanofibres [178].

1.5 Interplay of AQPs, block copolymers & polymer membranes

This subchapter is published in [1]

Provided that the performance of AqpZ proteopolymersome described by Kumar et al. [10] could be scaled up they could create a water separation membrane that reaches fluxes of 11000 $Lm^{-2}h^{-1}$, a value that is several orders of magnitude higher than conventional industrial membranes. In highly packed 2D AqpZ crystal arrays fluxes of up to 16000 $Lm^{-2}h^{-1}$ could be achieved in principle [214]. However these values will very probably never be achieved due to upscaling issues - but they show the huge potential of biomimetic membranes. The development is rapid: in 2011 ABPMs were regarded as the most revolutionary membrane advances, but also the ones most farthest away from a potential commercial viability [215]. Now, four years later ABPM membranes are commercially available with areas of tens of m^2 [193]. It will still take time before the technology is widespread but it has definitely moved outside the fundamental research domain. In the next sections we will highlight the AQP biomimetic membrane technology development in detail.

The first industrial approaches are made from two Danish companies, Aquaporin A/S, and AquaZ (now Applied Biomimetic). Together with the Danish Technical University (DTU), the University of Southern Denmark (SDU), DHI, Lund University, Sweden, Ben-Gurion University of the Negev, Israel, Malaga University, Spain, Vilnius University, Lithuania and Veolia Water, France, Aquaporin A/S joined the EU funded MEMBAQ project 2006-2010 which aimed at utilizing AQPs for industrial applications [216]. At the same time AquaZ started on membrane development based on a patent from Carlo Montemagno where he described conceptually how AQPs, embedded in polymeric or lipid bilayers, could function as a biomimetic membrane, although without any concrete design of such a membrane [217].
The first membrane design from Aquaporin A/S was based on an ethylene tetrafluoroethylene (ETFE) scaffold with holes of 300 μm, produced by laser-ablation, which are inspired by painting/folding lipid chambers from the 70's [6, 218] (Figure 18a-d). A freestanding lipid-bilayer film is established by "painting" a two-phase solution over the hole, where the lipids move from the organic solvent to the aqueous phase, accumulate around the holes and establish a bridging layer. Several membrane proteins and peptides were incorporated in the freestanding layer including porins [101]. Also freestanding PMOXA-PDMS-PMOXA polymer membranes with incorporated gramicidin A channels were de-

veloped [102] and characterized [219]. In subsequent designs the membrane is supported by PEO-dimethacrylate (PEO-DMA) based hydrogels [220] (Figure 18e) or stabilized using surface plasma polymerization [221]. Moreover, a strategy was explored to form interface lipid bilayer between lipid-coated water drops in a continuos oil phase, shown in Figure 18f [7]. A later liquid membrane approach investigated spinach AQP (SoPIP2;1) proteoliposomes in a sandwich between NF membranes that could prove an AQP fingerprint for the first time, however at modest water flux [222]. These designs [222–227] later paved the way for developing membrane-based biosensor designs [110]. The hydrogel approach from Aquaporin A/S was adapted in 2010, when Montemagno and AquaZ claimed an AQP-based biomimetic lipidic membrane (ABLM) design with internally UV cross linked and PA-interconnected proteoliposomes that are immobilized on a lipid-coated AL and supported with a PEO hydrogel [228].

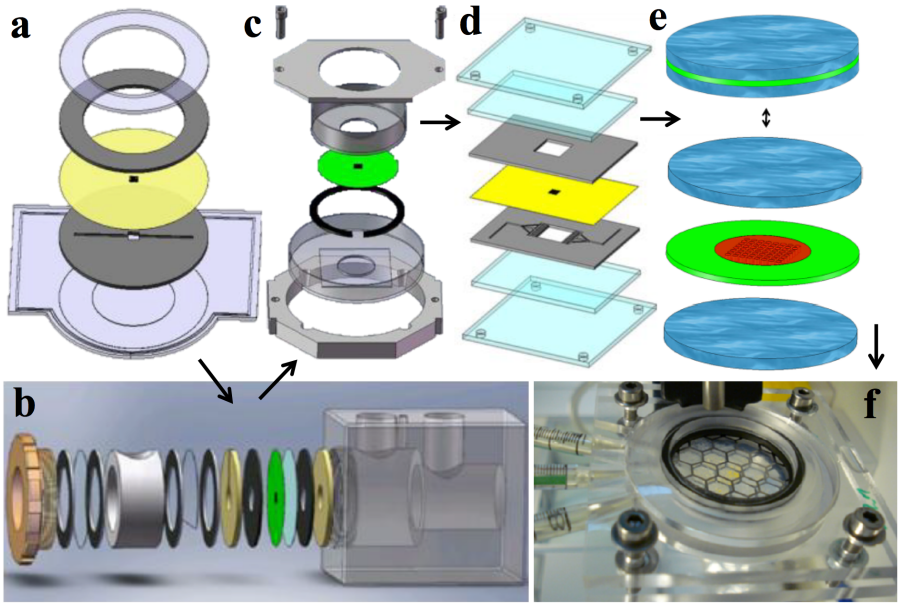

Figure 18: Various designs for potential AQP-based biomimetic lipidic membranes (ABLMs) with freestanding lipid bilayer, developed from Aquaporin A/S. Designs a-e are based on painting a two-phase-solution including lipids over a micrometer-hole scaffold, marked in yellow (a,d) or green (b,c,e) [229]. Model e provides further stabilization using a hydrogel support on both sides [220]. f) An alternative design that consists of lipid-coated water droplets in a oil emulsion where the lipid bilayer forms at the interface [7].

In 2009, Aquaporin A/S and DHI Singapore initiated collaborative research with the SMTC on biomimetic membranes. At the same time the Chung lab from NUS started biomimetic research in collaboration with Wolfgang Meier and coworkers. NUS followed up on Aquaporin's hydrogel approach and tried to achieve a planar proteobilayer, starting with AqpZ proteoliposome fusion on pure and PEO coated porous alumina and found an increasing stability with increasing mPAR [230]. In 2012, they described an

approach based on a Langmuir-Blodgett-film with Nickel-chelated lipids that bind to His-tagged AqpZ, similar to the approach from Kumar [26], but using lipids with subsequent Langmuir-Schäffer deposition-mediated transfer on a mica surface [231]. This was followed by Kaufman et al. who incoporated SoPIP2;1 in positively charged bolalipid micelles which were then fused on a negatively charged silica surface [232]. Chuyang Tang et al. investigated on fusion behavior of proteoliposoes on pure and polymer-coated silica via quartz crystal microbalance with dissipation (QCM-D) [190]. They found increasing robustness and fusion resistance with increasing mPAR, and further proteoliposome stabilization with polyelectrolyte layers at the highest mPAR (1:25) in 1,2-diphytanoyl-sn-glycero-3-phosphocholine (DPhPC) liposomes [190].
The SMTC group also investigated ABLMs, following Kaufman's approach of liposome fusion on nanofiltration (NF) membranes [233, 234] and fused AqpZ proteoliposomes on NF PA-polysulfone (PSf) membranes that were precoated with positively charged lipids via spin-coating [235]. The proteoliposomes were placed on the NF membrane and slightly pressurized with 0.5 bar. They found a linear relationship between the roughness of the ABLM surface and mPAR indicating AqpZ incorporation, but no effect from AqpZ on the water flux J_v and J_s could be observed [235].

A different approach was initiated jointly by SMTC and Aquaporin A/S in which AqpZ proteoliposomes were embedded in the standard AL made from interfacial polymerization of *m*-phenyl diamine (MPD) and trimesoyl chloride (TMC) on a PSf support structure [8, 236, 237]. ABLMs were tested with functional AqpZ proteoliposomes, proteoliposomes with an inactive AqpZ mutant and PA-PSf membranes without proteoliposomes. ABLMs were further benchmarked against commercially available membranes with cross-flow RO tests on 42 cm^2 effective coupon area. The ABLMs with AqpZ proteoliposomes had a significantly higher J_v than the ABLM with inactive AqpZ and the PA-PSf membrane while J_s values were similar in all cases. Furthermore the ABLMs were able to withstand 10 bar pressure making them well-suited for low pressure RO applications. J_v of the AqpZ ABLM was ~40% higher compared to the commercial brackish water RO membrane (BW30) and an order of magnitude higher compared to a seawater RO membrane (SW30HR).
This was followed up by a systematic study which revealed that 1,2-dioleoyl-sn-glycero-3-phosphocholine (DOPC)-based proteoliposomes and proteoliposomes of mPAR of 1:200 gave optimal water flux as judged by SFLS and that cholesterol addition could seal defects on the proteoliposomes [189]. To achieve higher loading and better sealing, the SMTC group coated proteoliposomes with polydopamine (PDA) and immobilized them on a 28 cm^2 NF PAI membrane by embedding them in branched PEI, cross linked per PA

bond at elevated temperature [191]. The SFLS data showed, that the elevated temperature had a higher negative influence on the permeability of the proteoliposomes than the PDA coating itself. Even so, AqpZ function was demonstrated with an optimal performance mPAR of 1:200 when reconstituted and integrated into the PAI-PEI layer. In contrast the best SFLS response was achieved at an mPAR of 1:100 [189]. This discrepancy could be due to AqpZ being affected by the PDA coating or the PEI branches. Still, the J_v was measured to be 36 $Lm^{-2}h^{-1}bar^{-1}$ making it the highest among all biomimetic membranes so far [191]. Also proteopolymersomes can be functionalized to get bound chemically to a counterpart functionalized membrane. Functionalization of both liposomes and polymersomes has been studied extensively since decades [238–240].

ABPMs with functionalized proteopolymersomes are first mentioned in a patent of Montemagno in 2011, where he claimed a concept of proteopolymersomes made of polyethyloxazoline-polydimethylsiloxane-polyethyloxazoline (PEOXA-PDMS-PEOXA) triblock copolymers, where the methacrylate-functionalized PEOXA block is immobilizing the proteopolymersomes on a methacrylate functionalized cellulosic membrane [241]. The first experimental results on this approach were presented by the NUS group [116]. They made proteopolymersomes containing AqpZ in methacrylate-functionalized PMOXA-PDMS-PMOXA and tested them with SFLS. In contrast to Kumar [10], no significant difference SFLS signals with varying mPAR was observed - likely a reflection of the issues with SFLS on rigid structures mentioned in section 3. Proteopolymersomes were deposited onto acrylate-functionalized PCTE membranes and immobilized by UV-crosslinking of the acrylate groups with the methacrylate of the PMOXA, as claimed from Montemagno et al. [241]. Afterwards, the proteopolymersomes were further immobilized by pressure-assisted adsorption and possibly ruptured by ”smooth extrusion”. AQP resulted in an increasing J_v with increasing mPAR, whereas there was no J_v with polymersomes alone, however AFM and field-emission SEM (FE-SEM) revealed that the layer had some defects [116]. In a subsequent study they followed the same approach using an acrylate-functionalized CA membrane [117]. Here, they found an increase in J_v and decrease in NaCl rejection with proteopolymersomes of higher mPAR. The increase in J_v could indicate AQP activity but the NaCl rejection was however still quite low (33%) and the measured membrane area was only 7 mm^2 [117].
In another approach, gold-disulphide binding to immobilize disulphide functionalized PMOXA-PDMS-PMOXA AqpZ proteopolymersomes on gold-coated porous alumina and silicon surfaces has been described [140]. Here FE-SEM revealed that full coverage of the pores was achieved at pore diameter of 55 nm, where larger (100 nm diameter) pores remained open. Again, an effect of incorporating AQP was observed but NaCl rejection

was modest [140]. To obtain a better sealing, cysteamine was added with PDA and histidine coatings after the proteopolymersome immobilization on gold-coated PCTE [114]. J_v increased and J_s decreased with increasing amount of PDA-His-layers, however the best sealing was obtained without proteopolymersomes. PRO mode testing (AL to the water receiving draw side) resulted in significantly higher J_s than FO mode testing (AL to feed side) [114]. Mathematical simulations on this ABPM indicated that in PRO mode, J_v is determined by vesicle size and permeability. In FO mode, hydrostatic pressure is determined by the vesicle interior solute concentration [115].
Another slightly different design has been experimentally realized afterwards with AqpZ and methacrylate- and carboxyl-functionalized PMOXA-PDMS-PMOXA on amine- functionalized CA [126]. Here proteopolymersomes are first covalently attached to the CA, where the carboxyl-groups of PMOXA and the amine groups on CA formed a PA bond. Then, a methacrylic cross linking polymerization is performed by dipping the membrane into a mixture of methyl methacrylate, ethylene glycol dimethacrylate and initiator. J_v is linearly increasing and NaCl rejection decreasing with polymerization time. An increase in J_v and decrease in NaCl rejection of ABPMs compared to only methacrylated CA and polymersome coated CA in both FO and NF mode evidenced the presence of AQP. However the NaCl rejection (61%) still indicated significant defects [126]. Another example of methacrylate cross-linking involves amine-functionalized AqpZ proteoliposomes on a PDA precoated UF PAN membrane [242]. Here proteoliposomes are internally cross linked via methacrylate and gently pressurized onto the PDA-PAN support, allowing the amines of PDA and functionalized lipids to react. Further stabilization is achieved via glutaraldehyde. The internal cross linking of the proteoliposomes has a positive effect on stability. J_v and NaCl rejection between liposome-coated membranes and ABLMs showed some effects of AqpZ presence, however FE-SEM images and low NaCl rejections revealed that defects in the ABLM played a strong role in the membrane performance [242].

Instead of chemical bonding, proteoliposomes or -polymersomes can be bound by electrostatic forces. Using this approach Kaufman et al. attempted to fuse positively charged bolamphiphilic proteoliposomes onto negatively charged NF AL and sulfonated PSf (PSS) membranes [243]. The proteoliposome loading was enhanced with the more negatively charged PSS membrane. However, proteoliposome loading also led to a decrease in J_v together with an increase in NaCl rejection, probably due to induced defects in the bolamphiphilic bilayer by SoPIP2;1 [243].
Another electrostatic-binding-based approach employed the embedment of positively charged poly-L-lysine covered AqpZ proteoliposomes in the anionic part of a LbL sandwich on an

UF PAN membrane [244]. The anionic part is made of PAA and PSS, where the cationic counterpart was polyallylamine hydrochloride (PAH). Here, a clear AqpZ effect could be observed as J_v increased by 30-50% after addition of proteoliposomes, where the effect was stronger when there was a higher amount of negatively charged lipids present. The $MgCl_2$ rejection was comparable to the work of Zhao et al. [8] however no NaCl rejection was presented [244]. This work was extended by encapsulating magnetic nanoparticles to force more proteoliposomes magnetically to adsorb on the polyanionic film. In FO mode, they measured an increase in both, J_v and J_s with increasing mPAR, which speaks for remaining defects despite the efforts to load more vesicles onto the supporting substrate [245]. Wang and coworkers from Ocean University of China followed up on that approach and immobilized AqpZ proteoliposomes with positively charged lipids on top of a negatively charged PSS layer, followed by PEI on an UF PAN membrane [246]. Modest NaCl rejection and J_v decrease indicated a highly defective membrane. An increase in J_v between liposomes and proteoliposomes as well as further increase in J_v with higher mPAR could indicate the presence of AQP. NaCl rejection remained however unchanged between all membranes. They further showed that membrane performance was compromised after detergent treatment [246].

All designs are summarized in Figure 19, and based on the results obtained so far we conclude that the embedment of proteopolymersomes or -liposomes in a layer results in more efficient membranes than layer-based immobilization. A great advantage of the PA-embedment technique is that no precoating/functionalization is needed which otherwise severely limits any upscaling [8]. All reported performances are however still modest compared to theoretical predictions and clearly more development is required. The major dilemma seems to be that with increasing mPAR J_v increases but the matrix layer becomes weaker and more prone to salt leakage. Introduction of sealing and stabilizing polymer networks could improve rejection but may also compromise J_v [214].
Next to ABPMs and ABLMs there are two main directions aiming to achieve biomimetic membranes by AQP mimicking artificial channels: carbon nanotubes (CNTs) and organic building block nano channels [247]. CNT is more prominent because fast water permeation is proven in theory [248] and experimentally [249]. With regard to organic nano channels, there are five promising structures found to compete with ABPMs, ABLMs and CNTs: zinc and N,N-diacetic acid imidazolium bromide based zwitterionic coordination polymers [250], helical pores of dendritic dipeptides [251], imidazole compounds with urea ribbons [252], hydrazine-appended pillar[5]arenes, macrocycles of m-phenylene ethynylene [253]. Their great advantage is their smaller size with comparable channel diameter (3-10 Å) [247].

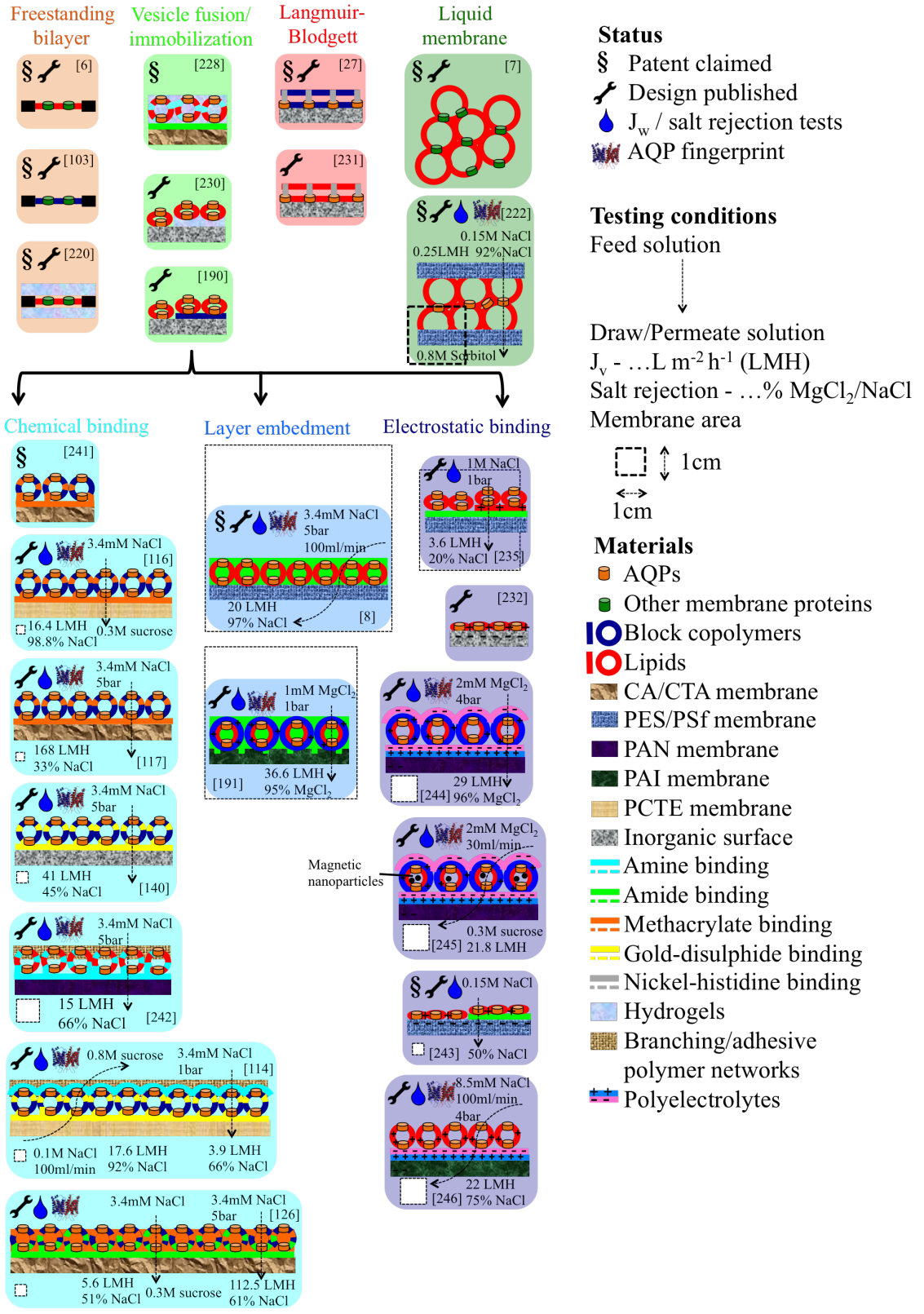

Figure 19: Schematic overview of all published designs for ABPMs and ABLMs. Pioneer work is mainly done by Kumar and Aquaporin A/S. The most experimental designs has been done by NUS, where NTU published the most promising layer embedment ABLMs. The main recent work is on LbL-based electrostatic binding, for example binding of proteoliposomes on a polyelectrolyte layer [246].

2 Interplay of AQPs & block copolymers

This chapter is published in [1]

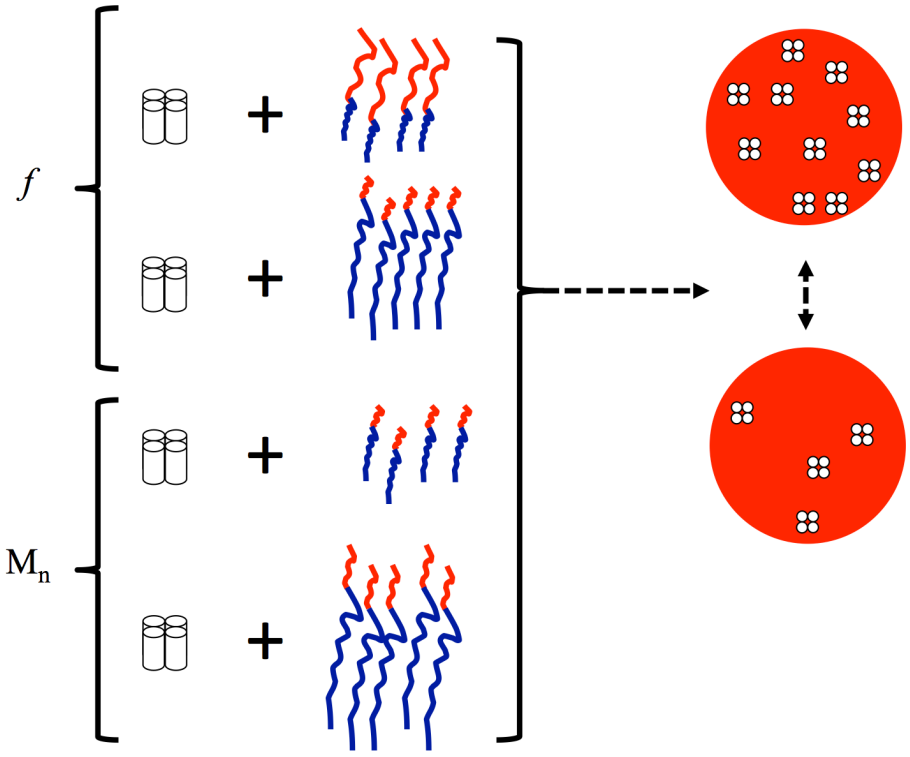

Figure 20: Schematic sketch of methodology. Length and hydrophilic volume ratio f of the block copolymers is varied in order to find out how these parameters influence AQP incorporation.

2.1 Introduction

This chapter is about how to manipulate how AQPs and block copolymers interact with each other and how to find the sweet spot where a functional membrane is obtained. To our knowledge, no systematic experimental studies have been performed on how molecular parameters of block copolymer influence membrane protein incorporation. From calculations and simulations we know that highly flexible hydrophobic chains and a high PDI_M are facilitating membrane protein incorporation, whereas too long hydrophilic chains could block membrane protein channels [86, 87].

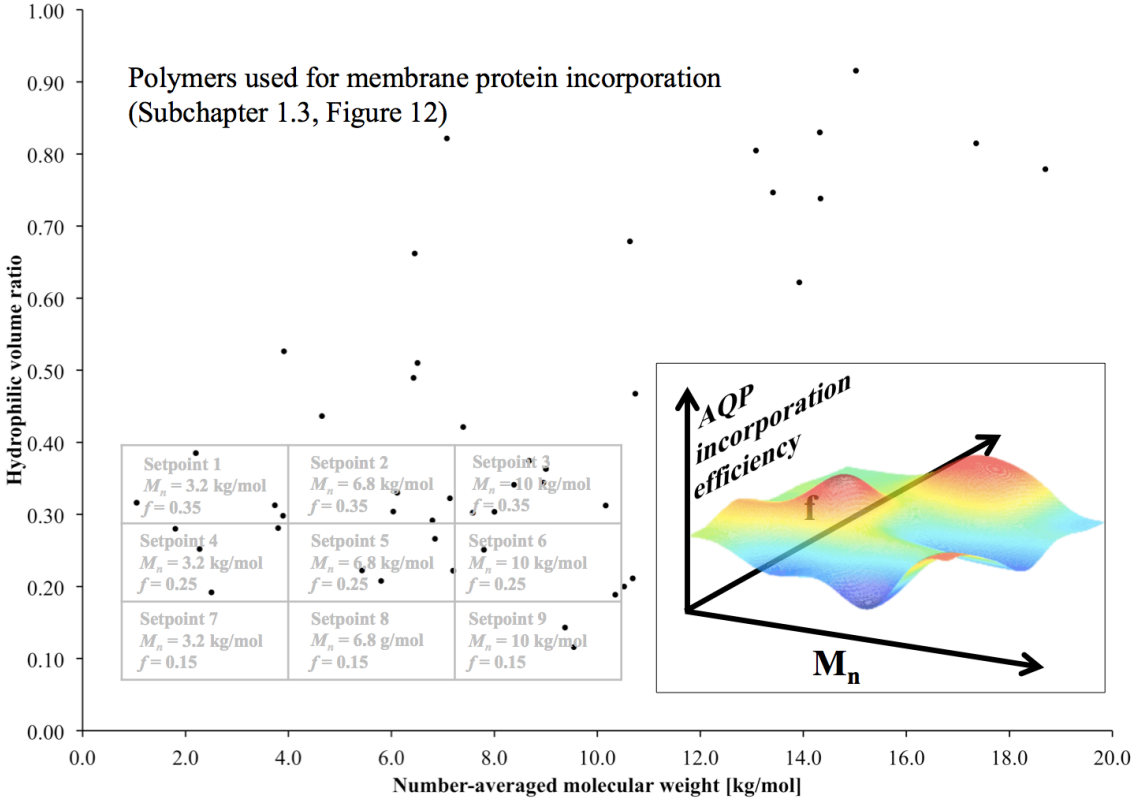

Figure 21: Lattice of nine setpoints over diagram 12 of all polymers used for membrane protein incorporation. The majority of polymers used has f between 0.1 and 0.4 and M_n between 2 and 12 kg/mol. Based on these findings, the nine lattice points were defined using three f values and three M_n values within this region. Each lattice window/setpoint represents one molecular parameter window of M_n and f. The inset shows a hypothetical function of M_n and f for AQP incorporation efficiency.

From Table 2 and Figure 12 from subchapter 1.3 we learnt that clear patterns from experimental studies for incorporation efficiency of membrane proteins remain a great challenge. In order to create a reasonable systematic study to find the sweet spot of membrane protein (AqpZ and AQP10 in our case) incorporation in block copolymers, we chose two molecular parameter of block copolymers (in our study PB-PEO): M_n and f. We set a

lattice of setpoints over the part of the diagram of where the majority of block copolymers with functional incorporated membrane proteins are located, where each setpoint respectively lattice window represents on window of a certain M_n and f range. We chose three M_n (3.2, 6.8 and 10.0 kg/mol) and three f (0.15, 0.25 and 0.35) in order to create 9 distinct molecular parameter windows. We planned to create a pool of polymers that fit these windows. As far as it was challenging to fit the exact number of Bd and EO units, we set the tolerance of 25% offset to the M_n and f values of the setpoints. We synthesized 11 polymers that meet the criteria for 8 of the 9 setpoints, listed in Table 3. PB_{29}-PEO_{16} was more than 25% off in M_n but we still chose to use it as small M_n polymers used to work well for AQP incorporation in previous studies we made [96]. Our aim is to find out which one is the optimal parameter window for AQP incorporation. If we incorporate AqpZ in each polymer in a equal ratio, with equal method and characterize them in equal manner, we hope to be able to define incorporation efficiency as a function of M_n and f, shown in the inset of Figure 21.

Table 3: List of polymers used for this study. $M_{n(set)}$ and f_{set} are the planned values that were related to the experimental values after the synthesis ($M_{n(exp)}$ and f_{exp}). For the calculation of the offsets (ΔM_n and Δf), $M_{n(set)}$ and f_{set} are set to 100%.

Setpoint	$M_{n(set)}$ [kg/mol]*	f_{set}	Used polymer	$M_{n(exp)}$ [kg/mol]	ΔM_n [%]	f_{exp}	Δf [%]
1	3.2	0.35	PB_{32}-PEO_{30}	3.0	-5.1	0.37	4.9
1	3.2	0.35	PB_{43}-PEO_{32}	3.8	18.1	0.32	-9.7
2	6.8	0.35	PB_{62}-PEO_{56}	5.8	-14.8	0.36	1.7
3	10.0	0.35	PB_{92}-PEO_{78}	8.4	-16.2	0.34	-1.7
4	3.2	0.25	PB_{33}-PEO_{18}	2.6	-19.5	0.25	0.4
4	3.2	0.25	PB_{29}-PEO_{16}	2.3	-28.3	0.26	3.2
4	3.2	0.25	PB_{46}-PEO_{32}	3.9	21.8	0.30	20.4
6	10.0	0.25	PB_{117}-PEO_{61}	9.1	-9.5	0.25	-2.0
7	3.2	0.15	PB_{45}-PEO_{15}	3.0	-4.9	0.16	7.3
8	6.8	0.15	PB_{104}-PEO_{31}	7.0	2.0	0.16	3.3
9	10.0	0.15	PB_{120}-PEO_{41}	8.3	-16.9	0.18	16.7

Detecting functional incorporation of AQPs is challenging as well, as the permeating solute is neutral water molecules. Protein mediated transport of neutral molecules (in particular at the single protein level) is harder to measure than transport of charged molecules (ion or protons) or a specific chemical reaction (e.g. ATPase enzyme activity). Although deuterated water labeling has been proposed for measurements via Raman spectroscopy [254] this type of measurements is complicated by the fact that water transport rate in the AQP channel is different for deuterated water molecules compared to that for normal water molecules [255].

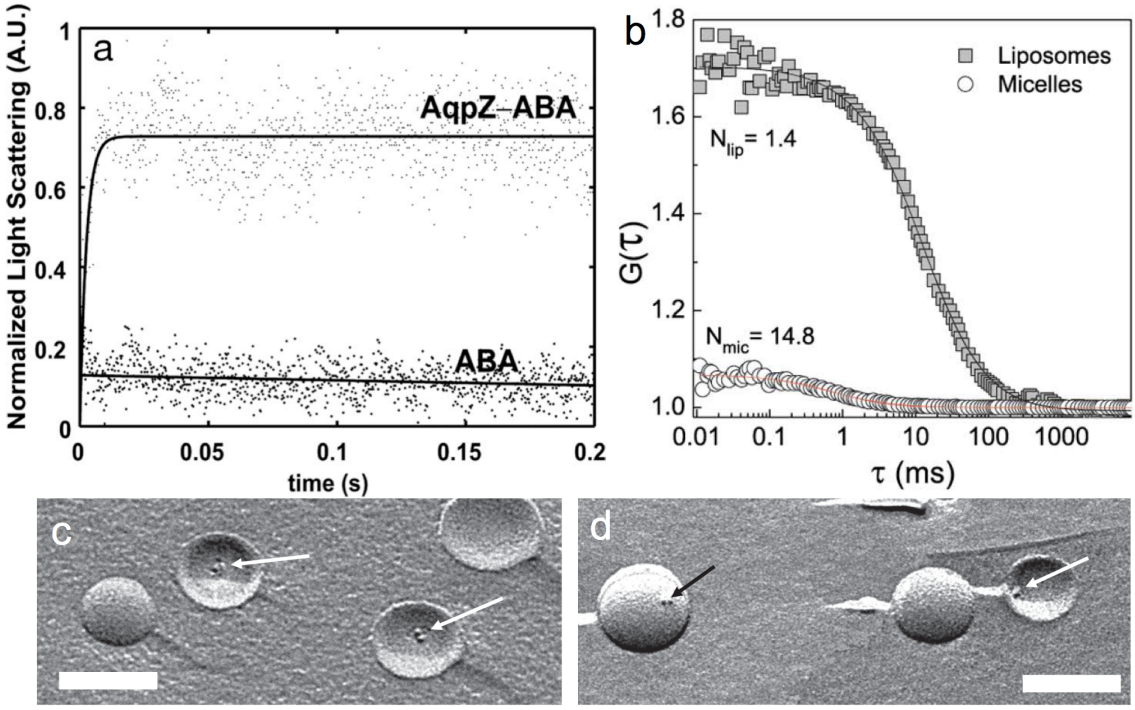

Figure 22: Exemplary diagrams of (a) SFLS [10] and (b) Fluorescence correlation spectroscopy (FCS) [111], and (c) + (d) FF-TEM micrographs of proteoliposomes [256]. The SFLS example shows the water permeability PMOXA-PDMS-PMOXA (here referred to as ABA) polymersomes alone and with AqpZ incorporated, where it is increased by several orders of magnitude. In the FCS example, the flourescence signal of fluorescence-labelled AqpZ is monitored in proteoliposomes and in micelles after proteoliposome solubilization, shown in an autocorrelation curve. Proteoliposomes with higher weight move slower and therefore stay longer in the confocal volume, resulting in a higher diffusion time τ, where it is decreased due to faster movement of the lighter micelles through the confocal volume. FF-TEM reveals AQP as small spots on the replica of freeze-fractured proteovesicles, as shown here in the case of proteoliposomes with AQP1 (left side) and AqpZ (right side) incorporated. Scale bar in (c) + (d) is 100 nm.

A popular method for measuring functional incorporation is SFLS (see Figure 22a). In SFLS, proteopolymersomes are rapidly mixed with an osmotically active agent (NaCl or sucrose) in a defined volume. In the case of a hyperosmotic shock, proteopolymersomes will shrink, which will give rise to an increase in light scattering. With increasing amount of incorporated AQPs the shrinking rate will increase as well. This method is however strongly affected by the quality (size distribution) of the polymersomes, of the AQP concentration in the polymersome and the concentration of the osmolyte [119].
Another method to show qualitatively the difference between proteopolymersomes and polymersomes is sodium dodecyl sulphate polyacrylamide gel electrophoresis (SDS-PAGE). In SDS-PAGE, proteins are placed on a polyacrylamide gel that is set in a current and separated by their electrophoretic mobility, which is related to M_w, charge and conformation of the proteins. SDS is added in order to denature the proteins and to apply a negative

charge on the proteins, relative to their M_w. After staining each protein can be observed as a band on a characteristic height that is related to its M_w respectively to the M_w of the denatured monomer.

In principle direct visual quantification can be achieved by FF-TEM (Figure 22c+d) although FF-TEM will not reveal any functional information. In FF-TEM, proteopolymersomes are captured in their original shape by quick-freezing. The frozen sample is fractured, where the fracture plane is along the proteopolymersome bilayer which is the weakest point of the whole system. The sample with incorporated AQPs (or the cavities, where AQPs were embedded in the bilayer) is then exposed to carbon/metal coating. The forming replica is removed from the thawed sample and AQPs/cavities can be observed on the replica as distinct spots on the proteopolymersomes.

Another method is FCS of fluorescently labelled AQP (see Figure 22b). In FCS time-dependent fluctuations of fluorescence intensities in a microscopic space, the so-called confocal volume, are monitored and subjected to an autocorrelation function. Dependent from the different diffusion time of the particles diffusing through the confocal volume, one can obtain the number of particles in the confocal volume within a given time interval. When proteoliposomes or proteopolymersomes are monitored, then solubilized to micelles and monitored again, the proteins-per-vesicle-ratio (mean number of membrane proteins incorporated in the bilayer of one vesicle) can be obtained by dividing the latter number by the first. It is assumed that micelles contain only one AQP, thus the micelle-per-vesicle ratio is equal to the proteins-per-vesicle-ratio. Further details to the theory are given in [111]. Alternatively, one can obtain the proteins-per-vesicle-ratio by correlating the proteopolymersome solution with the AQP stock solution. Both correlation have advantages and challenges that are further described in the FCS subsection.

In characterizing biological material, SAXS is also an versatile tool because it gives structural information on particles in solution on a length-scale from 1 to 100 nm where data are presented as scattering intensity as a function of the magnitude of the scattering vector q. This quantity is independent of the particular geometry of the experimental set-up and directly related to the scattering angle 2θ as $q = 4\pi \sin(\theta)/\lambda$ where λ is the wavelength of the x-ray beam. Two scattering points separated by a distance d within a particle gives rise to interference showing up as increased intensity in the scattering curve at $q = 2\pi/d$. This means that large features are probed at low q while smaller details are probed in the high-q region of the curves. The strength, with which a particle scatters, its contrast, is proportional to its excess electron density, i.e. the difference between the electron densities of the sample and the solvent. The downside is that SAXS requires access to elaborated synchrotron radiation sources.

Here, we will exemplify SFLS, SDS-PAGE, FF-TEM, FCS and SAXS analyses with pro-

teopolymersomes of diblock copolymers of Table 3. PB-PEO was chosen because it showed functional AQP incorporation as discussed before and the M_n and f range is easier to control compared to PMOXA-PDMS-PMOXA. For SFLS, FF-TEM and SAXS, AqpZ is used as the incorporated membrane protein, where human aquaglyceroporin AQP10 tagged with green fluorescent protein (GFP) is used for the FCS experiments. Details are provided in the Materials & Methods section.

2.2 Materials & methods

Materials

Lipids and OG (Anagrade) were purchased from Avanti Lipids, Alabaster, USA. AqpZ (10 mg/ml in 20 mM Tris pH 8.0, 300 mM NaCl, 300 mM imidazole and 30 mM OG) was kindly provided from Aquaporin A/S. His-tagged AQP10-GFP (50 mM phosphate, 500 mM NaCl, 250 mM imidazole and 0.75 mg/ml 5-cyclohexyl-1-pentyl-β-D-maltoside (CYMAL-5) at pH 7.5) was kindly provided by Per Amstrup Pedersen lab. All other chemicals except PB-PEO were purchased from Sigma-Aldrich, Brøndby, Denmark and used as received.

PB-PEO synthesis

PB-PEO was synthesized as described before [257]. Briefly, all used polymers except PB_{46}-PEO_{32} were synthesized via a one-step anionic polymerization in tetrahydrofuran (THF) as solvent according to Förster [72]. Bd was polymerized with *n*-butyl lithium (*n*-BuLi) as initiator, where EO was polymerized using 1-*tert*-Butyl-4,4,4-tris(dimethylamino)-2,2-bis[tris(dimethyl-amino)-phosphor-anylidenamino]-2λ^5,4λ^5-catenadi(phosphazene) (tBuP4). The polymer was precipitated in cold acetone and analyzed via SEC (for PDI_M) and NMR (for stochiometry). PB_{46}-PEO_{32} was synthesized via two-steps after Hillmyer [70]. After Bd polymerization in the same way, the polymer was precipitated and brought back in solution for EO polymerization with potassium naphthalenide as initiator. Precipitation and analysis was done the same way. For stock solution, polymer was dissolved in chloroform at a concentration of 10 mg/ml and stored at -20°C until use.

Proteo- and polymersomes preparation via FR

2.5 ml of 10 mg/ml polymer stock was injected in a 5 ml round flask, evaporated on a rotary evaporator at room temperature (RT), 2 mbar and 125 rpm for at least 2 h to form an even film on the glas wall. For polymersome preparation, the film was rehydrated with 200 μl of Tris buffer (10 mM Tris pH 8.0, 50 mM NaCl) with 13 mg/ml OG, For proteopolymersome preparation, the film was rehydrated with AqpZ stock of a volume

to achieve the desired mPAR and Tris buffer with 13 mg/ml OG was added up to 200 μl. The sample was left stirring overnight at 4°C. Then the sample was diluted with another 800 μl of Tris buffer and 20mg biobeads were added to remove OG. After 3 h on a shaker at 200 rpm at RT, another 20 mg were added, whereafter the sample was left overnight shaking at 200 rpm at 4°C. The final polymer concentration was 25 mg/ml.

SFLS

SFLS was measured with a SFLSM-300 (BioLogic, Claix, France) with a Xe-Hg lamp. 1M NaCl with Tris buffer was used as osmotic agent. 3 ml of 3 mg/ml proteopolymersome and polymersomes was measured in a timeframe of 1.2 s during 8000 measurement points at an excitation wavelength of 365 nm at a flow rate of 12 ml/s. 9 traces were averaged with BioKine software. Analysis and normalization of curves was performed with Excel, fitting was performed again with BioKine software.

SDS-PAGE

Prior to SDS-PAGE, samples were extruded 20 times through PCTE membranes with 200 nm pore size. 200 μl of 25 mg/ml of proteo- or polymersomes were taken out and dialyzed at 4°C against 500 ml Tris buffer for 3 d in a Float-a-lyzer with 300 kDa molecular weight cut-off (MWCO) and 1 ml volume size, where the volume to 1 ml was filled up with Tris buffer. Tris buffer was exchanged every 12 h and every 3 h on the last day. 500 μl of the sample were mixed with another 500 μl Tris buffer, the other 500 μl were mixed with 500 μl Tris buffer and 100 mg/ml, respectively 300 mg/ml OG. The last solution was left stirring for 1 h at 4°C. The gel used was 3-12% Tris-Glycine from Invitrogen, Carlsbad, USA. After sample incubation at 37°C for 15 min, the sample was mixed 1:1 with Tris-Glycin SDS sample buffer. The final AqpZ concentration when injected on the gel was 0.651 mg/ml. SDS-PAGE was done at 125 V, 198 mA for 90 min. After staining on a shaker for 12 h, the sample was rinsed in MilliQ and left another 12 h shaking.

FF-TEM

FF was done with a MED020 with EM VCT100 shuttle attached (Leica, Wetzlar, Germany). A 3 mm aluminium sample carrier was filled with 1.2 μl of 25 mg/ml proteo- or polymersomes in its deeper pit with 300 μm depth. Another sample carrier was placed on top with the 200 μm towards the sample drop. The sandwich was shock-frozen by plunging it in liquid ethane. It was fixed in a sample holder under liquid nitrogen atmosphere and brought in a vacuum chamber at -140°C. There, the lower carrier with the 200 μm pit towards the sample was removed abruptly to enable a clean crack through the sample. The sample was coated with 2 nm carbon and 4 nm platinum at 45° tilting and 19 nm

backing layer without tilt. Outside the chamber, the replica was thawed for 5 min and placed carefully in a bath of 100 mg/ml OG to solubilize the thawed vesicles. The replica, swimming on the surface, was caught on a uncoated 400 Mesh copper TEM grid (Agar scientific, Essex, UK).
TEM was done on a CM100 (Philips, Amsterdam, Netherlands) with an Veleta 2k CCD camera (Olympus, Shinjuku, Japan). The applied voltage on a tungsten source was 80 kV with a 100 μm objective sense aperture.

FCS

25 mg/ml of proteopolymersomes were extruded 20 times through 200 nm pore sized PCTE membranes and just before measurement centrifuged at 10000 rpm for 10 min to remove any aggregates that could disturb the sensitive FCS measurements. FCS was performed with an Fluorescence lifetime imaging confocal microscope (PicoQuant, Berlin, Germany) with an excitation length of 482 nm and a laser pulse frequency of 400 MHz during 600 s. Proteopolymersomes were diluted to 10 nM GFP concentration. 20 μl of sample were set on a cleaned specimen glass. For optimal measurement, the confocal volume was focussed 20 μm inside the sample volume.

SAXS

Prior to SAXS measurements, 20 mg/ml proteo- or polymersomes were extruded 20 times through 200 nm pore sized PCTE membranes and centrifuged at 20000 rpm for 10 min to remove aggregates. Measurements were carried out at the beamline I911-4 at MAXLAB synchrotron in Lund, Sweden. The 2D detector images were radially averaged and background subtracted using the dedicated software at the beamline. Absolute intensity calibration to units of cm^{-1} was done using water as a scattering standard.

2.3 Results & discussion

SFLS

In order to exemplify an SFLS analysis, data for PB_{45}-PEO_{14} and PB_{33}-PEO_{18} diblock copolymer proteo- and polymersomes (meaning with and without AqpZ) is shown in Figure 23. For PB_{33}-PEO_{18} the rate constant associated with the increase in light scattering intensity was slightly higher with AqpZ, for PB_{45}-PEO_{14} it was even lower. This illustrates one of the major challenges in SFLS. The absence of a significant response to the change in extravesicular osmolarity could be due to an increase in the bilayer bending modulus induced by the presence of (non-functional or blocked) ApqZ. We observed similar problems in previous experiments with AqpZ and SoPIP2;1, where only the smallest

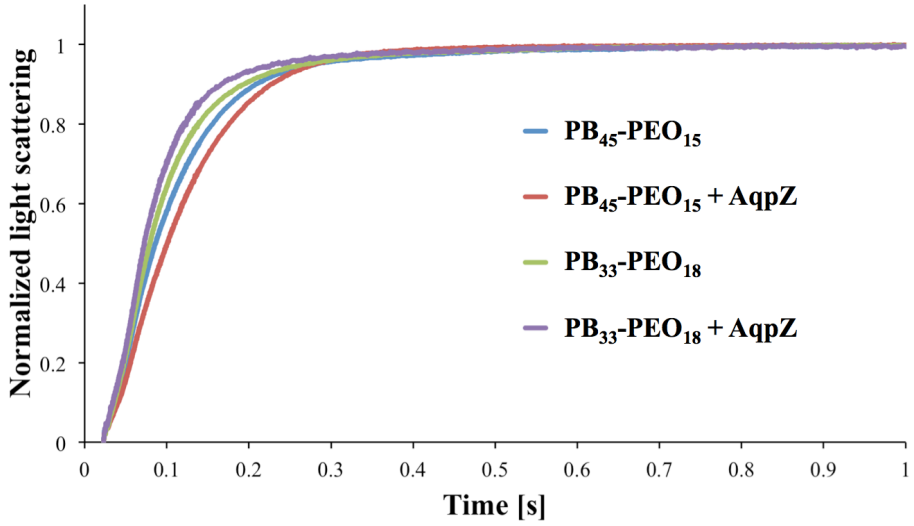

Figure 23: Normalized light scattering vs. time for proteo- and polymersomes of PB_{45}-PEO_{14} and PB_{33}-PEO_{18} at an mPAR of 1:100. For PB_{45}-PEO_{14} the apparent water permeability is slightly decreased for the proteopolymersomes versus polymersomes, whereas for PB_{33}-PEO_{18} it is slightly increased.

polymers (PB_{12}-PEO_{10} and PB_{22}-PEO_{23}) showed a significant difference in SFLS between proteo- and polymersomes (results not shown). Another reason for the similar SFLS signal might be the blockage of the AqpZ channels by PEO chains. In this case AqpZ would simply sit in the bilayer as an impermeable hydrophobic block, as suggested from Kumar et al. [50], because water permeation is blocked by the areas corresponding to the incorporated AqpZ, lower permeabilities of proteopolymersomes can be expected as compared to polymersomes. On the other hand the incorporated AqpZ could be fully functional but the polymer matrix is resistant to changes in volume. This underscores the notion that SFLS is not a stand-alone technique.

SDS-PAGE

SDS-PAGE did not give any reliable results. No characteristic bands of AqpZ tetrameters (~120 kDa), dimers (~60 kDa) or monomers (~30 kDa) could be observed on the gels, where proteopolymersomes (PB_{45}-PEO_{14}) were injected, solubilized in 100 mg/ml and later 300 mg/ml OG to ensure their solubilization (Figure 24 for 300 mg/ml OG). This could be due to OG that may induce polymer micelle aggregation, where AqpZ could be trapped. OG has a general tendency to aggregate amphiphilic molecules [258]. To remove AqpZ that is trapped in the proteopolymersome lumen, the sample was extruded and dialyzed later to remove all non-incorporated AqpZ or AqpZ polymer micelles. The smeared signal of the proteopolymersomes was significantly stronger compared to the polymersome sample that was given the same treatment. This would be a sign of AqpZ

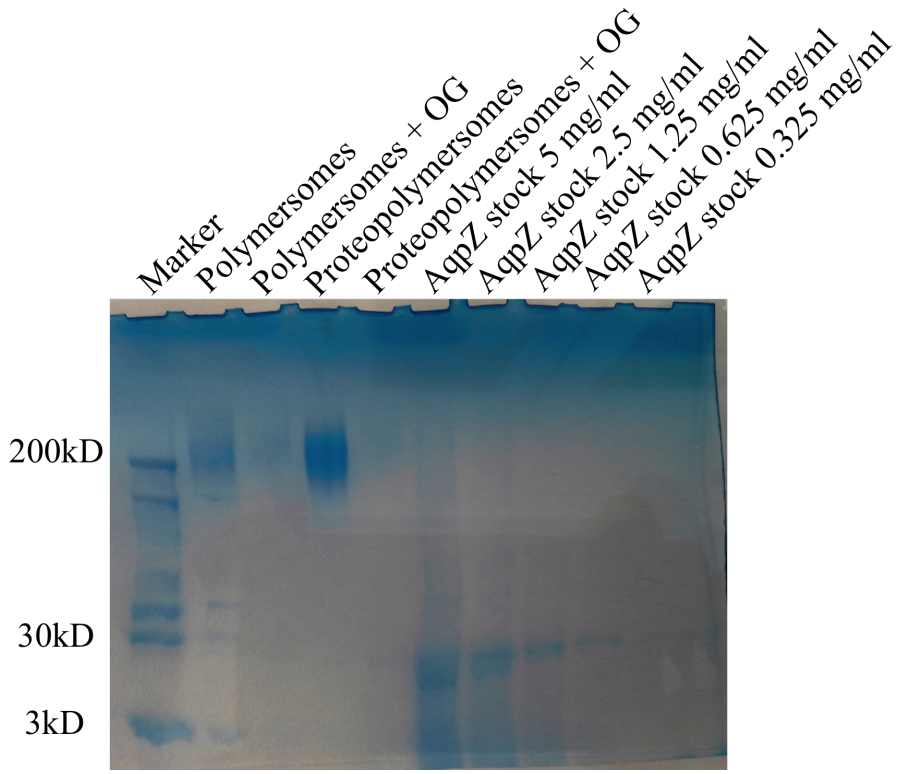

Figure 24: SDS-PAGE running gel of PB_{45}-PEO_{14} proteo- and polymersomes that has been treated with extrusion and dialysis. The first signals were in vesicular form, right next were the ones where they have been solubilized within 300 mg/ml OG. On the right hand are aliquots of AqpZ stock in several concentrations. The proteopolymersomes had a stronger signal than polymersomes, both signals fade out when the vesicles were solubilized.

incorporation. However, after adding OG, the signal vanished. Potentially, polymer micelles, including the trapped AqpZ, were interacting with the running gel. Other groups observed problems with Triton-X solubilized polymers on SDS-PAGE. Another possibility would be to try other protein characterization methods like Western blotting, or different detergents or running gels of varying concentrations, which was not possible within the time and resources of this project. However it is an interesting challenge for further research.

FF-TEM

Results of FF-TEM for PB_{45}-PEO_{14} proteopolymersomes are shown in Figure 25. Proteopolymersomes with an mPAR of 1:100 were produced using FR, frozen and fractured in a Leica MED20 station, where two planchets with frozen sample are separated, thus the fracture is more a ”crack” than a ”cut” thereby minimizing smearing effects from usual FF procedures (for details see supporting information). All proteo- and polymersome had a pronounced raspberry-like surface, potentially due to collapsed PB chains.

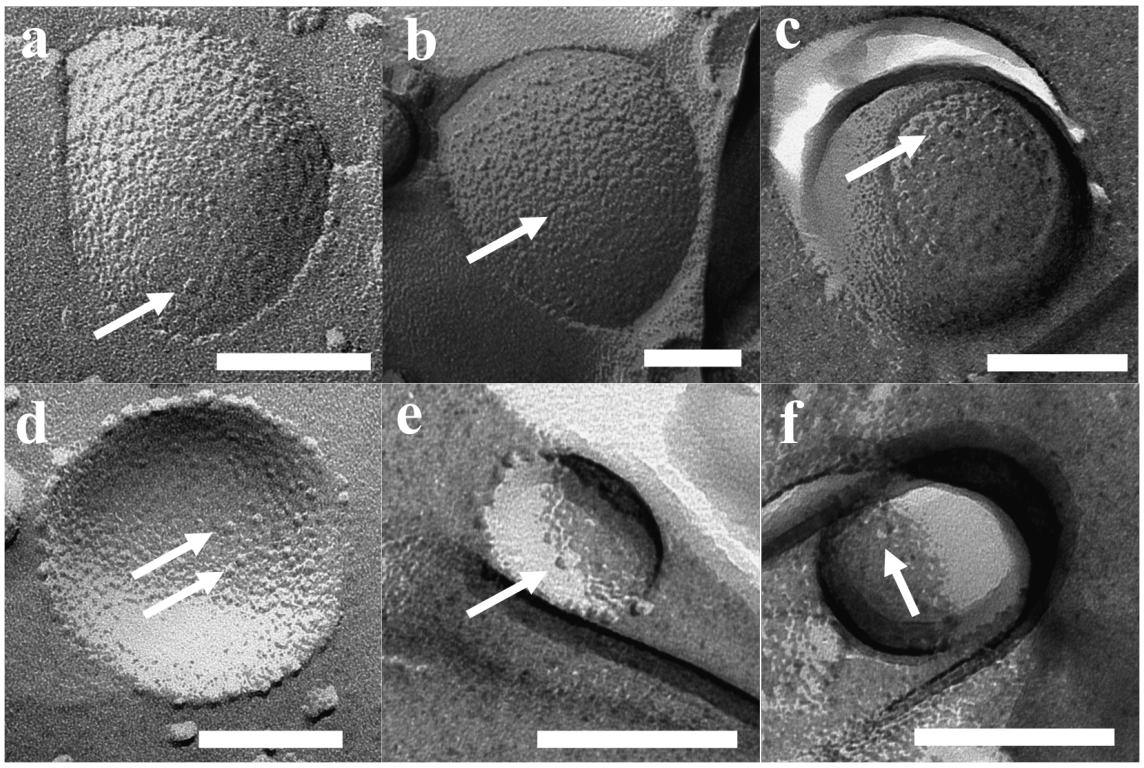

Figure 25: FF-TEM images of PB_{45}-PEO_{14} proteo- (b,c,e,f) and polymersomes (a,d). All vesicles revealed spots, potentially not from AqpZ but rather collapsed PB chains (a-c) or bad fracturing artifacts (d-f). Scale bar is 100 nm.

However, the 'typical' spots that have been claimed to be associated with AQP in a study on proteoliposomes[256] were not observed. In Figure 25 the bubble-like spots are distributed equally among polymersomes (Figure 25a+d) and proteopolymersomes (b,c,e,f). The spots could be either PB chain accumulations (Figure 25a-c) or artifacts due to bad fracturing (d-f). Proteo- and polymersomes of other PB-PEO polymers at other M_n and f showed similar behavior. It thus seems that FF-TEM sample preparation plays a major role in false positive results. Occasionally we observed dots all over the sample that were clearly not AqpZ, but potentially polymer micelles. These dots could be eliminated by omitting an upconcentration step and by carefully controlling temperature, sample and cutting handling or metal coating parameters (the optimized protocol is given in the supporting information). Even among the polymers with the shortest PB chains (PB_{32}-PEO_{30} and PB_{45}-PEO_{14}), we could not ascertain the presence of AqpZ. However, from these experiments alone we cannot exclude the possibility that AqpZ tetramers could be present as the hydrophilic PEO chains are still large compared to lipid head groups. Thus the AqpZ could be concealed in the PB core.

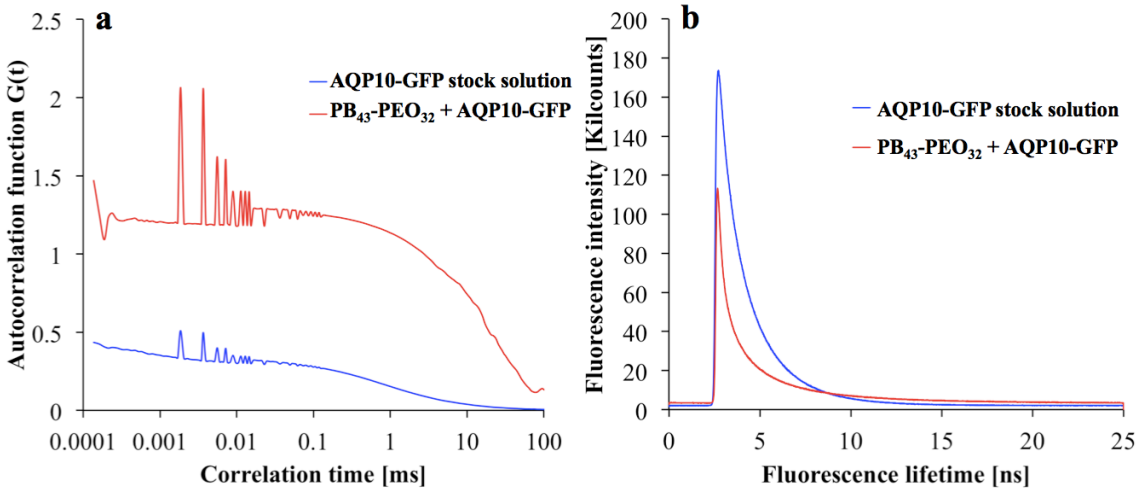

Figure 26: (a) Correlation diagram of proteopolymersomes and AQP10-GFP stock solution as a function of correlation time τ against autocorrelation function G(τ). The higher autocorrelation signal indicates a lower number of particles in the confocal volume, due to slower diffusion time. (b) Fluorescence lifetimes of the same samples as a function of lifetime against intensity signal. Where the intensities varied, the fluorescence lifetime was in a comparable range.

FCS

As both SFLS and FF-TEM present challenges as tools for evaluating protein incorporation into polymersomes we also evaluated FCS as a novel method for getting quantitative information about AQP incorporation. This was inspired by a recent paper by Erbakan et al. describing various AqpZ isoforms, tagged with a fluorophore in proteoliposomes, where the protein-per-vesicle ratio was determined and further substantiated using SFLS [111]. Initially we attempted to reproduce the proteoliposome experiments described in [111]. At a mPAR of 1:200, our measurements revealed a proteins-per-vesicle-ratio of 5.35, which was comparable to the ones obtained in Erbakan et al. (around 7.5). The difference could be due to the different AQP and tagged fluorophore used.

After having optimized the FCS instrument parameters for proteopolymersomes (for details please refer to the supporting information), we performed FCS on proteopolymersomes of PB_{45}-PEO_{14} (mPAR 1:100) with AQP10-GFP and with OG-solubilized protein micelles. The results are shown in Figure 26. We obtained a higher species number in the proteopolymersomes sample than in the protein micelle sample. This could be due to the same OG-induced aggregation. We therefore decided to correlate the proteopolymersomes to the AQP10-GFP stock. Erbakan et al. could not do this, because the fluorophore used (mBanana fluorescent protein) exhibited a decreased fluorescence lifetime in pure OG environment (stock solution) compared to lipid/OG environment (solubilized protein micelles). GFP however did not seem to alter fluorescence lifetime significantly whether the AQP10-GFP is in OG (1.8 ns) or polymer/OG environment (1.97 ns, Figure 26b).

They are comparable to fluorophore used by Erbakan et al. (4 ns [111]) and to standard GFP fluorescence lifetime (3 ns [259]). The difference between our GFP fluorescence lifetime and the standard one could be due to shielding of the attached AQP10 and the OG environment, as well as to the fitting algorithm of the instrument.

Accordingly it depends on the single components of the system which samples correlates the best. In the case of sensitive fluorophores it is better to compare AQP vesicles and AQP micelles not to influence the fluorophore environment. In the case of polymers as the protein matrix it is better to correlate the AQP-fluorophore stock solution as the polymeric AQP micelles aggregate easily. A disadvantage of correlating AQP-fluorophore stock with AQP vesicles is that the final concentration of AQP is not known complicating a correlation with similar AQP concentration.

Calculating the species number of pure AQP10-GFP from the stock in the confocal volume and the one from the proteopolymersome solution (Figure 26a), we obtained a proteins-per-vesicle-ratio of 2.87. These results demonstrate that FCS can serve as a tool to quantify AQPs in proteopolymersomes. This opens possibility for conducting a systematic study in which f and M_n are varied in order to obtain quantitative information about which polymers can be used to achieve the highest proteins-per-vesicle-ratio.

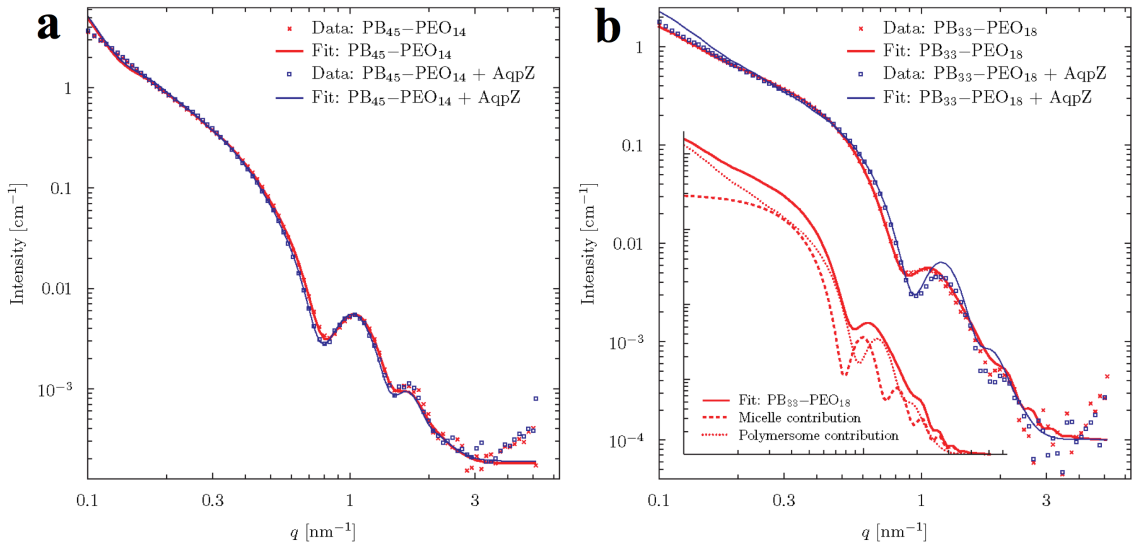

Figure 27: SAXS data for proteo- and polymersomes of (a) PB_{45}-PEO_{14} (left) and (b) PB_{33}-PEO_{18} (right). The fits were obtained using a vesicle model consisting of three concentric spherical shells. To fit the polymersomes of PB_{33}-PEO_{18} it was necessary to include an additional contribution from block-copolymer micelles as shown in the insert.

SAXS

Scattering curves for FR prepared proteo- and polymersomes of PB_{45}-PEO_{14} and PB_{33}-PEO_{18} are shown in Figure 27. The samples were extruded and centrifuged prior to measurements. At low q-values a typical linear slope is observed in the log-log plot, with the

intensity following a power law of q^{-2}. This behaviour is typical of flat laminar structures. The fact that the slope extends below the lowest detectable q-region indicates a low curvature (flat structure) even on the largest detectable length scale of $q = 2\pi/0.1$ nm $\approx$ 60 nm. At higher q a characteristic oscillatory behaviour is observed. This is attributed to the complex interference between the negative contrast of PB and the positive contrast of PEO.

The theoretical scattering from various simple geometrical objects such as spheres, cylinders and ellipsoids of varying contrast can readily be calculated. These can be combined to form simplified models of the studied particles. We choose to analyze the data using a vesicle-model consisting of three concentric spherical shells of alternating contrast. The thickness of the individual shells was varied to give the best fit to data using a least squares fitting routine.

Excellent fits were obtained for the PB_{45}-PEO_{14}-system meaning that data are in good agreement with the assumption that the diblock copolymers form spherical vesicles. The fits were especially sensitive to changes in the parameter determining the thickness of the central hydrophobic bilayer constituted by the PB-groups. These were fitted to 9.10±0.1 nm and 8.94±0.07 nm in the presence or absence of AqpZ respectively. Concerning the overall vesicle diameter we can conclude from the model that it is larger than 60 nm which is not surprising given the initial analysis above. It is evident from the data and the fit parameter values that well defined bilayer vesicles are formed and that the incorporation of AqpZ introduces only minor differences to the structure of the vesicles.

For the PB_{33}-PEO_{18} proteopolymersomes reasonably good fits were obtained with the vesicle model with a hydrophobic bilayer thickness of 7.66±0.05 nm. However for the polymersomes no fit to the data gave reasonable physical parameters. The data fit required the assumption that a population of block copolymer micelles co-exists with the vesicles. The combined model fit showed that 76 wt% of the population consisted of proteopolymersomes and 24 wt% were micelles with a hydrophobic core of diameter 11.7±0.3 nm gives a good fit with the data. The insert of Figure 27b shows the separate vesicle and micelle contributions.

SAXS analysis reveals that for PB_{45}-PEO_{14} vesicles are formed both with and without AQP where AQP incorporation leads to a minor differences in average hydrophobic vesicle wall thickness, which could indicate a dimpling or puckering of polymers close to the incorporated AQPs. In the case of PB_{33}-PEO_{18} some micelle-formation is observed, but this tendency is reduced when AQP is incorporated.

To summarize, the functional incorporation of AQPs in PB-PEO diblock copolymers with regard to the molecular parameters M_n and f was investigated. The main methods were

FF-TEM and FCS, where SDS-PAGE (AQP presence), SFLS (AQP functionality) and SAXS (Proteopolymersome bilayer properties) were used to substantiate the findings. Both, proteo- and polymersomes had spots, when observed with FF-TEM, so the differentiation of AQPs from artifacts is a challenge for this method. SAXS showed that the incorporation of AQPs in a polymersome bilayer changed its property to a more smooth and well-defined shape. FCS looks as a promising alternative to FF-TEM, where first incorporations of AQP in a small PB-PEO polymer showed an protein-to-vesicle-ratio of 2.78. Due to time restrictions of the project and lack of further AQP10-GFP, the systematic study with all PB-PEO polymers of Table 3 could not be finalized, however this could be an interesting challenge for future research.

3 Polymersomes I: Molecular parameters

This chapter has been submitted. In this online version of the thesis, the submitted manuscript is not included but can be obtained from electronic article databases e.g. via www.orbit.dtu.dk or on request from DTU Environment, Technical University of Denmark, Miljøvej, Building 113, 2800 Kgs. Lyngby, Denmark, info@env.dtu.dk.

4 Polymersomes II: Formation and modification methods

This chapter has been submitted. In this online version of the thesis, the submitted manuscript is not included but can be obtained from electronic article databases e.g. via www.orbit.dtu.dk or on request from DTU Environment, Technical University of Denmark, Miljøvej, Building 113, 2800 Kgs. Lyngby, Denmark, info@env.dtu.dk.

5 Polymersomes III: Analysis methods

This chapter has been accepted at RSC Advances. In this online version of the thesis, the accepted manuscript is not included but can be obtained from electronic article databases e.g. via www.orbit.dtu.dk or on request from DTU Environment, Technical University of Denmark, Miljøvej, Building 113, 2800 Kgs. Lyngby, Denmark, info@env.dtu.dk.

6 Interplay of AQPs, block copolymers & polymer membranes

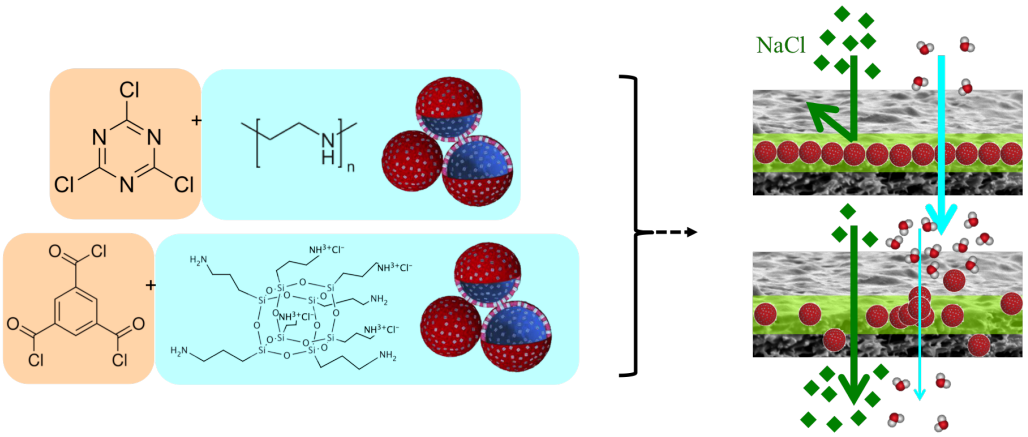

Figure 28: Schematic sketch of methodology. Depending on varying parameter during the integration of protoepolymersomes in an AL, the resulting membrane performance, exemplified at water flux and NaCl rejection, will be investigated.

Parts of this chapter have been published in [1]

6.1 Introduction

Nearly all RO and FO membranes are PA-based, often referred to as TFC membranes due to their superior performance compared to other membrane designs. An AL made of PA is generally generated by a reaction between an amine and an acyl chloride [204]. This reaction can be prepared by dissolving the amine group in an aqueous phase, and the acyl chloride group in an organic phase [260]. This principle is called interfacial polymerization and was first introduced in the 60's by Emerson et al.. The amine group is usually dissolved in the aqueous phase, where the acid chloride group is dissolved in the organic phase. Interfacial polymerization was brought into membrane technology by John Cadotte from FilmTec (now Dow Chemical) also in the 60's. Typically a membrane is wetted with the aqueous phase, containing the amine group and dried a little to remove visible liquid while keeping the surface moist. Then the organic phase with the acyl chloride group is added on top. The reaction growth is believed to be directed into the organic phase [261], due to a preferential solubility of the amine group in the organic phase compared to the solubility of the acyl chloride in the aqueous phase. This results in the well-known ridge and valley form of an AL, shown in chapter 1.5. The standard amine-acyl chloride combination is MPD and TMC, and typically these are supplemented

with additives (molecules with similar chemistries) in low concentrations to improve flux, rejection or chlorine resistance [204].

The ideal AL of a PA membrane for water separation has to be highly water permeable, while rejecting all other solutes and being resistant towards cleaning. An ideal AL of an ABPM could even be water impermeable if it enables sufficient integration of proteopolymersomes in such a way that water only passes the incorporated proteins. Therefore we explored novel AL components. An AL with homogenous thickness could facilitate such proteopolymersome integration.We elaborated two AL linker couples for their potential use for the integration of proteopolymersomes in ABPMs: Polyhedral oligomeric silsesquioxane (POSS, amine linker) & TMC and PEI (amine linker) & Cyanuric chloride (CC, chloride acid linker). All chemical structures are given in Figure 29. POSS is a well-defined nano-scale organic–inorganic structure that allows for constructing nanostructured hybrid materials and nanocomposites. With respect to membrane technology POSS has been investigated in terms of creating membranes for molecular separation at elevated temperatures [262] and membranes with anti-fouling properties [263]. However, it is not clear if POSS is compatible with proteopolymersome incorporation. In a recent study POSS has been introduced as an AL layer components and POSS-TMC-layer exhibited a well-defined layer without ridges and valleys but with high mechanical stability on PAN membranes [264]. This may be a better platform for the integration of proteopolymersomes compared to the ridge-and-valley MPD-TMC network. PEI and CC reacts to a polyamine layer on UF PES that is less sensitive to extreme pH conditions. Furthermore, the thickness of this AL can easily be tuned by varying the concentration of PEI [265], which is another practical feature for ABPMs.

We prepared PA, respectively polyamine layers in the case of PEI+CC (hereinafter referred to as AL) of POSS+TMC AL with polymersomes of PB_{29}-PEO_{16} in the aqueous phase, as well as PEI+CC AL with proteopolymersomes of AqpZ and PB_{45}-PEO_{15} (mPAR 1:100) in the aqueous phase. For the microfluidic approach (described later) of all AL we used proteopolymersomes (AqpZ, PB_{33}-PEO_{18}, mPAR 1:100). We selected PB_{29}-PEO_{16} due to its ability to form large amounts of stable polymersomes in aqueous phase compared to other PB-PEO polymersomes ([257], respectively chapter 3). PB_{45}-PEO_{15} and PB_{33}-PEO_{18} form large amounts of stable polymersomes in aqueous phase as well and showed successful AqpZ incorporation as evidenced by SAXS ([1], respectively chapter 2). We used MilliQ water as the aqueous phase and hexane as organic phase and in order to achieve the lowest possible polydispersity, polymersomes were sonicated resulting in 95% of the polymersomes with a diameter of 196±83 nm as determined by DLS.

We produced a non-supported AL by simply adding both phases after another in a beaker and an AL supported by MF PES layers using different coating procedures (for details see

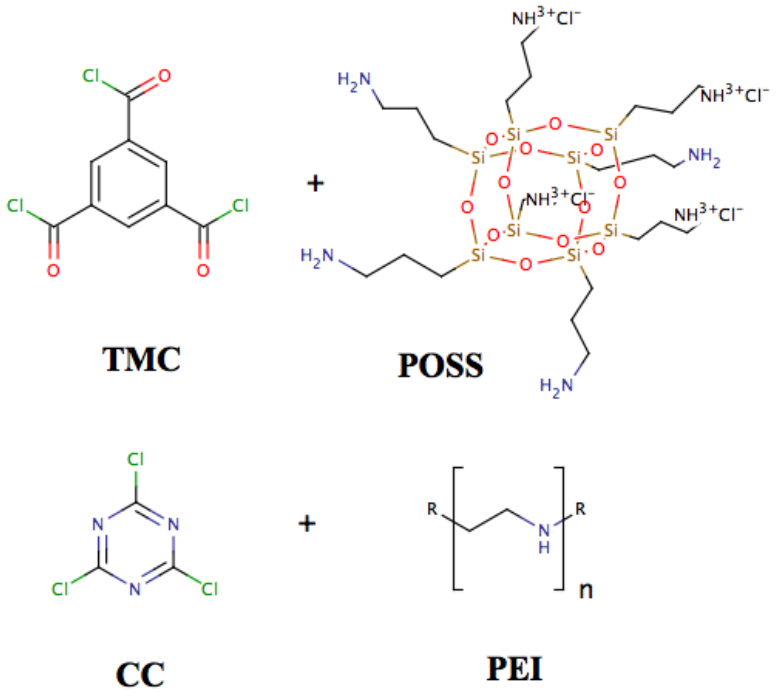

Figure 29: Chemical structure of novel AL linkers used for ABPM generation. POSS as the amine linker generate a highly stable and well-defined AL with TMC, where PEI (amine linker) and CC (acid chloride linker) forms a pH resistant polyamine layer that can be varied easily in thickness with PEI concentration.

Material & Methods). Characterization of the non-supported AL was done using FTIR, SEM and a novel, recently published microfluidic approach that allows for direct monitoring of the polymerization process [266]. Characterization of the supported AL was also achieved via FTIR and SEM, where it was also tested for functionality using standard flux and rejection test in FO mode and methylviolet staining.

6.2 Material & methods

Materials

MF PES and AqpZ in 10 mg/ml in 20 mM Tris pH8.0, 300 mM NaCl, 300 mM Imidazole and 30 mM OG) was kindly provided from Aquaporin A/S, Copenhagen, Denmark. PB-PEO was synthesized as described before [257]. Briefly, PB was polymerized within *n*-BuLi as initiator and EO within tBuP4 as initiator with dried THF as the solvent. The complete polymer was precipitated in acetone and analyzed via NMR (stochiometry) and SEC (PDI_M). The solid was dissolved in chloroform at 10 mg/ml and stored at -20°C until use. POSS was purchased from Hybridplastics, Hattiesburg, USA. OG (Anagrade)

was purchased from Avanti Lipids, Alabaster, USA. All other chemicals were purchased from Sigma-Aldrich, Denmark or Netherlands.

Proteo- and polymersomes preparation via FR

Polymerstock was injected in a round flask and evaporated at RT at approximately 125 rpm for several hours. For polymersome preparation, the film was rehydrated with Tris buffer (10 mM Tris pH 8.0, 50 mM NaCl) with 13 mg/ml OG, for proteopolymersomes the film was rehydrated with AqpZ stock and Tris buffer with 13 mg/ml OG and left stirring for 12h at RT. Then, four times the rehydration volume of Tris buffer was added to end up at a polymer concentration of 25 mg/ml. At the same time, 20 mg per ml solution was added and the sample was left shaking for 3 h at RT and another 12 h at RT after addition of another portion of the same amount of biobeads. The sample was sonicated for 5 min.

DLS

DLS was performed on a Nano Zetasizer (Malvern, Worcestershire, UK). 1 ml of 25 mg/ml polymersomes were introduced in a cuvette and measured 3*6 times for 10 s.

Non-supported AL formation

The polymersome sample was sonicated for 5 min. Approximately 20 ml of aqueous phase (9 g/l POSS adjusted with 1M NaOH to pH 9.5 in MilliQ with 0.4 g/l polymersomes if they were present) was poured in a beaker. Afterwards 20 ml of organic phase (0.5 g/l TMC in n-hexane) was added carefully. After 5 min, the AL was collected with a small spoon or a spatel and put on a petri dish to air dry and later in the vacuum oven to dry at 50°C for at least 12 h.

Formation of supported AL containing POSS and TMC

Supported ALs containing POSS and TMC were processed following Dalwani et al. [264]. A perforated metal frame with an effective area of 13.86 cm^2 was taped with double sided tape. A cellulose-based highly porous support was placed on top. Another layer of tape was put and the MF PES was set on top with the dense side up. This sandwich was connected to a vacuum pump and placed in a bath with 0.5 g/l SDS in MilliQ to wet the membrane. This solution was then soaked throught the MF PES at 0.5 bar pressure for 10 min. The frame was then placed in another batch containing the aqueous phase (9 g/l POSS adjusted to pH 9.5 using 1 M NaOH in MilliQ, if they are present 0.4 g/l polymersomes), whereafter it was again soaked for 10 min at 0.5 bar. It was then put in the organic phase (2 g/l TMC in n-hexane) and allowed to react for 5 min (no vacuum soaking). The

frame was removed from the bath and leftover TMC was rinsed with n-hexane. For J_v and J_s testing, the membrane was placed in a parafilm-taped petri dish with MilliQ until use. For FTIR and SEM characterization, a piece was cut out and vacuum dried at 50°C for 12 h.

Formation of supported AL containing PEI and CC

Supported ALs containing PEI and CC were processed according to Lee et al. [265]. MF PES was placed on a steel plate with an effective area of 96 cm^2 and tightened with an O-ring. The suction cell was connected to a vacuum pump. 100 ml of 0.5 g/l SDS in MilliQ was poured on the MF PES and soaked for 10 min with 0.5 bar pressure. The remaining solution was drained and 100 ml of the aqueous phase (1.25 g/l PEI in MilliQ, if they are present 0.4 g/l proteopolymersomes) was poured into the cell, followed by another 10 min soaking at 0.5 bar and draining afterwards. The cell was clamped vertically and air dried until the top film became dim. Finally, 50 ml of the organic phase (0.5 g/l CC in hexane) were added and allowed to react for 30 s. The organic phase was drained and the membrane rinsed with 20ml of hexane. Preparation for different characterization was done like for supported AL containing POSS and TMC.

FTIR

FTIR was performed on a Tensor 27 (Bruker, Billerica, USA) on a ZnSe crystal at RT. For each sample, an average of 32 scans per measurement were taken. Further analysis was done using Excel.

SEM

SEM analysis was performed on a JSM-6010LA (JEOL, Tokyo, Japan) with 5 kV electrons from tungsten source and a working distance of 10 mm.

Microfluidic approach

The microfluidic approach was performed like described in Zhang et al. [266]. The chip was produced on a silicon wafer by photolithography and ion etching and bonded to a glass wafer. The inner walls of the compartments were chemically hydrophobized using silicon oil. The chip was placed in a self-made holder with reservoir connections. The aqueous phase (9 g/l POSS pH 9.5, 0.4 g/l polymersomes in MilliQ) was introduced within applying a pressure of 2400 Pa. The organic phase (0.5 g/l TMC in hexane) was then introduced with a minimal introducing pressure. To allow AL formation without pressure differences, all connections were opened after introduction of both phases. The

AL formation was monitored with a AxioCam MRc 5 camera that was connected to a Axiovert 40 optical microscope (Carl-Zeiss, Jena, Germany).

J_s and J_v testing of supported AL

The supported AL, as well as the AIM was tested for J_v and J_s using an own-built measurement system for two parallel measurements. A small chamber (3.92 cm^2 for supported AL containing POSS and TMC) was connected with hard plastic tubes to the draw solution (1 L 1 M NaCl in MilliQ) on a balance and the feed solution (1 L MilliQ) as well as to the pumps. The speed velocity was set to 10ml/min in cross-flow mode. The membrane in the chamber was placed with AL up (FO mode). Weight increase and conductivity was measured manually approximately every 15 min for at least 2 h or longer if there was a reasonable weight increase of the draw solution. Further analysis was done with Excel.

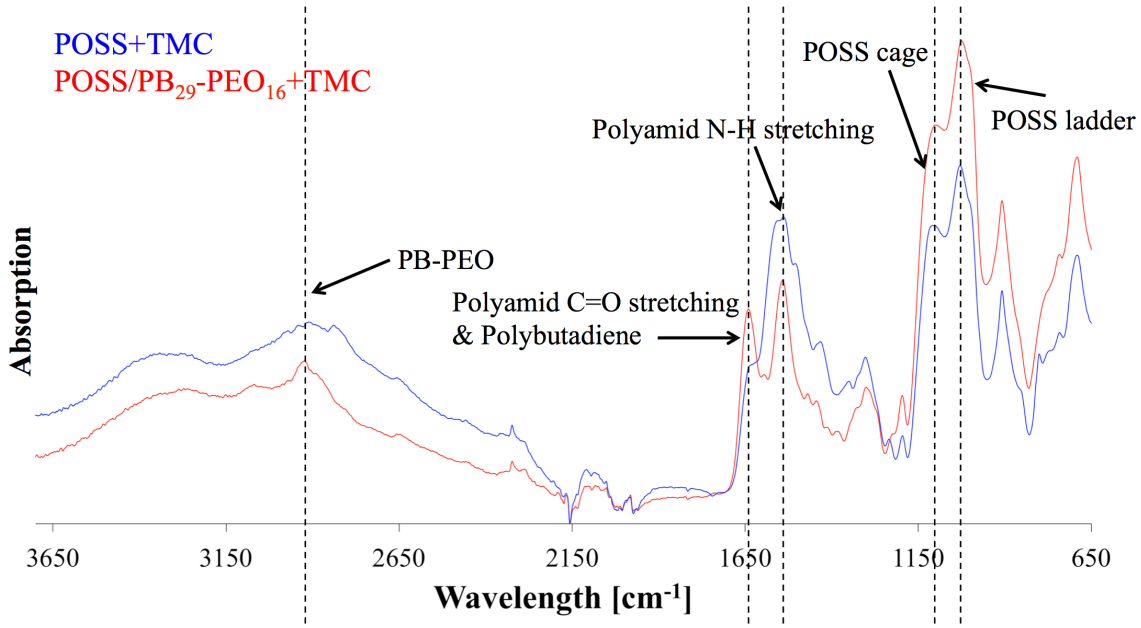

Figure 30: FTIR diagram of POSS/polymersomes+TMC AL (labelled red) and POSS+TMC control AL (labelled blue) as a function of wavelength against absorption. The AL with polymersomes had an absorption peak around 3000 cm^{-1}, that responds to PB and PEO, indicating their presence in the AL, where the characteristic absorption peaks for PA bonds and POSS were present as well.

6.3 Results & discussion

Non-supported POSS/polymersomes+TMC AL

After adding both phases, pieces of the formed (non-supported) AL were air dried then vacuum-dried where they crumbled to flake-like structures. FTIR analysis of POSS+TMC

with addition of polymersomes revealed the presence of block copolymers in the AL, see Figure 30. AL with polymersomes had an absorption peak around 3000 cm^{-1} (C-H stretch), which can also be found in spectra of PB and PEO [267, 268]. The polymersome-free AL exhibited a broad peak at that wavelength range but not a distinct maximum as for the polymersome-containing AL. This could indicate a successful polymersome integration in the AL. Polymersomes furthermore did not seem to block AL formation, because the characteristic peaks of a PA bond, the C=O stretch at 1636 cm^{-1}, as well as the N-H stretch at 1545 cm^{-1} [264] were clearly visible in the AL with polymersomes. Finally partial hydrolysis of the POSS leading to the AL formation is not substantially affected by the presence of the polymerosomes as far as the characteristic peaks for the POSS-cage and ladder (1125 cm^{-1} and 1040 cm^{-1} [264]) were present in both AL. There was however an apparent influence of the polymersomes on TMC reactivity. Originally, Dalwani et al. used 2 g/l TMC for their non-supported and supported AL [264]. In our case we could not form a non-supported AL with 2 g/l but with 0.5 g/l TMC. Potentially the TMC-POSS-stochiometry was artificially increased by the presence of another species in the aqueous phase. An excess of TMC could hinder network structure formation, because TMC will not connect POSS cages, resulting only in low molecular weight networks. We used 0.5 g/l TMC for the non-supported POSS+TMC AL and POSS/polymersomes+TMC AL.
The FTIR results were complemented with SEM analysis of the same samples, see in Figure 31. The POSS+TMC AL appeared smooth and well-defined, in agreement with previous work [264], see Figure 31a+b. When polymersomes were added (Figure 31c-e) a clear distinction can be made between the side towards the organic phase, that does not reveal presence of polymersomes (Figure 31c) and the side that faced the aqueous layer, which is well-covered with polymersomes (Figure 31e).
Most of the polymersomes seemed to sit loosely on top of the AL, whereas some polymersomes seemed to be covered to a certain extent by the AL: their shape less sharp than the others (indicated by the dotted circles in image d). A few polymersomes were directly embedded inside the AL, visible from its cracked profile (arrows in Figure 31d). This could indicate that the POSS approach can be used to embed polymersomes in such a way that they would be suitable for membrane fabrication.

Non-supported PEI/proteopolymersomes-CC AL

Experiments with PEI+CC did not succeed as good as POSS+TMC for the non-supported AL. We used proteopolymersomes (AqpZ & PB_{45}-PEO_{15}), as far as none the supported POSS+TMC or POSS/polymersomes+TMC did show a good membrane performance but the PEI/proteopolymersomes+CC did. However the non-supported layer was much more fragile and difficult to remove from the liquid. Flakes of non-supported PEI/proteopolymer-

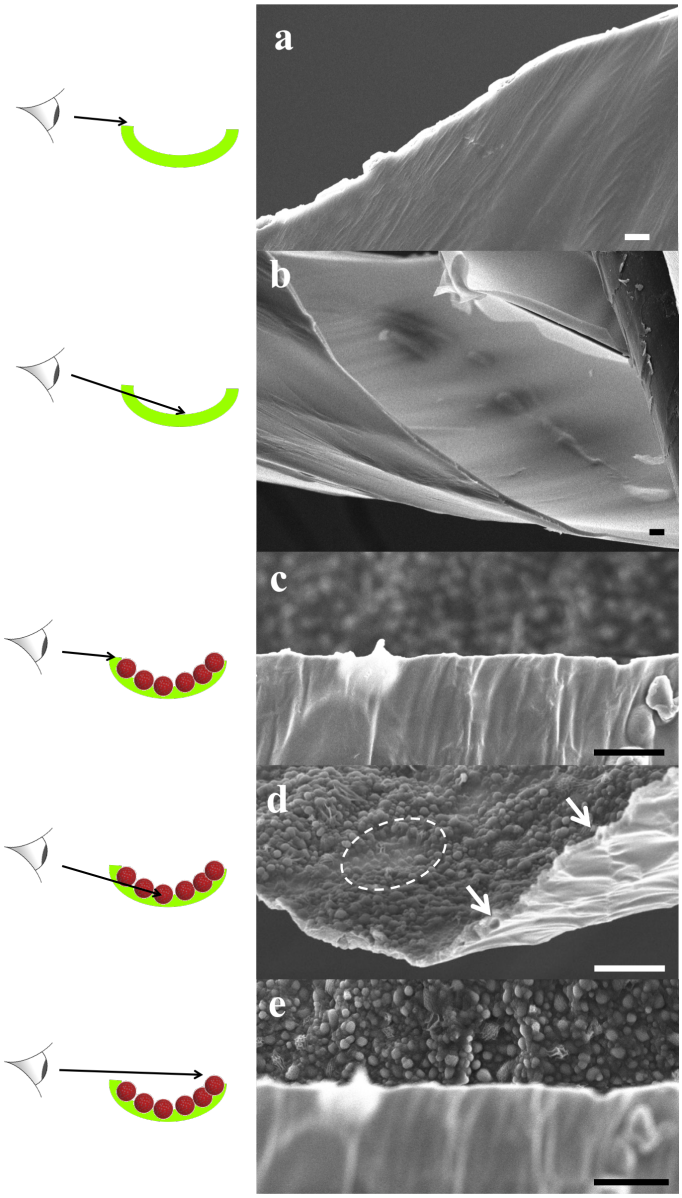

Figure 31: SEM images of POSS+TMC AL (a+b) and of POSS/polymersomes+TMC AL (c-e) with schematic sketches, which part of the layer is being captured. Images were taken from different parts of the flakes (labelled green in the sketch) of the AL, that were generated during the SEM preparation. The AL without polymersomes was smooth and well-defined, which remained on the organic side when polymersomes were added. The aqueous side was covered with loosely attached and half-covered polymersomes (dotted circle in image d). A few could be observed inside the AL (arrows in image d). Scale bar is 3 μm.

somes+CC were too small and brittle to be measured by FTIR. All our measurements on this AL only resulted in a signal close to zero without any peaks. Thus, we could only analyze the non-supported PEI+CC AL alone. At least we could prove that the linkers were still functional, as far as they had not been used for a while. From Figure 32 we could deduct that the AL was formed, however only to a small extent. The tertiary amine

bond of polyamine has an absorption peak at 720 cm^{-1}. There was a weak signal at this wavelength for the non-supported PEI+CC AL, as well as a absorption peak at 1480 cm^{-1} that is characteristic for PEI [265].

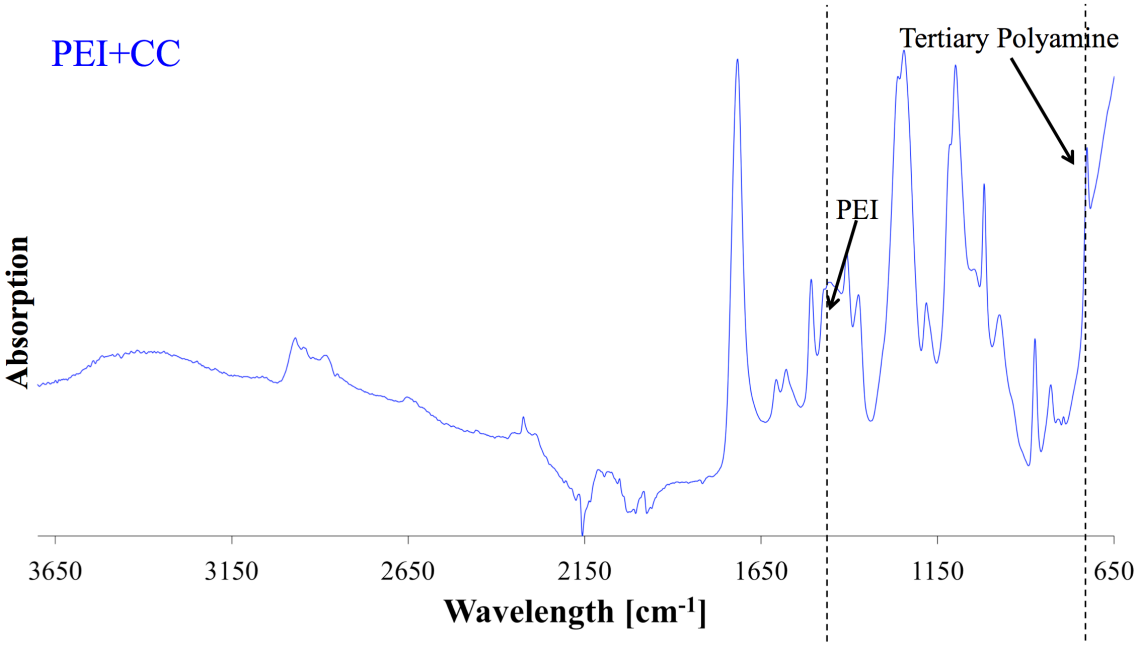

Figure 32: FTIR diagram of non-supported PEI+CC AL. Flakes of the non-supported PEI/proteopolymersomes+CC were too fragile to be investigated. Characteristic peaks for polyamine and PEI were observed, however they were not strong.

SEM revealed similar problems. The fragile flakes were mainly collapsed, so it was difficult to obtain any information on the AL profile. As shown in Figure 33a-c, the thickness of the non-supported PEI-CC was very small, where both sides of the AL were rather rough, possibly due to deformation during the drying process. As mentioned before, flakes of the non-supported PEI/proteopolymersomes+CC AL were too small to achieve a FTIR signal, however we could look at both the surfaces facing the organic phase (d) and the aqueous phase (e). This side was not covered with proteopolymersomes as in the case of POSS+TMC, but some single proteopolmyersomes could be seen, shown with arrows in Figure 33e, a few again covered. However there were holes in the layer as well. If there was proteopolymersome integration in the non-supported PEI+CC AL, it was at a far lower loading than non-supported POSS+TMC.

Recently, a novel approach from the microfluidic field was published [266] that allows visual study of the evolution of the location of interfacial polymerisation reactions. This involves a chip containing a hydrophobized micro-chamber that is separated in two compartments by an array of micro-pillars each with a diameter of 30 μm and a height of 50 μm. The aqueous phase with amine linker was introduced via micro capillary connec-

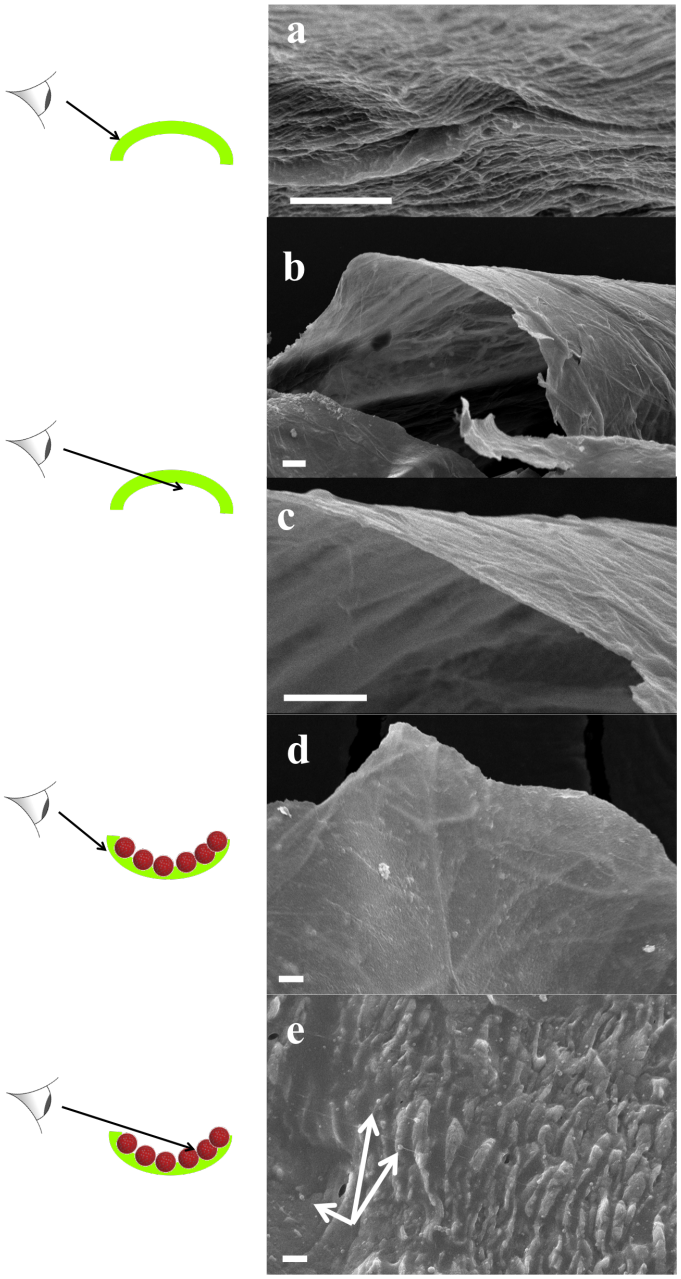

Figure 33: SEM images of the non-supported PEI+CC AL (a-c) and of the non-supported PEI/proteopolymersomes+CC AL (d+e) with schematic sketches, which part of the layer is being captured. AL flakes were more fragile and the surface of the empty non-supported AL less smooth than in the case of POSS+TMC. Integration of proteopolymersomes was at far lower rates, if at all. The side facing the aqueous phase revealed a few small proteopolymersomes, where a fraction of them could be covered. Scale bar is 3 μm.

tions into one compartment and formed a water-air-interface between the pillars. Then the organic phase with acyl chloride linker was introduced into the other compartment. AL formation at the interface between the solutions was observed using an optical microscope. Depending on the linkers, the resulting AL will have a different morphology and

formation time. POSS+TMC forms well-defined AL with a formation time within 4 s. In contrast, for instance the apparent growth of a film from Jeffamine+TMC is not finalized after 15 min and the film reveals the ridge and valley structures that are typical for AL formed by interfacial polymerization [266].

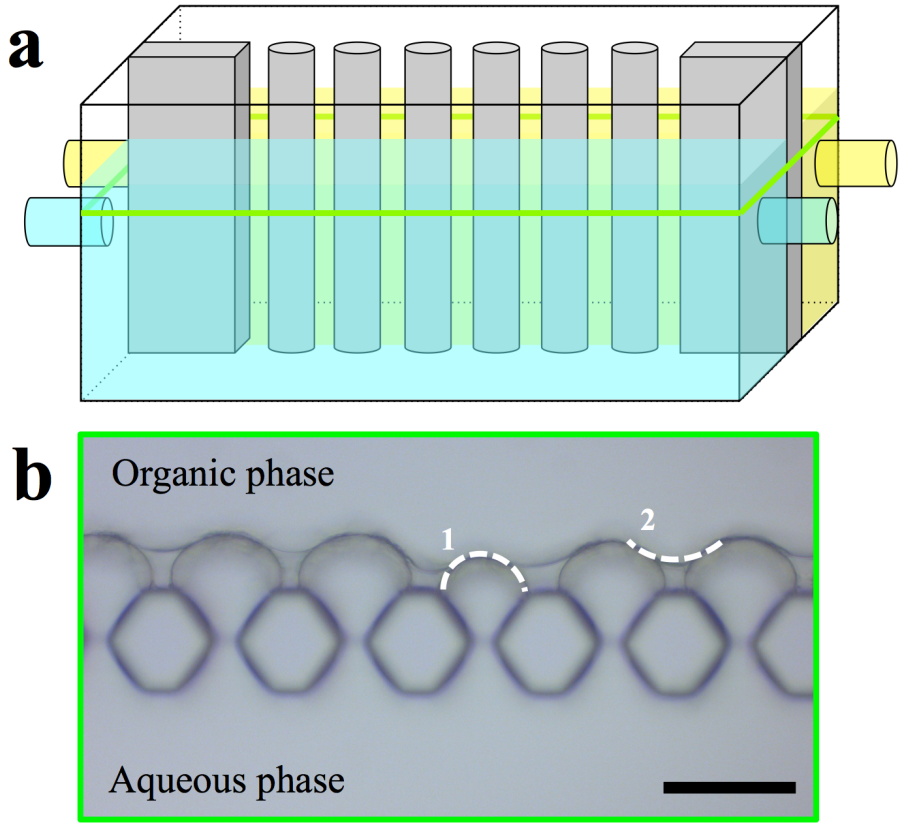

Figure 34: a) Schematic sketch of the microfluidic chamber and micrographs of POSS/proteopolymersomes+TMC AL and (b) micrograph of the compartment. The aqueous phase reached into the other compartment. After introducing the organic phase, a well-defined AL formed. Scale bar is 50 μm.

We used this approach to monitor POSS/proteopolymersomes+TMC AL (AqpZ & PB_{33}-PEO_{18}, mPAR 1:100), see Figure 34. The chip that was used was not hydrophobized optimally, which resulted in partial infusion of the aqueous phase into the channel with the organic phase. The hydrophobization was still sufficiently efficient to hinder the aqueous phase from passing entirely to the other compartment. Other reasons for the shift of the interface from the pillar structures to the organic phase could be overpressure from the aqueous phase, which is hard to control since the offered pressure is in the range of 10^4 Pa. When the organic phase containing TMC was introduced, the typical sharp AL was formed at the aqueous-organic interface (Figure 34b dotted line 1). After that, the reaction was continued by the diffused amine into the organic phase and the formed AL that connected the initial interfaces, exhibited a new aqueous-organic inter-

face (Figure 34b dotted line 2). Such observation demonstrates a less denser AL formed by POSS/proteopolymersomes-TMC compared to that formed by POSS-TMC reaction. The formation time was on the order of seconds. The film remained in the same shape and no further growth was observed in the following 12 h.

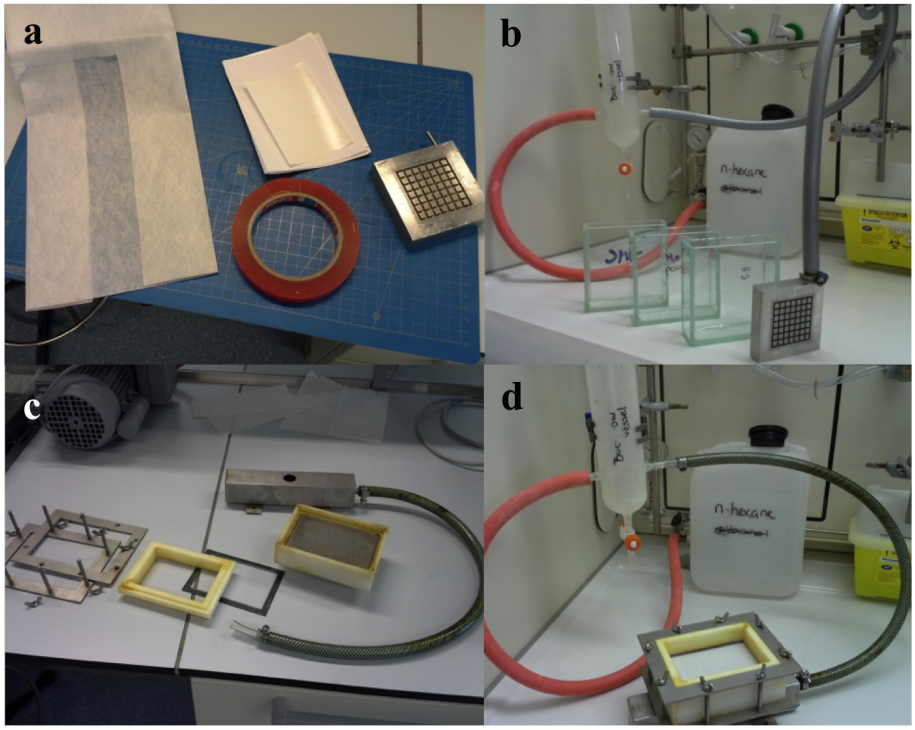

Figure 35: Setups for coating of POSS/polymersomes+TMC (a+b) and PEI/proteopolymersomes+CC (c+d). In the first "taping" protocol, a highly porous cellulose based support was taped on a roughly perforated metal frame, followed by MF PES. The frame was put in several baths, where the solution was soaked through the MF PES except for the organic phase. For the second protocol, MF PES was directly placed on the fine perforated frame and fixed with six screws, whereafter the frame was connected to a vacuum pump. Instead of baths, the different were poured in and drained afterwards. More solutions were therefore needed per membrane, but the AL was three times higher.

Supported POSS/polymersomes+TMC AL

We then investigated POSS+TMC on MF PES support material coated following the procedures in Dalwani et al. [264] (Coating setup in Figure 35a+b), which was further described in the Material & Methods section. The MF PES itself was supported by a nonwoven. FTIR spectroscopy revealed the presence of polymersomes in the supported AL, however, the AL formation is significantly reduced compared to the non-supported POSS/polymersomes+TMC AL, see Figure 36. A main challenge of analyzing supported AL with FTIR is the potential absorption of the PES support, which has a strong absorption especially in the region between 700 and 2000 cm^{-1}. Especially the POSS absorption peaks interfered strongly with PES peaks. In the supported POSS/polymersomes+TMC

AL the PB-PEO signal at 3000 cm^{-1} was present as well as another small peak around 1700 cm^{-1} that also appeared in the FTIR spectra of PB [267]. Interestingly, it could not be found in the non-supported AL. Potentially it was overlayed from the background signal in the region between 1600-3650 cm^{-1} that was more significant at the FTIR analysis spectra from the non-supported AL. Both PA bonds were present in the supported POSS+TMC AL, but strongly reduced in the one with polymersomes. The large peak (at 1580 cm^{-1}) close to the N-H stretching peak, is associated with PES. The N-H stretching peak (1545 cm^{-1}) was only present in the supported POSS+TMC AL. The broad peak of this AL from 3150-3650 cm^{-1} is likely associated to water and/or unreacted amine groups.

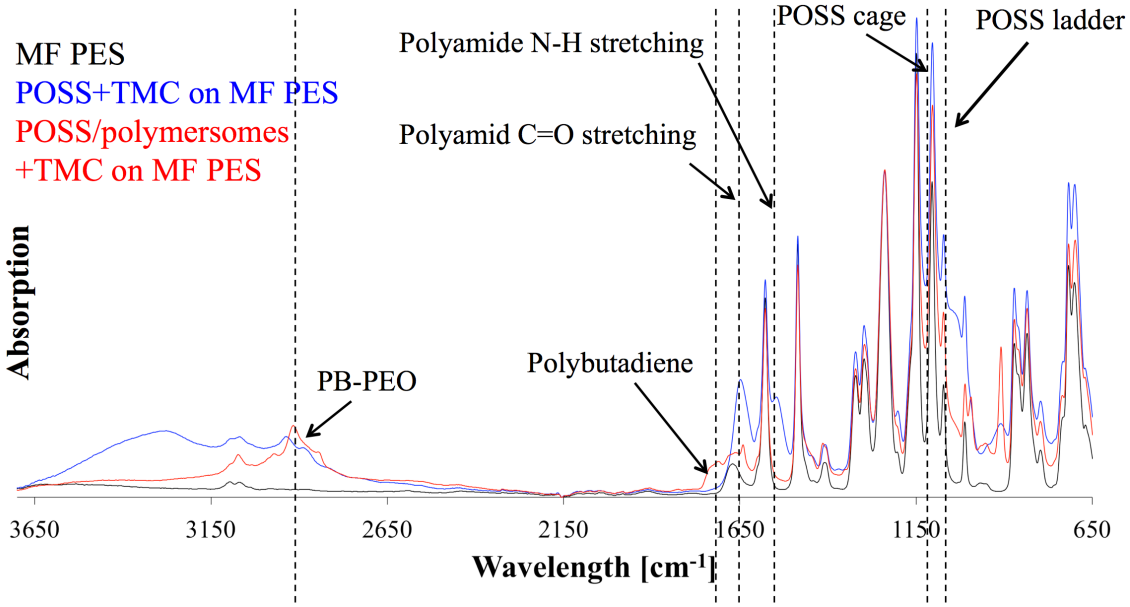

Figure 36: FTIR analysis of supported POSS/polymersomes+TMC AL (red) and POSS+TMC control AL (blue) on MF PES and pure MF PES (black). The PES supporting material had high absorption and interfered with many absorption peaks. A subtraction from the absorption spectra of pure PES resulted in negative peaks. We therefore only normalized the spectra. PB-PEO was present in the AL with polymersomes, however the PA formation was strongly suppressed.

The reason for the suppression of the PA-signal in the supported POSS/polymersomes+TMC AL is not clear. It may be related to the TMC reactivity as discussed before. We used 2 g/l TMC for the supported POSS+TMC AL and POSS/polymersomes+TMC AL, because there was no AL formation at 0.5 g/l. Another TMC concentration may be more optimal for the supported POSS/polymersomes+TMC AL. The potential blockage of AL formation induced by polymersomes should have suppressed the AL formation in the non-supported AL as well, which it did not. However AL formation was significantly decreased with supported POSS+TMC AL when changing from 2 g/l to 0.5 g/l. Another

hypothesis could be that POSS+TMC do not form easily on MF PES. To our knowledge, no former POSS+TMC AL formation on MF PES has been reported. MF PES has significantly bigger pore sizes than PAN. This could hamper the formation of a smooth layer.

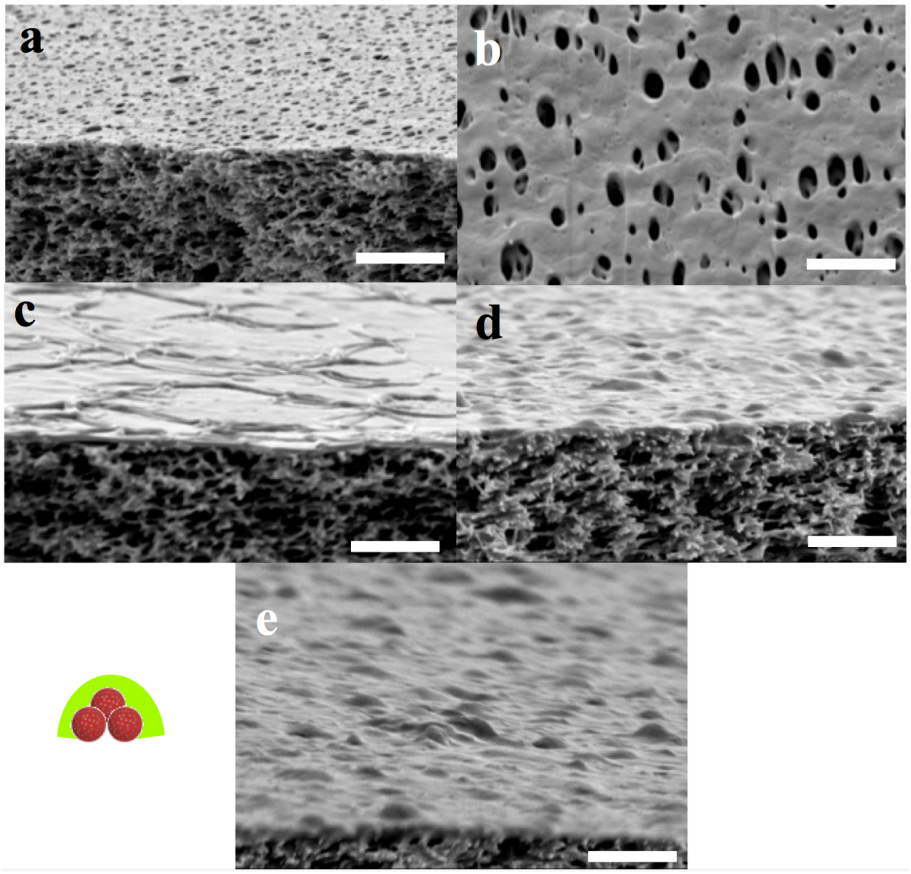

Figure 37: SEM images of MF PES (a+b) supported POSS+TMC AL on MF PES (c) and supported POSS/polymersomes+TMC on MF PES (d+e). Schematic sketch of polymersome coverage left to e). Micropores of the MF PES were covered completely by the POSS+TMC AL. After addition of polymersomes, small bumps with dimensions similar to the polymersomes were observed on the organic faced side of the AL. Greater bumps may be attributed to accumulations of covered polymersomes. Scale bar is 3 μm.

In contrast to the FTIR analysis, SEM analysis showed a completely covered POSS/polymersomes+TMC AL on the MF PES (Figure 37). Also POSS and TMC alone seemed to cover the microporous PES structure completely with the smooth layer, although less defined than for PAN substrates [264]. This could be due to the different pore size as mentioned before. When polymersomes were added, the AL exhibited sub-micron sized bumps. They are 1.5-2 μm in length and 0.5-1 μm in height. Considering a covering AL of 100 nm thickness [264] (Figure 37 sketch in bottom left corner) there would be groups of 6-9 polymersomes in a row in 1-3 layers. In contrast to the non-supported ALs we can only observe the side facing the organic phase. In the case of the supported

POSS/polymersomes+TMC AL, the polymersomes influence the shape of the AL side facing the organic phase to a far higher extent than in the non-supported form. This is most probably due to the different preparations, with regard to POSS/polymersomes being in solution at the non-supported AL formation and being at the water-air-interface or even dried on the MF PES at the supported AL formation. Thus, the chances of polymersomes being integrated in the AL is higher for the supported AL than for the non-supported one. In conclusion SEM analysis revealed a successful embedment of polymersomes in a supported AL, whereas FTIR data were less informative. A limitation of FTIR and SEM analysis of supported AL is that only a small fraction of the whole membrane is observed. Another aspect is that the AL could become brittle during drying, and delaminate, or break off when exposed to liquid nitrogen that is used for SEM sample preparation.

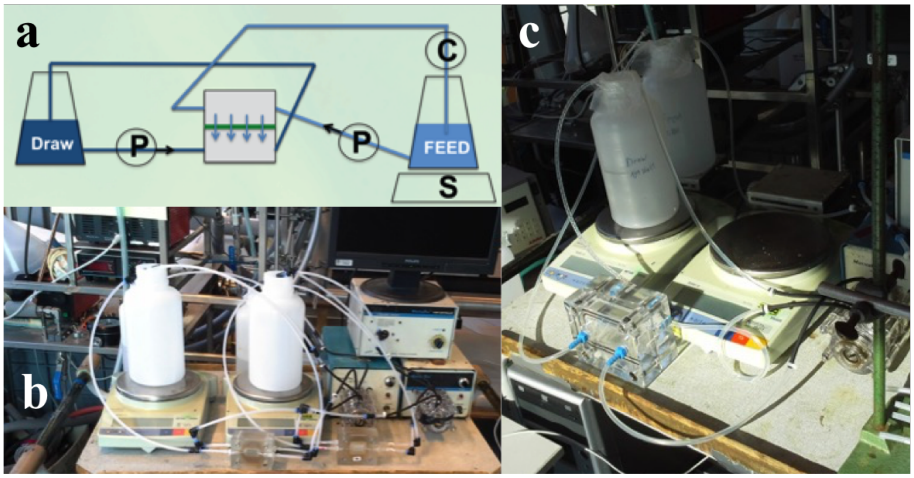

Figure 38: Setup for flux and rejection measurements. (a) Schematic sketch of measurement conditions. Feed and draw solutions will be introduced in reverse flow direction (cross-flow) and the membrane will be placed with AL to the feed side (FO mode). J_s was measured by salt increase per conductivity in the feed solution and J_v was measured by mass increase of the draw solution. (b) Setup for ALs containing POSS+TMC with small chamber and (c) setup for ALs containing PEI+CC with Sterlitech chamber.

We also attempted to test the POSS/polymersomes+TMC AL on MF PES in terms of flux and rejection measurements in FO mode. The whole setup is shown in Figure 38b (schematically in Figure 38a), further details described in the Material & Methods section. However we did not see any FO performance. Approximately one third of the membranes tested were impermeable to salt as evidenced by the low conductivity change in the feed solution within 2 h. The rest of the membranes were leaky as evidenced by an immediate increase in conductivity. The fraction of sealed and leaky membranes of POSS+TMC and POSS/polymersomes+TMC were comparable. In the sealed membranes, the pores are likely clogged by several accumulated layers of POSS+TMC AL. However, after staining

with methyl blue no pinholes or scratches were detected on the surface, suggesting that the supporting PES was covered with the AL. As mentioned before, MF PES may not be a suited support for POSS+TMC ALs in general. PAN support did not show any flux without hydraulic pressure, due to the small pore size (5-30 nm) [269]. It may be suited for POSS+TMC for a NF membrane, but not for FO. A compromise would be to use UF PES membranes as used by Lee et al. [265]. Another problem could be the measurement chamber. At a measurement area of only 3.9 cm^2 small effects such as air bubbles, fluctuations in turbulence or flow speed, as well as small gravity difference could affect the overall measurements to a higher extent compared to the Sterlitech chamber. It would have been a good idea to directly start the coating protocol for PEI+CC, as far as this led to a higher effective AL area, as will be explained later. However, our first aim was to stick to the original protocol as close as possible. Another difficulty was to keep the membrane from drying and at the same time prevent them sticking to the petri dish they are stored in. The petri dish was closed and taped with parafilm to avoid release of water, however parts of the membrane were still often exposed to air or stick. This could as well affect the membrane performance.

Supported PEI/proteopolymersomes+CC

For PEI/proteopolymersomes, another coating protocol was performed in a perforated frame with a greater area and smaller perforation holes, thus, no cellulose support was needed (Figure 35c+d). Instead of placing the frame in different bath, the solutions were poured into the frame. Care had to be taken with fixing of the membrane to the frame to not let one of the six screws fall on the AL. The advantage of this setup was a three times higher AL area. On the other hand, the solution that were poured in could not be reused again, in contrast to the other setup.

FTIR analysis of the supported PEI/proteopolymersomes+CC AL was difficult due to an overlay by PES of all relevant absorption peaks (Figure 39). The signal of PEI, as well as the one of the tertiary polyamine was hard to observe, only a weak PB-PEO signal was observed. From FTIR it seemed that there was no AL forming on MF PES, which was surprising, due to the fact that it worked on UF PES [265]. SEM substantiated the findings of FTIR, because in all three repeats of PEI+CC as well as PEI/proteopolymersomes+CC only the empty MF PES was observed (not shown). Potentially the higher pores made it impossible for the AL to form, as far as its stability was significantly lower compared to AL containing POSS+TMC.

A general problem of FTIR and SEM analysis of supported AL was that only a small fraction of the whole membrane could be observed. Obviously a complete coverage of an AL is seldom. Instead there are areas of better and worse coverage. Even with three repeats

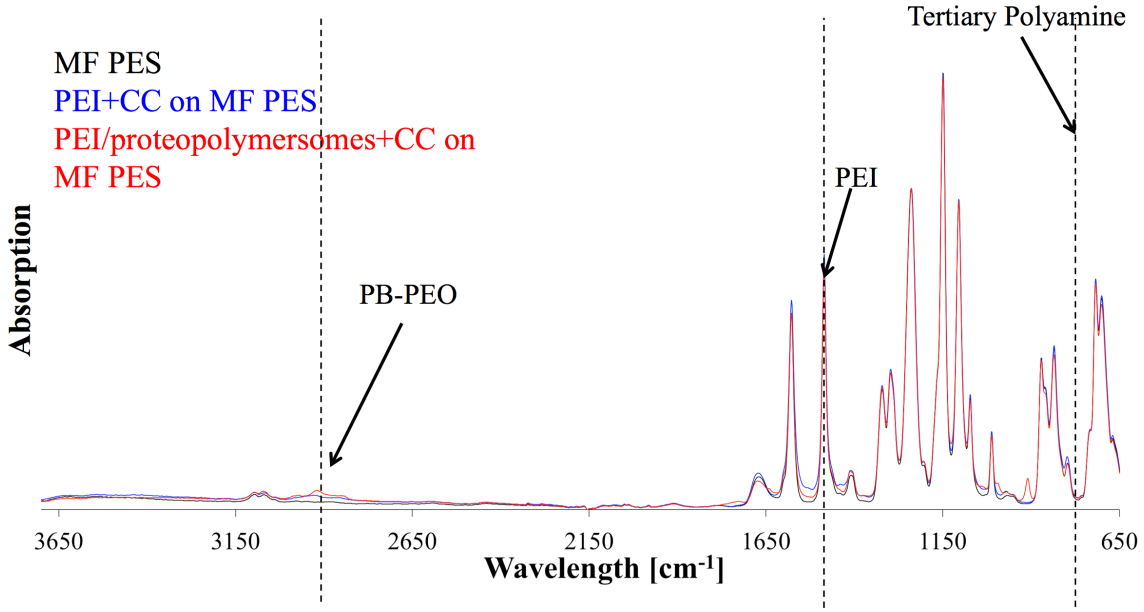

Figure 39: FTIR diagram of supported PEI/proteopolymersomes+CC AL (labelled red) and PEI+CC control AL (labelled grey) on MF PES and pure MF PES (labelled black) as a function of wavelength against absorption. PES interfered with the characteristic absorption peak of PEI and polyamine. A small absorption peak of PB-PEO was observed.

one cannot exclude that only regions of bad coverage were analyzed. Another aspect is the drying process. The AL could get brittle during the drying and delaminate more easily, or break off when exposed to liquid nitrogen as in the case for SEM preparation. To substantiate the findings, more repeats will be necessary.

When measured for J_v and J_s with the Sterlitech chamber, the supported PEI+CC AL showed a similar behavior to all supported AL containing POSS+TMC, even though, none of them had scratches or holes, as revealed with Methylblue staining. These finding would again substantiate the hypotheses made at FTIR and SEM characterization. PEI+CC did not form a proper AL, at least not on MF PES. One from the three repeats of the supported PEI/proteopolymersomes+CC AL revealed a J_v of 22.15 $Lm^{-2}h^{-1}$, exceeding the J_v of the AIM with a factor of almost four, however also with more than double J_s (108.6 $gm^{-2}h^{-2}$). It is common that higher J_v correlates with an increase J_s as well. The experiment was running for 4 h, where the weight of the draw increased by 383.7 g, where NaCl in the feed increased at the same time to 1.8 g. This result substantiate the fact that the membrane areas, chosen for characterization methods may be from a bad spot. However, the reproducibility was low, thus there are still some optimization steps are crucial.

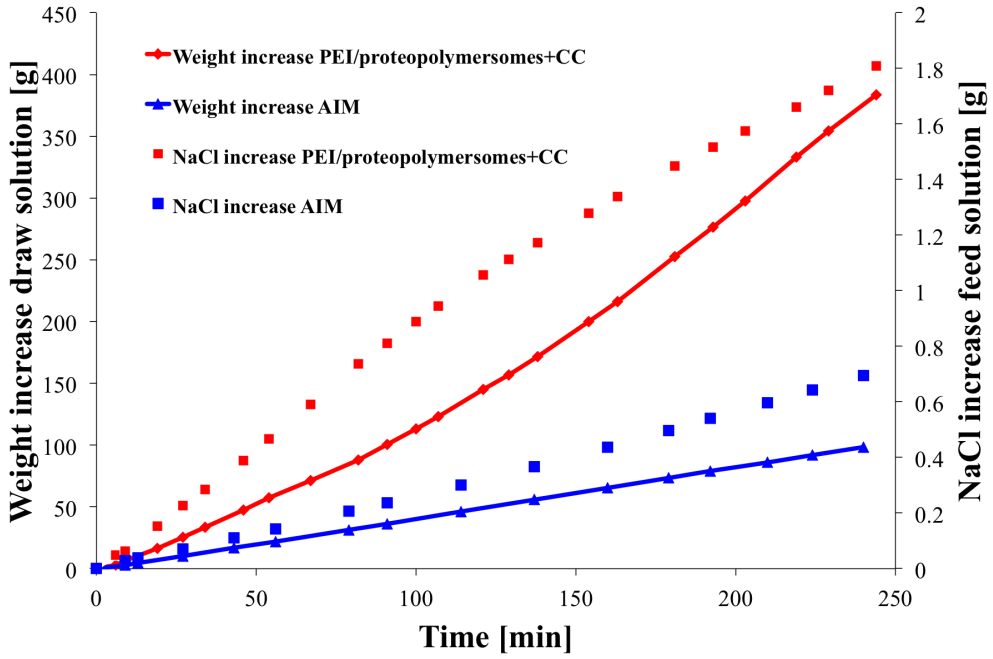

Figure 40: Diagram of measured membrane performance for AIMs (labelled blue) and supported PEI/proteopolmyersomes+CC AL on MF PES as a function of weight increase of the draw solution (lines) and NaCl increase in the feed solution (dots) against time. PEI/proteopolymersomes+CC membranes had a superior weight increase but were as well double as leaky as AIM. One out of three PEI/proteopolymersomes+CC membranes show that performance, the other two had no flux and were highly leaky to NaCl.

To conclude, we obtained insights in non-supported and supported AL containing POSS with polymersomes in the aqueous phase and TMC in the organic phase, respectively PEI with proteopolymersomes in the aqueous phase and CC in the organic phase. The non-supported POSS/polymersomes+TMC AL was formed successfully with high amounts of polymersomes covered and some of them even integrated inside the AL. The supported POSS/polymersomes+TMC showed a different characteristics. FTIR data indicated a high suppression of the AL formation at polymersome addition, whereas SEM images showed a completely covered and significantly different AL upon polymersome addition. None of the membranes produced, containing POSS and TMC had any reasonable performance, probably due to incomplete coverage of the AL. Still it was interesting to get an insight how POSS, TMC and proteopolymersomes are interacting. Formation of non-supported and supported PEI/proteopolymersomes+CC was only marginally, mostly due to the marginally reactive components. However one out of three PEI/proteopolymersomes +CC membranes showed a three times superior J_v but as well a more than double J_s compared to J_s. The microfluidic approach is a great tool to observe a non-supported AL in solution. There was no microscopic effect of polymersome addition to the POSS+TMC

AL. These finding could help to get a closer insight in how proteo- and polymersomes can influence AL formation. Further challenges will be to create a functional water separation membrane from these components.

7 Conclusion & Outlook

The dependence of the interaction of AQPs and PB-PEO diblock copolymers on the molecular parameter of the latter (M_n and f) was investigated. It was characterized using FF-TEM and FCS as the main methods SDS-PAGE (AQP presence), SFLS (AQP functionality), SAXS/SANS (Proteopolymersome bilayer properties) to substantiate the findings. No clear differences between proteopolymersomes and polymersomes could be obtained within FF-TEM as far as both revealed spots that looked like AQPs in the fractured polymersome bilayer. SAXS/SANS showed that the incorporation of AQPs in a polymersome bilayer changed its property to a more smooth and well-defined shape. Furthermore, almost only proteopolymersomes were obtained, where for polymersomes there were as well micelles present. FCS looks as a promising alternative to FF-TEM, where first incorporations of AQP in a low M_n PB-PEO polymer showed an protein-to-vesicle-ratio of 2.78.

Polymersomes formed in a different manner depending on their M_n and f. If both values are increasing d_P of the assembled polymersomes increased as well. The polydispersity increased on the other hand with decreasing M_n at high f. Three main regions of a distinct assembling behavior has been found using FF-TEM and DLS: Low M_n/high f (mixed d_P/polydisperse), low f (small d_P/monodisperse) and high M_n/high f (large d_P/monodisperse). This could be described as a function of free energy to form polymersomes where the more monodisperse polymersomes had only a few energetic minima but the polydisperse ones had several. Furthermore, polymersomes were found to exhibit more brittle bilayers when SE formed, compared to FR. This results in a lower SFLS signal and a resistance to extrusion with a sharp edge, whereafter they break down to micelles. There seems furthermore to be a threshold for SE prepared polymersomes between 3.75 kg/mol (PB_{43}-PEO_{32}) and 3.8 kg/mol (PB_{46}-PEO_{32}). The first polymersomes and polymersomes of lower M_n the break down to micelles, where they keep their vesicular structure at PB_{46}-PEO_{32} and polymers of higher M_n. A sleightly higher brittleness for SE prepared polymersomes was observed at 5 mg/ml polymer concentration compared to 10, 20 and 25 mg/ml. For detergent-mediated FR it does not matter for the polymersome properties if detergent is removed via biobeads or dialysis, as well as which temperature or time is used. For analysis, novel methods like AFM or NTA can provide reliable information about d_P in contrast to DLS. Cryo-TEM is a safe standard for d_P or lamellarity but requires an elaborate setup. SAXS and SANS can provide the best accuracy to obtaining bilayer thickness.

Finally, the interaction of AQPs and polymers (proteopolymersomes) and membranes was investigated. Novel AL linkers (POSS+TMC, PEI+CC) were used for their potential pur-

pose for ABPMs, as far as the optimal AL for usual PA membranes and ABPMs can be quite different. Polymersomes could be integrated successfully in a POSS+TMC AL, as shown with FTIR, SEM and a novel microfluidic approach. On SEM images, polymersomes could be found in the opened cross section of the non-supported AL. This indicated that they were directly in the right position to be actively involved in the water separation process of the membrane. The membrane performance of empty and polymersome added POSS+TMC AL was not promising, which may be due to the measurement setup. PEI+CC was a worse performing candidate for proteopolymersomes integration, however the membrane performance resulted in a three times higher J_v and more than double J_s compared to the standard AIM measured.

Taken together these findings provide valuable insights in research fields as membrane protein-polymer interaction, polymer synthesis, polymer self-assembly, soft matter and colloidal science, membrane research as well as in applied fields as drug delivery, polymer chemistry, biomimetic membrane, PA membrane and general membrane technology. These findings are also opening up to many further steps to investigate on each single component, for example on AQPs. AqpZ and AQP10 to a smaller extent were used as the first component for ABPMs. Potentially other AQPs are worth investigating as well, such as plant AQPs who exhibit far higher water fluxes than AqpZ. PB-PEO was used as the second component. Additionally to PB-PEO and PMOXA-PDMS-PMOXA, the other block copolymer that is often used for membrane protein incorporation, there could be further block copolymers that could be used to incorporated membrane proteins and potentially self-assemble to monodisperse polymersomes directly.

In terms of polymersomes this project is a step towards understanding the dependence of internal factors on polymer self-assembly. Another challenge could be to investigate further internal factors like PDI_M, zeta potential or polymer chemistry as well as external factors, which is done in a greater perspective mainly on chemistries that do not self-assemble in water. Further steps towards upscaling of polymersome production with the aim of integrating biomolecules could be investigated, such as trying other solvent-free formation and further modification methods and compare the resulting polymersomes.

As the third component, MF PES revealed some challenges to function as a membrane. There are various other polymer membranes that are worth investigating for the role as a mechanical support for ABPMs for example PAI or PSf. More AL linkers can be investigated in the design of impermeable, stable and well-defined AL, capable of integrating high numbers of proteopolymersomes.

Finally, for ABPMs and other biomimetic membranes, a long journey is still to be done in the integration even though there are ABMs available on the market already. Even though great breakthoughs has been achieved, the theoretical J_v and NaCl rejection values for

biomimetic membranes are still by far higher than the numbers from recent upcoming biomimetic membrane designs. Further research on those membranes are crucial to fight and prevent upcoming clean water scarcity.

References

[1] J. Habel et al., *Aquaporin-Based Biomimetic Polymeric Membranes: Approaches and Challenges*. Membranes, 5 (3) **2015**, pp. 307–351.

[2] WHO, *Chloride in water*. Guidelines for drinking-water quality, 2 **2003**.

[3] S. Törnroth-Horsefield, *Aquaporins*. Biochim. Biophys. Acta - Gen. Subjects, 1840 (5) **2014**, pp. 1465–1624.

[4] P. Agre, *Aquaporin Water Channels*. Bioscience Rep., 24 (3) **2004**, pp. 127–163.

[5] K. P. Lee, T. C. Arnot, and D. Mattia, *A review of reverse osmosis membrane materials for desalination - Development to date and future potential*. J. Membr. Sci., 370 (1-2) **2011**, pp. 1–22.

[6] J. S. Hansen et al., *Development of an automation technique for the establishment of functional lipid bilayer arrays*. J. Micromech. Microeng., 19 (2) **2009**, p. 025014.

[7] C. Rein, "Stabilization and characterization of 2D and 3D biomimetic membranes". PhD thesis. Copenhagen, Denmark: University of Copenhagen, June 2011.

[8] Y. Zhao et al., *Synthesis of robust and high-performance aquaporin-based biomimetic membranes by interfacial polymerization-membrane preparation and RO performance characterization*. J. Membr. Sci., 423-424 (C) **2012**, pp. 422–428.

[9] D. E. Discher and A. Eisenberg, *Polymer Vesicles*. Science, 297 (5583) **2002**, pp. 967–973.

[10] M. Kumar et al., *Highly permeable polymeric membranes based on the incorporation of the functional water channel protein Aquaporin Z*. Proc. Natl. Acad. Sci. USA, 104 (52) **2007**, pp. 20719–20724.

[11] K Ishibashi et al., *The evolutionary aspects of aquaporin family*. Am. J. Physiol. Regul. Integr. Comp. Physiol., 300 **2011**, R566–R576.

[12] A. S. Verkman, M. O. Anderson, and M. C. Papadopoulos, *Aquaporins: important but elusive drug targets*. Nat. Rev. Drug Discov., 13 (4) **2014**, pp. 259–277.

[13] B. de Groot and H. Grubmüller, *Water permeation across biological membranes: mechanism and dynamics of aquaporin-1 and GlpF*. Science, 294 **2001**, pp. 2353–2357.

[14] P. Agre, *The Aquaporin Water Channels*. Proc. Am. Thorac. Soc., 3 (1) **2006**, pp. 5–13.

[15] M. Borgnia et al., *Cellular and molecular biology of the aquaporin water channels*. Annu. Rev. Biochem., 68 **1999**, 425–458.

[16] N. Uehlein et al., *Gas-tight triblock-copolymer membranes are converted to CO_2 permeable by insertion of plant aquaporins*. Sci. Rep., 2 **2012**, p. 538.

[17] S. Törnroth-Horsefield et al., *Structural insights into eukaryotic aquaporin regulation*. FEBS Lett., 584 (12) **2010**, pp. 2580–2588.

[18] T Braun et al., *The 3.7 Å projection map of the glycerol facilitator GlpF: a variant of the aquaporin tetramer*. EMBO Rep., 1 (2) **2000**, pp. 183–189.

[19] D. F. Savage et al., *Architecture and Selectivity in Aquaporins: 2.5 Å X-Ray Structure of Aquaporin Z*. PLoS Biol., 1 (3) **2003**, pp. 334–340.

[20] D. Wree et al., *Requirement for asparagine in the aquaporin NPA sequence signature motifs for cation exclusion*. FEBS J., 278 (5) **2011**, pp. 740–748.

[21] U Kosinska Eriksson et al., *Subangstrom Resolution X-Ray Structure Details Aquaporin-Water Interactions*. Science, 340 (6138) **2013**, pp. 1346–1349.

[22] E. Beitz et al., *Point mutations in the aromatic/arginine region in aquaporin 1 allow passage of urea, glycerol, ammonia, and protons*. Proc. Natl. Acad. Sci. USA, 103 (2) **2006**, pp. 269–274.

[23] D. Fu and M. Lu, *The structural basis of water permeation and proton exclusion in aquaporins (Review)*. Mol. Membr. Biol., 24 (5-6) **2007**, pp. 366–374.

[24] L. Xin et al., *Population Shift between the Open and Closed States Changes the Water Permeability of an Aquaporin Z Mutant*. Biophys. J., 103 (2) **2012**, pp. 212–218.

[25] B. Wu et al., *Concerted action of two cation filters in the aquaporin water channel*. EMBO J., 28 (15) **2009**, pp. 2188–2194.

[26] M. Kumar, "Biomimetic membranes as new materials for applications in environmental engineering and biology". PhD thesis. Champaign, IL, USA: University of Illinois, July 2010.

[27] N Chakrabarti, B. Roux, and R. Pomès, *Structural Determinants of Proton Blockage in Aquaporins*. J. Mol. Biol., 343 (2) **2004**, pp. 493–510.

[28] N Chakrabarti et al., *Molecular basis of proton blockage in aquaporins*. Structure, 12 **2004**, pp. 65–74.

[29] B. L. de Groot et al., *The Mechanism of Proton Exclusion in the Aquaporin-1 Water Channel*. J. Mol. Biol., 333 (2) **2003**, pp. 279–293.

[30] B. de Groot and H. Grubmüller, *The dynamics and energetics of water permeation and proton exclusion in aquaporins*. Curr. Opin. Struc. Biol., 15 (2) **2005**, pp. 176–183.

[31] M. Borgnia et al., *Functional reconstitution and characterization of AqpZ, the E. coli water channel protein*. J. Mol. Biol., 291 (5) **1999**, pp. 1169–1179.

[32] B. Yang and A Verkman, *Water and Glycerol Permeabilities of Aquaporins 1–5 and MIP Determined Quantitatively by Expression of Epitope-tagged Constructs in* Xenopus *Oocytes*. J. Biol. Chem., 272 (26) **1997**, pp. 16140–16146.

[33] X. Ding et al., *Water and CO_2 permeability of SsAqpZ, the cyanobacterium Synechococcussp. PCC7942 aquaporin*. Biol. Cell, 105 (3) **2013**, pp. 118–128.

[34] G. Calamita et al., *Molecular cloning and characterization of AqpZ, a water channel from Escherichia coli*. J. Biol. Chem., 270 (49) **1995**, pp. 29063–29066.

[35] J. Preiner et al., *High-Speed AFM Images of Thermal Motion Provide Stiffness Map of Interfacial Membrane Protein Moieties*. Nano Lett., 15 (1) **2015**, pp. 759–763.

[36] A. Laganowsky et al., *Membrane proteins bind lipids selectively to modulate their structure and function*. Nature, 510 (7503) **2014**, pp. 172–175.

[37] X. Kong et al., *Surface tension effects on the phase transition of a DPPC bilayer with and without protein: a molecular dynamics simulation*. Phys. Chem. Chem. Phys., 16 (18) **2014**, pp. 8434–8440.

[38] G. Hu, L. Y. Chen, and J. Wang, *Insights into the mechanisms of the selectivity filter of Escherichia coli aquaporin Z*. J. Mol. Model., 18 (8) **2012**, pp. 3731–3741.

[39] L. Xin et al., *Water permeation dynamics of AqpZ: A tale of two states*. Biochim. Biophys. Acta - Biomembr., 1808 (6) **2011**, pp. 1581–1586.

[40] M Akai et al., *Aquaporin AqpZ Is Involved in Cell Volume Regulation and Sensitivity to Osmotic Stress in Synechocystis sp. Strain PCC 6803*. J. Bacteriol., 194 (24) **2012**, pp. 6828–6836.

[41] X. Zhang et al., *Enhanced functional expression of aquaporin Z via fusion of in situ cleavable leader peptides in Escherichia coli cell-free system*. Enzyme Microb. Tech., 55 **2014**, pp. 26–30.

[42] D. A. Hajduk et al., *Complex phase behavior in aqueous solutions of poly(ethylene oxide)-poly(ethylethylene) block copolymers*. J. Phys. Chem. B, 102 (22) **1998**, pp. 4269–4276.

[43] M Antonietti and S Förster, *Vesicles and Liposomes: A Self-Assembly Principle Beyond Lipids*. Adv. Mater., 15 (16) **2003**, pp. 1323–1333.

[44] M. Xiao et al., *Biomimetic membrane control of block copolymer vesicles with tunable wall thickness*. Soft Matter, 9 (8) **2013**, pp. 2434–2442.

[45] L. Zhang and A. Eisenberg, *Multiple Morphologies of "Crew-Cut" Aggregates of Polystyrene-b-poly(acrylic acid) Block Copolymers*. Science, 268 (5218) **1995**, pp. 1728–1731.

[46] A. D. Bangham, M. M. Standish, and J. C. Watkins, *Diffusion of univalent ions across the lamellae of swollen phospholipids*. J. Mol. Biol., 13 (1) **1965**, pp. 238–252.

[47] B. M. Discher et al., *Polymersomes: Tough Vesicles Made from Diblock Copolymers*. Science, 284 (5417) **1999**, pp. 1143–1146.

[48] D. E. Discher and F. Ahmed, *Polymersomes*. Annu. Rev. Biomed. Eng., 8 **2006**, pp. 323–341.

[49] C. Lopresti et al., *Polymersomes: nature inspired nanometer sized compartments*. J. Mater. Chem., 19 (22) **2009**, pp. 3557–3776.

[50] M. Kumar et al., *High-Density Reconstitution of Functional Water Channels into Vesicular and Planar Block Copolymer Membranes*. J. Am. Chem. Soc, 134 (45) **2012**, pp. 18631–18637.

[51] C. Nardin et al., *Polymerized ABA Triblock Copolymer Vesicles*. Langmuir, 16 (3) **2000**, pp. 1035–1041.

[52] K. Kita-Tokarczyk et al., *Monolayer Interactions between Lipids and Amphiphilic Block Copolymers*. Langmuir, 25 (17) **2009**, pp. 9847–9856.

[53] K. Kita-Tokarczyk and W. P. Meier, *Biomimetic block copolymer membranes*. Chimia, 62 (10) **2008**, pp. 820–825.

[54] H Aranda-Espinoza et al., *Electromechanical limits of polymersomes*. Phys. Rev. Lett., 87 (20) **2001**, p. 208301.

[55] R Dimova et al., *Hyperviscous diblock copolymer vesicles*. Eur. Phys. J. E, 7 **2002**, pp. 241–250.

[56] L Luo and A. Eisenberg, *Thermodynamic stabilization mechanism of block copolymer vesicles*. J. Am. Chem. Soc, 123 **2001**, pp. 1012–1013.

[57] D. D. Lasic et al., *Spontaneous vesiculation*. Adv. Colloid Interface Sci., 89–90 (0) **2001**, pp. 337–349.

[58] J. Lee et al., *From membranes to melts, rouse to reptation: Diffusion in polymersome versus lipid bilayers*. Macromolecules, 35 (2) **2002**, pp. 323–326.

[59] J. Lee et al., *Preparation, stability, and in vitro performance of vesicles made with diblock copolymers*. Biotechnol. Bioeng., 73 (2) **2001**, pp. 135–145.

[60] Z. Bai, B. Zhao, and T. P. Lodge, *Bilayer Membrane Permeability of Ionic Liquid-Filled Block Copolymer Vesicles in Aqueous Solution*. J. Phys. Chem. B, 116 (28) **2012**, pp. 8282–8289.

[61] F. Itel et al., *Molecular Organization and Dynamics in Polymersome Membranes: A Lateral Diffusion Study*. Macromolecules, 47 **2014**, pp. 7588–7596.

[62] R. Stoenescu, W. P. Meier, and H. Wennemers, "Asymmetric amphiphilic triblock copolymers". PhD thesis. Basel, Switzerland: University of Basel, July 2004.

[63] E. Blasco et al., *Light induced molecular release from vesicles based on amphiphilic linear-dendritic block copolymers*. Polym. Chem., 4 (7) **2013**, pp. 2246–2254.

[64] Q. Yan et al., *Breathing Polymersomes: CO 2-Tuning Membrane Permeability for Size-Selective Release, Separation, and Reaction*. Angew. Chem. Int. Ed., 52 (19) **2013**, pp. 5070–5073.

[65] A. Leson et al., *Molecular Exchange through Membranes of Poly(2-vinylpyridine-block-ethylene oxide) Vesicles*. Small, 3 (6) **2007**, pp. 1074–1083.

[66] G. Battaglia, A. J. Ryan, and S. Tomas, *Polymeric Vesicle Permeability: A Facile Chemical Assay*. Langmuir, 22 (11) **2006**, pp. 4910–4913.

[67] B. M. Discher et al., *Polymer vesicles in various media*. Curr. Opin. Colloid. In., 5 (1-2) **2000**, pp. 125–131.

[68] I. Eggens et al., *Separation, quantitation and distribution of dolichol and dolichyl phosphate in rat and human tissues*. Biochim. Biophys. Acta - Lipid. Lipid Met., 751 (3) **1983**, pp. 355–368.

[69] F. He and Y. W. Tong, *A mechanistic study on amphiphilic block co-polymer poly(butadiene-b-(ethylene oxide)) vesicles reveals the water permeation mechanism through a polymeric bilayer*. RSC Adv., 4 (29) **2014**, pp. 15304–15313.

[70] M. A. Hillmyer and F. S. Bates, *Synthesis and Characterization of Model Polyalkane-Poly(ethylene oxide) Block Copolymers*. Macromolecules, 29 (22) **1996**, pp. 6994–7002.

[71] M. Szwarc, *'Living' Polymers*. Nature, 178 (4543) **1956**, pp. 1168–1169.

[72] S. Förster and E. Krämer, *Synthesis of PB-PEO and PI-PEO Block Copolymers with Alkyllithium Initiators and the Phosphazene Base t-BuP4*. Macromolecules, 32 (8) **1999**, pp. 2783–2785.

[73] D. R. Arifin and A. F. Palmer, *Polymersome Encapsulated Hemoglobin: A Novel Type of Oxygen Carrier*. Biomacromolecules, 6 (4) **2005**, pp. 2172–2181.

[74] S. Li et al., *Self-Assembled Poly(butadiene)-b-poly(ethylene oxide) Polymersomes as Paclitaxel Carriers*. Biotechnol Progr., 23 (1) **2007**, pp. 278–285.

[75] Z. Bai and T. P. Lodge, *Polymersomes with Ionic Liquid Interiors Dispersed in Water*. J. Am. Chem. Soc, 132 (45) **2010**, pp. 16265–16270.

[76] W. F. Paxton, D. Price, and N. J. Richardson, *Hydroxide ion flux and pH-gradient driven ester hydrolysis in polymer vesicle reactors*. Soft Matter, 9 (47) **2013**, pp. 11295–11302.

[77] R. C. Amos et al., *Tuning polymersome surfaces: functionalization with dendritic groups*. Soft Matter, 8 (21) **2012**, pp. 5947–5958.

[78] S. Belegrinou et al., *Biomimetic supported membranes from amphiphilic block copolymers*. Soft Matter, 6 (1) **2010**, pp. 179–186.

[79] Y. Kagawa and E. Racker, *Partial Resolution of the Enzymes Catalyzing Oxidative Phosphorylation*. J. Biol. Chem., 246 (17) **1971**, pp. 5477–5487.

[80] C. Nardin et al., *Nanoreactors based on (polymerized) ABA-triblock copolymer vesicles*. Chem. Commun. **2000**, pp. 1433–1434.

[81] X. Zhang et al., *Mimicking the cell membrane with block copolymer membranes*. J. Polym. Sci. A Polym. Chem., 50 (12) **2012**, pp. 2293–2318.

[82] P. Tanner et al., *Polymeric Vesicles: From Drug Carriers to Nanoreactors and Artificial Organelles*. Acc. Chem. Res., 44 (10) **2011**, pp. 1039–1049.

[83] H.-J. Choi and C. D. Montemagno, *Artificial organelle: ATP synthesis from cellular mimetic polymersomes*. Nano Lett., 5 (12) **2005**, pp. 2538–2542.

[84] D. M. Vriezema et al., *Positional Assembly of Enzymes in Polymersome Nanoreactors for Cascade Reactions*. Angew. Chem. Int. Ed., 46 (39) **2007**, pp. 7378–7382.

[85] O Andersen and R. E. Koeppe, *Bilayer thickness and membrane protein function: an energetic perspective*. Annu. Rev. Biophys. Biomol. Struct., 36 **2007**, pp. 107–130.

[86] V. Pata and N. Dan, *The Effect of Chain Length on Protein Solubilization in Polymer-Based Vesicles (Polymersomes)*. Biophys. J., 85 (4) **2003**, pp. 2111–2118.

[87] G. Srinivas, D. E. Discher, and M. Klein, *Key Roles for Chain Flexibility in Block Copolymer Membranes that Contain Pores or Make Tubes*. Nano Lett., 5 (12) **2005**, pp. 2343–2349.

[88] D. E. Discher et al., *Emerging applications of polymersomes in delivery: From molecular dynamics to shrinkage of tumors*. Prog. Polym. Sci., 32 (8-9) **2007**, pp. 838–857.

[89] C. Aponte-Santamaría et al., *Molecular driving forces defining lipid positions around aquaporin-0*. Proc. Natl. Acad. Sci. USA, 109 (25) **2012**, pp. 9887–9892.

[90] J. S. Hansen et al., *Interaction between sodium dodecyl sulfate and membrane reconstituted aquaporins: A comparative study of spinach SoPIP2;1 and* E. coli *AqpZ*. Biochim. Biophys. Acta - Biomembr., 1808 (10) **2011**, pp. 2600–2607.

[91] R. Stoenescu, A. Graff, and W. P. Meier, *Asymmetric ABC-Triblock Copolymer Membranes Induce a Directed Insertion of Membrane Proteins*. Macromol. Biosci., 4 (10) **2004**, pp. 930–935.

[92] R. K. Hite, Z. Li, and T. Walz, *Principles of membrane protein interactions with annular lipids deduced from aquaporin-0 2D crystals*. EMBO J., 29 (10) **2010**, pp. 1652–1658.

[93] R. Nehring et al., *Amphiphilic Diblock Copolymers for Molecular Recognition: Metal-Nitrilotriacetic Acid Functionalized Vesicles*. Langmuir, 25 (2) **2009**, pp. 1122–1130.

[94] S. M. Kelly, T. J. Jess, and N. C. Price, *How to study proteins by circular dichroism*. Biochim. Biophys. Acta, 1751 (2) **2005**, pp. 119–139.

[95] University of Illinois et al., "Highly permeable polymeric membranes". Pat. WO 2009/078174. June 2009.

[96] J. Habel, "Structural and functional characterization of Aquaporin 0 incorporated in block copolymers and their resulting aggregate morphologies". MA thesis. Basel, Switzerland: University of Basel, 2011.

[97] T Gonen et al., *Aquaporin-0 membrane junctions reveal the structure of a closed water pore*. Nature, 429 **2004**, pp. 193–197.

[98] G Chandy et al., *Comparison of the Water Transporting Properties of MIP and AQP1*. J. Membr. Biol., 159 (1) **1997**, pp. 29–39.

[99] Pennsylvania State University et al., "High density membrane protein membranes". Pat. WO 2014/028923. Feb. 2014.

[100] C. Hélix-Nielsen, *Biomimetic membranes for sensor and separation applications*. Anal. Bioanal. Chem., 395 (3) **2009**, pp. 697–718.

[101] K. Pszon-Bartosz et al., *Assessing the efficacy of vesicle fusion with planar membrane arrays using a mitochondrial porin as reporter*. Biochem. Biophys. Res. Commun., 406 (1) **2011**, pp. 96–100.

[102] A González-Pérez et al., *Biomimetic triblock copolymer membrane arrays: A stable template for functional membrane proteins*. Langmuir, 25 (18) **2009**, pp. 10447–10450.

[103] M. Andreasson-Ochsner et al., *Selective Deposition and Self-Assembly of Triblock Copolymers into Matrix Arrays for Membrane Protein Production*. Langmuir, 28 (4) **2012**, pp. 2044–2048.

[104] S. Gulati et al., *Detergent-free purification of ABC (ATP-binding-cassette) transporters*. Biochem. J., 461 (2) **2014**, pp. 269–278.

[105] T. J. Knowles et al., *Membrane Proteins Solubilized Intact in Lipid Containing Nanoparticles Bounded by Styrene Maleic Acid Copolymer*. J. Am. Chem. Soc, 131 (22) **2009**, pp. 7484–7485.

[106] A. R. Hall et al., *Hybrid pore formation by directed insertion of α-haemolysin into solid-state nanopores*. Nat. Nanotechnol., 5 (12) **2010**, pp. 874–877.

[107] S. Balme et al., *New Bioinspired Membrane Made of a Biological Ion Channel Confined into the Cylindrical Nanopore of a Solid-State Polymer.* Nano Lett., 11 (2) **2011**, pp. 712–716.

[108] S. Bodor et al., *Electrochemical methods for the determination of the diffusion coefficient of ionophores and ionophore–ion complexes in plasticized PVC membranes*. Analyst, 133 (5) **2008**, pp. 635–642.

[109] S. Ibragimova, "Supporting and stabilizing biomimetic membranes". PhD thesis. Kgs. Lyngby, Denmark: Danish Technical University, May 2011.

[110] A. Mech-Dorosz et al., *A reusable device for electrochemical applications of hydrogel supported black lipid membranes*. Biomed. Microdevices, 17 (1) **2015**, p. 21.

[111] M. Erbakan et al., *Molecular Cloning, Overexpression and Characterization of a Novel Water Channel Protein from Rhodobacter sphaeroides*. PLoS ONE, 9 (1) **2014**, e86830.

[112] A. Graff et al., *Amphiphilic Copolymer Membranes Promote NADH:Ubiquinone Oxidoreductase Activity: Towards an Electron-Transfer Nanodevice*. Macromol. Chem. Phys., 211 (2) **2010**, pp. 229–238.

[113] D. Wong, T.-J. Jeon, and J. Schmidt, *Single molecule measurements of channel proteins incorporated into biomimetic polymer membranes*. Nanotechnology, 17 (15) **2006**, pp. 3710–3717.

[114] H. L. Wang et al., *Mechanically robust and highly permeable AquaporinZ biomimetic membranes*. J. Membr. Sci., 434 **2013**, pp. 130–136.

[115] H. Wang, T.-S. Chung, and Y. W. Tong, *Study on water transport through a mechanically robust Aquaporin Z biomimetic membrane*. J. Membr. Sci., 445 (C) **2013**, pp. 47–52.

[116] H. Wang et al., *Highly Permeable and Selective Pore-Spanning Biomimetic Membrane Embedded with Aquaporin Z*. Small, 8 (8) **2012**, pp. 1185–1190.

[117] P. S. Zhong et al., *Aquaporin-embedded biomimetic membranes for nanofiltration*. J. Membr. Sci., 407-408 **2012**, pp. 27–33.

[118] C. De Vocht et al., *Assessment of stability, toxicity and immunogenicity of new polymeric nanoreactors for use in enzyme replacement therapy of MNGIE*. J. Control. Release, 137 (3) **2009**, pp. 246–254.

[119] M. Grzelakowski et al., *A framework for accurate evaluation of the promise of aquaporin based biomimetic membranes*. J. Membr. Sci., 479 **2015**, pp. 223–231.

[120] M. Grzelakowski et al., *Immobilized Protein-Polymer Nanoreactors*. Small, 5 (22) **2009**, pp. 2545–2548.

[121] S. Ihle et al., *Nanocompartments with a pH release system based on an engineered OmpF channel protein*. Soft Matter, 7 (2) **2011**, pp. 532–539.

[122] P. Tanner, V. Balasubramanian, and C. G. Palivan, *Aiding Nature's Organelles: Artificial Peroxisomes Play Their Role*. Nano Lett., 13 (6) **2013**, pp. 2875–2883.

[123] P. Tanner et al., *Enzymatic Cascade Reactions inside Polymeric Nanocontainers: A Means to Combat Oxidative Stress*. Chem. Eur. J., 17 (16) **2011**, pp. 4552–4560.

[124] J. Ł. Kowal et al., *Functional surface engineering by nucleotide-modulated potassium channel insertion into polymer membranes attached to solid supports*. Biomaterials, 35 (26) **2014**, pp. 7286–7294.

[125] M Winterhalter et al., *Controlling membrane permeability with bacterial porins: application to encapsulated enzymes*. Talanta, 55 (5) **2001**, pp. 965–971.

[126] W. Xie et al., *An aquaporin-based vesicle-embedded polymeric membrane for low energy water filtration*. J. Mater. Chem. A, 1 (26) **2013**, pp. 7592–7600.

[127] T. Heinisch et al., *Fluorescence-Based Assay for the Optimization of the Activity of Artificial Transfer Hydrogenase within a Biocompatible Compartment*. ChemCatChem, 5 (3) **2013**, pp. 720–723.

[128] P. Broz et al., *Toward Intelligent Nanosize Bioreactors: A pH-Switchable, Channel-Equipped, Functional Polymer Nanocontainer*. Nano Lett., 6 (10) **2006**, pp. 2349–2353.

[129] K. Langowska, C. G. Palivan, and W. P. Meier, *Polymer nanoreactors shown to produce and release antibiotics locally*. Chem. Commun., 49 (2) **2013**, pp. 128–130.

[130] A. Graff et al., *Virus-assisted loading of polymer nanocontainer*. Proc. Natl. Acad. Sci. USA, 99 (8) **2002**, pp. 5064–5068.

[131] A. Ranquin et al., *Therapeutic Nanoreactors: Combining Chemistry and Biology in a Novel Triblock Copolymer Drug Delivery System*. Nano Lett., 5 (11) **2005**, pp. 2220–2224.

[132] M. Sauer et al., *Ion-carrier controlled precipitation of calcium phosphate in giant ABA triblock copolymer vesicles*. Chem. Commun., 23 **2001**, pp. 2452–2453.

[133] T. Haefele, K. Kita-Tokarczyk, and W. P. Meier, *Phase Behavior of Mixed Langmuir Monolayers from Amphiphilic Block Copolymers and an Antimicrobial Peptide*. Langmuir, 22 (3) **2006**, pp. 1164–1172.

[134] M. Nallani et al., *A nanocompartment system (Synthosome) designed for biotechnological applications*. J. Biotechnol., 123 (1) **2006**, pp. 50–59.

[135] M. Nallani, "A novel nanocompartment system named Synthosome for biotechnological applications". PhD thesis. Bremen, Germany: University of Bremen, Dec. 2005.

[136] O. Onaca, "Functionalized polymer vesicles and interactions with Polymyxin B and derivates". PhD thesis. Bremen, Germany: University of Bremen, July 2007.

[137] A. Graff, "Insertion of Membrane Proteins in Artificial Polymer Membranes". PhD thesis. Basel, Switzerland: University of Basel, Apr. 2006.

[138] W. P. Meier, C Nardin, and M Winterhalter, *Reconstitution of channel proteins in (polymerized) ABA triblock copolymer membranes*. Angew. Chem. Int. Ed., 39 (24) **2000**, 4599–4602.

[139] C Nardin et al., *Amphiphilic block copolymer nanocontainers as bioreactors*. Eur. Phys. J. E, 4 (4) **2001**, pp. 403–410.

[140] P. H. H. Duong et al., *Planar biomimetic aquaporin-incorporated triblock copolymer membranes on porous alumina supports for nanofiltration*. J. Membr. Sci., 409-410 **2012**, pp. 34–43.

[141] H.-J. Choi, H. Lee, and C. D. Montemagno, *Toward hybrid proteo-polymeric vesicles generating a photoinduced proton gradient for biofuel cells*. Nanotechnology, 16 (9) **2005**, pp. 1589–1597.

[142] H. Lee et al., *Vectorial insertion of bacteriorhodopsin for directed orientation assays in various polymeric biomembranes*. Polymer, 47 (9) **2006**, pp. 2935–2941.

[143] H.-J. Choi, J Germain, and C. D. Montemagno, *Effects of different reconstitution procedures on membrane protein activities in proteopolymersomes*. Nanotechnology, 17 **2006**, pp. 1825–1830.

[144] H.-J. Choi and C. D. Montemagno, *Biosynthesis within a bubble architecture*. Nanotechnology, 17 (9) **2006**, pp. 2198–2202.

[145] H.-J. Choi and C. D. Montemagno, *Light-Driven Hybrid Bioreactor Based on Protein-Incorporated Polymer Vesicles*. IEEE Trans. Nanotechnol., 6 (2) **2007**, pp. 171–176.

[146] D. Dobrunz et al., *Polymer Nanoreactors with Dual Functionality: Simultaneous Detoxification of Peroxynitrite and Oxygen Transport*. Langmuir, 28 (45) **2012**, pp. 15889–15899.

[147] J. Thoma et al., *Membrane protein distribution in composite polymer-lipid thin films*. Chem. Commun., 48 (70) **2012**, pp. 8811–8813.

[148] O. Onaca et al., *Functionalized Nanocompartments (Synthosomes) with a Reduction-Triggered Release System*. Angew. Chem. Int. Ed., 120 **2008**, pp. 7137–7139.

[149] D Ho et al., *Protein-driven energy transduction across polymeric biomembranes*. Nanotechnology, 15 **2004**, pp. 1084–1094.

[150] D. Ho et al., *Fabrication of biomolecule–copolymer hybrid nanovesicles as energy conversion systems*. Nanotechnology, 16 (12) **2005**, pp. 3120–3132.

[151] J. Z. Xi et al., *Lessons Learned from Engineering Biologically Active Hybrid Nano/Micro Devices*. Adv. Funct. Mater., 15 (8) **2005**, pp. 1233–1240.

[152] D Ho et al., *Hybrid Protein-Polymer Biomimetic Membranes*. IEEE Trans. Nanotechnol., 3 (2) **2004**, pp. 256–263.

[153] J. Habel, *Functional and chemical characterization of vesicular diblock copolymer bilayers with Aquaporin included*. Tech. rep. Copenhagen, Denmark, Oct. 2011.

[154] M. Espina, "Barrier properties of biomimetic membranes". MA thesis. Kgs. Lyngby: Danish Technical University, Oct. 2012.

[155] M. Nallani et al., *Proteopolymersomes:* In vitro *production of a membrane protein in polymersome membranes*. Biointerphases, 6 (4) **2011**, pp. 153–157.

[156] J. Bomholt, "Human Aquaporins - From *in vivo* detection to industrial scale production". PhD thesis. Copenhagen, Denmark: University of Copenhagen, Dec. 2014.

[157] X. Zhang et al., *Natural channel protein inserts and functions in a completely artificial, solid-supported bilayer membrane*. Sci. Rep., 3 **2013**, p. 2196.

[158] J. Dorn et al., *Planar Block Copolymer Membranes by Vesicle Spreading*. Macromol. Biosci., 11 (4) **2011**, pp. 514–525.

[159] K. Vijayan et al., *Interactions of Membrane-Active Peptides with Thick, Neutral, Nonzwitterionic Bilayers*. J. Phys. Chem. B, 109 (30) **2005**, pp. 14356–14364.

[160] S. Toughrai, "Functional surfaces through biomimetic block copolymer membranes". PhD thesis. Basel, Switzerland: University of Basel, Dec. 2014.

[161] E. Amado et al., *Spontaneous Formation of Giant Bioactive Protein-Block Copolymer Vesicles in Water*. ACS Macro Lett., 1 (8) **2012**, pp. 1016–1019.

[162] M. Noor et al., *Polymersome surface decoration by an EGFP fusion protein employing Cecropin A as peptide "anchor"*. J. Biotechnol., 157 (1) **2012**, pp. 31–37.

[163] L. Kuang et al., *"Frozen" Block Copolymer Nanomembranes with Light-Driven Proton Pumping Performance*. ACS Nano, 8 (1) **2014**, pp. 537–545.

[164] D. Hua, L. Kuang, and H. Liang, *Self-Directed Reconstitution of Proteorhodopsin with Amphiphilic Block Copolymers Induces the Formation of Hierarchically Ordered Proteopolymer Membrane Arrays*. J. Am. Chem. Soc, 133 (8) **2011**, pp. 2354–2357.

[165] L. Kuang et al., *Interface for Light-Driven Electron Transfer by Photosynthetic Complexes Across Block Copolymer Membranes*. J. Phys. Chem. Lett., 5 (5) **2014**, pp. 787–791.

[166] R. H. Perry, *Perry's Chemical Engineers' Handbook*. 7th ed. New York, NY, USA: McGraw-Hill, 1997.

[167] M. Mulder, *Basic principles of membrane technology*. 2nd ed. Dordrecht, The Netherlands: Kluwer academic publishers, Feb. 1996.

[168] R. Baker, *Membrane technology and applications*. 2nd ed. Chichester, UK: Jon Wiley & Sons, Nov. 2004.

[169] R. Valladares-Linares et al., *Forward osmosis niches in seawater desalination and wastewater reuse*. Water Res., 66 (C) **2014**, pp. 122–139.

[170] T. Y. Cath, A. E. Childress, and M. Elimelech, *Forward osmosis: Principles, applications, and recent developments*. J. Membr. Sci., 281 **2006**, pp. 70–78.

[171] F. Helfer, C. Lemckert, and Y. G. Anissimov, *Osmotic power with Pressure Retarded Osmosis: Theory, performance and trends - A review*. J. Membr. Sci., 453 (c) **2014**, pp. 337–358.

[172] J. Duan, E. Litwiller, and I. Pinnau, *Solution-diffusion with defects model for pressure-assisted forward osmosis*. J. Membr. Sci., 470 (C) **2014**, pp. 323–333.

[173] A. Tiraferri et al., *A method for the simultaneous determination of transport and structural parameters of forward osmosis membranes*. J. Membr. Sci., 444 (C) **2013**, pp. 523–538.

[174] K. Lutchmiah et al., *Forward osmosis for application in wastewater treatment: A review*. Water Res., 58 (C) **2014**, pp. 179–197.

[175] M. Elimelech and W. A. Phillip, *The Future of Seawater Desalination: Energy, Technology, and the Environment*. Science, 333 (6043) **2011**, pp. 712–717.

[176] D. L. Shaffer et al., *Forward osmosis: Where are we now?* Desalination, 356 (C) **2015**, pp. 271–284.

[177] J. R. McCutcheon et al., "Method of modifying thin film composite membrane support structures for engineered osmosis applications". Pat. US 2012/0048805. Mar. 2012.

[178] N.-N. Bui and J. R. McCutcheon, *Hydrophilic Nanofibers as New Supports for Thin Film Composite Membranes for Engineered Osmosis*. Environ. Sci. Technol., 47 **2013**, pp. 1761–1769.

[179] J. Ren and J. R. McCutcheon, *A new commercial thin film composite membrane for forward osmosis*. Desalination, 343 (C) **2014**, pp. 187–193.

[180] Y. Cui, X.-Y. Liu, and T.-S. Chung, *Enhanced osmotic energy generation from salinity gradients by modifying thin film composite membranes*. Chem. Eng. J., 242 (C) **2014**, pp. 195–203.

[181] L. Luo et al., *Novel thin-film composite tri-bore hollow fiber membrane fabrication for forward osmosis*. J. Membr. Sci., 461 (C) **2014**, pp. 28–38.

[182] Z. Thong et al., *Novel Nanofiltration Membranes Consisting of a Sulfonated Pentablock Copolymer Rejection Layer for Heavy Metal Removal*. Environ. Sci. Technol., 48 (23) **2014**, pp. 13880–13887.

[183] N. T. Hancock, N. D. Black, and T. Y. Cath, *A comparative life cycle assessment of hybrid osmotic dilution desalination and established seawater desalination and wastewater reclamation processes*. Water Res., 46 (4) **2012**, pp. 1145–1154.

[184] K. L. Hickenbottom et al., *Forward osmosis treatment of drilling mud and fracturing wastewater from oil and gas operations*. Desalination, 312 **2013**, pp. 60–66.

[185] N. T. Hancock et al., *Towards direct potable reuse with forward osmosis: Technical assessment of long-term process performance at the pilot scale*. J. Membr. Sci., 445 (C) **2013**, pp. 34–46.

[186] Nanyang Technological University et al., "Forward osmosis hollow fibre membrane". Pat. WO 2012/074487. June 2012.

[187] L. Setiawan et al., *Fabrication of poly(amide-imide)-polyethersulfone dual layer hollow fiber membranes applied in forward osmosis by combined polyelectrolyte cross-linking and depositions*. Desalination, 312 **2013**, pp. 99–106.

[188] X. Yang et al., *Membrane module design and dynamic shear-induced techniques to enhance liquid separation by hollow fiber modules: a review*. Desalin. Water Treat., 51 (16-18) **2013**, pp. 3604–3627.

[189] Y. Zhao et al., *Effects of Proteoliposome Composition and Draw Solution Types on Separation Performance of Aquaporin-Based Proteoliposomes: Implications for Seawater Desalination Using Aquaporin-Based Biomimetic Membranes*. Environ. Sci. Technol., 47 **2013**, pp. 1496–1503.

[190] X. Li et al., *Fusion behaviour of aquaporin Z incorporated proteoliposomes investigated by quartz crystal microbalance with dissipation (QCM-D)*. Colloids Surf. B: Biointerfaces, 111 **2013**, pp. 446–452.

[191] X. Li et al., *Preparation of high performance nanofiltration (NF) membranes incorporated with aquaporin Z*. J. Membr. Sci., 450 (C) **2014**, pp. 181–188.

[192] http://www.htiwater.com/.

[193] http://www.aquaporin.dk/.

[194] http://porifera.com/.

[195] http://oasyswater.com/.

[196] http://www.csmfilter.com/.

[197] http://www.toyobo-global.com/.

[198] http://www.modernwater.com/.

[199] http://cdmsmith.com/en-EU.aspx.

[200] http://trevisystems.com/.

[201] http://www.forwardwater.com/.

[202] S. Phuntsho et al., *Fertiliser drawn forward osmosis desalination: the concept, performance and limitations for fertigation*. Rev. Environ. Sci. Biotechnol., 11 (2) **2012**, pp. 147–168.

[203] S. Zhao et al., *Recent developments in forward osmosis: Opportunities and challenges*. J. Membr. Sci., 396 **2012**, pp. 1–21.

[204] I. Alsvik and M.-B. Hägg, *Pressure Retarded Osmosis and Forward Osmosis Membranes: Materials and Methods*. Polymers, 5 (1) **2013**, pp. 303–327.

[205] C. Zhao et al., *Modification of polyethersulfone membranes - A review of methods*. Prog. Mater. Sci., 58 (1) **2013**, pp. 76–150.

[206] A. L. Ahmad et al., *Recent development in additives modifications of polyethersulfone membrane for flux enhancement*. Chem. Eng. J., 223 (C) **2013**, pp. 246–267.

[207] C Barth et al., *Asymmetric polysulfone and polyethersulfone membranes: effects of thermodynamic conditions during formation on their performance*. J. Membr. Sci., 169 (2) **2000**, pp. 287–299.

[208] C. Klaysom et al., *Forward and pressure retarded osmosis: potential solutions for global challenges in energy and water supply*. Chem. Soc. Rev., 42 (16) **2013**, pp. 6959–6989.

[209] K. Y. Wang, T.-S. Chung, and J.-J. Qin, *Polybenzimidazole (PBI) nanofiltration hollow fiber membranes applied in forward osmosis process*. J. Membr. Sci., 300 (1-2) **2007**, pp. 6–12.

[210] L. Setiawan et al., *Fabrication of novel poly(amide-imide) forward osmosis hollow fiber membranes with a positively charged nanofiltration-like selective layer*. J. Membr. Sci., 369 (1-2) **2011**, pp. 196–205.

[211] G. P. Robertson et al., *Structural determination of Torlon® 4000T polyamide-imide by NMR spectroscopy*. Polymer, 45 (4) **2004**, pp. 1111–1117.

[212] N. Y. Yip et al., *High Performance Thin-Film Composite Forward Osmosis Membrane*. Environ. Sci. Technol., 44 (10) **2010**, pp. 3812–3818.

[213] J. de Groot, "A tale of two charges: zwitterionic polyelectrolyte multilayer membranes". PhD thesis. Enschede, The Netherlands: University of Twente, Oct. 2014.

[214] H.-J. Choi and C. D. Montemagno, *Recent Progress in Advanced Nanobiological Materials for Energy and Environmental Applications*. Materials, 6 (12) **2013**, pp. 5821–5856.

[215] M. M. Pendergast and E. M. V. Hoek, *A review of water treatment membrane nanotechnologies*. Energy Environ. Sci., 4 (6) **2011**, pp. 1946–1971.

[216] http://cordis.europa.eu/result/rcn/47761_en.html.

[217] M. T. Technologies et al., "Biomimetic membranes". Pat. WO 2004/011600. Feb. 2004.

[218] J. S. Hansen, "Development of supported biomimetic membranes for insertion of aquaporin protein water channels for novel water filtration applications ". PhD thesis. Kgs. Lyngby, Denmark: Danish Technical University, Oct. 2010.

[219] C. Rein et al., *Free-Standing Biomimetic Polymer Membrane Imaged with Atomic Force Microscopy*. Langmuir, 27 (2) **2011**, pp. 499–503.

[220] S. Ibragimova et al., *Hydrogels for* in situ *encapsulation of biomimetic membrane arrays*. Polym. Adv. Technol., 23 (2) **2010**, pp. 182–189.

[221] M. Perry et al., *Surface Modifications of Support Partitions for Stabilizing Biomimetic Membrane Arrays*. J. Membr. Sci. Technol., (1) **2011**, S1:001.

[222] Aquaporin AS et al., "Biomimetic membranes and uses thereof". Pat. WO 2010/146365. Dec. 2010.

[223] Aquaporin AS, P. H. Jensen, and D. Keller, "Membrane for filtering of water". Pat. WO 2006/122566. Nov. 2006.

[224] Aquaporin AS and P. H. Jensen, "Biomimetic water membrane comprising Aquaporins used in the production of salinity power". Pat. WO 2007/033675. Mar. 2007.

[225] Aquaporin AS et al., "Scaffold for composite biomimetic membrane". Pat. WO 2009/074155. June 2009.

[226] Aquaporin AS and J. S. Hansen, "Assays relating to biomimetic membranes and their uses". Pat. WO 2010/146366. Dec. 2010.

[227] Aquaporin AS, T. Vissing, and J. S. Hansen, "Liquid membrane suitable for water extraction". Pat. WO 2012/080946. June 2012.

[228] Danfoss et al., "Nanofabricated membrane using polymerized proteoliposomes". Pat. WO 2010/091078. Aug. 2010.

[229] K. Pszon-Bartosz, "Microfluidic devices for investigation of biomimetic membranes for sensor". PhD thesis. Kgs. Lyngby, Denmark: Danish Technical University, Nov. 2011.

[230] H. Wang et al., *Preparation and characterization of pore-suspending biomimetic membranes embedded with Aquaporin Z on carboxylated polyethylene glycol polymer cushion*. Soft Matter, 7 (16) **2011**, pp. 7274–7280.

[231] G. Sun et al., *A novel method of AquaporinZ incorporation via binary-lipid Langmuir monolayers*. Colloids Surf. B: Biointerfaces, 89 **2012**, pp. 283–288.

[232] Y Kaufman et al., *Fusion of Bolaamphiphile Micelles: A Method to Prepare Stable Supported Biomimetic Membranes*. Langmuir, 29 (4) **2013**, pp. 1152–1161.

[233] Y Kaufman, A Berman, and V. Freger, *Supported lipid bilayer membranes for water purification by reverse osmosis*. Langmuir, 26 (10) **2010**, pp. 7388–7395.

[234] V. Freger, A. Berman, and Y. Kaufman, "Biomimetic membranes, their production and uses thereof in water purification". Pat. US 2011/0084026. Apr. 2011.

[235] X. Li et al., *Preparation of supported lipid membranes for aquaporin Z incorporation*. Colloids Surf. B: Biointerfaces, 94 **2012**, pp. 333–340.

[236] Nanyang Technological University et al., "Aquaporin based thin film composite membranes". Pat. WO 2013/043118. Mar. 2013.

[237] Aquaporin AS et al., "Systems for water extraction". Pat. WO 2014/128293. Aug. 2014.

[238] P. Tanner, "Design and development of protein-polymer assemblies to engineer artificial organelles". PhD thesis. Basel, Switzerland: University of Basel, Sept. 2013.

[239] P. V. Pawar et al., *Functionalized polymersomes for biomedical applications*. Polym. Chem., 4 (11) **2013**, pp. 3160–3176.

[240] A. Jesorka and O. Orwar, *Liposomes: Technologies and Analytical Applications*. Annu. Rev. Anal. Chem., 1 (1) **2008**, pp. 801–832.

[241] Danfoss, AquaZ, and C. D. Montemagno, "Biomimetic membrane formed from a vesicle-thread conjugate". Pat. WO 2010/040353. Apr. 2010.

[242] G. Sun et al., *Stabilization and immobilization of aquaporin reconstituted lipid vesicles for water purification*. Colloids Surf. B: Biointerfaces, 102 **2012**, pp. 466–471.

[243] Y Kaufman et al., *Towards supported bolaamphiphile membranes for water filtration: Roles of lipid and substrate*. J. Membr. Sci., 457 (C) **2014**, pp. 50–61.

[244] G. Sun et al., *A layer-by-layer self-assembly approach to developing an aquaporin-embedded mixed matrix membrane*. RSC Adv., 3 (2) **2013**, pp. 473–481.

[245] G. Sun et al., *Highly permeable aquaporin-embedded biomimetic membranes featuring a magnetic-aided approach*. RSC Adv., 3 (24) **2013**, pp. 9178–9184.

[246] M. Wang et al., *Layer-by-Layer Assembly of Aquaporin Z-Incorporated Biomimetic Membranes for Water Purification*. Environ. Sci. Technol., 49 (6) **2015**, pp. 3761–3768.

[247] Y.-x. Shen et al., *Biomimetic membranes: A review*. J. Membr. Sci., 454 (C) **2014**, pp. 359–381.

[248] J. A. Thomas and A. J. H. McGaughey, *Reassessing Fast Water Transport Through Carbon Nanotubes*. Nano Lett., 8 (9) **2008**, pp. 2788–2793.

[249] J. Holt et al., *Fast Mass Transport Through Sub-2-Nanometer Carbon Nanotubes*. Science, 312 (5776) **2006**, pp. 1034–1037.

[250] Z. Fei et al., *A Synthetic Zwitterionic Water Channel: Characterization in the Solid State by X-ray Crystallography and NMR Spectroscopy*. Angew. Chem. Int. Ed., 44 (35) **2005**, pp. 5720–5725.

[251] V. Percec et al., *Self-assembly of amphiphilic dendritic dipeptides into helical pores*. Nature, 430 (7001) **2004**, pp. 764–768.

[252] M. Barboiu, *Artificial Water Channels*. Angew. Chem. Int. Ed., 51 (47) **2012**, pp. 11674–11676.

[253] X. Zhou et al., *Self-assembling subnanometer pores with unusual mass-transport properties*. Nat. Commun., 3 **2012**, p. 949.

[254] K. Ibata et al., *Analysis of Aquaporin-Mediated Diffusional Water Permeability by Coherent Anti-Stokes Raman Scattering Microscopy*. Biophys. J., 101 (9) **2011**, pp. 2277–2283.

[255] A. B. Mamonov et al., *Water and Deuterium Oxide Permeability through Aquaporin 1: MD Predictions and Experimental Verification*. J. Gen. Physiol., 130 (1) **2007**, pp. 111–116.

[256] F. Itel et al., *CO_2 permeability of cell membranes is regulated by membrane cholesterol and protein gas channels*. FASEB J., 26 (12) **2012**, pp. 5182–5191.

[257] J. Habel et al., *How molecular internal-geometric parameters affect PB-PEO polymersome size in aqueous solution*. J. Polym. Sci. B Polym. Phys., submitted.

[258] U Kragh-Hansen, M le Maire, and J. V. Møller, *The mechanism of detergent solubilization of liposomes and protein-containing membranes.* Biophys. J., 75 (6) **1998**, pp. 2932–2946.

[259] http://www.iss.com/.

[260] E. L. Wittbecker and P. W. Morgan, *Interfacial polycondensation. I.* J. Polym. Sci., 40 (137) **1959**, pp. 289–297.

[261] A. K. Ghosh et al., *Impacts of reaction and curing conditions on polyamide composite reverse osmosis membrane properties*. J. Membr. Sci., 311 (1-2) **2008**, pp. 34–45.

[262] M. J. T. Raaijmakers et al., *Sieving of Hot Gases by Hyper-Cross-Linked Nanoscale-Hybrid Membranes*. J. Am. Chem. Soc, 136 (1) **2014**, pp. 330–335.

[263] P Ajit Walter, T Muthukumar, and B. Reddy, *Assessment of antifouling efficacy of polyhedral oligomeric silsesquioxane based poly (urea-urethane-imide) hybrid membranes*. Lett. Appl. Microbiol., 61 (3) **2015**, pp. 274–282.

[264] M. Dalwani et al., *Ultra-thin hybrid polyhedral silsesquioxane-polyamide films with potentially unlimited 2D dimensions*. J. Mater. Chem., 22 (30) **2012**, pp. 14835–14838.

[265] K. P. Lee et al., *pH stable thin film composite polyamine nanofiltration membranes by interfacial polymerisation*. J. Membr. Sci., 478 (C) **2015**, pp. 75–84.

[266] Y. Zhang, N. E. Benes, and R. G. H. Lammertink, *Visualization and characterization of interfacial polymerization layer formation*. Lab Chip, 15 **2015**, pp. 575–580.

[267] http://webbook.nist.gov/cgi/cbook.cgi?ID=B6002924&Mask=80.

[268] http://webbook.nist.gov/cgi/cbook.cgi?ID=B6002924&Mask=80.

[269] L Germic et al., *Characterization of polyacrylonitrile ultrafiltration membranes*. J. Membr. Sci., 132 (1) **1997**, pp. 131–145.

[270] O. W. Webster, *Living Polymerization Methods*. Science, 251 (4996) **1991**, pp. 887–893.

[271] R. Nehring, "Amphiphilic Diblock Copolymers for Molecular Recognition". PhD thesis. Basel, Switzerland: University of Basel, Feb. 2009.

8 Appendices

8.1 Appendix I: PB-PEO diblock copolymer synthesis

PB-PEO polymerization was accomplished via living anionic polymerization. Compared to other polymerization methods like free radical initiation or chemical condensation, this kind of polymerization has the advantage of narrow PDI_M, defined chain ends and high conversion [270, 271]. In contrast to free radical polymerization, termination reactions can be prevented and the active species can be maintained until quenched with a desired end group. Anionic living polymerization contains three steps: initiation, propagation and termination. Chain growth is initiated via a Lewis-Base, producing an active carbanion that reacts with other monomers and so performs chain propagation. Protons inactivate the active carbanion, so every proton donor can work as a quenching agent for anionic living polymerizations. THF turned out to be a good solvent [71]. As far as anionic polymerization is very sensitive to oxygen and moist, air- and waterfree conditions are crucial for the success of this polymerization [271].

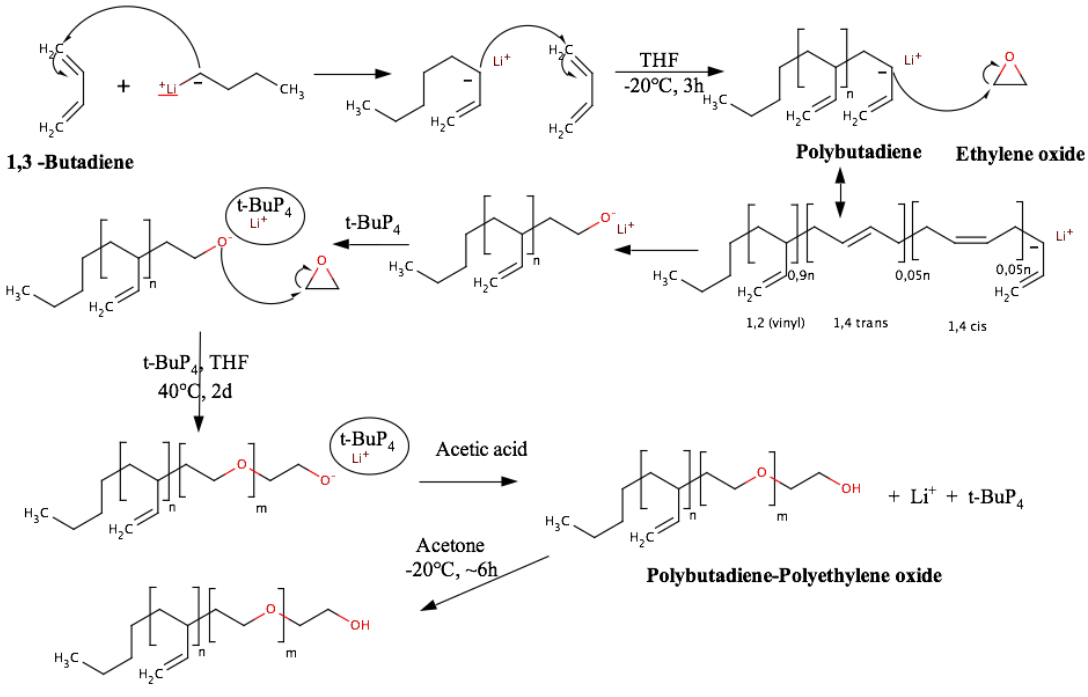

Figure 41: Chemical sketch of PB-PEO synthesis

In this case, Bd was polymerized with *n*-BuLi as initiator (Figure 41). PB has the molar ratio between 1,2 addition, 1,4 *trans*-addition and 1,4 *cis*-addition of 9:(1) in THF. Adding of EO shuts down this polymerization, whereas the EO end is still active. Polymerization

of further EO is however hindered by the Li^+ cations that strongly bind to this living end. tBuP4 reduces this association so that the EO polymerization is allowed to run in presence of tBuP4. Due to the basic character of tBuP4, the reaction can be easily quenched within adding of protons, in forms of usual acids like acetic acid, as used in this work [271].
According to the findings made in chapter 2, nine promising regions in a diagram of M_n against f for incorporation capable polymersomes, stated as setpoints, were chosen as a baseline for a systematic study. As a result, block lengths for Bd and EO were calculated from given M_n and f values and an assumed PDI_M of 1.1.
Unfortunately, there was a lack of PB-PEO references for calculating dn/dc to obtain M_w and PDI_M from the SEC analysis. The existing Polystyrene standards couldn't achieve reasonable M_w. Therefore, SEC was only used to check if the PDI_M is generally broad, meaning only one and a narrow peak, and if the peak was shifted from the PB precursor to PB-PEO. ^{1}H-NMR was used to obtain the block lengths, respectively M_n, which was then used as the new internal-geometrical factor instead of M_w. This is also reasonable as far as M_n is more sensitive to low molecular weight polymers.

After four optimizations of the protocol, there were 31 synthesis approaches, whereas 24 of them led to a polymer, 17 of them could be used for polymersome formation and 8 of them met the criteria of the setpoints that were described in chapter 2 (Table 4). Bd was always purified first and weighted to get the volume (measured dividing by the temperature-adjusted density). The EO volume to achieve the desired stoichiometry was calculated from the obtained Bd volume. All further calculated values (f_{cal}, $M_{n(cal)}$, $N_{Bd(cal)}$ and $N_{EO(cal)}$) were calculated from the obtained EO volume. Due to the difference between the obtained and the calculated EO volume, f_{set} and f_{cal} as well as $M_{n(set)}$ and $M_{n(cal)}$ are not the same value. Note that the offsets (Δf, ΔN_{Bd} and ΔN_{EO}) are always referring to the difference between the experimental and the calculated (not the originally set) value.
The protocol for purification of the monomers as well as the synthesis was a result of several optimization steps, compared to the original protocol from Förster [72].
The criteria for optimization (in contrast to the systematic study of chapter 2 were always the offset of the block lengths of Bd and EO from the targeted value. The reasonable range was set to ±25% for both monomers. A polymer with too high block length of the one monomer and too low of the other could probably be in a reasonable M_n range. On the other hand could a polymer with too high, respectively too low block length of both monomers probably reveal a reasonable f. Therefore, M_n and f were not taken as criteria as far as they could be misleading.

Table 4: Overview table of all synthesized polymers with set $M_{w(set)}$, PDI_M (calculated with Polystyrene standard) and $f_{(set)}$, $f_{(cal)}$, block lengths $N_{Bd(cal)}$ and $N_{EO(cal)}$ and $M_{n(cal)}$ (calculated from the obtained monomer volumes) compared to all experimental values except M_w that couldn't be obtained due to missing PB-PEO standard at SEC analysis. It has to be mentioned that PB_{43}-PEO_{32}. PB_{74}-PEO_{60} and PB_{107}-PEO_{22} were synthesized with a different synthesis than the other polymers after Hillmyer, starting with the finished PB [70], they were therefore left out for analysis. PB_{29}-PEO_{19} and PB_{46}-PEO_{32} contain wrong calculation. Therefore, all these polymers have different $N_{Bd(cal)}$ and $N_{EO(cal)}$.

Polymer	Setpoint	Synthesis	Polymersomes?	$M_{w(set)}$ [kg/mol]	PDI_M	$f_{(set)}$	$f_{(cal)}$	$f_{(exp)}$	Δf [%]	$N_{Bd(cal)}$	$N_{Bd(exp)}$	ΔN_{Bd} [%]	$N_{EO(cal)}$	$N_{EO(exp)}$	ΔN_{EO} [%]	$M_{n(cal)}$ [kg/mol]	$M_{n(exp)}$ [kg/mol]	ΔM_n [%]
PB_{28}-PEO_{24}	1	2 SEC peaks	Not used	3.5	1.1	0.35	0.35	0.35	-0.55	34	28	-17.82	30	24	-18.53	3.2	2.6	-18.12
PB_{32}-PEO_{30}	1	Run to end	Yes	3.5	1.02	0.35	0.35	0.37	3.96	34	32	-6.91	30	30	-1.08	3.2	3.0	-4.48
PB_{62}-PEO_{56}	2	Run to end	Yes	7.5	1.01	0.35	0.35	0.36	2.05	74	62	-15.88	64	56	-13.2	6.8	5.8	-14.77
PB_{92}-PEO_{78}	3	Run to end	Yes	11	1.08	0.35	0.35	0.34	-1.71	108	92	-15.07	94	78	-17.29	10.0	8.4	-15.99
PB_{104}-PEO_{77}	3	Run to end	Yes	11	1.05	0.35	0.35	0.31	-10.3	108	104	-3.61	94	77	-18.09	10.0	9.0	-9.61
PB_{59}-PEO_{3}	4	Run to end	No	3.5	1.02	0.25	0.25	0.03	-89.41	41	59	44.7	22	3	-88.18	3.2	3.3	4.32
PB_{43}-PEO_{32}	4	Run to end	Yes	3.5	1.03	0.25	0.19	0.32	71.35	41	43	5.37	15	32	115.33	2.9	3.8	30.58
PB_{29}-PEO_{19}	4	Run to end	Yes	3.2	1.01	0.25	0.19	0.29	59.23	41	29	-30.49	15	19	27.83	2.9	2.4	-17.11
PB_{33}-PEO_{18}	4	Run to end	Yes	3.5	1.01	0.25	0.25	0.84	41	33	-19.88	22	18	-18.98	3.2	2.6	-19.6	
PB_{41}-PEO_{22}	4	Failed		7.5		0.25												
PB_{80}-PEO_{5}	5	Run to end	No	7.5	1.04	0.25	0.25	0.04	-85.08	88	80	-8.64	47	5	-89.36	6.8	4.6	-33.08
PB_{74}-PEO_{60}	5	Run to end	Yes	7.5	1.01	0.25	0.23	0.33	46.09	88	74	-15.46	42	60	42.98	6.6	6.7	0.88
PB_{46}-PEO_{32}	5	Run to end	Yes	7.3	1.00	0.25	0.23	0.30	31.84	88	46	-48.01	42	32	-24.35	6.6	3.9	-41.39
PB_{29}-PEO_{16}	5	Run to end	Yes	7.5	1.00	0.25	0.25	0.26	3.78	88	29	-67.1	47	16	-65.43	6.8	2.3	-66.59
PB_{117}-PEO_{61}	6	Run to end	Yes	11	1.11	0.25	0.25	0.25	-1.53	129	117	-9.07	69	61	-10.91	10.0	9.1	-9.63
PB_{47}-PEO_{7}	7	Run to end	Yes	3.5	1.03	0.15	0.15	0.09	-42.08	48	47	-2.81	14	7	-47.68	3.2	2.9	-11.42
PB_{45}-PEO_{14}	7	Run to end	Yes	3.5	1.01	0.15	0.15	0.16	5.38	48	45	-7.03	14	14	-1.07	3.2	3.0	-5.89
PB_{104}-PEO_{31}	8	Run to end	Yes	7.5	1.12	0.15	0.15	0.16	3.66	102	104	1.54	29	31	5.95	6.8	7.0	2.37
PB_{98}-PEO_{42}	8	2 SEC peaks	Not used	7.5	1.18	0.15	0.15	0.21	40.18	102	98	-3.53	29	42	45.52	6.8	7.2	5.68
PB_{150}-PEO_{43}-1	9	Run to end	No	11		0.15												
PB_{150}-PEO_{43}-2	9	Failed		11		0.15												
PB_{150}-PEO_{43}-3	9	Failed		11		0.15												
PB_{150}-PEO_{43}-4	9	Failed		11		0.15												
PB_{95}-PEO_{2}	9	Run to end	No	11	1.078	0.15	0.15	0.01	-91.5	150	95	-36.4	43	2	-95.35	10.0	5.3	-47.55
PB_{150}-PEO_{43}-5	9	Failed		11		0.15												
PB_{150}-PEO_{43}-6	9	1 broad peak	Not used	11	7.053	0.15												
PB_{142}-PEO_{53}	9	2 SEC peaks	Not used	11	1.184	0.15	0.15	0.19	24.82	150	142	-5.6	43	53	23.26	10.0	10.0	-0.14
PB_{121}-PEO_{25}	9	Run to end	Yes	11	1.012	0.15	0.15	0.11	-26.13	150	121	-19.05	43	25	-42.85	10.0	7.7	-23.55
PB_{107}-PEO_{22}	9	Run to end	No	11	1.015	0.15	0.15	0.12	-22.07	150	107	-28.95	42	22	-46.67	10.0	6.8	-32.24
PB_{60}-PEO_{25}	9	Run to end	Yes	11	1.006	0.15	0.15	0.21	37.63	150	60	-60.3	43	25	-41.45	10.0	4.3	-56.74
PB_{120}-PEO_{41}	9	Run to end	Yes	11	1.000	0.15	0.15	0.18	16.13	150	120	-19.95	43	41	-4.3	10.0	8.3	-16.99

Regarding to Förster, Bd should be distilled over *n*-Bu_2Mg and *n*-BuLi, whereas EO was supposed to be distilled over calcium hydride (CaH_2), sodium mirror and *n*-BuLi. In the first protocol, CaH_2 and *n*-Bu_2Mg were chosen for Bd purification as far as *n*-BuLi was also the polymerization initiator for Bd, so there would be a loss of Bd when using *n*-BuLi for purification. The *n*-BuLi step was left out at EO purification.
Förster added tBuP4 into the reactor even before Bd polymerization to avoid contamination of the tBuP4 solvent hexane. The polymerization was thought to last for 4-6 h at -78°C. In order to save time, the reaction was speeded up to 3 h at -20°C for the first protocol. Furthermore, tBuP4 was added just before EO polymerization as far as its influence on Bd polymerization was thought to be greater than hexanes' influence on the EO polymerization.
For the endcapping, Förster added a small amount of EO first at -40°C. Instead of one amount for endcapping and the rest for polymerization, the whole EO was added once, due to the difficulty to add EO separately, as far as the used volumes were small. The further polymerization of EO was then allowed to run for 2 d at 40°C following Förster, whereas there should appear a deep blue color after 1 d. This was performed as well in the first protocol, however a blue color only appeared once during all reactions. The warming up from -40°C to 40°C was performed quickly. Polymer quenching was done with acetic acid in a molar ratio to the tBuP4 initiator of 1:3, and the resulting polymer was precipitated over 400 ml -20°C cold acetone as described in Förster.
The outcoming polymer of the first protocol was a yellowish honey-like solid. No EO was attached and the Bd block length was off by 35%. SEC analysis revealed a sharp peak, so the PDI_M was reasonable. Reasons for no attachment could be insufficient purification or leaks in the vacuum during the polymerization.

As far as EO polymerization is a first-order-reaction and therefore known to polymerize slowly at small volume concentrations, the amount of THF was reduced to approximately 500 ml for the second protocol, instead of approximately 1000 ml like previously used. To further increase the reaction speed, the temperature was set up to 45°C and only run for 1.5 d. EO was again added in two portions.
Here, EO was attached for the first time, visible from the characteristic peak for EO at 3.65 ppm from the NMR (Figure 42, top panel). SEC analysis of the resulting polymer however revealed a bad PDI_M (see Figure 42, bottom panel). It seemed that at least one of the monomers were dirty.

Therefore, the focus for the third protocol was on monomer purification. Both monomers were now distilled over 1ml *n*-Bu_2Mg and 1 ml *n*-BuLi. Furthermore, a degassing step

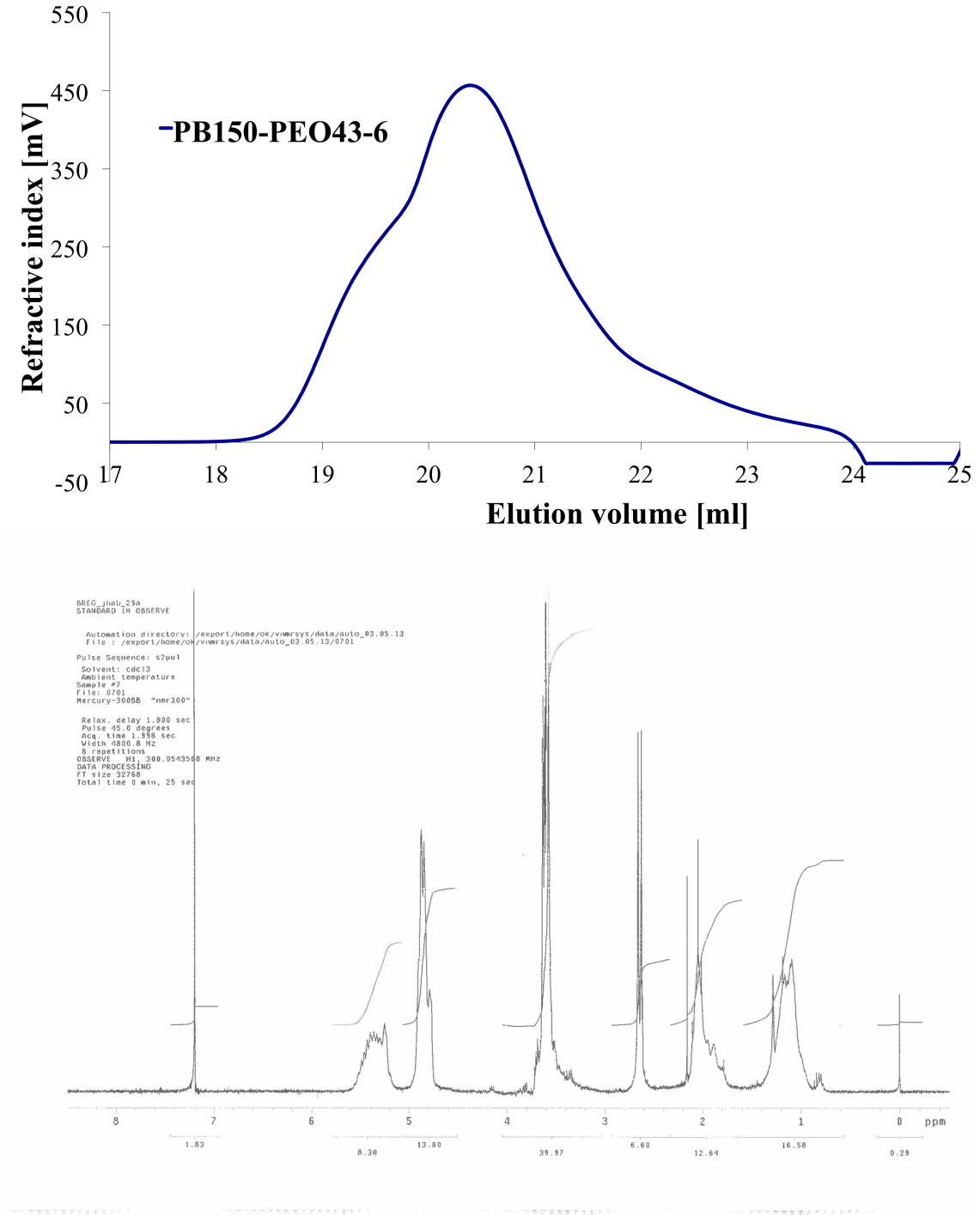

Figure 42: *Top*: SEC elugram of PB_{150}-PEO_{43}-6, produced with second synthesis protocol. The peak was broad, which indicates a bad PDI_M. *Bottom*: ^{1}H-NMR of PB_{150}-PEO_{43}-6. EO was attached for the first time, which can be seen from the high peak at approximately 3.56 ppm.

was added. This procedure contained freezing the monomer via liquid nitrogen for 10 min and evacuating the flask afterwards. The procedure was repeated, whereas the pressure should be approximately 10^{-2} mbar in both degassing procedures, to ensure that the

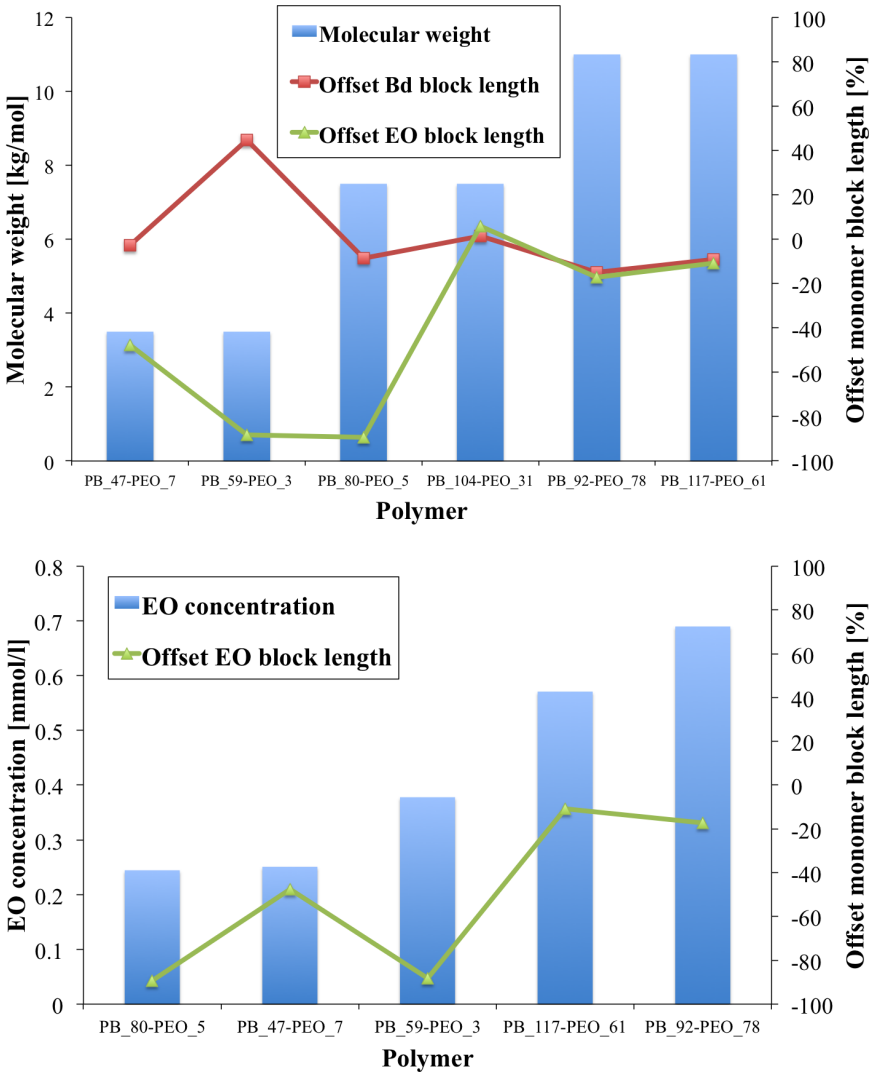

Figure 43: Top panel: Comparison of $M_{w,PB-PEO}$s of PB-PEO samples, synthesized with the fourth protocol. Surprisingly, the higher $M_{w,PB-PEO}$ samples had a better EO conversion than the low $M_{w,PB-PEO}$ samples. Bottom panel: Comparison of EO concentrations of the same samples. There was a slight indication that higher EO concentration leads to better EO conversion.

monomer is completely free of oxygen. The CaH_2 step was left out due to time reasons. After degassing, the monomer is thawed and warmed to 0°C within ice water. The reaction took place for 20 min in order to clean the monomer completely but in terms of Bd not to polymerize too much. In summary, both monomers were distilled into a flask with 1 ml *n*-Bu_2Mg, where the solvent was first evaporated, degassed with liquid nitrogen two times, allowed to react with *n*-Bu_2Mg for 20min, distilled in another flask with a film of 1 ml *n*-BuLi and again degassed and allowed to react in the same manner. The reaction was performed the same like in the second protocol.

Eight polymers were synthesized according to the third protocol that was the first reason-

able amount to do comparisons. All polymers had EO attached, three of them had Bd and EO block length inside the reasonable range of below 25% off from the desired length, three polymers were beyond that range and two polymers revealed two peaks with SEC analysis and therefore couldn't be analyzed for block length numbers. During the synthesis of PB_{104}-PEO_{31}, the stopcock flew out after half a day, however the EO block length fitted well to another value, so the polymer can be used as well. This polymer has to be analyzed with regard to that fact.
It was thought first that polymers with higher $M_{w,PB-PEO}$ perform worse due to other effects rising from the polymer length. Contrary to this thought, the highest $M_{w,PB-PEO}$ polymers performed the best, whereas the lower one did not (see Figure 43, top panel). When looking at EO concentrations in Figure 43, bottom panel, one could indicate a decreasing polymerization performance with decreasing concentration. PB_{59}-PEO_3 did not have proper EO polymerization even though the EO concentration was higher than PB_{47}-PEO_7. Samples performed reasonable with an EO volume concentration of at least 2%.

The fourth protocol was developed, based on the findings mentioned above. The Bd polymerization was elongated to 4 h to make sure it's complete, when EO is added. Besides, the THF volume was decreased by half to approximately 250 ml or lower, depending on the EO volume, in order not to undergo an EO volume concentration of 2% to enhance the concentration of the complex of the active carbanion, tBuP4 and Li^+ that could increase the EO conversion rate. Finally, the temperature of the EO polymerization was set between 40°C and 45°C, depending on the pressure that should not exceed 1.5 bar to avoid further stopcock releases.
Two of the resulting polymers performed well in terms of EO and Bd block length, one had again two peaks at SEC analysis and one had 42% less EO units than expected. Even more than the EO volume concentration, it was the pure EO volume that was significantly different between the sample with bad conversion (40a; 4.5 ml EO) and the samples with good conversion (39a and 41a; 14.5 ml and 16.5 ml). From that finding, the EO volume that got lost during polymerization was calculated, defined as the difference between the EO volume that was added to the reactor and the theoretical volume EO would have with the mol number of the EO block length in the resulting PB-PEO. It turned out that even in the well performing polymers, there was always a loss of approximately 2 ml of EO.

Taking these findings into account, 2 ml EO was always added extra to the calculated amount in the final protocol. To minimize monomer loss, the reactor was cooled down to -70°C in a bath with isopropanol, completely saturated with dry ice; after addition of Bd as well as after the second addition of EO. It was left at this temperature for 10 min

to ensure that the major volume of the monomer went into solution. The temperature was then set to the values of the certain reaction. To avoid wasting expensive tBuP4, a PB precursor was drawn after endcapping of PB and analysed via SEC to make sure that there was only one polymer in the solution. After quenching of the EO polymerization, PB-PEO was precipitated in 800 ml acetone, cooled in dry ice, to get the highest possible solid amount.

The next two synthesized polymers following that protocol, worked fine. Due to stock limitations from Sigma-Aldrich, there was only little volume of tBuP4 left for the last three polymers. Consequently, the volume dimension had to be decreased, meaning less THF, Bd and EO, so that EO would be again in the volume range of bad performing samples (< 10 ml), however its volume concentration would be in the range of good performing samples (> 2% v/v).

None of the following three polymers were in the reasonable range for the EO block length. The same was unfortunately valid for Bd as well. This could be an indication that there was too much dead volume in the reactor with standard volume of 1 L for the volume dimension of the samples (THF volumes: 60-90 ml). As a consequence, a majority of the monomer stayed in the gas phase and did not participate in the polymerization process. On the other hand this could as well indicate that not EO concentration but pure EO volume was the crucial factor for the EO polymerization process.

From the last four synthesis performed, two went successful, two did not. In one of the two unsuccessful ones the reactor got under too high pressure due to a defect temperature sensor. The second unsuccessful one (over 60% offset for both monomer block lengths) was in a reasonable EO volume range at first sight. At second sight, it could be that this sample marked the line between complete and incomplete EO conversion within 2 d. Comparing all polymers in terms of EO conversion and EO volumes, a clear pattern could be seen, showing a sharp decrease in EO conversion efficiency between 10 and 12 ml EO (Figure 44, top panel). It may be as well noteworthy to compare EO's mol numbers as far as they are fixed values, whereas the volumes are dependent on the temperature sensitive density varying from sample to sample. The sharp decrease, here between 0.22 and 0.26 mol was also visible there (Figure 44, bottom panel).

From a kinetic point of view there was as well a correlation between offset and the apparent rate constant of first-order-reactions k_{app}, however not as good as the one with EO volume and mol number (Figure 45 top panel). The sample with highest offset above 60% was significantly below k_{app} of 1. The doubling of k_{app} from approximately 3 to approximately 6 did not find an analogy in the EO block offset. The best performing samples were in the range between k_{app} 1 and 3, together with significantly worse performing sample without a clear pattern. As far as the EO block length is dependent on the Bd

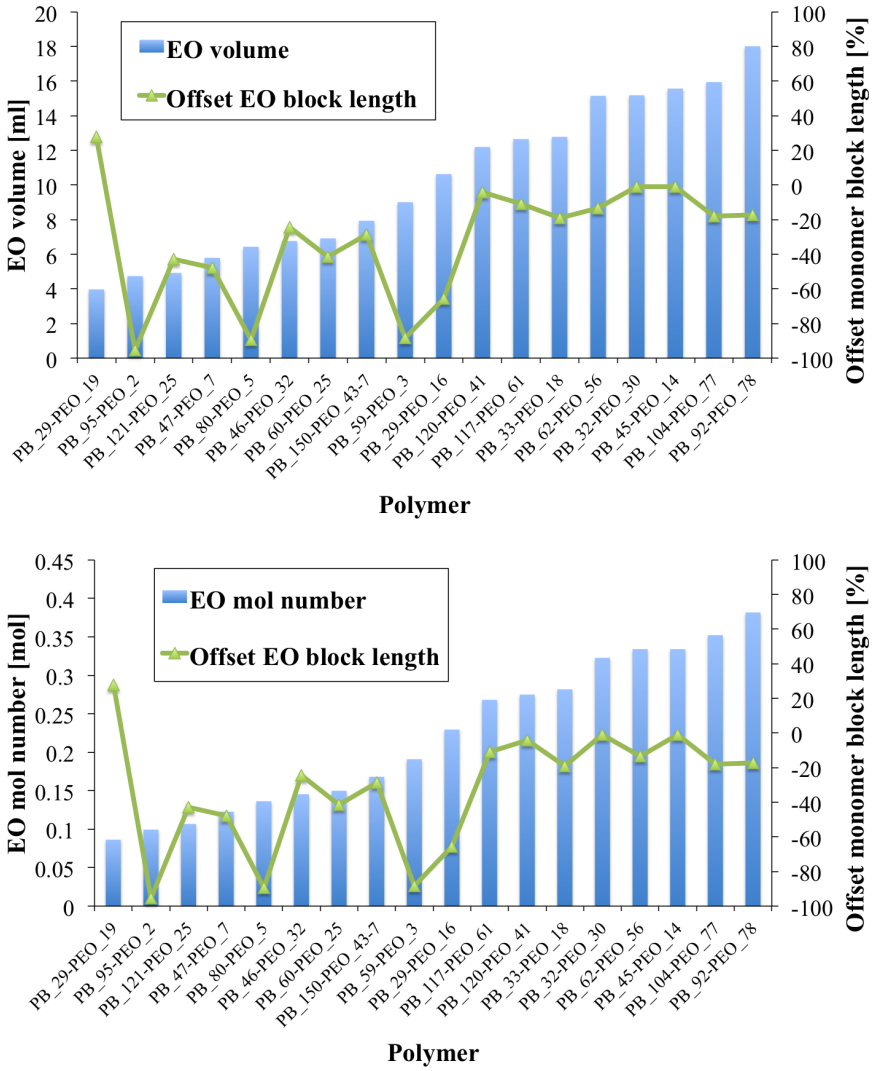

Figure 44: Comparison of EO volumes (top panel) and EO mol number (bottom panel) with regard to offset of EO block length. There was obviously a sharp decrease in conversion efficiency between 10 and 12 ml, respectively between 0.22 and 0.26 mol. The mol number comparison was more reliable than the volume comparison, as far as mol number was a fixed number, whereas volume was dependent from EO's density that varied with the temperature dry ice of the EO container that was different from sample to sample.

conversion, k_{app} was furthermore compared with the EO conversion. However, a pattern could not neither be found at that comparison (Figure 45 bottom panel).

There seemed to be a similar line for Bd as well, however with a lower accuracy. Bd volume (Figure 46 top panel) and mol number (Figure 46 bottom panel) was compared with regard to Bd conversion. The focus will be on the mol number as far as Bd had higher volumes revealing higher inaccuracy due to density dependence. When setting the line at the mol number of PB_{29}-PEO_{16}, the second unsuccessful sample with the last protocol mentioned above, one could argue that PB_{95}-PEO_2 was an early protocol generation sam-

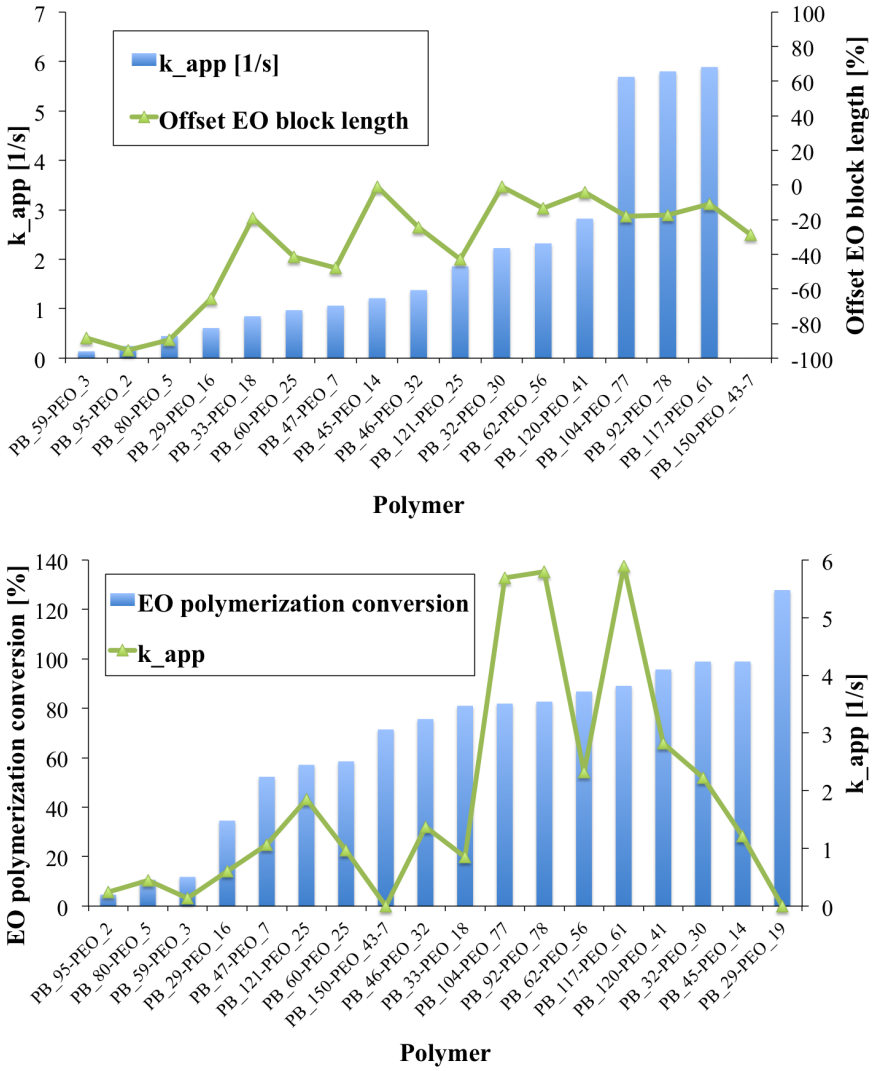

Figure 45: *Top panel*: Comparison of apparent rate constant k_{app} with regard to offset of EO block length. There is a rough correlation in the sense that the worst performing polymers also had the lowest k_{app}. However in a range between k_{app} 1 and 3, one can find polymers with a offset of EO block length of 1% between offsets of 40%. *Bottom panel*: Comparison of k_{app} with regard to EO conversion. No clear correlation can be found here neither.

ple with several errors contained and PB_{60}-PEO_{25} in the low volume dimension did not perform well due to the reactor dead volume problem discussed before. PB_{59}-PEO_3 with 50% more Bd block length than expected, remained unclear. Furthermore, the pressure values during Bd degassing were significantly high, however sample PB_{80}-PEO_5 from the same purification batch had a good Bd conversion.

The mol number of PB_{29}-PEO_{16} were almost identical to sample PB_{32}-PEO_{30} and PB_{121}-PEO_{25} with good Bd conversion, in contrast to significantly different EO mol numbers at the line. Additionally, the reaction times had been changed during the protocols. To sum it up, the conversion success line for Bd has to be questioned.

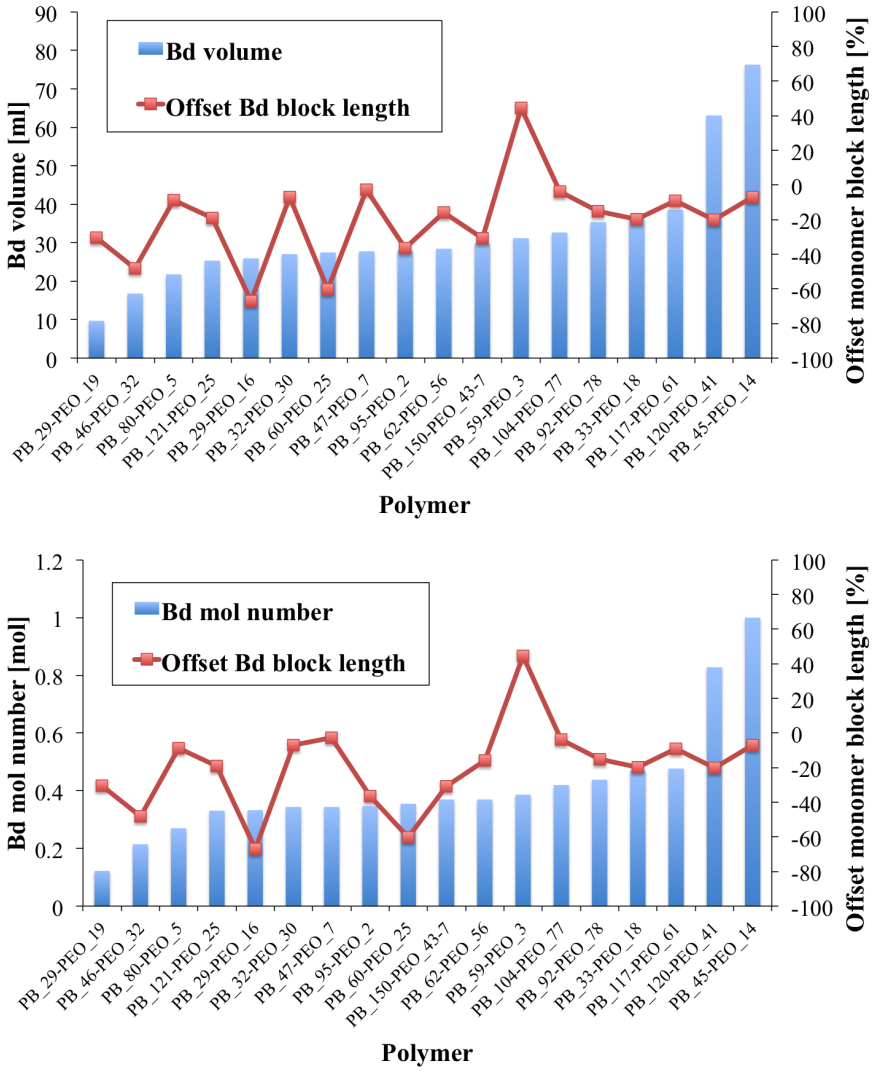

Figure 46: Comparison of Bd volumes (top panel) and Bd mol number (bottom panel) with regard to offset of both monomer's block lengths. There was hardly a line between good and bad conversion like it is the case for EO. Furthermore, reaction times were changed during protocol optimization, so a direct comparison remained problematic.

There were no other parameters where a link between conversion efficiency could be obtained. The following parameters were chosen for comparison with regard offset of both monomer block lengths, respectively of only one, if there is no contribution of the parameter to one monomer:

- $M_{w,PB-PEO}$ and f_{phil} in Figure 47
- Concentration of both monomers in Figure 48
- Concentration, mol number and volume of *n*-BuLi in Figure 49

- Concentration of tBuP4 (for tBuP4, only the volume was shown, as far as concentration and mol number were identical to *n*-BuLi), volume of THF and acetic acid in Figure 50
- Conversion of Bd and EO in Figure 51
- Time, pressure and temperature of the Bd polymerization in Figure 52
- Time, pressure and temperature of the Bd endcapping in Figure 53
- Time, pressure and temperature of the EO polymerization in Figure 54
- Sensor temperatures during EO polymerization and color development in Figure 55
- Yield and overall efficiency in Figure 56

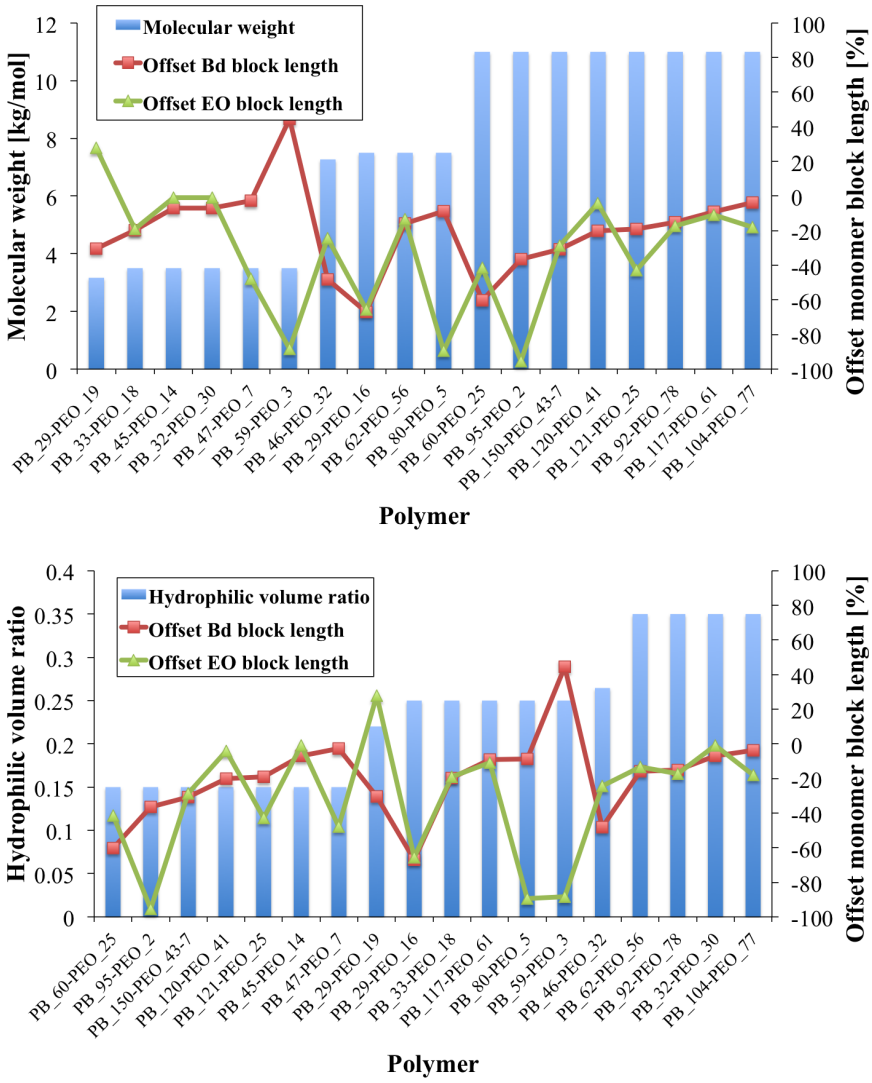

Figure 47: Comparison of $M_{w,PB-PEO}$ (top panel) and f_{phil} (bottom panel) with regard to the offset of both monomer block lengths.

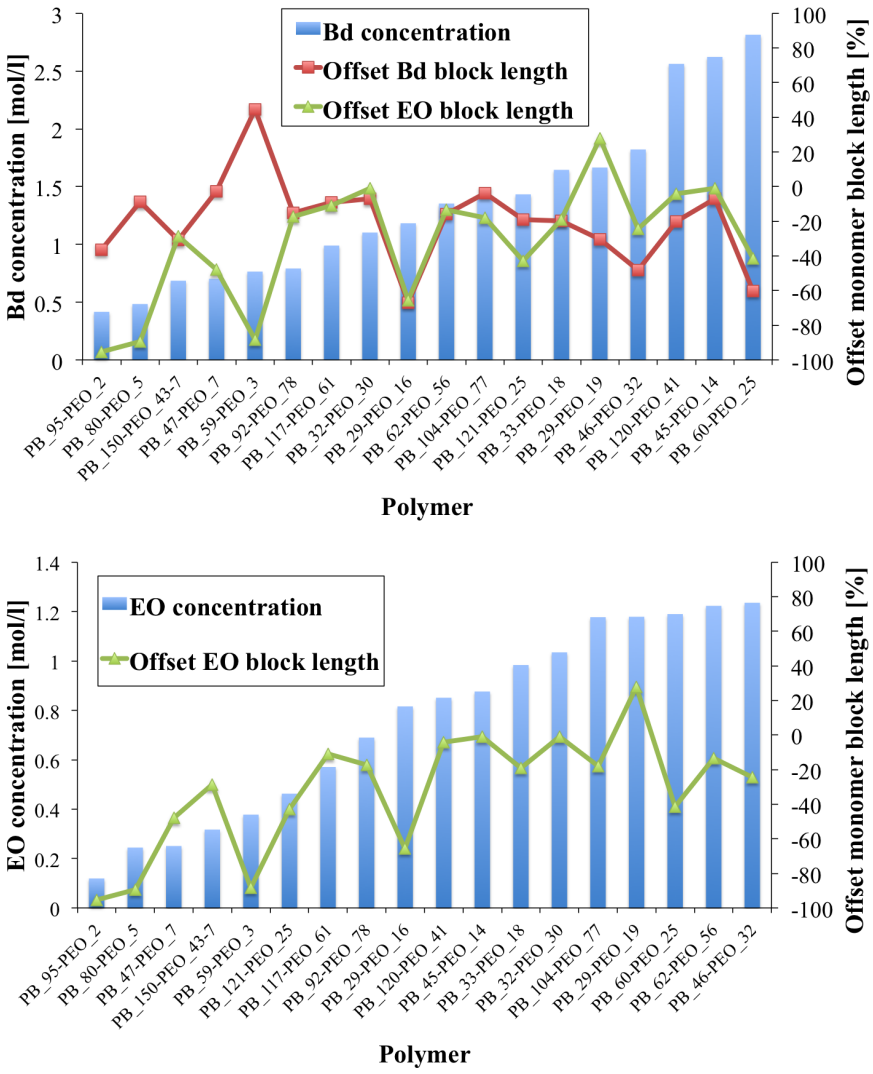

Figure 48: Comparison of Bd (top panel) and EO (bottom panel) concentration with regard to the offset of both monomer block lengths.

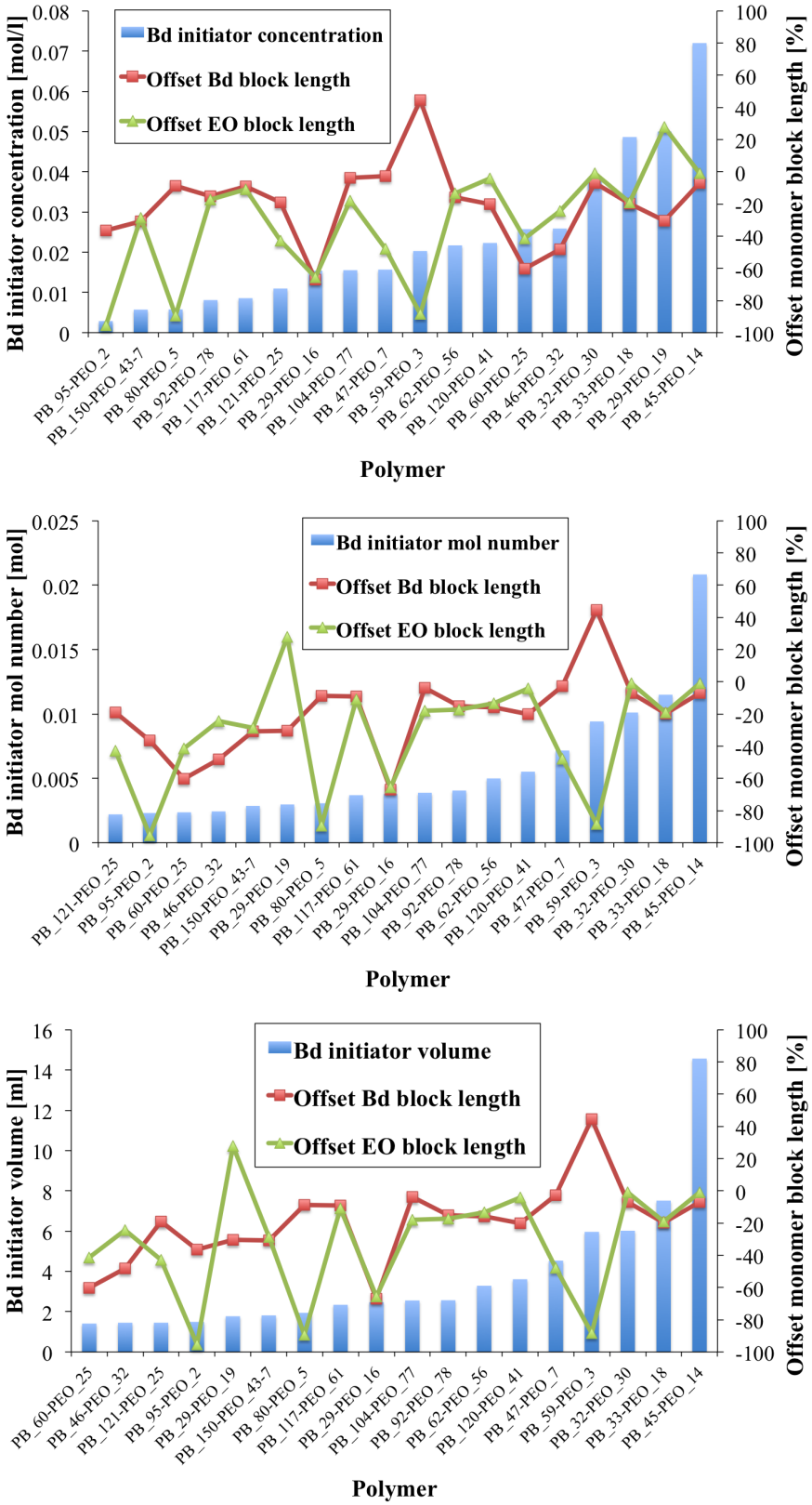

Figure 49: Comparison of concentration (top panel), mol number (middle panel) and volume (bottom panel) of *n*-BuLi (stated as Bd initiator) with regard to the offset of both monomer block lengths. There could potentially be an influence of *n*-BuLi for the EO polymerization as far as it is still present.

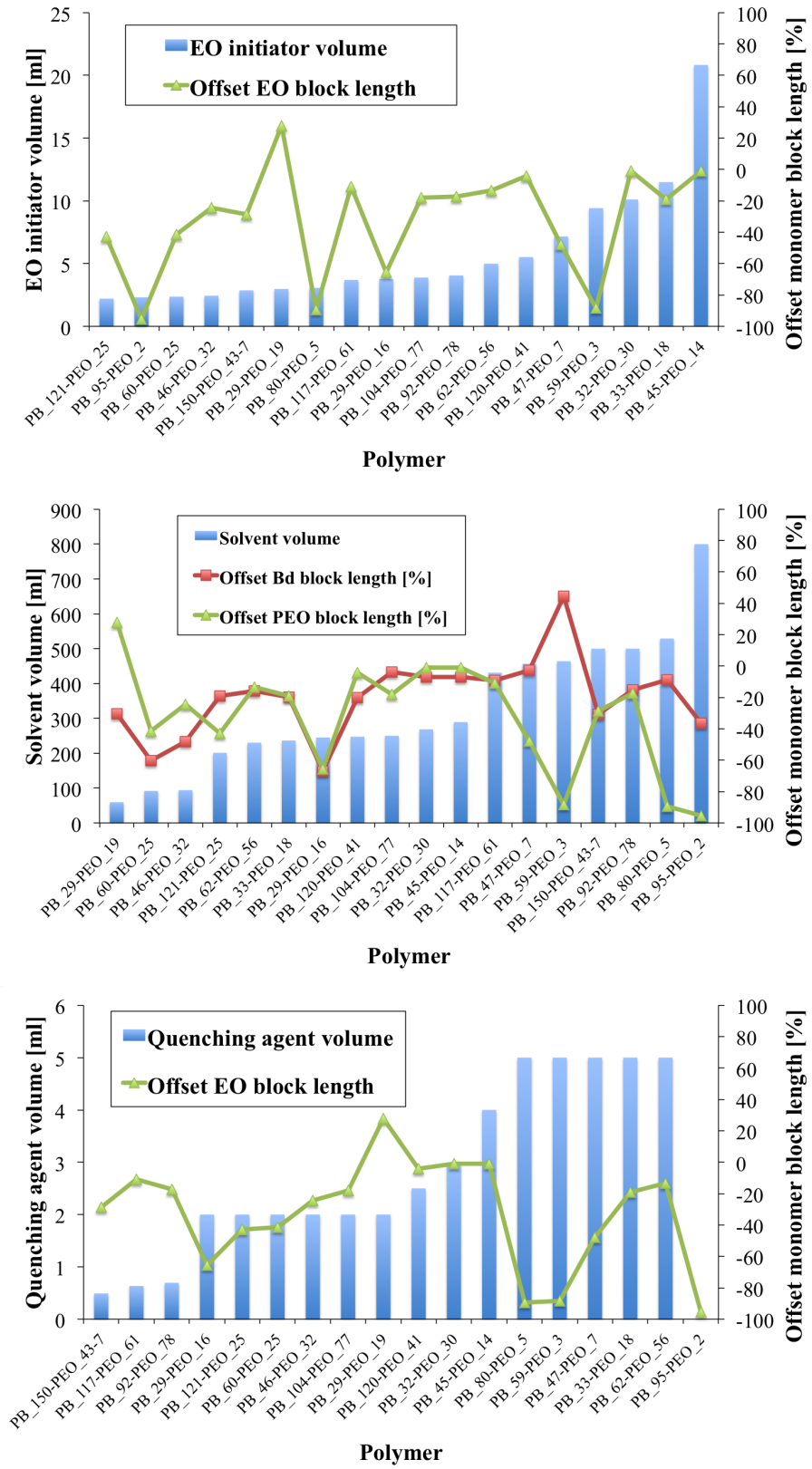

Figure 50: Comparison of tBuP4 concentration (bottom panel, stated as EO initiator), THF volume (middle panel) and acetic acid volume (stated as quenching agent, only quenching the EO polymerization, bottom panel) with regard to the offset of both monomer block lengths. As far as there is no contribution of tBuP4 to the Bd polymerization, the offset for the Bd block length was left out.

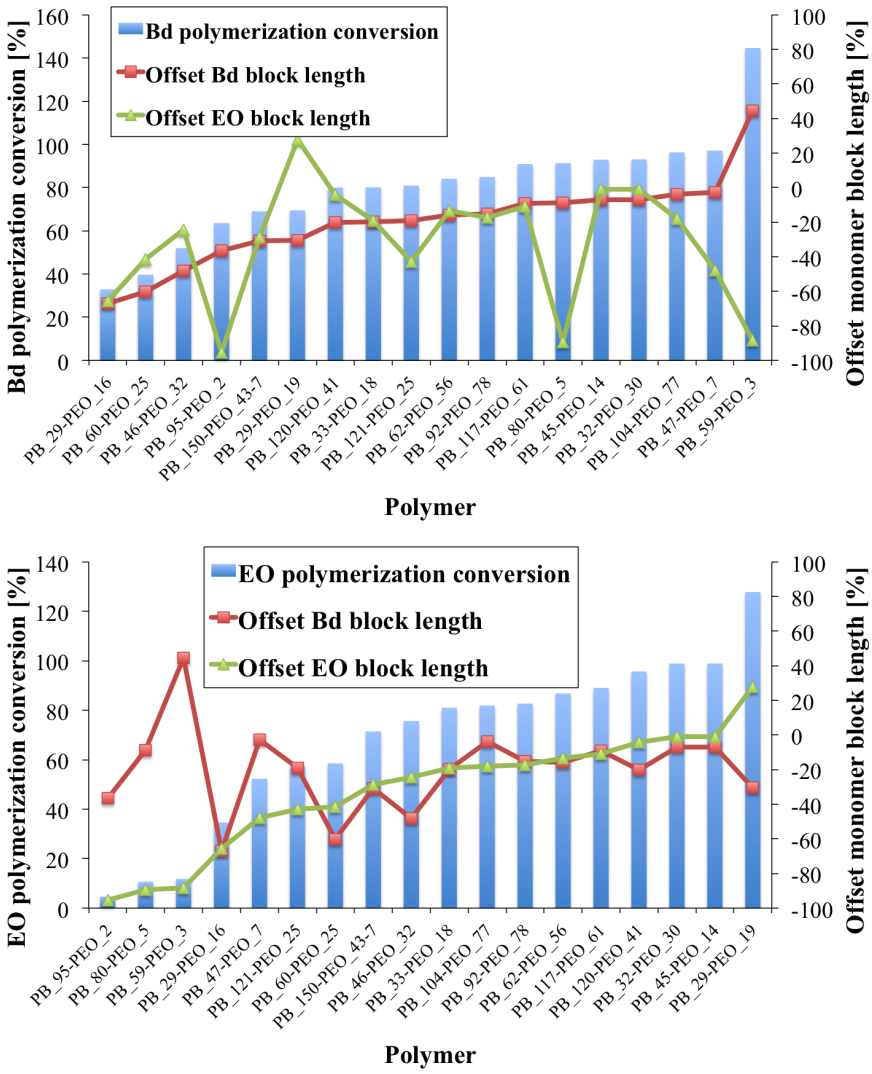

Figure 51: Comparison of Bd (top panel) and EO (bottom panel) conversion with regard to the offset of both monomer block lengths.

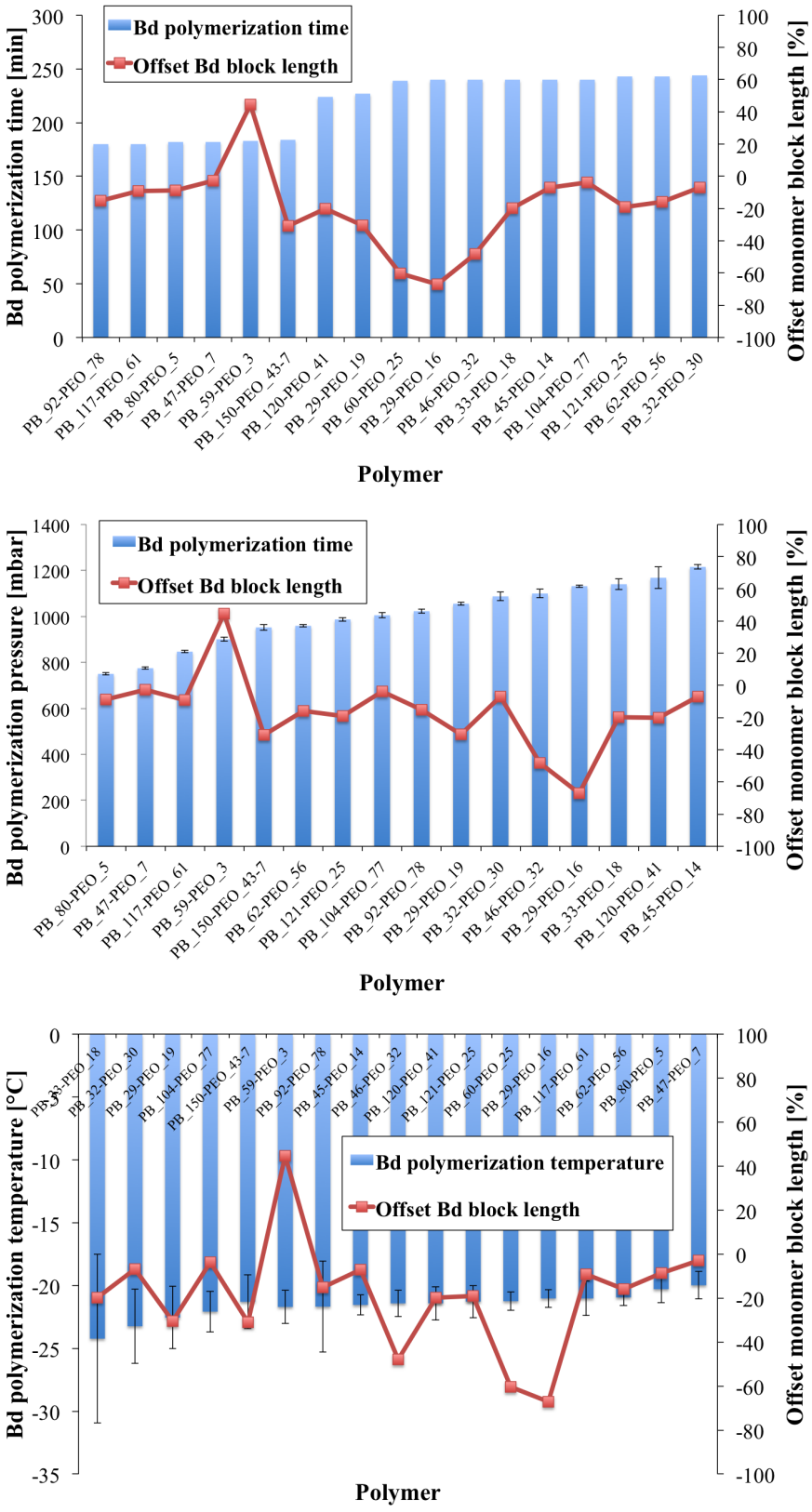

Figure 52: Comparison of time (top panel), pressure (middle panel) and temperature (bottom panel) of the Bd polymerization with regard to the offset of the Bd block length.

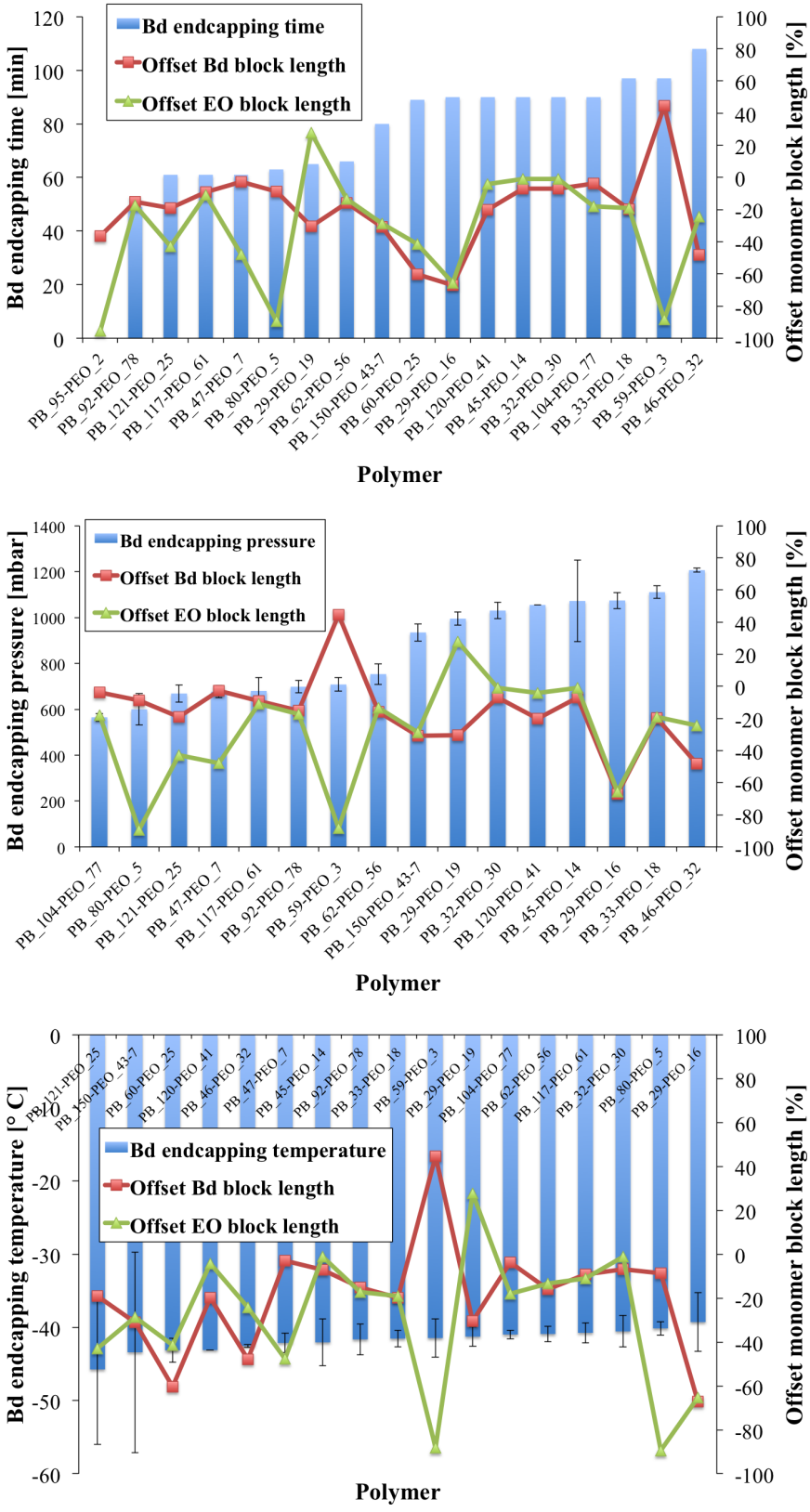

Figure 53: Comparison of time (top panel), pressure (middle panel) and temperature (bottom panel) of the Bd endcapping with regard to offset of monomer block lengths.

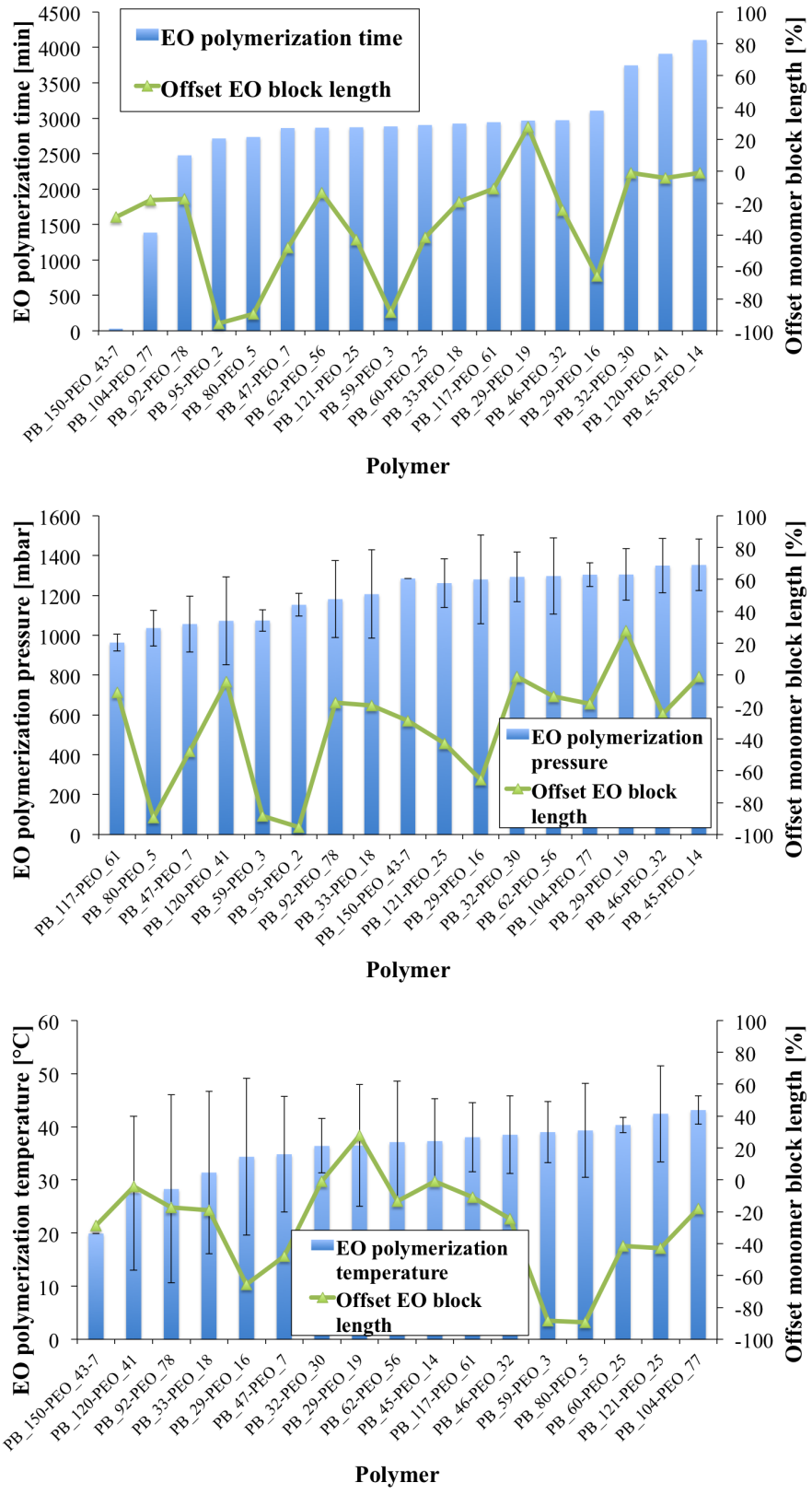

Figure 54: Comparison of time (top panel), pressure (middle panel) and temperature (bottom panel) of the EO polymerization with regard to the offset of the EO block length.

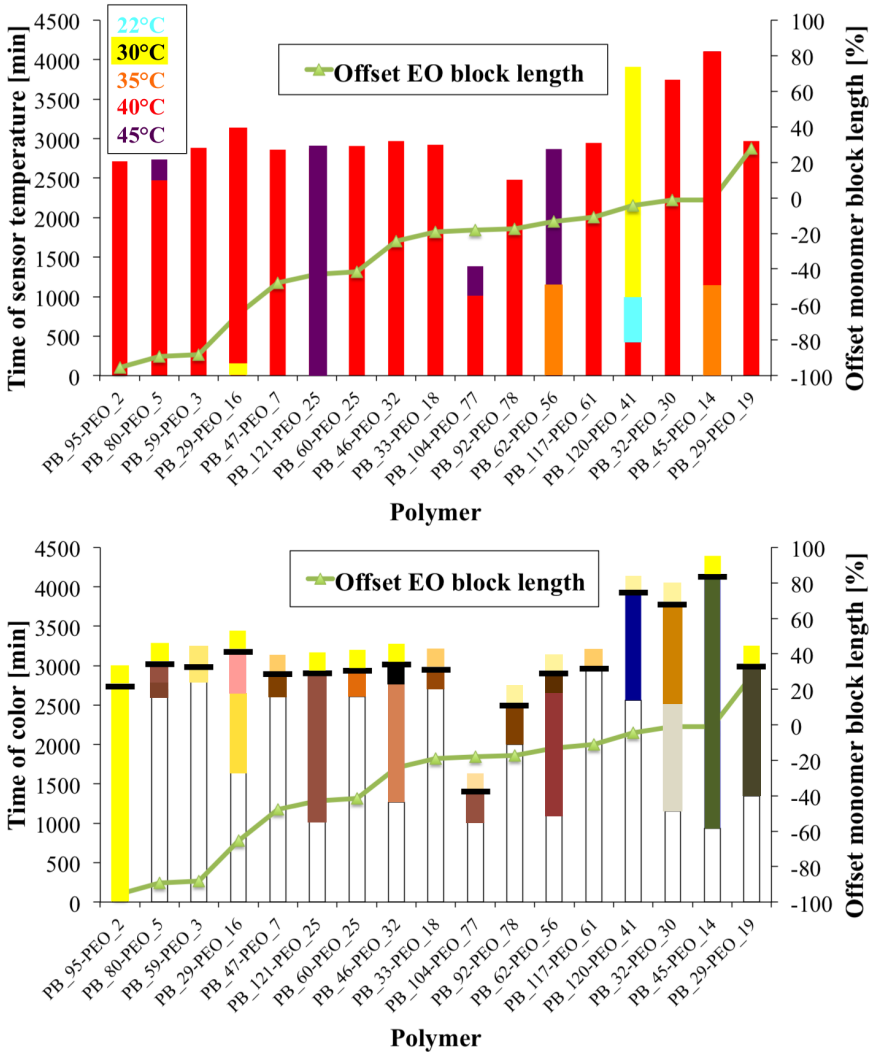

Figure 55: Comparison of sensor temperatures during EO polymerization (top panel) and color development (bottom panel) with regard to the offset of the EO block length. PB_{150}-PEO_{43}-7 wasn't included in the comparison because the EO polymerization only lasted for 30min.

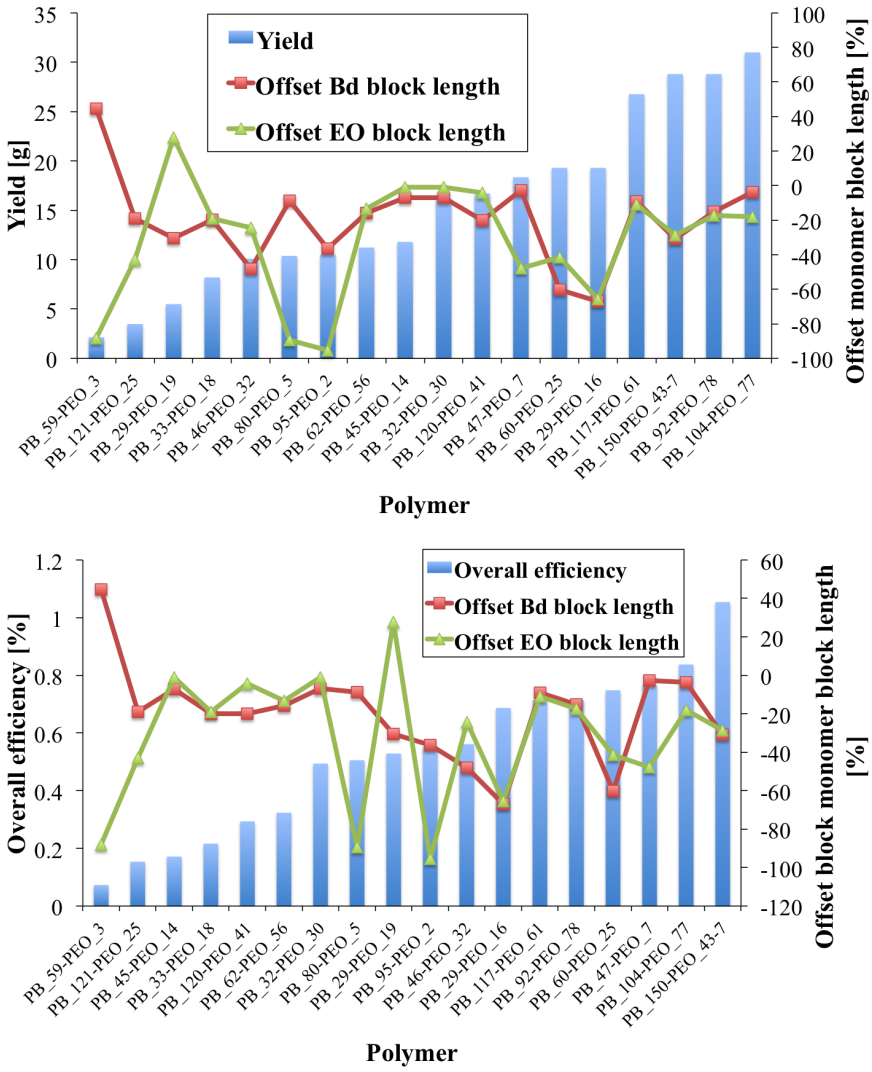

Figure 56: Comparison of yield (top panel) and overall efficiency (bottom panel) with regard to the offset of both monomer block lengths.

Förster's one-pot anionic polymerization of PB-PEO-based diblock copolymers was optimized during six modifications of the original protocol. Both monomers could be dried best from moisture and oxygen by distilling over *n*-Bu_2Mg and *n*-BuLi and degassing until approximately 10^{-2} mbar.
During these reactions, Bd polymerization worked optimal for 4 h at -20°C, endcapping was optimal at 1.5 h at -40°C. The best conditions for optimal EO polymerization was 2 d between 40°C and 45°C where care should be taken that the pressure does not exceed 1.5 bar.
Regarding EO, it seemed that approximately 2 ml go lost during the reaction, so it would be feasible to always add 2 ml extra. There seemed furthermore to be a sharp decrease in conversion efficiency between 10 and 12 ml and even more accurate, between 0.22 and 0.26 mol EO, regardless of the EO volume concentration. Sure statements about that findings would of course require more experiments. No similar pattern could be found for Bd. This loss was not obtained for the Hillmyer polymerization without tBuP4. Therefore, a potential reason for the decreases could be that the complexation of tBuP4 is affected when the EO mol number sinks below a certain value. Förster only stated a successful conversion for PEO between 2 and 20 kg/mol. The majority of the synthesized polymers were below that value. Furthermore, Förster didn't mention volume or mol number of EO that he used. Potentially the performance of the complexation ability of tBuP4 reaches its limit below a certain EO mol number.
Remaining challenges would be to find out the reaction time for full conversion of EO for smaller dimensions than the conversion efficiency line, to find similar patterns for Bd or to optimize the maximal and minimal solution volume for successful reaction in a standard reactor. These challenges remain interesting, but are beyond the scope of this project, whose goal was to optimize polymersome formation, not to optimize polymer synthesis.

8.2 Appendix II: Published version of Paper 1

Aquaporin-based biomimetic polymeric membranes: approaches and challenges

Joachim Habel, Michael Hansen, Nanna Larsen, Søren Kynde, Søren Roi Midtgaard, Grethe Vestergaard Jensen, Julie Bomholt, Anayo Ogbonna, Kristoffer Almdal, Alexander Schulz, and Claus Hélix-Nielsen

Membranes 2015, 5 (3) 307-351

doi: 10.3390/membranes5030307

Membranes **2015**, *5*, 307-351; doi:10.3390/membranes5030307

OPEN ACCESS

membranes

ISSN 2077-0375

www.mdpi.com/journal/membranes

Review

Aquaporin-Based Biomimetic Polymeric Membranes: Approaches and Challenges

Joachim Habel [1,2], Michael Hansen [3], Søren Kynde [4], Nanna Larsen [5], Søren Roi Midtgaard [4], Grethe Vestergaard Jensen [4], Julie Bomholt [2], Anayo Ogbonna [2], Kristoffer Almdal [6], Alexander Schulz [3] and Claus Hélix-Nielsen [1,2,7,*]

1 Technical University of Denmark, Department of Environmental Engineering, Miljøvej, Building 113, 2800 Kgs. Lyngby, Denmark; E-Mail: joachim.habel@gmx.de

2 Aquaporin A/S, Ole Maaløes Vej 3, 2200 Copenhagen, Denmark; E-Mails: jbo@aquaporin.dk (J.B.); annyogbonna@yahoo.com (A.O.)

3 University of Copenhagen, Department of Plant and Environmental Sciences, Thorvaldsensvej 40, 1871 Frederiksberg, Denmark; E-Mails: mh@plen.ku.dk (M.H.); als@plen.ku.dk (A.S.)

4 University of Copenhagen, Copenhagen Biocenter, Ole Maaløes Vej 5, 2200 Copenhagen, Denmark; E-Mails: kynde@nbi.ku.dk (S.K.); soromi@nbi.ku.dk (S.R.M.); gvjensen@nbi.ku.dk (G.V.J.)

5 University of Copenhagen, Niels Bohr Institute, Hans Christian Ørsted building D, Universitetsparken, 5, 2100 Copenhagen, Denmark; E-Mail: nanna.skaarup@gmail.com

6 Technical University of Denmark, Department of Micro- and Nanotechnology, Produktionstorvet, Building 423, 2800 Kgs. Lyngby; E-Mail: kral@nanotech.dtu.dk

7 University of Maribor, Laboratory for Water Biophysics and Membrane Processes, Faculty of Chemistry and Chemical Engineering, Smetanova ulica 17, 2000 Maribor, Slovenia

* Author to whom correspondence should be addressed; E-Mail: clhe@env.dtu.dk; Tel.: +45-27-10-20-76.

Academic Editor: Chuyang Y. Tang and Zhining Wang

Received: 8 July 2015 / Accepted: 22 July 2015 / Published: 31 July 2015

Abstract: In recent years, aquaporin biomimetic membranes (ABMs) for water separation have gained considerable interest. Although the first ABMs are commercially available, there are still many challenges associated with further ABM development. Here, we discuss the interplay of the main components of ABMs: aquaporin proteins (AQPs), block copolymers for AQP reconstitution, and polymer-based supporting structures. First, we briefly cover challenges and review recent developments in understanding the interplay between AQP and block copolymers. Second, we review some experimental characterization methods for

investigating AQP incorporation including freeze-fracture transmission electron microscopy, fluorescence correlation spectroscopy, stopped-flow light scattering, and small-angle X-ray scattering. Third, we focus on recent efforts in embedding reconstituted AQPs in membrane designs that are based on conventional thin film interfacial polymerization techniques. Finally, we describe some new developments in interfacial polymerization using polyhedral oligomeric silsesquioxane cages for increasing the physical and chemical durability of thin film composite membranes.

Keywords: biomimetic membranes; aquaporins; block copolymers; proteopolymersomes; polyhedral oligomeric silsesquioxanes; polyamide layer; microfluidics; membrane proteins; protein-polymer-interactions

1. Introduction

Aquaporin biomimetic membranes (ABMs) have attracted interest recently due to their potentially superior performance in terms of water flux and solute rejection as compared to conventional membranes. Their superior performance has been demonstrated experimentally [1–3]. The number of Web of Science entries for biomimetic membranes has increased by a factor of four from 2000 to 2011. The general ABM approach has been reviewed recently [4–6]. Basically, the ABMs developed until now are made from combining three components: Aquaporins (AQPs) which are membrane protein water channels; amphiphilic molecules in which the AQPs are embedded; and a polymer support structure. The amphiphilic molecules generally can be either lipids or polymers. Due to superior performance in terms of stability and flexibility [7], block copolymers (di- or triblock) have been predominantly investigated resulting in aquaporin-based biomimetic polymeric membranes (ABPMs), but a number of studies also address aquaporin-based biomimetic lipidic membranes (ABLMs).

Here, we attempt to provide a broad overview of how AQPs, block copolymers and polymer support structures interact and how these interactions can be characterized. In the first section, we will discuss the interplay between AQPs and block copolymers including general membrane protein incorporation into block copolymers, resulting in AQP-block copolymer complexes in vesicular (proteopolymersomes) or planar form. Many aspects of AQP incorporation were lessons learnt from the study of incorporation of other membrane proteins. We then review characterization methods for studying proteopolymersomes including freeze-fracture transmission electron microscopy (FF-TEM), stopped-flow light scattering (SFLS), fluorescence correlation spectroscopy (FCS) and small-angle X-ray scattering (SAXS). In order to fabricate membranes, the reconstituted AQPs need to be integrated in a suitable supporting matrix. Here, we will describe recent advances with emphasis on how to understand the interplay between proteopolymersomes and polymer-based supporting structures in the form of polyamide active layer (PA-AL) formation. PA-based thin film composite membranes represent a classical approach to membrane fabrication. However, it remains a challenge to control stability, surface roughness and other material properties of the PA-AL. We have therefore investigated if proteo- and polymersomes can be integrated in PA-AL containing polyhedral oligomeric silsesquioxanes (POSS) and how the AL is influenced by this integration in terms of physical and chemical stability and surface roughness. POSS

is a well-defined nano-scale organic-inorganic structure that allows for constructing nano-structured hybrid materials and nanocomposites. With respect to membrane technology, POSS has been investigated in terms of creating membranes for molecular separation at elevated temperatures [8] and membranes with anti-fouling properties [9]. However, it is not clear if POSS is compatible with proteopolymersome incorporation. Here, we briefly describe methods to investigate POSS-proteopolymersome interactions using a microfluidic approach for membrane formation [10].

2. Interactions between Aquaporin Proteins and Block Copolymer Matrixes

Although most work on membrane protein incorporation has been performed with lipids as host matrix components (first proteoliposomes publication appeared in 1971 [11]), polymer-based incorporation has gained considerable interest since the first proteopolymersomes publication appeared in 2000 [12]. The early work focused on incorporation of membrane-spanning proteins including ATPases and bacteriorhodopsin into polymethyloxazoline-polydimethylsiloxane-polymethyloxazoline (PMOXA-PDMS-PMOXA) triblock copolymer bilayers in planar [13] or vesicular form [14–16].

It is intriguing that membrane proteins can be incorporated functionally in polymeric bilayers (e.g., based on PMOXA-PDMS-PMOXA) that can be up to 10 times thicker than their lipidic counterparts [17]. In fact, proteopolymersomes have been observed with protein densities that exceed proteoliposomes by far [18].

A theoretical approach has been established for general membrane protein incorporation into amphiphilic structures. In this approach, the membrane protein incorporation efficiency depends on its hydrophobicity and its coupling to the host membrane, which is directly related to hydrophobic mismatch. To minimize the mismatch, the host membrane has to deform to match the hydrophobic length of the transmembrane segment of the membrane protein about 3–4 nm. The alternative mode of adaption, a host membrane-induced membrane protein deformation is unlikely as far as the compressibility of membrane proteins is generally one to two orders of magnitude higher than lipids [19]. For polymers, the compression-expansion modulus is assumed to rise linearly with increasing molecular weight (M_w), in which chain compression is favorable over chain stretching. This linear increase is consistent with the notion that the hydrophobic mismatch energy can be balanced with a decrease in stretching energy in the polymer chains around the incorporated membrane protein [20]. Srinivas and Discher found by using coarse-grain simulations that flexible hydrophobic chains can allow protein incorporation, even when the hydrophobic mismatch between membrane protein and hydrophobic interior of the chain region is greater than 22% [21,22]. Thus, membrane proteins can be incorporated more effectively if the hydrophobic chains are flexible [20]. Because flexible chains may however block the channel, no functionality of proteopolymersomes might be observed, even if the membrane protein has been incorporated functionally [21]. Moreover, high polydispersity can as well lead to a higher incorporation efficiency because the shorter chains can gather around the membrane protein and compensate for the hydrophobic mismatch. The good incorporation observed with PMOXA-PDMS-PMOXA could therefore also be attributed to their significantly high polydispersity index (*P DI*). In contrast, for natural lipid environment, the annual lipids around the incorporated protein can be selected in part by affinity to the protein surface and lateral diffusion [23]. The effect of hydrophobic mismatch is significant

for ATPases, co-transporter proteins and ion channels [19], whereas for AQPs, the effects appear smaller—likely because the protein itself is structurally more rigid [24].

The first incorporation of AQPs in polymer bilayer was done in 2004 by Stoenescu and coworkers [25]. They incorporated AQP0 that is derived from the mammalian eye-lens, in polymersomes of three different block architectures (ABA, ABC, CBA, where A stands for PMOXA, B for PDMS and C for polyethylene oxide, PEO). The block configuration dictates the orientation of the incorporated AQP0. Where ABA had 50% of incorporated AQP0 with an orientation similar to that observed in liposomes, CBA had only 20% and ABC 80%, as evidenced by antibody labeling. In all cases, incorporation is achieved by adding AQP0 in detergent during the polymersome formation and removing the non-incorporated protein by size exclusion chromatography (SEC) [25].

The first demonstration of functional AQP incorporation was presented by Kumar in 2007 who incorporated bacterial AqpZ from *E.coli* in PMOXA-PDMS-PMOXA polymersomes [17] and proved their functionality within SFLS. SFLS is a common permeability characterization method, in which the polymersome shrinkage due to a response to osmolarity change is monitored over time by light scattering. Incorporation of AqpZ led to 800 times higher osmotic response of proteopolymersomes compared to empty polymersomes and showed that the activation energy, meaning the barrier for water to pass through the AqpZ, was comparable to that of AQP reconstituted in proteoliposomes and frog oocytes. The molar protein-to-amphiphile-ratio (mPAR) for optimal AqpZ performance in the triblock copolymer system was found to be 1:50 which would correspond to 1:100 in a (diblock- or lipid) bilayer system [17]. The high density reconstitution of AQP is further exemplified by the formation of 2D AQP crystals to achieve structural (crystallographic) information about AQP—analogous to what has been done with lipid based 2D AQP crystals [26]. For this purpose, a monolayer of nickel-functionalized polybutadiene-polyethylene oxide (PB-PEO) is accumulated at the water-interface, where in the aqueous solution, mixed micelles of detergent, histidine-tagged AqpZ and PDMS-PMOXA-PDMS were present [27]. The nickel affinity to the histidine binds the AqpZ to the PB-PEO layer [28], facilitating a high packing of AqpZ in this layer. After removing the detergent via biobeads and the PB-PEO via imidazole, densely packed AqpZ PMOXA-PDMS-PMOXA crystals were left, unfortunately not of sufficient quality to obtain any structural information [29,30].

2D crystals can in fact be used to investigate the influence of AQP on polymer self-assembly in general. AQP0 is known to easily form 2D crystals due to its natural occurrence in stacks in the eye lens [31]. The findings here were that AQP0 dictates the self-assembling behavior of both polymers in a reciprocal way to the hydrophilic volume ratio *f*. With increasing mPAR, the interfacial curvature decreases and polymersomes turn into membrane sheets and partly crystals (see Figures 1 and 2). In the case of PB-PEO, formation of polymersomes only occurred by adding AQP0, whereas without AQP0 only cylindrical structures are observed. The highest measured packing densities of functional AQPs into vesicular structures are observed at PB-PEO polymersomes with an mPAR of 1:15, which is significantly higher than what has been achieved in proteoliposomes or frog oocytes. Although not all AQP0 protein was incorporated, the seven-fold increase in osmotic response is consistent with a high-packing density given the relatively low permeability of AQP0 [32]. In this case incorporation was done via mixing detergent-solubilized polymers with detergent-solubilized AQP0 and subsequently dialyzing out the detergent [18,33].

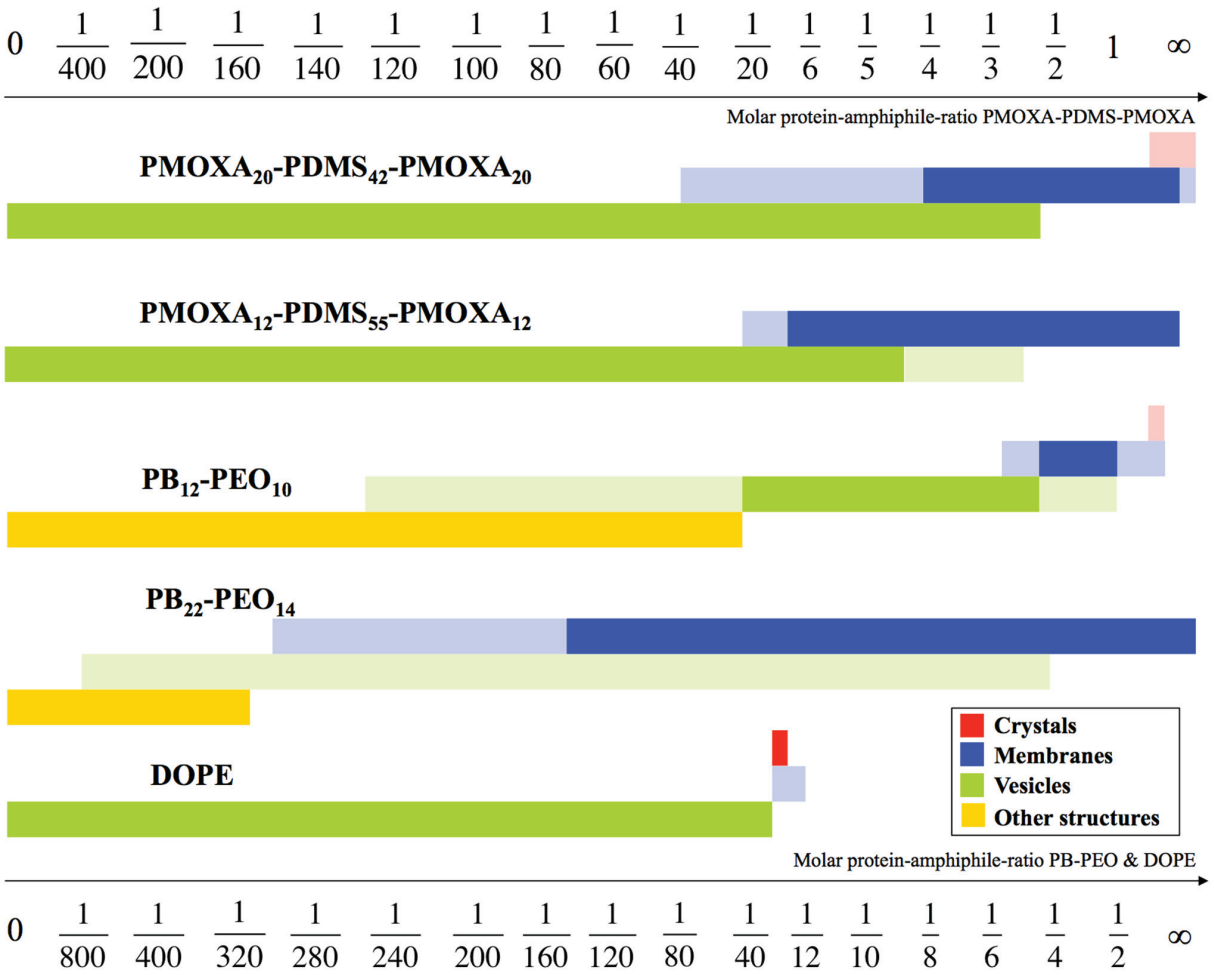

Figure 1. Schematic drawing of aggregate morphologies as a function of mPAR. PB_{12}-PEO_{10} undergoes four transitions. Surprisingly, the vesicle shape remained at significantly higher densities at block copolymers, compared to a standard lipid like 1,2-dioleoyl-sn-glycero-3-phosphoethanolamine (DOPE). The mPAR of the one-molecule-bilayer-forming ABA triblock copolymers was divided by two enabling direct comparison with the PB-PEO diblock copolymers and DOPE, both forming bilayers. The morphologies in full color are the main morphologies, pale colors denote coexisting morphologies. Adapted from [34].

With respect to fabrication of biomimetic membranes for technological purposes the first protein incorporation approaches from 2009–2011 were mainly lipid based [35,36], but also planar polymeric membranes have been demonstrated with functional incorporation of gramicidin A [37]. These efforts were pioneered by the Danish company Aquaporin A/S. Their later achievements in fabricating biomimetic membrane will be discussed in the next sections, as well as the work coming out of the groups at the Singapore Membrane Technology Center (SMTC) at Nanyang Technological University (NTU) and the National University of Singapore (NUS).

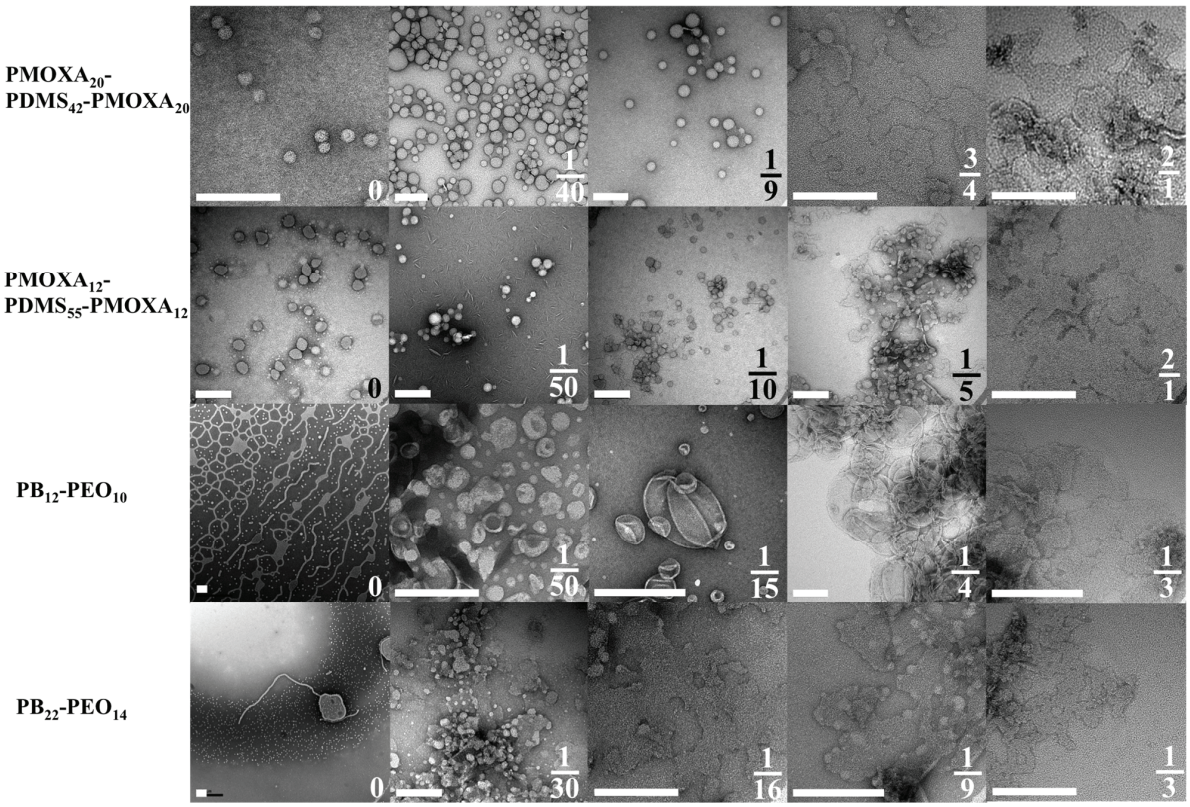

Figure 2. TEM images of aggregate morphologies as a function mPAR. Where the PMOXA-PDMS-PMOXA copolymers self-assemble to vesicles, PB-PEO forms network- and sperm-like structures and only after incorporation of AQP0 vesicular structures are observed. Scale bar is 200nm. Adapted from [33].

Table 1 summarizes all experimental membrane protein (and peptide) incorporations in block copolymer membranes, including polymer chemistry and stochiometry, *PDI*, the number-average molecular weight (M_n), f, the incorporated membrane protein, the transport cargo (e.g., water for AQP), if there was functional incorporation, mPAR, the shape of the polymer self-assembled structure, how polymer and membrane protein were mixed and how the function incorporation was measured. M_n (which can be quantified using NMR) is related to M_w as $PDI = M_w/M_n$. The table excludes those incorporation studies which do not involve block copolymer-protein interactions, such as cell-free expression systems [38–40], encapsulation in hydrophobic interior [16], nanopores [41,42], non-amphiphilic polymers [43] and hydrogel approaches [44,45]. With this limitation, the table shows that most results were published by Wolfgang Meier and coworkers using on PMOXA-PDMS-PMOXA triblock copolymers.

Table 1. Overview of studies of membrane protein incorporation into amphiphilic block copolymers. Most studies are done with the porin OmpF, followed by AqpZ. For explanations please refer to the list of abbreviations.

Polymer	M_n	PDI	*f*	Membrane Protein	Transport Cargo	FI?	mPAR	S	Incorporation method	Main Functional incorporation measurement	References
$PMOXA_{13}$–$PDMS_{23}$–$PMOXA_{13}$	3.9				e^-	X	1:3300	V	MAq, biobeads & SEC	Cargo → Reduction of MP → EPR signal	[49]
$PMOXA_{13}$–$PDMS_{23}$–$PMOXA_{13}$	4.7	NA	0.44	Alamethicin		X	1:590	P	MAq	Current change	[50]
$PMOXA_{13}$–$PDMS_{23}$–$PMOXA_{13}$	4.7	NA	0.44	Hemolysin		X	1:110,000,000	P	MAq	Current change	[50]
$PMOXA_{13}$–$PDMS_{23}$–$PMOXA_{13}$	4.7	NA	0.44	OmpG		X	1:33,000,000	P	MAq	Current change	[50]
$PMOXA_{20}$-$PDMS_{41}$-$PMOXA_{20}$	6.4	1.61	0.49	NtAQP1	CO_2	X	1:360	P	MOr	Cargo → Reaction inside vesicle → pH change	[51]
$PMOXA_{20}$-$PDMS_{41}$-$PMOXA_{20}$	6.4	1.61	0.49	NtPIP2:1	CO_2	X	1:360	P	MOr	Cargo → Reaction inside vesicle → pH change	[51]
$PMOXA_{20}$-$PDMS_{41}$-$PMOXA_{20}$	6.5	<1.2	0.51	AQP0	H_2O	ND	10:1–1:1	P	MAq & dialysis		[18]
$PMOXA_{20}$-$PDMS_{41}$-$PMOXA_{20}$	6.5	<1.2	0.51	AQP0	H_2O	ND	10:1–1:50	V	MAq & dialysis		[18]
$PMOXA_{20}$-$PDMS_{41}$-$PMOXA_{20}$	6.5	<1.2	0.51	AQP0	H_2O	-	1:2.5–0	V	MAq & dialysis	Vesicle size change	[18]
$PMOXA_{12}$-$PDMS_{54}$-$PMOXA_{12}$	6.0	1.01	0.2	AqpZ	H_2O	X	1:100–1:1600	V	MAq & biobeads	Vesicle size change	[3,52]
$PMOXA_{19}$-$PDMS_{74}$-$PMOXA_{19}$	8.7	1.46	0.23								
$PMOXA_{12}$-$PDMS_{54}$-$PMOXA_{12}$	6.0	1.01	0.30	AqpZ	H_2O	X	1:50–1:400	V	MAq & biobeads	Vesicle size change	[53,54]
$PMOXA_{12}$-$PDMS_{54}$-$PMOXA_{12}$	6.0	1.01	0.30	Hemolysin		-	1:83,000,000	P	MAq	Current change	[50]
$PMOXA_{20}$-$PDMS_{54}$-$PMOXA_{20}$	7.4	NA	0.42	TsX	Nucleosides	X	1:450	V	MOr, SI & SEC	Cargo → Encapsulated enzyme activity → Color change	[55]
$PMOXA_{8}$-$PDMS_{55}$-$PMOXA_{8}$	5.4	NA	0.22	AqpZ	H_2O	X	1:3500	V	PFR, biobeads & SEC	Vesicle size change	[56]
$PMOXA_{12}$-$PDMS_{55}$-$PMOXA_{12}$	6.1	1.64	0.30	OmpF	ELF97	X	1:1200	V	MAq & SECCargo	Precipitation inside vesicle → Color change	[57]
$PMOXA_{12}$-$PDMS_{55}$-$PMOXA_{12}$	6.1	1.64	0.30	OmpF	Acridine orange	X	1:9,100,000	V	PPFR & SEC	Cargo release → Color change	[58]
$PMOXA_{12}$-$PDMS_{55}$-$PMOXA_{12}$	6.1	1.64	0.30	OmpF	Paraquat. Pyocyanin	X	1:640	V	MAq & dialysis	No cargo → No detoxication of encapsulated enzyme→ Cell death	[59,60]
$PMOXA_{12}$-$PDMS_{55}$-$PMOXA_{12}$	6.1	1.64	0.30	AQP0	H_2O	ND	10:1–1:25	P	MAq & dialysis		[18]

Table 1. *Cont.*

Polymer	M_n	PDI	*f*	Membrane Protein	Transport Cargo	FI?	mPAR	S	Incorporation method	Main Functional incorporation measurement	References
$PMOXA_{12}$-$PDMS_{55}$-$PMOXA_{12}$	6.1	1.64	0.30	AQP0	H_2O	-	1:3–0	V	MAq & dialysis	Vesicle size change	[18]
$PMOXA_{12}$-$PDMS_{55}$-$PMOXA_{12}$	6.1	1.64	0.30	AqpZ	H_2O	ND	1:4	Cr. V	MAq & biobeads		[29]
$PMOXA_{7}$-$PDMS_{60}$-$PMOXA_{7}$	5.6	NA	0.19	Gramicidin A	Monovalent cations	X	1:81,000	P	MOr	Current change	[37]
$PMOXA_{8}$-$PDMS_{60}$-$PMOXA_{8}$	5.8	NA	0.21	AqpZ	H_2O	X	1:3800	V	PFR, biobeads & SEC	Vesicle size change	[56]
$PMOXA_{13}$-$PDMS_{62}$-$PMOXA_{13}$	6.8	1.47	0.29	NADH reductase	e^-	X	1:1900	V	MAq, biobeads & SEC	Cargo → Reduction of MP → EPR signal	[49]
$PMOXA_{15}$-$PDMS_{62}$-$PMOXA_{15}$	7.1	1.50	0.32	NADH reductase	e^-	X	1:1800	V	MAq, biobeads & SEC	Cargo → Reduction of MP → EPR signal	[49]
$PMOXA_{12}$-$PDMS_{65}$-$PMOXA_{12}$	6.9	1.67	0.27	MloK1	Potassium	X	1:390	P	MAq & biobeads	Current change	[61]
$PMOXA_{15}$-$PDMS_{68}$-$PMOXA_{15}$	7.6	NA	0.30	LamB	Maltohexaose	X	NA	P	MAq	Current change at varying cargo concentrations	[62]
$PMOXA_{15}$-$PDMS_{68}$-$PMOXA_{15}$	7.6	NA	0.30	OmpF	Actylthiocholine	X	1:10000	V	PFR	Cargo → Encapsulated enzyme activity → Color change	[62]
$PMOXA_{15}$-$PDMS_{68}$-$PMOXA_{15}$	7.6	1.20	0.30	AqpZ	H_2O	X	1:10–1:1000	V	PFR & biobeads	Vesicle size change	[63]
$PMOXA_{15}$-$PDMS_{68}$-$PMOXA_{15}$	7.6	1.20	0.30	Hemolysin			1:66,000,000	V	MAq	Current change	[50]
$PMOXA_{21}$-$PDMS_{69}$-$PMOXA_{21}$	8.7	2.00	0.37	NADH reductase	e^-	X	1:1500	V	MAq, biobeads & SEC	Cargo → Reduction of MP → EPR signal	[49]
$PMOXA_{16}$-$PDMS_{72}$-$PMOXA_{16}$	8.0	1.17	0.30	OmpF	Enone	X	1:220	V	PPFR & dialysis	Cargo → Encapsulated enzyme activity → Color change	[64]
PMOXA-PDMS-PMOXA	8.8	NA	NA	OmpF	ELF97	X	1:50	V	MAq & SEC	Cargo → Precipitation inside vesicle → Color change	[65]
$PMOXA_{32}$-$PDMS_{72}$-$PMOXA_{32}$	10.7	1.83	0.47	OmpF	7-ADCA. PGME	X	NA	V	PFR & dialysis	Cargo → Encapsulated enzyme activity → Bacterial death	[66]
$PMOXA_{11}$-$PDMS_{73}$-$PMOXA_{11}$	7.2	1.70	0.22	LamB	DNA	X	1:390	V	MOr, SI & SEC	Fluorescence-labelled cargo	[67]
$PMOXA_{11}$-$PDMS_{73}$-$PMOXA_{11}$	7.2	1.70	0.22	OmpF	Nucleosides	X	1:10, 1:100	V	PPFR & SEC	Cargo → Encapsulated enzyme activity → Color change	[68]
$PMOXA_{11}$-$PDMS_{73}$-$PMOXA_{11}$	7.2	1.70	0.22	TsX	Nucleosides	X	1:10, 1:100	V	PPFR & SEC	Cargo → Encapsulated enzyme activity → Color change	[68]
$PMOXA_{11}$-$PDMS_{73}$-$PMOXA_{11}$	7.2	1.70	0.22	LamB	DNA	X	NA	P	MAq		[67]

Table 1. *Cont.*

Polymer	M_n	PDI	*f*	Membrane Protein	Transport Cargo	FI?	mPAR	S	Incorporation method	Main Functional incorporation measurement	References
Lipids											
$PMOXA_{21}$-$PDMS_{73}$-$PMOXA_{21}$	9.0	1.70	0.36	Alamethicin	Calcium	X	1:24	V	MAq	Cargo precipitation inside vesicle	[69,70]
$PMOXA_{21}$-$PDMS_{73}$-$PMOXA_{21}$	9.0	1.70	0.36	FhuA	Sulphorhodamine B	X	1:6,000,000	V	MOr, SI & SEC	Cargo → Quenching inside vesicle → Color change	[71–73]
$PMOXA_{21}$-$PDMS_{73}$-$PMOXA_{21}$	9.0	1.70	0.36	FhuA	TMB	X	1:4500. 1:3,600,000	V	MAq/ & biobeads/MOr, SI & SEC	Cargo → Encapsulated enzyme activity → Color change	[71,72,74]
$PMOXA_{21}$-$PDMS_{73}$-$PMOXA_{21}$	9.0	1.70	0.36	FhuA		ND	3000:1	P	MAq		[72]
$PMOXA_{21}$-$PDMS_{73}$-$PMOXA_{21}$	9.0	1.70	0.36	FhuA	NAD	-	NA	V	MAq	Cargo → Encapsulated enzyme activity→ Absorbance change of cargo	[73]
$PMOXA_{21}$-$PDMS_{73}$-$PMOXA_{21}$	9.0	1.70	0.36	FhuA	DNA	-	NA	V	MOr, SI & SEC	Fluorescence-labelled cargo	[73]
$PMOXA_{21}$-$PDMS_{73}$-$PMOXA_{21}$	9.0	1.70	0.36	LamB	Sugar	X	NA	P	MAq	Current change at varying cargo concentration	[75]
$PMOXA_{21}$-$PDMS_{73}$-$PMOXA_{21}$	9.0	1.70	0.36	OmpF	e^-	X	NA	P	MAq	Current change	[75]
$PMOXA_{21}$-$PDMS_{73}$-$PMOXA_{21}$	9.0	1.70	0.36	OmpF	Ampicillin	X	1:1000	V	MOr & SEC	Cargo → Hydrolysis inside vesicle → Color change	[12,76]
$PMOXA_{20}$-$PDMS_{75}$-$PMOXA_{20}$	9.0	1.46	0.34	AqpZ	H_2O	X	1:25, 1:50, 1:200	V	PFR & biobeads	Vesicle size change	[77]
$PMOXA_{11}$-$PDMS_{76}$-$PMOXA_{11}$	7.8	1.48	0.25	BR	H^+	X	NA	V/Mc	MOr & SI	pH change	[78,79]
$PMOXA_{11}$-$PDMS_{76}$-$PMOXA_{11}$	7.8	1.48	0.25	BR & ATPase	H^+	X	1:180	V	MOr & dialysis	pH change & bioluminescence assay	[15]
$PMOXA_{11}$-$PDMS_{76}$-$PMOXA_{11}$	7.8	1.48	0.25	BR & ATPase	H^+	X	1:20	V	PBR & dialysis	pH change	[80–82]
$PMOXA_6$-$PDMS_{90}$-$PMOXA_6$	9.5	NA	0.12	OmpF	L-ascorbic acid, CO, $Na_2S_2O_4$, $ONOO^-$	X	1:1300	V	PFR, dialysis & SEC	Cargo → Absorbance change of encapsulated protein	[83]
$PMOXA_{21}$-$PDMS_{97}$-$PMOXA_{21}$	9.0	1.70	0.30	Hemaglutinin		X	1:3800	V	MAq & biobeads	MP → Fusion with fluorescence-labelled liposomes	[74]
$PMOXA_9$-$PDMS_{106}$-$PMOXA_9$	9.4	1.38	0.14	NADH reductase	e^-	X	1:1400	V	MAq, biobeads & SEC	Cargo → Reduction of MP → EPR signal	[49]
$PMOXA_{13}$-$PDMS_{110}$-$PMOXA_{13}$	10.4	1.44	0.19	NADH reductase	e^-	X	1:1200	V	MAq, biobeads & SEC	Cargo → Reduction of MP → EPR signal	[49]
$PMOXA_{14}$-$PDMS_{110}$-$PMOXA_{14}$	10.5	1.36	0.20	NADH reductase	e^-	X	1:1200	V	MAq, biobeads & SEC	Cargo → Reduction of MP → EPR signal	[49]

Table 1. *Cont.*

Polymer	M_n	PDI	*f*	Membrane Protein	Transport Cargo	FI?	mPAR	S	Incorporation method	Main Functional incorporation measurement	References
$PMOXA_{15}$-$PDMS_{110}$-$PMOXA_{15}$	10.7	1.62	0.21	AqpZ	H_2O	X	1:25–1:500	V	PFR & SEC	Vesicle size change	[17,29]
$PMOXA_{15}$-$PDMS_{110}$-$PMOXA_{15}$	10.7	1.62	0.21	OmpF		ND	NA	P	MAq		[84]
PMOXA-PDMS-PMOXA	20.0	NA		FhuA	Calcein	X	1:2,700,000	V	MOr, SI & SEC	Cargo release → Color change	[85]
$PMOXA_{65}$-$PDMS_{165}$-$PMOXA_{65}$		23.3	1.63	NADH reductase	e^-	X	1:550	V	MAq, biobeads & SEC	Cargo → Reduction of MP → EPR signal	[49]
PMOXA-PDMS-PMOXA	NA	NA	NA	BR	H^+	X	NA	P	MAq	pH change	[86,87]
PMOXA-PDMS-PMOXA	NA	NA	NA	BR & CcO	H^+ & e^-	X	NA	V	MOr, SI & SEC	Current & pH change	[87,88]
PMOXA-PDMS-PMOXA	NA	NA	NA	CcO	e^-	X	NA	P	MOr, SI & SEC	Current change	[86,87]
PMOXA-PDMS-PMOXA	NA	NA	NA	OmpF	H^+	X	NA	P	MAq	Current change	[89]
$PMOXA_{110}$-$PDMS_{40}$-PEO_{25}	13.4	NA	0.75	AQP0	H_2O	ND	1:200	V	MOr, SI & SEC		[25]
$PMOXA_{45}$-$PDMS_{40}$-$PMOXA_{67}$	10.6	NA	0.68	AQP0	H_2O	ND	1:200	V	MOr, SI & SEC		[25]
MPEG-PVL	6.5	<1.2	0.00	Polymyxin B	Calcein	X	1:2	V	MAq	Cargo release → Color change	[73]
P2VP-PEO	NA	NA	NA	FhuA	NAD	-	NA	V	MOr, SI & SEC	Cargo → Enzyme reaction inside vesicle → Absorbance change of cargo	[73]
PB_{12}-PEO_{10}	1.1	1.09	0.32	AQP0	H_2O	X	1:5–1:250	V	MAq & dialysis	Vesicle size change	[18]
PB_{12}-PEO_{10}	1.1	1.09	0.32	AQP0	H_2O	ND	1:1.3	Cr	MAq & dialysis		[18]
PB_{12}-PEO_{10}	1.1	1.09	0.32	AQP0	H_2O	ND	1:1–1:10	P	MAq & dialysis		[18]
PB_{12}-PEO_{10}	1.1	1.09	0.3	AqpZ	H_2O	X	1:50-1:1000	V	MAq & dialysis	Vesicle size change	[90]
PB_{12}-PEO_{10}	1.1	1.09	0.32	BR	H^+	X	1:500	V	MAq & biobeads	pH change	[91]
PB_{12}-PEO_{10}	1.1	1.09	0.3	SoPIP2;1	H_2O	-	1:200	V	MAq & biobeads	Vesicle size change	[90]
PB_{12}-PEO_{10}	1.1	NA	0.34	Hemolysin	Calcein	X	1:33,000	V	MAq & dialysis	Cargo release → Color change	[92]
PB_{22}-PEO_{14}	1.8	1.17	0.28	AQP0	H_2O	ND	2:1–1:300	P	MAq & dialysis		[18]
PB_{22}-PEO_{23}	2.2	1.09	0.39	AqpZ	H_2O	X	1:15–1:200	V	MAq & dialysis	Vesicle size change	[90]
PB_{22}-PEO_{23}	2.2	1.09	0.39	SoPIP2;1	H_2O	-	1:15, 1:200	V	MAq & dialysis	Vesicle size change	[90]
PB_{29}-PEO_{16}	2.3	1.00	0.25	AQP10	H_2O	-	1:990	V	PFR & SE	Vesicle size change	-
PB_{35}-PEO_{14}	2.5	1.09	0.19	AqpZ	H_2O	-	1:15	V	MAq & dialysis	Vesicle size change	[90]
PB_{35}-PEO_{14}	2.5	1.09	0.19	SoPIP2;1	H_2O	-	1:15	V	MAq & dialysis	Vesicle size change	[90]

Table 1. *Cont.*

Polymer	M_n	PDI	*f*	Membrane Protein	Transport Cargo	FI?	mPAR	S	Incorporation method	Main Functional incorporation measurement	References
PB_{43}-PEO_{32}	3.7	1.03	0.31	AQP10	H_2O	X	1:600	V	PFR & SE	Vesicle size change	[93]
PB_{46}-PEO_{30}	3.8	1.04	0.28	AqpZ	H_2O	-	1:50,1:100,1:200	V	MAq & dialysis	Vesicle size change	[90]
PB_{46}-PEO_{32}	3.9	1.00	0.30	AQP10	H_2O	-	1:580	V	PFR & SE	Vesicle size change	-
PB_{52}-PEO_{29}	4.1	<1.1	0.25	Hemolysin	e^-	X	NA	P	MAq	Current change	[94]
PB_{52}-PEO_{29}	4.1	<1.1	0.25	Polymyxin B		X	NA	P	MAq	Current change	[95]
PB_{52}-PEO_{29}-LA	4.1	<1.1	0.25	Hemolysin	e^-	X	NA	P	MAq	Current change	[94]
PB_{52}-PEO_{29}-LA	4.1	<1.1	0.25	Polymyxin B		X	NA	P	MAq	Current change	[95]
PB_{92}-PEO_{78}	8.4	1.08	0.34	AQP10	H_2O	-	1:270	V	PFR & SE	Vesicle size change	-
PB_{125}-PEO_{80}	8.9	<1.1	0.28	Alamethicin	Calcein	-	1:2-1:8	V	MAq	Cargo release → Color change	[96]
$PHEMA_{25}$-$PBMA_{25}$-$PHEMA_{25}$	14.3	1.30	0.83	AqpZ		-	NA	P	MAq & biobeads	Current change	[97]
$PHEMA_{25}$-$PBMA_{25}$-$PHEMA_{25}$	14.3	1.30	0.83	Hemolysin		X	NA	P	MAq	Current change	[97]
$PHEMA_{25}$-$PBMA_{25}$-$PHEMA_{25}$	14.3	1.30	0.83	OmpF		-	1:70	P	MAq & biobeads	Current change	[97]
PEE_{37}-PEO_{40}	3.9	<1.1	0.39	Alamethicin	Calcein	X	1:2–1:8	V	MAq	Cargo release → Color change	[96]
PPO_{34}-PGM_{14}	6.5	1.30	0.66	Strepatividin-BSA		ND	1:5, 1:15, 1:50	V	PPFR		[98]
PI_{93}-PEO_{87}	10.2	1.00	0.31	FhuA	TMB	X	1:6700. 1:5,300,000	V	MOr, SI & SEC	Cargo → Encapsulated enzyme activity → Color change	[73]
PEO_{136}-PIB_{18}-PEO_{136}	8.0	1.86	0.90	Cecropin A	Calcein	X	1:30	V	MAq & SEC	Cargo release → Color change	[99]
$P4MVP_{21}$-PS_{26}-$P4MVP_{21}$	13.1	NA	0.80	PR		X	1:10	V	MAq & precipitation	Absorbance change in membrane protein	[100]
$P4MVP_{21}$-PS_{38}-$P4MVP_{21}$	14.3	1.19	0.74	PR		X	1:10	V	MAq & precipitation	Absorbance change in membrane protein	[100]
$P4MVP_{29}$-PS_{42}-$P4MVP_{29}$	18.7	NA	0.78	PR		X	1:10	V	MAq & precipitation	Absorbance change in membrane protein	[100]
$P4MVP_{22}$-PB_{28}-$P4MVP_{22}$	15.0	NA	0.92	PR		ND	1:10	V	MAq & precipitation		[101]
$P4MVP_{22}$-PB_{28}-$P4MVP_{22}$	15.0	NA	0.92	RC	e^-	X	1:25	V	MAq & precipitation	Cargo → Reduction of MP → EPR signal	[102]
$P4VP_{22}$-PB_{28}-$P4VP_{22}$	7.1	NA	0.82	PR		ND	1:10	V	MAq & precipitation		[101]
$P4MVP_{29}$-PB_{56}-$P4MVP_{29}$	17.4	1.08	0.81	RC	e^-	X	1:25	V	MAq & precipitation	Cargo → Reduction of MP → EPR signal	[102]
$P4MVP_{18}$-PB_{93}-$P4MVP_{18}$	13.9	1.06	0.62	PR		ND	1:10	V	MAq & precipitation		[101]

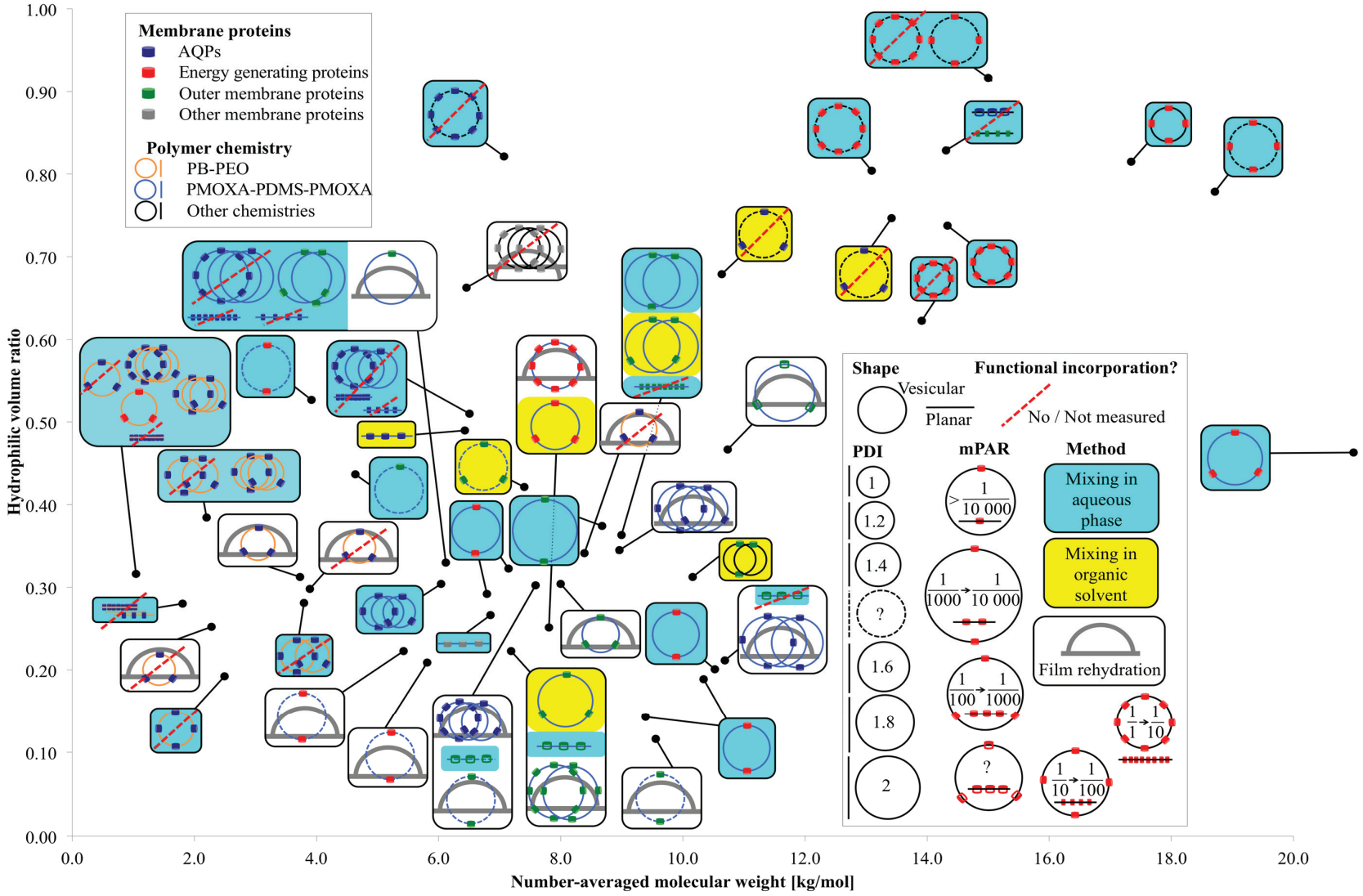

Figure 3. Overview of relevant parameters for membrane protein incorporation into amphiphilic block copolymers

Figure 3 presents an overview of membrane protein incorporation into polymers with a known M_n and *f*. Each black dot represents one polymer. The connected box shows the polymer chemistry, the incorporated membrane protein family, the self-assembled morphology (vesicular or planar), the incorporation method, the *PDI* of the polymer (not of the polymersomes), the mPAR and if the incorporation was functional or not, or respectively not measured. If there are several sketches in the box, several different experiments have been performed on the polymer. If there are two crossing circles and two close lines respectively, two different mPARs were investigated, where all other parameters remained the same. If there are three crossing circles, three or more mPARs were investigated. In the case of varying another parameter than mPAR (incorporation method, polymer chemistry, incorporated membrane protein *etc.*) a new sketch is drawn. Generally, polymers capable of functional incorporation have an *f* between 0.2 and 0.35 and M_n was in between 2 and 12 kg/mol. Compared with PB-PEO, PMOXA-PDMS-PMOXA has a far broader *PDI* [46], its bilayer is highly water impermeable [17] and they do not collapse in dried form [47]. PB-PEO is more lipid-like as far it collapses easier and has higher water permeability [18]. The polymers that did not achieve functional AQP incorporation were mainly PB-PEO polymers with small M_n and *PDI*. Energy generating (BR, CcO, NADH reductase, ATPase, RC, PR) and outer membrane proteins (OmpF, OmpG, FhuA, TsX) were incorporated mainly into PMOXA-PDMS-PMOXA polymers, but outer membrane proteins have also been incorporated in more exotic chemistries in an *f* range where one would not expect vesicular structures. The great majority of functional incorporation trials were performed with vesicular structures, where mixing was done in aqueous phase. Generally, at smaller *PDI* values, no functional membrane proteins can be incorporated, which is in agreement with the findings from Pata *et al.* [20]. A wide range of mPARs have been used with no optimal ratios detected. However, mPARs are based on the initial or nominal concentrations of membrane proteins and polymers and the final mPAR after incorporation may be different [48]. In the next section, we will discuss how to quantify membrane proteins (with focus on AQPs) after incorporation.

3. Evaluation of AQP Incorporation Characterization Methods

Detecting functional incorporation of AQPs is challenging, as the permeating solute is neutral water molecules. Protein mediated transport of neutral molecules (in particular at the single protein level) is harder to measure than transport of charged molecules (ion or protons) or a specific chemical reaction (e.g., ATPase enzyme activity). Although deuterated water labeling has been proposed for measurements via Raman spectroscopy [103], these type of measurements is complicated by the fact that water transport rate in the AQP channel is different for deuterated water molecules compared to that for normal water molecules [104].

A popular method for measuring functional incorporation is SFLS. In SFLS, proteopolymersomes are rapidly mixed with an osmotically active agent (NaCl or sucrose) in a defined volume. In the case of a hyperosmotic shock, proteopolymersomes will shrink, which will give rise to an increase in light scattering. With an increasing amount of incorporated AQPs, the shrinking rate will increase as well. This method is however strongly affected by the quality (size distribution) of the polymersomes, of the AQP concentration in the polymersome and the concentration of the osmolytes [56].

In principle, direct visual quantification can be achieved by FF-TEM, although FF-TEM will not reveal any functional information. In FF-TEM, proteopolymersomes are captured in their original shape

by quick-freezing. The frozen sample is fractured, where the fracture plane is along the proteopolymersome bilayer, which is the weakest point of the whole system. The sample with incorporated AQPs (or the cavities, where AQPs were embedded in the bilayer) is then exposed to carbon/metal coating. The forming replica is removed from the thawed sample and AQPs/cavities can be observed on the replica as distinct spots on the proteopolymersomes.

Another method is FCS of fluorescently labelled AQP. In FCS time-dependent fluctuations of fluorescence intensities in a microscopic space, the so-called confocal volume, are monitored and subjected to an autocorrelation function. Dependent from the different diffusion time of the particles diffusing through the confocal volume, one can obtain the number of particles in the confocal volume within a given time interval. When proteoliposomes or proteopolymersomes are monitored, then solubilized to micelles and monitored again, the proteins-per-vesicle-ratio (mean number of membrane proteins incorporated in the bilayer of one vesicle) can be obtained by dividing the latter number by the first. It is assumed that micelles contain only one AQP, thus the micelle-per-vesicle ratio is equal to the proteins-per-vesicle-ratio. Further details to the theory are given in [48]. Alternatively, one can obtain the proteins-per-vesicle-ratio by correlating the proteopolymersome solution with the AQP stock solution. Both correlations have advantages and challenges that are further described in the FCS subsection.

In characterizing biological material, SAXS is also a versatile tool because it gives structural information on particles in solution on a length-scale from 1 to 100 nm where data are presented as scattering intensity as a function of the magnitude of the scattering vector q. This quantity is independent of the particular geometry of the experimental set-up and directly related to the scattering angle 2θ as $q = 4\pi \sin(\theta)/\lambda$ where λ is the wavelength of the X-ray beam. Two scattering points separated by a distance d within a particle gives rise to interference showing up as increased intensity in the scattering curve at $q = 2\pi/d$. This means that large features are probed at low q while smaller details are probed in the high-q region of the curves. The strength, with which a particle scatters, its contrast, is proportional to its excess electron density, *i.e.*, the difference between the electron densities of the sample and the solvent. The downside is that SAXS requires access to elaborated synchrotron radiation sources.

Here, we will exemplify SFLS, FF-TEM, FCS and SAXS analyses with a series of diblock copolymers with optimal M_n and f range for functional membrane protein incorporation: PB_{29}-PEO_{16}, PB_{33}-PEO_{18}, PB_{45}-PEO_{14}, PB_{43}-PEO_{32}, PB_{46}-PEO_{32} and PB_{92}-PEO_{78}. PB-PEO was chosen because it showed functional AQP incorporation as discussed before and the M_n and f range is easier to control compared to PMOXA-PDMS-PMOXA. For SFLS, FF-TEM and SAXS, AqpZ is used as the incorporated membrane protein, where GFP-tagged human aquaglyceroporin AQP10 is used for the FCS experiments. Details are provided in the supporting material.

3.1. Stopped-Flow Light Scattering

In order to exemplify an SFLS analysis, data for PB_{45}-PEO_{14} and PB_{33}-PEO_{18} diblock copolymer proteo- and polymersomes (meaning with and without AqpZ) is shown in Figure 4. For PB_{33}-PEO_{18} the rate constant associated with the increase in light scattering intensity was slightly higher with AqpZ, for PB_{45}-PEO_{14} it was even lower. This illustrates one of the major challenges in SFLS. The absence of a significant response to the change in extravesicular osmolarity could be due to an increase in the bilayer bending modulus induced by the presence of (non-functional or blocked) ApqZ. We observed similar

problems in previous experiments with AqpZ and SoPIP2; 1, where only the smallest polymers (PB_{12}-PEO_{10} and PB_{22}-PEO_{23}) showed a significant difference in SFLS between proteo- and polymersomes (results not shown). Another reason for the similar SFLS signal might be the blockage of the AqpZ channels by PEO chains. In this case, AqpZ would simply sit in the bilayer as an impermeable hydrophobic block, as suggested from Kumar *et al.* [18], because water permeation is blocked by the areas corresponding to the incorporated AqpZ, lower permeabilities of proteopolymersomes can be expected as compared to polymersomes. On the other hand the incorporated AqpZ could be fully functional, but the polymer matrix is resistant to changes in volume. This underscores the notion that SFLS is not a stand-alone technique.

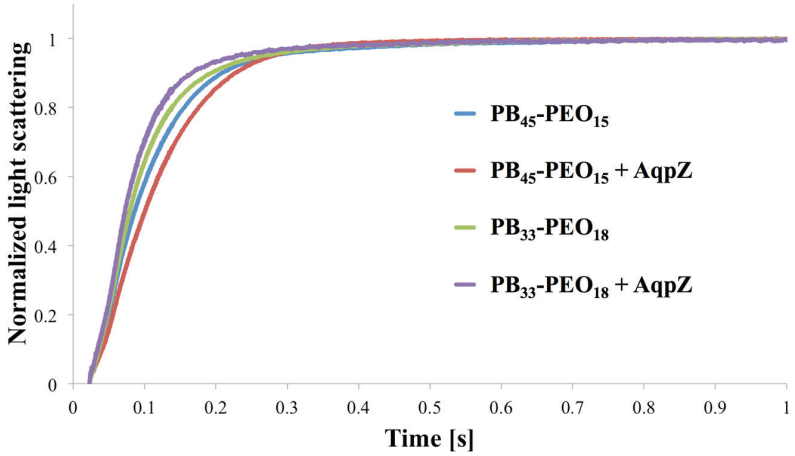

Figure 4. Normalized light scattering *vs.* time for proteo- and polymersomes of PB_{45}-PEO_{14} and PB_{33}-PEO_{18} at an mPAR of 1:100. For PB_{45}-PEO_{14} the apparent water permeability is slightly decreased for the proteopolymersomes *versus* polymersomes, whereas for PB_{33}-PEO_{18} it is slightly increased.

3.2. Freeze Fracture Transmission Electron Microscopy

Results of FF-TEM for PB_{45}-PEO_{14} proteopolymersomes are shown in Figure 5. Proteopolymersomes with an mPAR of 1:100 were produced using film rehydration (FR), frozen and fractured in a Leica MED20 station, where two planchets with frozen sample are separated, thus the fracture is more a "crack" than a "cut," thereby minimizing smearing effects from usual FF procedures (for details see supporting information). All proteo- and polymersome had a pronounced raspberry-like surface, potentially due to collapsed PB chains. However, the "typical" spots that have been claimed to be associated with AQP in a study on proteoliposomes [105] were not observed. In Figure 5, the bubble-like spots are distributed equally among polymersomes (Figure 5a–d) and proteopolymersomes (b,c,e,f). The spots could be either PB chain accumulations (Figure 5a–c) or artifacts due to bad fracturing (d–f). Proteo- and polymersomes of other PB-PEO polymers at other M_n and f showed similar behavior. It thus seems that FF-TEM sample preparation plays a major role in false positive results. Occasionally, we observed dots all over the sample that were clearly not AqpZ but potentially polymer micelles. These dots could be eliminated by omitting an up concentration step and by carefully controlling temperature, sample and cutting handling or metal coating parameters (the optimized protocol is given in the supporting

information). Even among the polymers with the shortest PB chains (PB_{32}-PEO_{30} and PB_{45}-PEO_{14}), we could not ascertain the presence of AqpZ. However, from these experiments alone we cannot exclude the possibility that AqpZ tetramers could be present as the hydrophilic PEO chains are still large compared to lipid head groups. Thus the AqpZ could be concealed in the PB core.

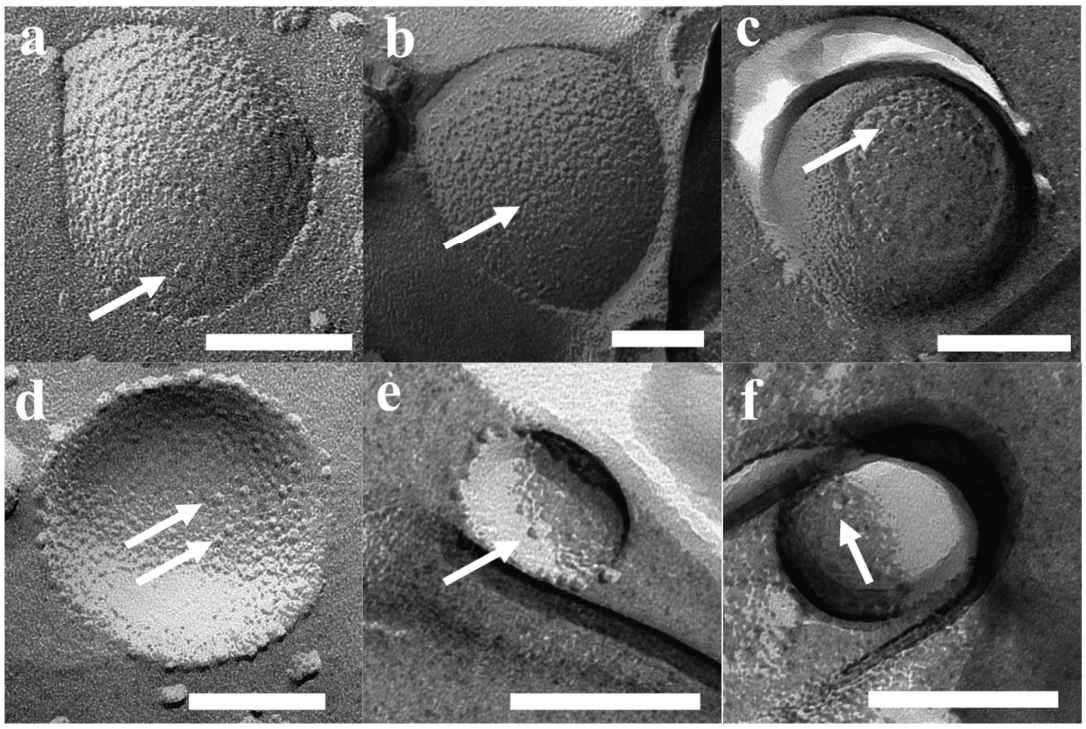

Figure 5. FF-TEM images of PB_{45}-PEO_{14} proteo—(**b**,**c**,**e**,**f**) and polymersomes (**a**,**d**). All vesicles revealed spots, potentially not from AqpZ but rather collapsed PB chains (**a**–**c**) or bad fracturing artifacts (**d**–**f**). Scale bar is 100 nm.

3.3. Fluorescence Correlation Spectroscopy

As both SFLS and FF-TEM present challenges as tools for evaluating protein incorporation into polymersomes, we also evaluated FCS as a novel method for getting quantitative information about AQP incorporation. This was inspired by a recent paper by Erbakan *et al.* describing various AqpZ isoforms, tagged with a fluorophore in proteoliposomes, where the protein-per-vesicle ratio was determined and further substantiated using SFLS [48]. Initially, we attempted to reproduce the proteoliposome experiments described in [48]. At an mPAR of 1:200, our measurements revealed a proteins-per-vesicle-ratio of 5.35, which was comparable to the ones obtained in Erbakan *et al.* (around 7.5). The difference could be due to the different AQP and tagged fluorophore used.

After having optimized the FCS instrument parameters for proteopolymersomes (for details please refer to the supporting information), we performed FCS on proteopolymersomes of PB_{45}-PEO_{14} (mPAR 1:100) with AQP10-GFP and with OG-solubilized protein micelles. The results are shown in Figure 6. We obtained a higher species number in the proteopolymersomes sample than in the protein micelle sample. This could be due to the same OG-induced aggregation. We therefore decided to correlate the proteopolymersomes to the AQP10-GFP stock. Erbakan *et al.* could not do this, because

the fluorophore used (mBanana fluorescent protein) exhibited a decreased fluorescence lifetime in pure OG environment (stock solution) compared to lipid/OG environment (solubilized protein micelles). GFP, however, did not seem to alter fluorescence lifetime significantly whether the AQP10-GFP is in OG (1.8 ns) or polymer/OG environment (1.97 ns, Figure 6b). They are comparable to fluorophore used by Erbakan *et al.* (4 ns [48]) and to standard GFP fluorescence lifetime (3 ns [106]). The difference between our GFP fluorescence lifetime and the standard one could be due to shielding of the attached AQP10 and the OG environment, as well as to the fitting algorithm of the instrument.

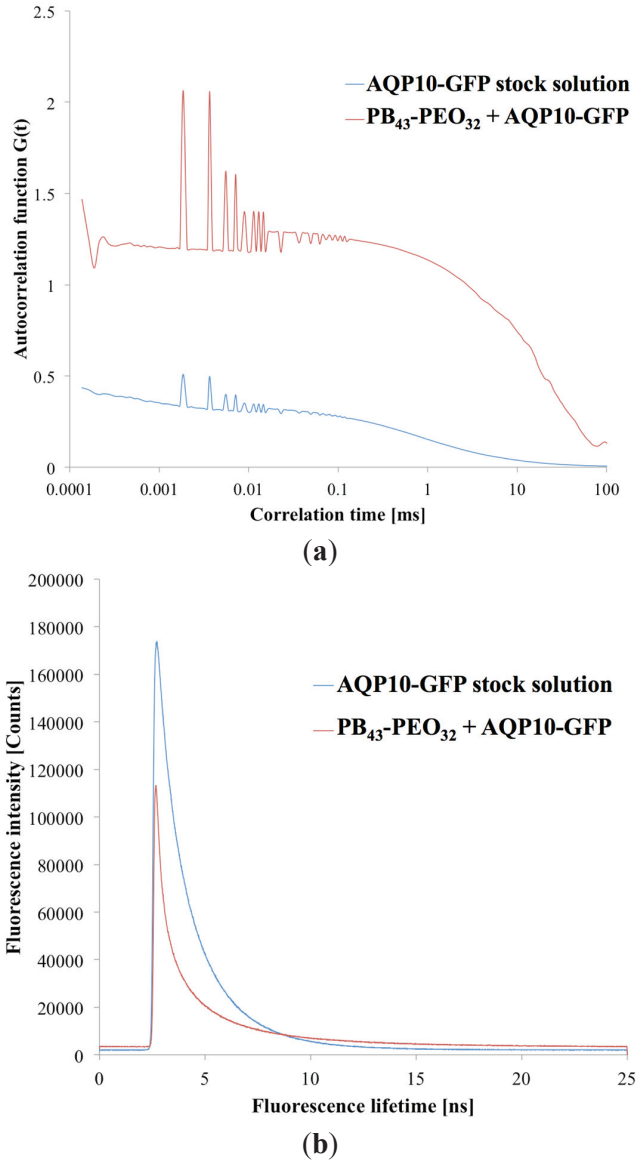

Figure 6. (**a**) Correlation diagram of proteopolymersomes and AQP10-GFP stock solution as a function of correlation time τ against autocorrelation function G(τ). The higher autocorrelation signal indicates a lower number of particles in the confocal volume, due to slower diffusion time. (**b**) Fluorescence lifetimes of the same samples as a function of lifetime against intensity signal. Where the intensities varied, the fluorescence lifetime was in a comparable range.

Accordingly, the sample correlation depend on the single components of the system. In the case of sensitive fluorophores, it is better to compare AQP vesicles and AQP micelles not to influence the fluorophore environment. In the case of polymers as the protein matrix, it is better to correlate the AQP-fluorophore stock solution as the polymeric AQP micelles aggregate easily. A disadvantage of correlating AQP-fluorophore stock with AQP vesicles is that the final concentration of AQP is not known, complicating a correlation with similar AQP concentration.

Calculating the species number of pure AQP10-GFP from the stock in the confocal volume and the one from the proteopolymersome solution (Figure 6a), we obtained a proteins-per-vesicle-ratio of 2.87. These results demonstrate that FCS can serve as a tool to quantify AQPs in proteopolymersomes. This opens possibility for conducting a systematic study in which f and M_n are varied in order to obtain quantitative information about which polymers can be used to achieve the highest proteins-per-vesicle-ratio.

3.4. Small-Angle X-Ray Scattering

Scattering curves for FR prepared proteo- and polymersomes of PB_{45}-PEO_{14} and PB_{33}-PEO_{18} are shown in Figure 7. The samples were extruded and centrifuged prior to measurements. At low q-values a typical linear slope is observed in the log-log plot, with the intensity following a power law of q^{-2}. This behaviour is typical of flat laminar structures. The fact that the slope extends below the lowest detectable q-region indicates a low curvature (flat structure) even on the largest detectable length scale of $q = 2\pi/0.1$ nm $\approx$ 60 nm. At higher q, a characteristic oscillatory behaviour is observed. This is attributed to the complex interference between the negative contrast of PB and the positive contrast of PEO.

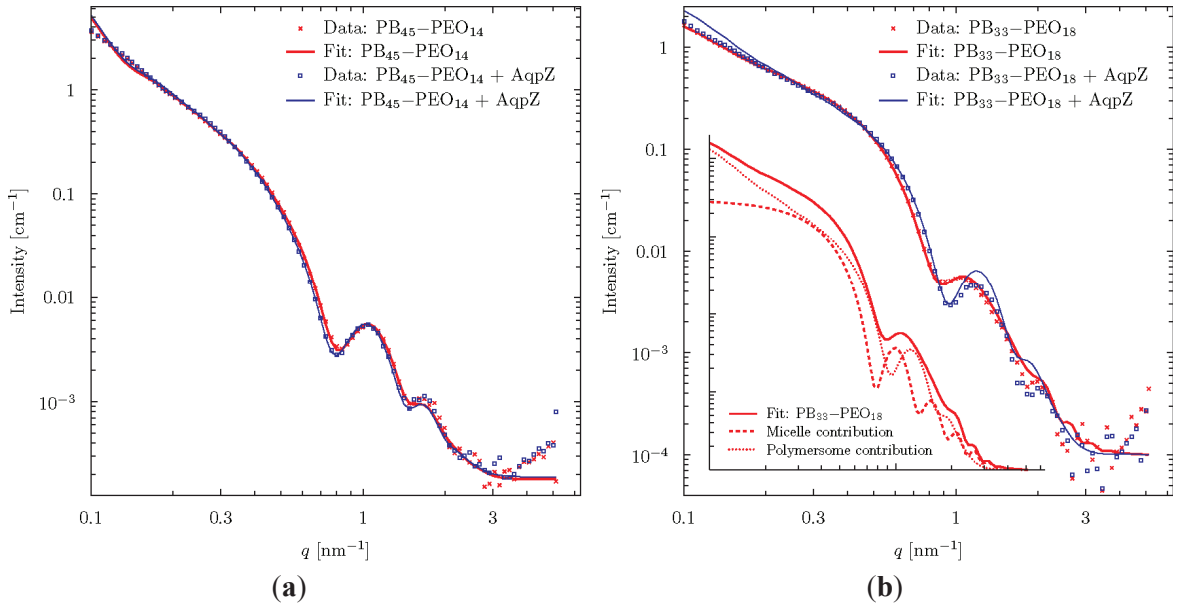

Figure 7. SAXS data for proteo- and polymersomes of PB_{45}-PEO_{14} (**a**) and PB_{33}-PEO_{18} (**b**). The fits were obtained using a vesicle model consisting of three concentric spherical shells. To fit the polymersomes of PB_{33}-PEO_{18}, it was necessary to include an additional contribution from block-copolymer micelles as shown in the insert.

The theoretical scattering from various simple geometrical objects such as spheres, cylinders and ellipsoids of varying contrast can readily be calculated. These can be combined to form simplified models of the studied particles. We choose to analyze the data using a vesicle-model consisting of three concentric spherical shells of alternating contrast, corresponding to shells of PEO, PB, and PEO, respectively. The thickness of the individual shells was varied to give the best fit to data using a least squares fitting routine.

Excellent fits were obtained for the PB_{45}-PEO_{14}-system meaning that data are in good agreement with the assumption that the diblock copolymers form spherical vesicles. The fits were especially sensitive to changes in the parameter determining the thickness of the central hydrophobic bilayer constituted by the PB-groups. These were fitted to 9.10 ± 0.1 nm and 8.94 ± 0.07 nm in the presence or absence of AqpZ respectively. Concerning the overall vesicle diameter, we can conclude from the model that it is larger than 60 nm, which is not surprising given the initial analysis above. It is evident from the data and the fit parameter values that well defined bilayer vesicles are formed and that the incorporation of AqpZ introduces only minor differences to the structure of the vesicles.

For the PB_{33}-PEO_{18} proteopolymersomes, reasonably good fits were obtained with the vesicle model with a hydrophobic bilayer thickness of 7.66 ± 0.05 nm. However, for the polymersomes, no fit to the data gave reasonable physical parameters. The data fit required the assumption that a population of block copolymer micelles co-exists with the vesicles. The combined model fit showed that 76 wt% of the population consisted of proteopolymersomes and 24 wt% were micelles with a hydrophobic core of diameter 11.7 ± 0.3 nm gives a good fit with the data. The insert of Figure 7 shows the separate vesicle and micelle contributions.

In conclusion, the SAXS analysis reveals that, for PB_{45}-$PEO_{14,}$ vesicles are formed both with and without AQP where AQP incorporation leads to a minor differences in average hydrophobic vesicle wall thickness, which could indicate a dimpling or puckering of polymers close to the incorporated AQPs. In the case of PB_{33}-PEO_{18}, some micelle-formation is observed, but this tendency is reduced when AQP is incorporated.

To summarize this chapter, the characterization methods for functional incorporation of AQPs in PB-PEO diblock copolymers were investigated. SFLS and FF-TEM are in principle powerful tools but, for polymer systems, the analysis can give ambiguous results. On the other hand, FCS and SAXS can provide detailed information, but the latter requires access to large-scale facilities in the form of synchrotron radiation sources.

4. Recent Developments in AQP Membrane Designs

Provided that the performance of AqpZ proteopolymersome described by Kumar *et al.* [17] could be scaled up, they could create a water separation membrane that reaches fluxes of 11,000 L m^{-2} h^{-1}, a value that is several orders of magnitude higher than conventional industrial membranes. In highly packed 2D AqpZ crystal arrays, fluxes of up to 16,000 L m^{-2} h^{-1} could be achieved in principle [107]. However, these values will very probably never be achieved due to upscaling issues—but they show the huge potential of biomimetic membranes. The development is rapid: in 2011, ABPMs were regarded as the most revolutionary membrane advances but also the ones most farthest away from a potential commercial viability [108]. Now, four years later, ABPM membranes are commercially available with areas of tens of m^2 [109]. It will still take time before the technology is widespread, but it has definitely

moved outside the fundamental research domain. In the next sections, we will highlight the AQP biomimetic membrane technology development in detail.

4.1. Membrane Designs Based on Planar Biomimetic Structures

The first industrial approaches are made from two Danish companies, Aquaporin A/S, and AquaZ (now Applied Biomimetic). Together with the Danish Technical University (DTU), the University of Southern Denmark (SDU), DHI, Lund University, Sweden, Ben-Gurion University of the Negev, Israel, Malaga University, Spain, Vilnius University, Lithuania and Veolia Water, France, Aquaporin A/S joined the EU funded MEMBAQ project 2006–2010 which aimed at utilizing AQPs for industrial applications [110]. At the same time, AquaZ started on membrane development based on a patent from Carlo Montemagno where he described conceptually how AQPs, embedded in polymeric or lipid bilayers, could function as a biomimetic membrane, although without any concrete design of such a membrane [111].

The first membrane design from Aquaporin A/S was based on an ethylene tetrafluoroethylene (ETFE) scaffold with holes of 300 μm, produced by laser-ablation, which are inspired by painting/folding lipid chambers from the 70s [112,113]. A freestanding lipid-bilayer film is established by "painting" a two-phase solution over the hole, where the lipids move from the organic solvent to the aqueous phase, accumulate around the holes and establish a bridging layer. Several membrane proteins and peptides were incorporated in the freestanding layer including porins [36]. In addition, freestanding PMOXA-PDMS-PMOXA polymer membranes with incorporated gramicidin A channels were developed [37] and characterized [114]. In subsequent designs, the membrane is supported by PEO-dimethacrylate (PEO-DMA) based hydrogels [115] or stabilized using surface plasma polymerization [116]. Moreover, a strategy was explored to form interface lipid bilayer between lipid-coated water drops in a continuous oil phase [117]. A later liquid membrane approach investigated SoPIP2;1 proteoliposomes in a sandwich between NF membranes that could prove an AQP fingerprint for the first time, however at modest water flux [118]. These designs [118–122] later paved the way for developing membrane-based biosensor designs [45]. The hydrogel approach from Aquaporin A/S was adapted in 2010, when Montemagno and AquaZ claimed an ABLM design with internally UV cross linked and PA-interconnected proteoliposomes that are immobilized on a lipid-coated PA layer and supported with a PEO hydrogel [123].

In 2009, Aquaporin A/S and DHI Singapore initiated collaborative research with the SMTC on biomimetic membranes. At the same time, the Chung lab from NUS started biomimetic research in collaboration with Wolfgang Meier and coworkers. NUS followed up on Aquaporin's hydrogel approach and tried to achieve a planar proteobilayer, starting with AqpZ proteoliposome fusion on pure and PEO coated porous alumina and found an increasing stability with increasing mPAR [124]. In 2012, they described an approach based on a Langmuir-Blodgett-film with Nickel-chelated lipids that bind to His-tagged AqpZ, similar to the approach from Kumar [29] but using lipids with subsequent Langmuir-Schäffer deposition-mediated transfer on a mica surface [125]. This was followed by Kaufman *et al.* who incoporated spinach AQP (SoPIP2;1) in positively charged bolalipid micelles which were then fused on a negatively charged silica surface [126]. Chuyang Tang *et al.* investigated on fusion behavior of proteoliposoes on pure and polymer-coated silica via quartz crystal microbalance with dissipation

(QCM-D) [127]. They found increasing robustness and fusion resistance with increasing mPAR, and further proteoliposome stabilization with polyelectrolyte layers at the highest mPAR (1:25) in 1,2-diphytanoyl-sn-glycero-3-phosphocholine (DPhPC) liposomes [127].

The SMTC group also investigated ABLMs, following Kaufman's approach of liposome fusion on nanofiltration (NF) membranes [128,129] and fused AqpZ proteoliposomes on NF PA-polysulfone (PSf) membranes that were precoated with positively charged lipids via spin-coating [130]. The proteoliposomes were placed on the NF membrane and slightly pressurized with 0.5 bar. They found a linear relationship between the roughness of the ABLM surface and mPAR indicating AqpZ incorporation, but no effect from AqpZ on the water flux J_v and the reverse salt flux J_s could be observed [130].

4.2. Membrane Designs Based on Vesicular Biomimetic Structures

A different approach was initiated jointly by SMTC and Aquaporin A/S in which AqpZ proteoliposomes were embedded in the standard PA layer made from interfacial polymerization of *m*-phenyl diamine (MPD) and trimesoyl chloride (TMC) on a PSf support structure [1,131,132]. ABLMs were tested with functional AqpZ proteoliposomes, proteoliposomes with an inactive AqpZ mutant and PA-PSf membranes without proteoliposomes. ABLMs were further benchmarked against commercially available membranes with cross-flow RO tests on 42 cm^2 effective coupon area. The ABLMs with AqpZ proteoliposomes had a significantly higher J_v than the ABLM with inactive AqpZ and the PA-PSf membrane while J_s values were similar in all cases. Furthermore the ABLMs were able to withstand 10 bar pressure making them well-suited for low pressure RO applications. J_v of the AqpZ ABLM was ~40% higher compared to the commercial brackish water RO membrane (BW30) and an order of magnitude higher compared to a seawater RO membrane (SW30HR).

This was followed up by a systematic study, which revealed that 1,2-dioleoyl-sn-glycero-3-phosphocholine (DOPC)-based proteoliposomes and proteoliposomes of mPAR of 1:200 gave optimal water flux as judged by SFLS and that cholesterol addition could seal defects on the proteoliposomes [133].

To achieve higher loading and better sealing, the SMTC group coated proteoliposomes with polydopamine (PDA) and immobilized them on a 28 cm^2 NF polyamide imide (PAI) membrane by embedding them in branched polyethyleneimine (PEI), cross linked per PA bond at elevated temperature [134]. The SFLS data showed, that the elevated temperature had a higher negative influence on the permeability of the proteoliposomes than the PDA coating itself. Even so, AqpZ function was demonstrated with an optimal performance mPAR of 1:200 when reconstituted and integrated into the PAI-PEI layer. In contrast, the best SFLS response was achieved at an mPAR of 1:100 [133]. This discrepancy could be due to AqpZ being affected by the PDA coating or the PEI branches. Still, the J_v was measured to be 36 L m^{-2} h^{-1} bar^{-1}) making it the highest among all biomimetic membranes so far [134].

In addition, proteopolymersomes can be functionalized to get bound chemically to a counterpart functionalized membrane. Functionalization of both liposomes and polymersomes has been studied extensively since decades [135–137].

ABPMs with functionalized proteopolymersomes are first mentioned in a patent of Montemagno in 2011, where he claimed a concept of proteopolymersomes made of polyethyloxazoline-polydimethylsiloxane-polyethyloxazoline (PEOXA-PDMS-PEOXA) triblock copolymers, where the

methacrylate-functionalized PEOXA block is immobilizing the proteopolymersomes on a methacrylate functionalized cellulosic membrane [138].

The first experimental results on this approach were presented by the NUS group [53]. They made proteopolymersomes containing AqpZ in methacrylate-functionalized PMOXA-PDMS-PMOXA and tested them with SFLS. In contrast to Kumar [17], no significant difference SFLS signals with varying mPAR was observed—likely a reflection of the issues with SFLS on rigid structures mentioned in Section 3. Proteopolymersomes were deposited onto acrylate-functionalized polycarbonate track-etched (PCTE) membranes and immobilized by UV-crosslinking of the acrylate groups with the methacrylate of the PMOXA, as claimed from Montemagno *et al.* [138]. Afterwards, the proteopolymersomes were further immobilized by pressure-assisted adsorption and possibly ruptured by "smooth extrusion". AQP resulted in an increasing J_v with increasing mPAR, whereas there was no J_v with polymersomes alone; however, AFM and field emission-scanning electron microscopy (FE-SEM) revealed that the layer had some defects [53]. In a subsequent study, they followed the same approach using an acrylate-functionalized cellulose acetate membrane [54]. Here, they found an increase in J_v and decrease in NaCl rejection with proteopolymersomes of higher mPAR. The increase in J_v could indicate AQP activity, but the NaCl rejection was however still quite low (33%) and the measured membrane area was only 7 mm^2 [54].

In another approach, gold-disulphide binding to immobilize disulphide functionalized PMOXA-PDMS-PMOXA AqpZ proteopolymersomes on gold-coated porous alumina and silicon surfaces has been described [77]. Here, FE-SEM revealed that full coverage of the pores was achieved at pore diameter of 55 nm, where larger (100nm diameter) pores remained open. Again, an effect of incorporating AQP was observed but NaCl rejection was modest [77]. To obtain a better sealing, cysteamine was added with PDA and histidine coatings after the proteopolymersome immobilization on gold-coated PCTE [3]. J_v increased and J_s decreased with increasing amount of PDA-His-layers; however, the best sealing was obtained without proteopolymersomes. Pressure retarded osmosis (PRO) mode testing (AL to the water receiving draw side) resulted in significantly higher J_s than forward osmosis (FO) mode testing (AL to feed side) [3]. Mathematical simulations on this ABPM indicated that in PRO mode, J_v is determined by vesicle size and permeability. In FO mode, hydrostatic pressure is determined by the vesicle interior solute concentration [52].

Another slightly different design has been experimentally realized afterwards with AqpZ and methacrylate- and carboxyl-functionalized PMOXA-PDMS-PMOXA on amine-functionalized CA [63]. Here, proteopolymersomes are first covalently attached to the CA, where the carboxyl-groups of PMOXA and the amine groups on CA formed a PA bond. Then, a methacrylic cross linking polymerization is performed by dipping the membrane into a mixture of methyl methacrylate, ethylene glycol dimethacrylate and initiator. J_v is linearly increasing and NaCl rejection decreasing with polymerization time. An increase in J_v and decrease in NaCl rejection of ABPMs compared to only methacrylated CA and polymersome coated CA in both FO and NF mode evidenced the presence of AQP. However the NaCl rejection (61%) still indicated significant defects [63].

Another example of methacrylate cross-linking involves amine-functionalized AqpZ proteoliposomes on a PDA precoated ultrafiltration (UF) polyacrylonitrile (PAN) membrane [139]. Here, proteoliposomes are internally cross linked via methacrylate and gently pressurized onto the PDA-PAN support, allowing the amines of PDA and functionalized lipids to react. Further stabilization is achieved via glutaraldehyde. The internal cross linking of the proteoliposomes has a positive effect on stability. J_v and NaCl rejection

between liposome-coated membranes and ABLMs showed some effects of AqpZ presence; however, FE-SEM images and low NaCl rejections revealed that defects in the ABLM played a strong role in the membrane performance [139].

Instead of chemical bonding, proteoliposomes or -polymersomes can be bound by electrostatic forces. Using this approach, Kaufman *et al.* attempted to fuse positively charged bolamphiphilic proteoliposomes onto negatively charged NF PA and sulfonate PSf (PSS) membranes [140]. The proteoliposome loading was enhanced with the more negatively charged PSS membrane. However, proteoliposome loading also led to a decrease in J_v together with an increase in NaCl rejection, probably due to induced defects in the bolamphiphilic bilayer by SoPIP2;1 [140].

Another electrostatic-binding-based approach employed the embedment of positively charged poly-L-lysine covered AqpZ proteoliposomes in the anionic part of a layer-by-layer (LbL) sandwich on an UF PAN membrane [2]. The anionic part is made of polyacrylic acid (PAA) and PSS, where the cationic counterpart was polyallylamine hydrochloride (PAH). Here, a clear AqpZ effect could be observed as J_v increased by 30%–50% after addition of proteoliposomes, where the effect was stronger when there was a higher amount of negatively charged lipids present. The $MgCl_2$ rejection was comparable to the work of Zhao *et al.* [1]; however, no NaCl rejection was presented [2]. This work was extended by encapsulating magnetic nanoparticles to force more proteoliposomes magnetically to adsorb on the polyanionic film. In FO mode, they measured an increase in both, J_v and J_s with increasing mPAR, which speaks for remaining defects despite the efforts to load more vesicles onto the supporting substrate [141].

Wang and coworkers from Ocean University of China followed up on that approach and immobilized AqpZ proteoliposomes with positively charged lipids on top of a negatively charged PSS layer, followed by PEI on an UF PAN membrane [142]. Modest NaCl rejection and J_v decrease indicated a highly defective membrane. An increase in J_v between liposomes and proteoliposomes as well as further increase in J_v with higher mPAR could indicate the presence of AQP. NaCl rejection remained however unchanged between all membranes. They further showed that membrane performance was compromised after detergent treatment [142].

All designs are summarized in Figure 8, and based on the results obtained so far, we conclude that the embedment of proteopolymersomes or -liposomes in a layer results in more efficient membranes than layer-based immobilization. A great advantage of the PA-embedment technique is that no precoating/functionalization is needed which otherwise severely limits any upscaling [1]. All reported performances are however still modest compared to theoretical predictions and clearly more development is required. The major dilemma seems to be that with increasing mPAR, J_v increases, but the matrix layer becomes weaker and more prone to salt leakage. Introduction of sealing and stabilizing polymer networks could improve rejection but may also compromise J_v [107].

Next to ABPMs and ABLMs, there are two main directions aiming to achieve biomimetic membranes by AQP mimicking artificial channels: carbon nanotubes (CNTs) and organic building block nano channels [143]. CNT is more prominent because fast water permeation is proven in theory [144] and experimentally [145]. With regard to organic nano channels, there are five promising structures found to compete with ABPMs, ABLMs and CNTs: zinc and N,N-diacetic acid imidazolium bromide based zwitterionic coordination polymers [146], helical pores of dendritic dipeptides [147], imidazole compounds with urea ribbons [148], hydrazine-appended pillar[5]arenes, macrocycles of m-phenylene ethynylene [149]. Their great advantage is their smaller size with comparable channel diameter (3–10 Å) [143].

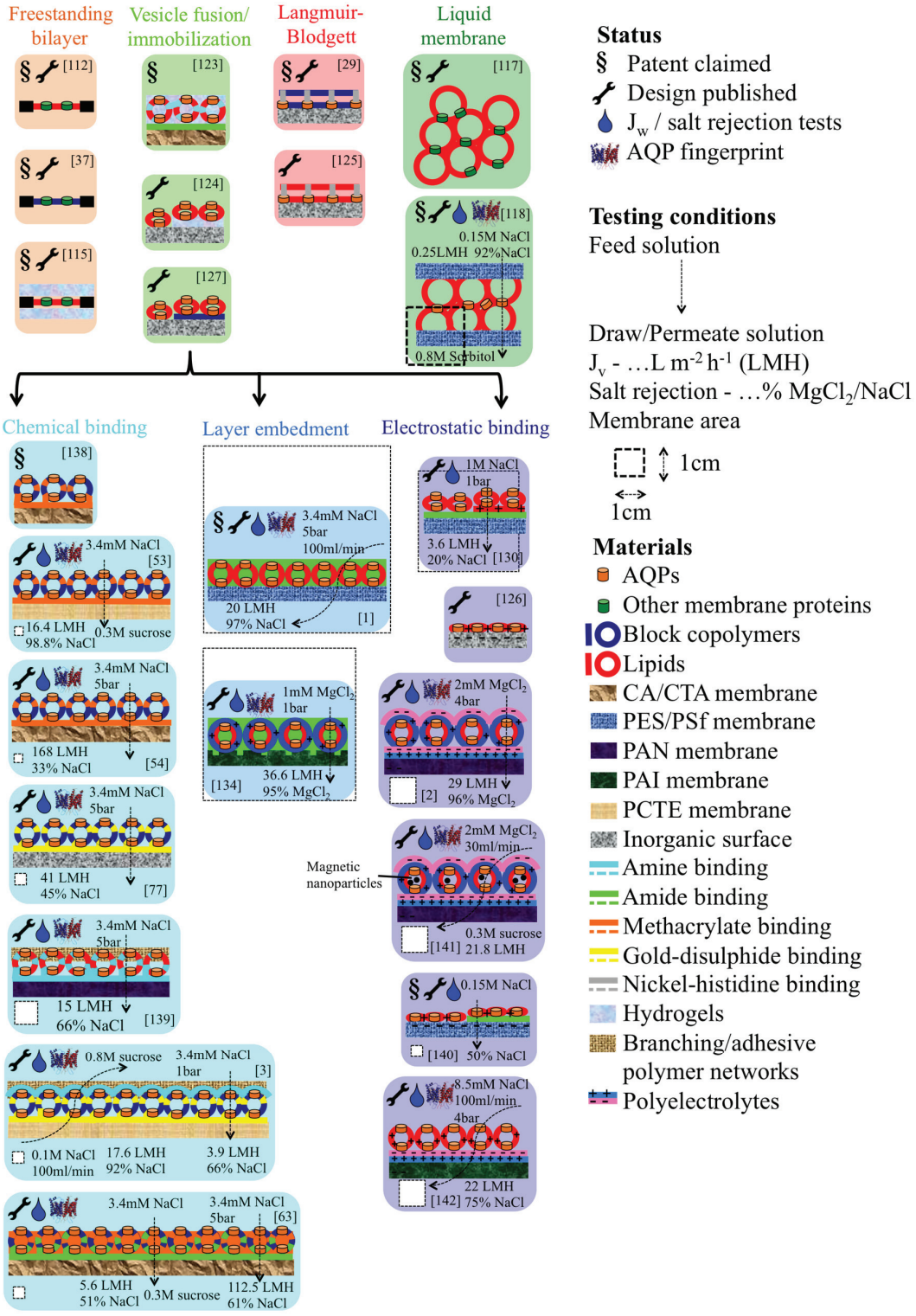

Figure 8. Schematic overview of all published designs for ABPMs and ABLMs. Pioneer work is mainly done by Kumar and Aquaporin AIS. The most experimental designs has been done by NUS, where NTU published the most promising layer embedment ABLMs. The main recent work is on LbL-based electrostatic binding, for example binding of proteoliposomes on a polyelectrolyte layer [142].

4.3. POSS—A Novel Element in Interfacial Polymerization

Nearly all RO and FO membranes are PA-based, often referred to as thin film composite (TFC) membranes due to their superior performance compared to other membrane designs. A PA-layer is generally generated by a reaction between an amine and an acyl chloride [150]. This reaction can be prepared by dissolving the amine group in an aqueous phase, and the acyl chloride group in an organic phase [151]. Typically, a membrane is wetted with the aqueous phase, containing the amine group and dried a little to remove visible liquid while keeping the surface moist. Then the organic phase with the acyl chloride group is added on top. The reaction growth is believed to be directed into the organic phase [152], due to a preferential solubility of the amine group in the organic phase compared to the solubility of the acyl chloride in the aqueous phase. This results in the well-known ridge and valley form of PA layer. The standard amine-acyl chloride combination is MPD and TMC, and typically these are supplemented with additives (molecules with similar chemistries) in low concentrations to improve flux, rejection or chlorine resistance [150].

The ideal AL of a PA membrane for water separation has to be highly water permeable, while rejecting all other solutes and being resistant against cleaning. An ideal AL of an ABPM could even be water impermeable if it enables sufficient integration of proteopolymersomes in such a way that water only passes the incorporated proteins. Therefore, novel AL components have to be explored. An AL with homogenous thickness could facilitate such proteopolymersome integration.

We have used POSS (amine linker) and TMC (acyl chloride linker) for their potential use for the integration of proteopolymersomes in ABPMs. In a recent study POSS has been introduced as an AL layer components and POSS-TMC-layer exhibited a well-defined layer without ridges and valleys but with high mechanical stability on PAN membranes [153]. This may be a better platform for the integration of proteopolymersomes compared to the ridge-and-valley MPD-TMC network. The reaction is schematically depicted in Figure 9.

Here, we prepared PA layers (hereinafter referred to as AL) of POSS+TMC containing polymersomes of PB_{29}-PEO_{16} in the aqueous phase. The influence of vesicles on the AL properties were determined, in order to provide a basis for subsequent addition of AQPs. We selected PB_{29}-PEO_{16} due to its ability to form large amounts of stable polymersomes in aqueous phase compared to other PB-PEO polymersomes [154]. For the microfluidic approach, we used proteopolymersomes (AqpZ, PB_{33}-PEO_{18}, mPAR 1:100). PB_{33}-PEO_{18} forms large amounts of stable polymersomes in aqueous phase as well and showed successful AqpZ incorporation as evidenced by SAXS. We used MilliQ water as the aqueous phase and hexane as organic phase and in order to achieve the lowest possible polydispersity, polymersomes were sonicated resulting in 95% of the polymersomes with a diameter of 196±83 nm as determined by dynamic light scattering (DLS).

We produced a non-supported AL by simply adding both phases after another in a beaker and an AL supported by microfiltration (MF) polyethersulfone (PES) layers using different coating procedures (for details see supplementary information). Characterization of the non-supported AL was done using Fourier-transformed infrared spectroscopy (FTIR), SEM and a novel, recently published microfluidic approach that allows for direct monitoring of the polymerization process [10]. Characterization of the supported AL was also achieved via FTIR and SEM, where it was also tested for functionality using standard flux and rejection test in FO mode and methylviolet staining.

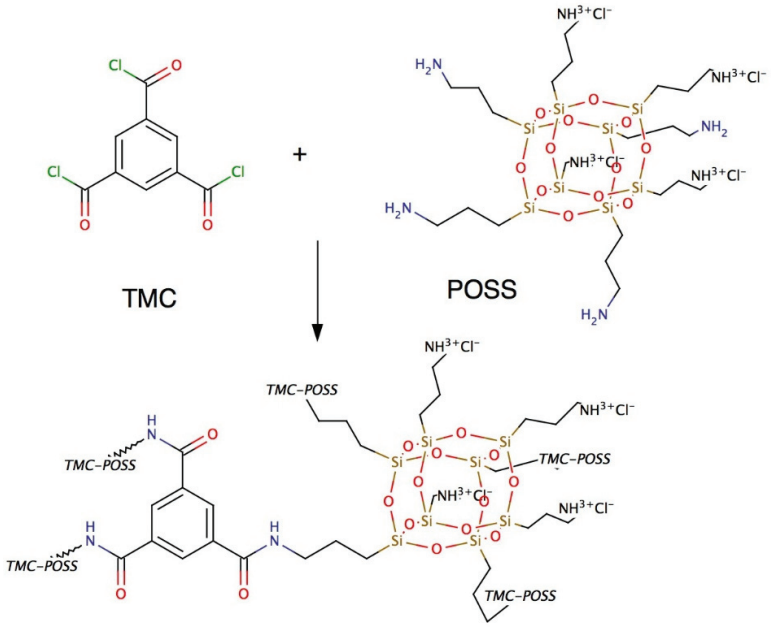

Figure 9. Chemical structure of POSS and TMC and the resulting AL. POSS as the amine linker generate a highly stable and well-defined AL with TMC.

After adding both phases, pieces of the formed (non-supported) AL were air dried then vacuum-dried where they crumbled to flake-like structures. FTIR analysis of POSS+TMC with addition of polymersomes revealed the presence of block copolymers in the AL, see Figure 10. AL with polymersomes had an absorption peak around 3000 cm^{-1} (C-H stretch), which can also be found in spectra of PB and PEO [155,156]. The polymersome-free AL exhibited a broad peak at that wavelength range but not a distinct maximum as for the polymersome-containing AL. This could indicate a successful polymersome integration in the AL. Polymersomes furthermore did not seem to block PA formation, because the characteristic peaks of a PA bond, the C=O stretch at 1636 cm^{-1}, as well as the N-H stretch at 1545 cm^{-1} [153] were clearly visible in the AL with polymersomes. Finally, partial hydrolysis of the POSS leading to the AL formation is not substantially affected by the presence of the polymerosomes as far as the characteristic peaks for the POSS-cage and ladder (1125 cm^{-1} and 1040 cm^{-1} [153]) were present in both AL. There was however an apparent influence of the polymersomes on TMC reactivity. Originally, Dalwani *et al.* used 2g/L TMC for their non-supported and supported AL [153]. In our case we could not form a non-supported AL with 2 g/L but with 0.5 g/L TMC. Potentially the TMC-POSS-stochiometry was artificially increased by the presence of another species in the aqueous phase. An excess of TMC could hinder network structure formation, because TMC will not connect POSS cages, resulting only in low molecular weight networks. We used 0.5 g/L TMC for the non-supported POSS+TMC AL and POSS/polymersomes+TMC AL.

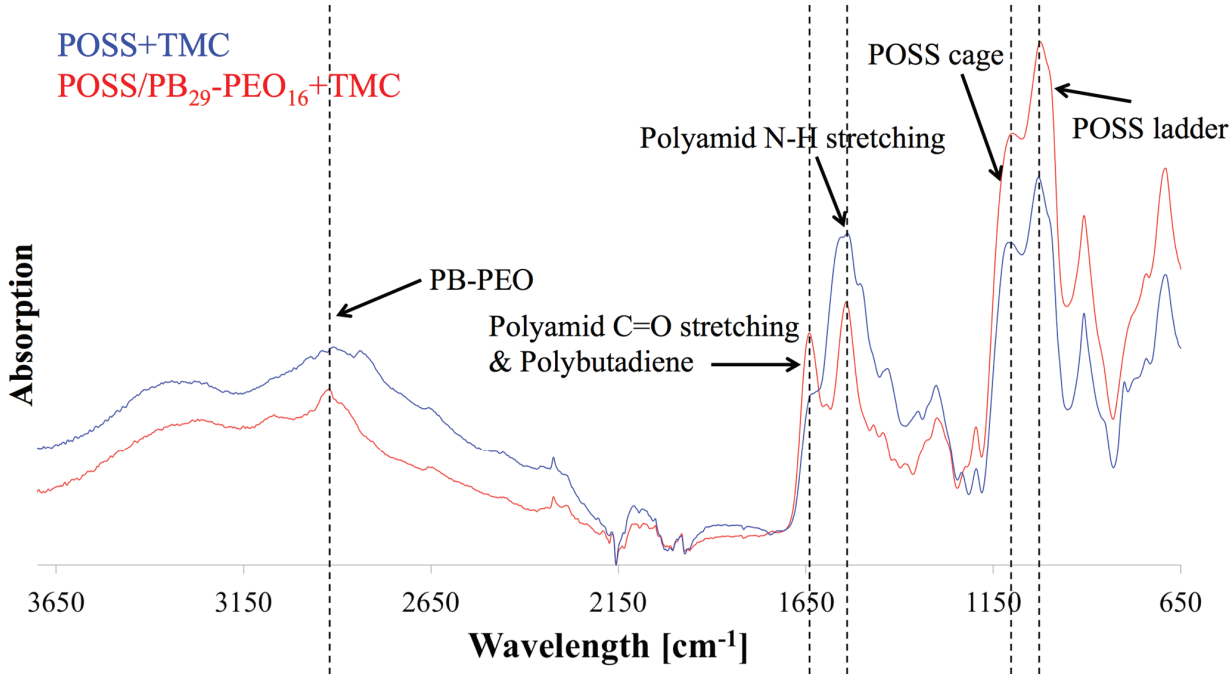

Figure 10. FTIR diagram of POSS/polymersomes+TMC AL (labelled red) and POSS+TMC control AL (labelled blue) as a function of wavelength against absorption. The AL with polymersomes had an absorption peak around 3000 cm^{-1}, that responds to PB and PEO, indicating their presence in the AL, where the characteristic absorption peaks for PA bonds and POSS were present as well.

The FTIR results were complemented with SEM analysis of the same samples, see in Figure 11. The POSS+TMC AL appeared smooth and well-defined, in agreement with previous work [153], see Figure 11a,b. When polymersomes were added (Figure 11c–e) a clear distinction can be made between the side towards the organic phase, that does not reveal presence of polymersomes (Figure 11c) and the side that faced the aqueous layer, which is well-covered with polymersomes (Figure 11e).

Most of the polymersomes seemed to sit loosely on top of the AL, whereas some polymersomes seemed to be covered to a certain extent by the AL, their shape less sharp than the others (indicated by the dotted circles in image Figure 11d). A few polymersomes were directly embedded inside the AL, visible from its cracked profile (arrows in Figure 11d). This could indicate that the POSS approach can be used to embed polymersomes in such a way that they would be suitable for membrane fabrication.

Recently, a novel approach from the microfluidic field was published [10] that allows visual study of the evolution of the location of interfacial polymerisation reactions. This involves a chip containing a hydrophobized micro-chamber that is separated in two compartments by an array of micro-pillars each with a diameter of 30 µm and a height of 50 µm. The aqueous phase with amine linker was introduced via micro capillary connections into one compartment and formed a water-air-interface between the pillars. Then the organic phase with acyl chloride linker was introduced into the other compartment. AL formation at the interface between the solutions was observed using an optical microscope. Depending on the linkers, the resulting AL will have a different morphology and formation time. POSS+TMC forms well-defined AL with a formation time within 4 s. In contrast, for instance the apparent growth of a film

from Jeffamine+TMC is not finalized after 15 min and the film reveals the ridge and valley structures that are typical for AL formed by interfacial polymerization [10].

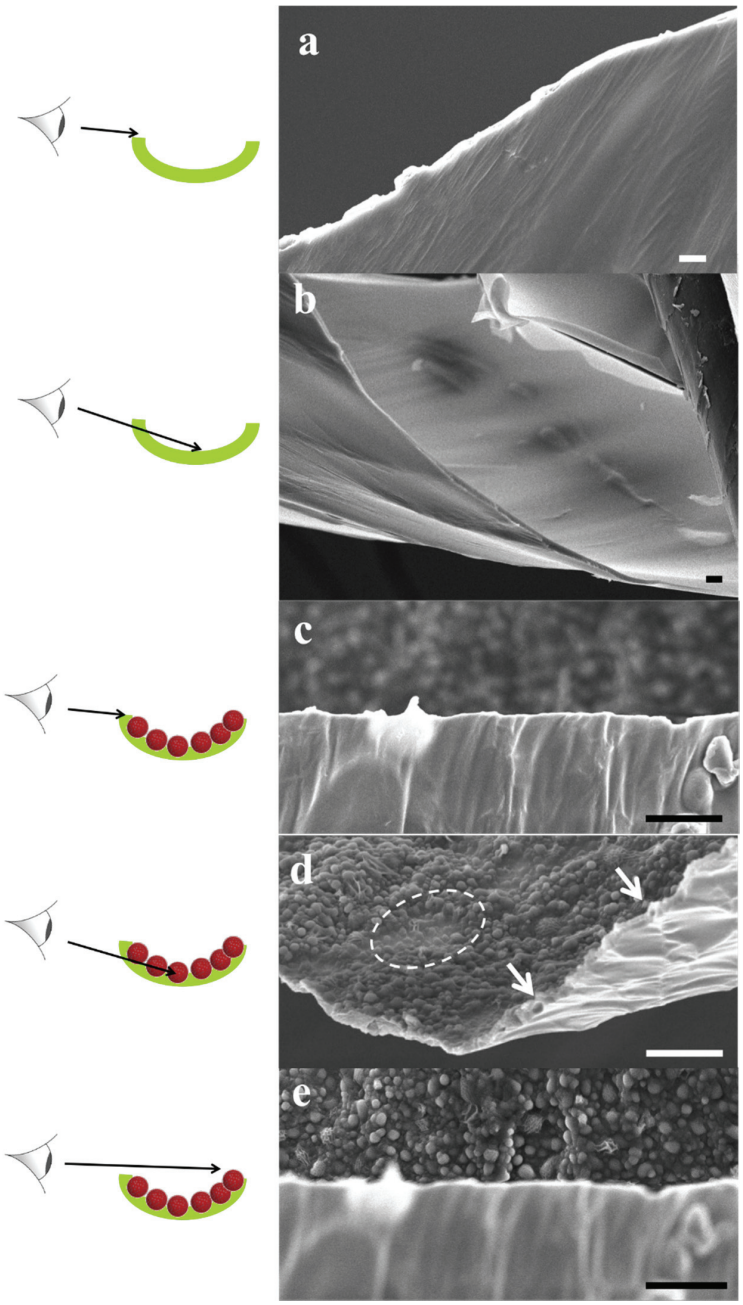

Figure 11. SEM images of POSS+TMC AL (**a**,**b**) and of POSS/polymersomes+TMC AL (**c**–**e**) with schematic sketches, which part of the layer is being captured. Images were taken from different parts of the flakes (labelled green in the sketch) of the AL, that were generated during the SEM preparation. The AL without polymersomes was smooth and well-defined, which remained on the organic side when polymersomes were added. The aqueous side was covered with loosely attached and half-covered polymersomes (dotted circle in (**d**)). A few could be observed inside the AL (arrows in (**d**)). Scale bar is 3 µm.

We used this approach to monitor POSS/proteopolymersomes+TMC AL (AqpZ & PB_{33}-PEO_{18}, mPAR 1:100), see Figure 12. The chip that was used was not hydrophobized optimally, which resulted in partial infusion of the aqueous phase into the channel with the organic phase. The hydrophobization was still sufficiently efficient to hinder the aqueous phase from passing entirely to the other compartment. Other reasons for the shift of the interface from the pillar structures to the organic phase could be overpressure from the aqueous phase, which is hard to control since the offered pressure is in the range of 10^4 Pa. When the organic phase containing TMC was introduced, the typical sharp AL was formed at the aqueous-organic interface (Figure 12b dotted line 1). After that, the reaction was continued by the diffused amine into the organic phase and the formed AL that connected the initial interfaces, exhibited a new aqueous-organic interface (Figure 12b dotted line 2). Such observation demonstrates a less denser AL formed by POSS/proteopolymersomes-TMC compared to that formed by POSS-TMC reaction. The formation time was on the order of seconds. The film remained in the same shape and no further growth was observed in the following 12 h.

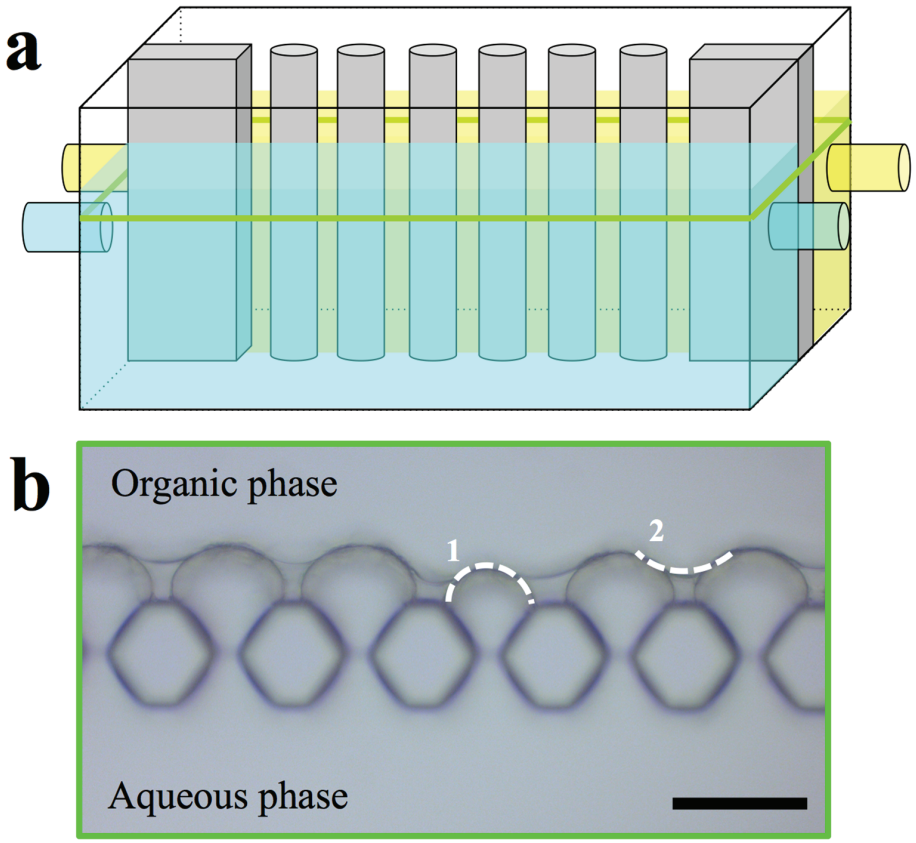

Figure 12. (**a**) Schematic sketch of the microfluidic chamber and micrographs of POSS/proteopolymersomes+TMC AL and (**b**) micrograph of the compartment. The aqueous phase reached into the other compartment. After introducing the organic phase, a well-defined AL formed. Scale bar is 50 µm.

We then investigated POSS+TMC on MF PES support material coated following the procedures in Dalwani *et al.* [153], which is further described in the supporting information. The MF PES itself was supported by a nonwoven. FTIR spectroscopy revealed the presence of polymersomes in the supported

AL, however, the PA formation is significantly reduced compared to the non-supported POSS/polymersomes+TMC AL, see Figure 13. A main challenge of analyzing supported AL with FTIR is the potential absorption of the PES support, which has a strong absorption especially in the region between 700 and 2000 cm^{-1}. Especially, the POSS absorption peaks interfered strongly with PES peaks. In the supported POSS/polymersomes+TMC AL the PB-PEO signal at 3000 cm^{-1} was present as well as another small peak around 1700 cm^{-1} that also appeared in the FTIR spectra of PB [155]. Interestingly, it could not be found in the non-supported AL. Potentially, it was overlayed from the background signal in the region between 1600–3650 cm^{-1} that was more significant at the FTIR analysis spectra from the non-supported AL. Both PA bonds were present in the supported POSS+TMC AL but strongly reduced in the one with polymersomes. The large peak (at 1580 cm^{-1}) close to the N-H stretching peak, is associated with PES. The N-H stretching peak (1545 cm^{-1}) was only present in the supported POSS+TMC AL. The broad peak of this AL from 3150–3650 cm^{-1} is likely associated to water and/or unreacted amine groups.

The reason for the suppression of the PA-signal in the supported POSS/polymersomes+TMC AL is not clear. It may be related to the TMC reactivity as discussed before. We used 2 g/L TMC for the supported POSS+TMC AL and POSS/polymersomes+TMC AL, because there was no AL formation at 0.5 g/L. Another TMC concentration may be more optimal for the supported POSS/polymersomes+TMC AL. The potential blockage of PA formation induced by polymersomes should have suppressed the PA formation in the non-supported AL as well, which it did not. However, AL formation was significantly decreased with supported POSS+TMC AL when changing from 2 g/L to 0.5 g/L. Another hypothesis could be that POSS+TMC do not form easily on MF PES. To our knowledge, no former POSS+TMC AL formation on MF PES has been reported. MF PES has significantly bigger pore sizes than PAN. This could hamper the formation of a smooth layer.

In contrast to the FTIR analysis, SEM analysis showed a completely covered POSS/polymersomes+TMC AL on the MF PES (Figure 14). In addition, POSS and TMC alone seemed to cover the microporous PES structure completely with the smooth layer, although less defined than for PAN substrates [153]. This could be due to the different pore size as mentioned before. When polymersomes were added, the AL exhibited sub-micron sized bumps. They are 1.5–2 μm in length and 0.5–1 μm in height. Considering a covering AL of 100 nm thickness [153] (Figure 14 sketch in bottom left corner) there would be groups of 6–9 polymersomes in a row in 1–3 layers. In contrast to the non-supported ALs, we can only observe the side facing the organic phase. In the case of the supported POSS/polymersomes+TMC AL, the polymersomes influence the shape of the AL side facing the organic phase to a far higher extent than in the non-supported form. This is most probably due to the different preparations, with regard to POSS/polymersomes being in solution at the non-supported AL formation and being at the water-air-interface or even dried on the MF PES at the supported AL formation. Thus, the chances of polymersomes being integrated in the AL is higher for the supported AL than for the non-supported one.

In conclusion, SEM analysis revealed a successful embedment of polymersomes in a supported AL, whereas FTIR data were less informative. A limitation of FTIR and SEM analysis of supported AL is that only a small fraction of the whole membrane is observed. Another aspect is that the AL could become brittle during drying, and delaminate, or break off when exposed to liquid nitrogen that is used for SEM sample preparation.

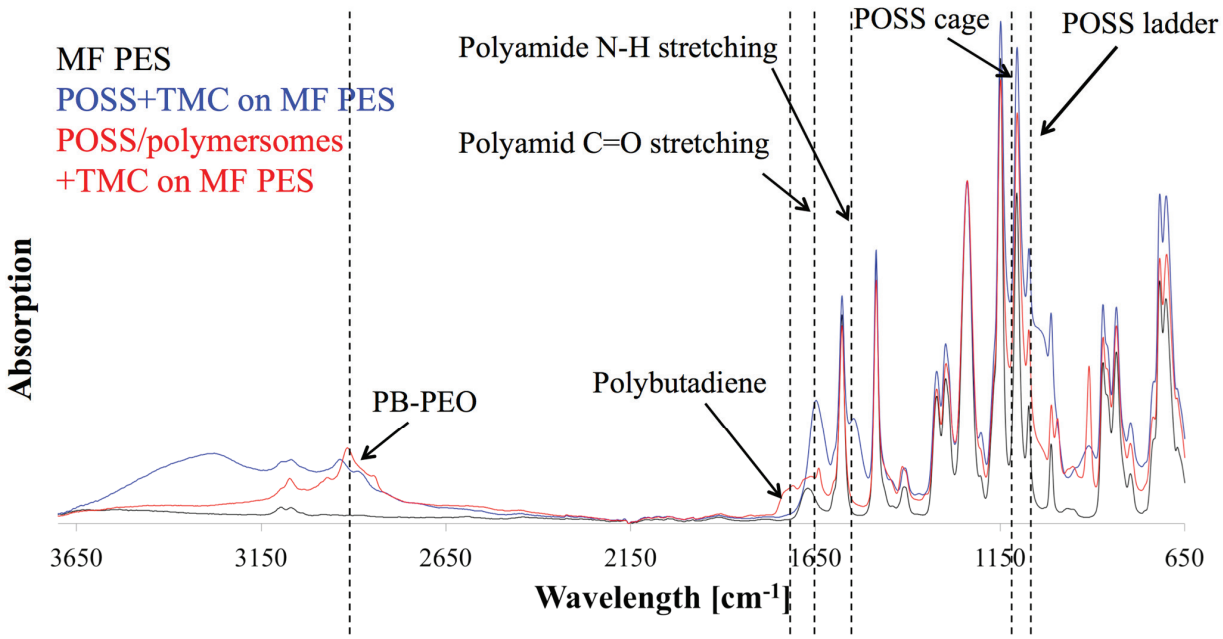

Figure 13. FTIR analysis of supported POSS/polymersomes+TMC AL (**red**) and POSS+TMC control AL (**blue**) on MF PES and pure MF PES (**black**). The PES supporting material had high absorption and interfered with many absorption peaks. A subtraction from the absorption spectra of pure PES resulted in negative peaks. We therefore only normalized the spectra. PB-PEO was present in the AL with polymersomes; however, the PA formation was strongly suppressed.

We also attempted to test the POSS/polymersomes+TMC AL on MF PES in terms of flux and rejection measurements in FO mode. However, we did not see any FO performance. Approximately one third of the membranes tested were impermeable to salt as evidenced by the low conductivity change in the feed solution within 2 h. The rest of the membranes were leaky as evidenced by an immediate increase in conductivity. The fraction of sealed and leaky membranes of POSS+TMC and POSS/polymersomes+TMC were comparable. In the sealed membranes, the pores are likely clogged by several accumulated layers of POSS+TMC AL. However, after staining with methyl blue no pinholes or scratches were detected on the surface, suggesting that the supporting PES was covered with the AL. As mentioned before, MF PES may not be a suited support for POSS+TMC ALs in general. PAN support did not show any flux without hydraulic pressure, due to the small pore size (5–30 nm) [157]. It may be suited for POSS+TMC for a NF membrane, but not for FO. A compromise would be to use UF PES membranes as used by Lee *et al.* [158].

To conclude this subchapter, we obtained insights in non-supported and supported AL containing POSS with polymersomes in the aqueous phase and TMC in the organic phase. The non-supported POSS/polymersomes+TMC AL was formed successfully with high amounts of polymersomes covered and some of them even integrated inside the AL. The supported POSS/polymersomes+TMC showed a different characteristics. FTIR data indicated a high suppression of the AL formation at polymersome addition, whereas SEM images showed a completely covered and significantly different AL upon polymersome addition. None of the membranes produced, containing POSS and TMC had any

reasonable performance, probably due to incomplete coverage of the AL. Still, it was interesting to get an insight into how POSS, TMC and proteopolymersomes are interacting. Further challenges will be to create a functional water separation membrane from these components.

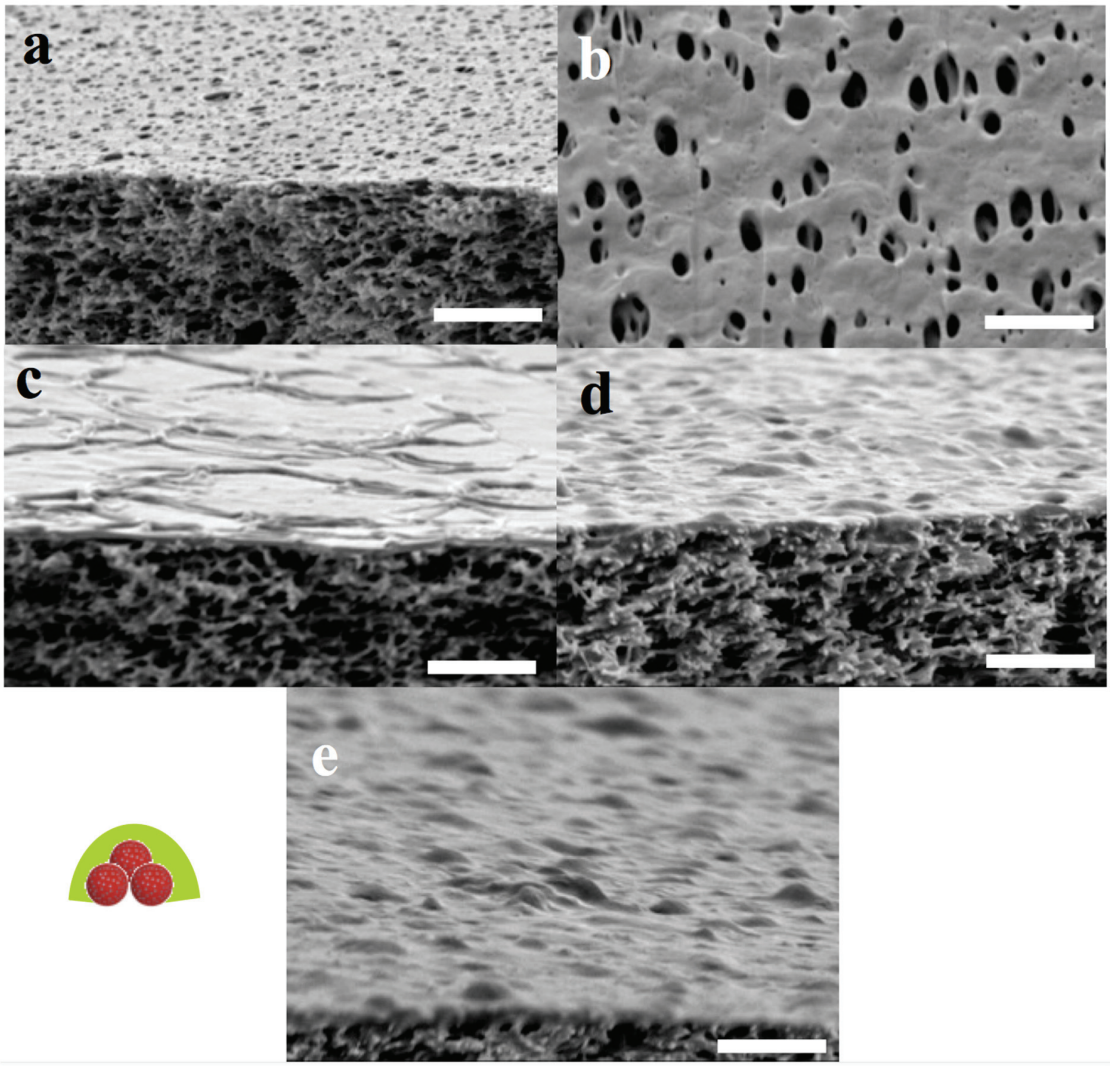

Figure 14. SEM images of MF PES (**a**,**b**) supported POSS+TMC AL on MF PES (**c**) and supported POSS/polymersomes+TMC on MF PES (**d**,**e**). Schematic sketch of polymersome coverage left to (**e**). Micropores of the MF PES were covered completely by the POSS+TMC AL. After addition of polymersomes, small bumps with dimensions similar to the polymersomes were observed on the organic faced side of the AL. Greater bumps may be attributed to accumulations of covered polymersomes. Scale bar is 3 µm.

5. Perspectives

As mentioned in other reviews [4], ABPMs are rapidly evolving and coming of age. Future challenges will be the upscaling production of both AQPs and block copolymers. Another relevant economic issue is the use of AQP-solubilizing detergents that have a broad price range. ABPMs need to be comparable to established membrane technologies in terms of cost and scale. As seen in Figure 8, all published

studies about ABPMs are tested in small-scale laboratory experiments. Even though there are commercially available ABPMs in m^2-scale, more development will be needed. The lessons learnt from nature are not completely transferred yet.

Acknowledgments

We thank Michiel Raaijmakers, Yali Zhang, Evelien Maaskant and Nieck Benes, University of Twente, especially Michiel Raaijmakers and Yali Zhang for helpful discussion and assistance in the lab for all experiments with POSS+TMC membranes; Daniela Pirner, University of Bayreuth, Germany, and Sokol Ndoni, DTU Nanotech, for helpful discussions and Simon Levinsen, DTU Nanotech for assistance in polymer synthesis; Fabian Itel and Mohamed Chami, both University of Basel, Switzerland, and Manish Kumar, Pennsylvania State University, USA, for useful discussions about polymersomes in general and freeze fracture; Fadoua Sbai, Aquaporin A/S for assistance with polymersome preparation; Per Amstrup Pedersen for providing AQP10-GFP; Klaus Qvortrup and Ramon Liebrechts, University of Copenhagen, for providing assistance with freeze fracture and access to the Leica freeze fracture instruments, Krzysztof Trzaskus, Joris de Grooth and Harmen Zwijnenberg for providing assistance with the membrane flux and rejection tests. We thank NXUS for the collection and analysis of the SAXS-data. NXUS is a pilot project enabling industrial use of large scale research facilities in collaboration with university experts in the field of neutron and X-ray science. NXUS is funded by the University of Copenhagen and the capital region of Denmark. JH was supported by an industrial PhD grant from Innovation Fund Denmark. CHN was supported by the IBISS—Industrial Biomimetic Sensing and separation platform (http://www.ibiss.dtu.dk) funded by the Danish Innovation Fund Grant No. 097-2012-4.

Author Contributions

Conceived and designed the experiments: Joachim Habel, Anayo Ogbonna. Performed the experiments: Joachim Habel, Michael Hansen, Nanna Larsen, Søren Kynde, Søren Roi Midtgaard. Analyzed the data: Joachim Habel, Michael Hansen, Søren Kynde, Søren Roi Midtgaard, Grethe Vestergaard Jensen. Contributed reagents/materials/analysis tools: Joachim Habel, Michael Hansen, Søren Kynde, Søren Roi Midtgaard, Grethe Vestergaard Jensen, Julie Bomholt, Anayo Ogbonna, Kristoffer Almdal, Alexander Schulz, Claus Hélix-Nielsen. Wrote the paper: Joachim Habel, Søren Kynde, Claus Hélix-Nielsen.

Conflicts of Interest

The authors declare no conflict of interest.

Abbreviations/Nomenclature

ABLM	Aquaporin-based lipidic biomimetic membrane
ABM	Aquaporin-based biomimetic membrane
ABPM	Aquaporin-based polymeric biomimetic membrane
7-ADCA	7-aminodesacetoxycephalosporanic acid

AFM	Atomic force microscopy
AL	Active layer
AQP	Aquaporin
AqpZ	Aquaporin Z
BR	Bacteriorhodopsin
BSA	Bovine serum albumin
CA	Cellulose acetate
CcO	Cytochrome c oxidase
CNT	Carbon nanotube
Cr	Planar shape with protein crystals
DLS	Dynamic light scattering
DMA	Dimethacrylate
DOPE	1,2-dioleoyl-sn-glycero-3-phosphoethanolamine
DPhPC	1,2-diphytanoyl-sn-glycero-3-phosphocholine
DTU	Danish Technical University
EFTE	Ethylene tetrafluoroethylene
ELF	Enzyme-labelled fluorescence
EPR	Electron paramagnetic resonance
f	Hydrophilic volume ratio
FCS	Fluorescence correlation spectroscopy
FE-SEM	Field-emission scanning electron microscopy
FF-TEM	Freeze-fracture transmission electron microscopy
FhuA	Ferric hydroxamate uptake protein
FI	Functional incorporation
FO	Forward osmosis
FTIR	Fourier-transformed infrared spectroscopy
FR	Film rehydration
J_s	Membrane reverse salt flux
J_v	Membrane water flux
LA	Lipoic acid
LamB	Phage lambda receptor
LbL	Layer-by-layer
M_n	Number-averaged molecular weight
M_w	Weight-averaged molecular weight
MAq	Mixing in aqueous phase
Mc	Micellar shape
MF	Microfiltration
MloK1	Potassium channel from Mesorhizobium loti
MPD	*m*-phenyl diamine
MPEG	Methyl polyethyleneglycol
mPAR	Molecular amphiphile-to-protein-ratio
MOr	Mixing in organic phase

PVL	Polyvalerolactone
NA	Not announced
NAD	β-nicotinamide adenine dinucleotide
NADH	Hydrogenated β-nicotinamide adenine dinucleotide
ND	Not determined
NF	Nanofiltration
NtAQP1	Tobacco plasma membrane intrinsic protein 1
NtPIP2;1	Tobacco plasma membrane intrinsic protein 2
NUS	National University of Singapore
OG	*n*-Octyl-β-D-Glucopyranoside
OmpF	Outer membrane protein F
OmpG	Outer membrane protein G
P	Planar shape
P2VP	Poly-2-vinyl pyridine
P4MVP	Poly-4-vinyl methylpyridine iodide
P4VP	Poly-4-vinyl pyridine iodide
PA	Polyamide
PAA	Polyacrylic acid
PAI	Polyamide imide
PAH	Polyallylamine hydrochloride
PAN	Polyacrylonitrile
PB	Polybutadiene
PBR	Polymer bulk rehydration
PBMA	Polybutyl methacrylate
PCTE	Polycarbonate track-etched
PDA	Polydopamine
PDA	Polydopamine
PDI	Polydispersity index
PDMS	Polydimethylsiloxane
PEE	Polyethylethylene
PEOXA	Polyethylene oxazoline
PEO	Polyethylene oxide
PES	Polyethersulfone
PFR	Polymer film rehydration
PGM	Polyglycerol monomethacrylate
PGME	Phenylglycine methyl ester
PHEMA	Polyhydroxyethyl methacrylate
PI	Polyisoprene
PIB	Polyisobutylene
PMOXA	Polymethyloxazoline
POSS	Polyhedral oligomeric silsesquioxane
PPFR	Protein/polymer film rehydration

PPO	Polypropylene oxide
PR	Proteorhodopsin
PRO	Pressure retarded osmosis
PS	Polystyrene
PSf	Polysulfone
PSS	Sulfonate polysulfone
QCM-D	Quartz crystal microbalance with dissipation
RC	Reaction centre
RO	Reverse osmosis
S	Shape
SFLS	Stopped-flow light scattering
SAXS	Small-angle X-ray scattering
SDU	Southern Danish University
SE	Solvent evaporation
SEC	Size exclusion chromatography
SEM	Scanning electron microscopy
SI	Solvent injection
SMTC	Singapore Membrane technology Centre
SoPIP2;1	Spinach plasma membrane intrinsic protein 2;1
TFC	Thin film composite
TMB	3,3,5,5-tetramethyl-benzidine
TMC	Trimesoyl chloride
UF	Ultrafiltration
V	Vesicular shape

References

1. Zhao, Y.; Qiu, C.; Li, X.; Vararattanavech, A.; Shen, W.; Torres, J.; Hélix-Nielsen, C.; Wang, R.; Hu, X.; Fane, A.G.; *et al*. Synthesis of robust and high-performance aquaporin-based biomimetic membranes by interfacial polymerization-membrane preparation and RO performance characterization. *J. Membr. Sci.* **2012**, *423–424*, 422–428.
2. Sun, G.; Chung, T.S.; Jeyaseelan, K.; Armugam, A. A layer-by-layer self-assembly approach to developing an aquaporin-embedded mixed matrix membrane. *RSC Adv.* **2013**, *3*, 473.
3. Wang, H.L.; Chung, T.S.; Tong, Y.W.; Jeyaseelan, K.; Armugam, A.; Duong, H.H.P.; Fu, F.; Seah, H.; Yang, J.; Hong, M. Mechanically robust and highly permeable AquaporinZ biomimetic membranes. *J. Membr. Sci.* **2013**, *434*, 130–136.
4. Tang, C.Y.; Wang, Z.; Petrinic´, I.; Fane, A.G.; Hélix-Nielsen, C. Biomimetic aquaporin membranes coming of age. *Desalination* **2015**, *368*, 89–105.
5. Tang, C.Y.; Zhao, Y.; Wang, R.; Hélix-Nielsen, C.; Fane, A.G. Desalination by biomimetic aquaporin membranes: Review of status and prospects. *Desalination* **2013**, *308*, 34–40.
6. Hélix-Nielsen, C. *Biomimetic Membranes for Sensor and Separation Applications*; Springer: Dordrecht, The Netherlands, 2012.

7. Kita-Tokarczyk, K.; Meier, W. Biomimetic block copolymer membranes. *CHIMIA* **2008**, *62*, 820–825.
8. Raaijmakers, M.J.T.; Hempenius, M.A.; Schön, P.M.; Vancso, G.J.; Nijmeijer, A.; Wessling, M.; Benes, N.E. Sieving of Hot Gases by Hyper-Cross-Linked Nanoscale-Hybrid Membranes. *J. Am. Chem. Soc.* **2014**, *136*, 330–335.
9. Ajit Walter, P.; Muthukumar, T.; Reddy, B. Assessment of antifouling efficacy of polyhedral oligomeric silsesquioxane based poly (urea-urethane-imide) hybrid membranes. *Lett. Appl. Microbiol.* **2015**, doi:10.1111/lam.12457.
10. Zhang, Y.; Benes, N.E.; Lammertink, R.G.H. Visualization and characterization of interfacial polymerization layer formation. *Lab Chip* **2015**, *15*, 575–580.
11. Kagawa, Y.; Racker, E. Partial Resolution of the Enzymes Catalyzing Oxidative Phosphorylation. *J. Biol. Chem.* **1971**, *246*, 5477–5487.
12. Nardin, C.; Thoeni, S.; Widmer, J.; Winterhalter, M.; Meier, W. Nanoreactors based on (polymerized) ABA-triblock copolymer vesicles. *Chem. Commun.* **2000**, 1433–1434.
13. Zhang, X.; Tanner, P.; Graff, A.; Palivan, C.G.; Meier, W. Mimicking the cell membrane with block copolymer membranes. *J. Polym. Sci. Part A: Polym. Chem.* **2012**, *50*, 2293–2318.
14. Tanner, P.; Baumann, P.; Enea, R.; Onaca, O.; Palivan, C.; Meier, W. Polymeric Vesicles: From Drug Carriers to Nanoreactors and Artificial Organelles. *Acc. Chem. Res.* **2011**, *44*, 1039–1049.
15. Choi, H.J.; Montemagno, C. Artificial organelle: ATP synthesis from cellular mimetic polymersomes. *Nano Lett.* **2005**, *5*, 2538–2542.
16. Vriezema, D.M.; Garcia, P.M.L.; Sancho Oltra, N.; Hatzakis, N.S.; Kuiper, S.M.; Nolte, R.J.M.; Rowan, A.E.; van Hest, J.C.M. Positional Assembly of Enzymes in Polymersome Nanoreactors for Cascade Reactions. *Angew. Chem. Int. Ed.* **2007**, *46*, 7378–7382.
17. Kumar, M.; Grzelakowski, M.; Zilles, J.; Meier, W.P. Highly permeable polymeric membranes based on the incorporation of the functional water channel protein Aquaporin Z. *Proc. Natl. Acad. Sci. USA* **2007**, *104*, 20719–20724.
18. Kumar, M.; Habel, J.; Shen, Y.x.; Meier, W.; Walz, T. High-Density Reconstitution of Functional Water Channels into Vesicular and Planar Block Copolymer Membranes. *J. Am. Chem. Soc.* **2012**, *134*, 18631–18637.
19. Andersen, O. Bilayer thickness and membrane protein function: An energetic perspective. *Annu. Rev. Biophys. Biomol. Struct.* **2007**, *36*, 107–130.
20. Pata, V.; Dan, N. The Effect of Chain Length on Protein Solubilization in Polymer-Based Vesicles (Polymersomes). *Biophys. J.* **2003**, *85*, 2111–2118.
21. Srinivas, G.; Discher, D.; Klein, M. Key Roles for Chain Flexibility in Block Copolymer Membranes that Contain Pores or Make Tubes. *Nano Lett.* **2005**, *5*, 2343–2349.
22. Discher, D.E.; Ortiz, V.; Srinivas, G.; Klein, M.L.; Kim, Y.; Christian, D.; Cai, S.; Photos, P.; Ahmed, F. Emerging applications of polymersomes in delivery: From molecular dynamics to shrinkage of tumors. *Prog. Polym. Sci.* **2007**, *32*, 838–857.
23. Aponte-Santamaría, C.; Briones, R.; Schenk, A.; Walz, T.; de Groot, B. Molecular driving forces defining lipid positions around aquaporin-0. *Proc. Natl. Acad. Sci. USA* **2012**, *109*, 9887–9892.
24. Hansen, J.S.; Vararattanavech, A.; Plasencia, I.; Greisen, P.J.; Bomholt, J.; Torres, J.; Emnéus, J.; Hélix-Nielsen, C. Interaction between sodium dodecyl sulfate and membrane reconstituted

aquaporins: A comparative study of spinach SoPIP2;1 and *E. coli* AqpZ. *Biochim. Biophys. Acta (BBA)—Biomembr.* **2011**, *1808*, 2600–2607.

25. Stoenescu, R.; Graff, A.; Meier, W. Asymmetric ABC-Triblock Copolymer Membranes Induce a Directed Insertion of Membrane Proteins. *Macromol. Biosci.* **2004**, *4*, 930–935.
26. Hite, R.K.; Li, Z.; Walz, T. Principles of membrane protein interactions with annular lipids deduced from aquaporin-0 2D crystals. *EMBO J.* **2010**, *29*, 1652–1658.
27. Nehring, R.; Palivan, C.G.; Casse, O.; Tanner, P.; Tüxen, J.; Meier, W. Amphiphilic Diblock Copolymers for Molecular Recognition: Metal-Nitrilotriacetic Acid Functionalized Vesicles. *Langmuir* **2009**, *25*, 1122–1130.
28. Kelly, D.; Abeyrathne, P.; Dukovski, D. The Affinity Grid: A pre-fabricated EM grid for monolayer purification. *J. Mol. Boil.* **2008**, *382*, 423–433.
29. Kumar, M. Biomimetic Membranes as New Materials for Applications in Environmental engineering and Biology. Ph.D. Thesis, University Illinois, Champaign, IL, USA, 2010.
30. Kumar, M.; Meier, W. Highly Permeable Polymeric Membranes. Patent WO 2009/078174, 18 June 2009.
31. Gonen, T.; Sliz, P.; Kistler, J.; Cheng, Y.; Walz, T. Aquaporin-0 membrane junctions reveal the structure of a closed water pore. *Nature* **2004**, *429*, 193–197.
32. Chandy, G.; Zampighi, G.; Kreman, M.; Hall, J. Comparison of the Water Transporting Properties of MIP and AQP1. *J. Membr. Biol.* **1997**, *159*, 29–39.
33. Kumar, M.; Walz, T. High Density Membrane Protein Membranes. Patent WO 2014/028923, 20 February 2014.
34. Habel, J. Structural and Functional Characterization of Aquaporin 0 Incorporated in Block Copolymers and Their Resulting Aggregate Morphologies. Master Thesis, Universität Basel, Basel, Switzerland, 2011.
35. Hélix-Nielsen, C. Biomimetic membranes for sensor and separation applications. *Anal. Bioanal. Chem.* **2009**, *395*, 697–718.
36. Pszon-Bartosz, K.; Hansen, J.S.; Stibius, K.B.; Groth, J.S.; Emnéus, J.; Geschke, O.; Hélix-Nielsen, C. Assessing the efficacy of vesicle fusion with planar membrane arrays using a mitochondrial porin as reporter. *Biochem. Biophys. Res. Commun.* **2011**, *406*, 96–100.
37. González-Pérez, A.; Stibius, K.; Vissing, T. Biomimetic triblock copolymer membrane arrays: A stable template for functional membrane proteins. *Langmuir* **2009**, *25*, 10447–10450.
38. Andreasson-Ochsner, M.; Fu, Z.; May, S.; Ying Xiu, L.; Nallani, M.; Sinner, E.K. Selective Deposition and Self-Assembly of Triblock Copolymers into Matrix Arrays for Membrane Protein Production. *Langmuir* **2012**, *28*, 2044–2048.
39. Gulati, S.; Jamshad, M.; Knowles, T.J.; Morrison, K.A.; Downing, R.; Cant, N.; Collins, R.; Koenderink, J.B.; Ford, R.C.; Overduin, M.; *et al*. Detergent-free purification of ABC (ATP-binding-cassette) transporters. *Biochem. J.* **2014**, *461*, 269–278.
40. Knowles, T.J.; Finka, R.; Smith, C.; Lin, Y.P.; Dafforn, T.; Overduin, M. Membrane Proteins Solubilized Intact in Lipid Containing Nanoparticles Bounded by Styrene Maleic Acid Copolymer. *J. Am. Chem. Soc.* **2009**, *131*, 7484–7485.
41. Hall, A.R.; Scott, A.; Rotem, D.; Mehta, K.K.; Bayley, H.; Dekker, C. Hybrid pore formation by directed insertion of α-haemolysin into solid-state nanopores. *Nat. Nanotechnol.* **2010**, *5*, 874–877.

42. Balme, S.; Janot, J.M.; Berardo, L.; Henn, F.; Bonhenry, D.; Kraszewski, S.; Picaud, F.; Ramseyer, C. New Bioinspired Membrane Made of a Biological Ion Channel Confined into the Cylindrical Nanopore of a Solid-State Polymer. *Nano Lett.* **2011**, *11*, 712–716.
43. Bodor, S.; Zook, J.M.; Lindner, E.; Tóth, K.; Gyurcsányi, R.E. Electrochemical methods for the determination of the diffusion coefficient of ionophores and ionophore-ion complexes in plasticized PVC membranes. *Analyst* **2008**, *133*, 635–642.
44. Ibragimova, S. Supporting and stabilizing biomimetic membranes. Ph.D. Thesis, Danish Technical University, Kgs. Lyngby, Denmark, 2011.
45. Mech-Dorosz, A.; Heiskanen, A.; Bäckström, S.; Perry, M.; Muhammad, H.B.; Hélix-Nielsen, C.; Emnéus, J. A reusable device for electrochemical applications of hydrogel supported black lipid membranes. *Biomed. Microdevices* **2015**, *17*, 21.
46. Discher, D.E. Polymer Vesicles. *Science* **2002**, *297*, 967–973.
47. Nardin, C.; Hirt, T.; Leukel, J.; Meier, W. Polymerized ABA Triblock Copolymer Vesicles. *Langmuir* **2000**, *16*, 1035–1041.
48. Erbakan, M.; Shen, Y.X.; Grzelakowski, M.; Butler, P.J.; Kumar, M.; Curtis, W.R. Molecular Cloning, Overexpression and Characterization of a Novel Water Channel Protein from Rhodobacter sphaeroides. *PLoS ONE* **2014**, *9*, e86830.
49. Graff, A. Amphiphilic Copolymer Membranes Promote NADH: Ubiquinone Oxidoreductase Activity: Towards an Electron-Transfer Nanodevice. *Macromol. Chem. Phys.* **2010**, *211*, 229–238.
50. Wong, D.; Jeon, T.J.; Schmidt, J. Single molecule measurements of channel proteins incorporated into biomimetic polymer membranes. *Nanotechnology* **2006**, *17*, 3710–3717.
51. Uehlein, N.; Otto, B.; Eilingsfeld, A.; Itel, F.; Meier, W.; Kaldenhoff, R. Gas-tight triblock-copolymer membranes are converted to CO2 permeable by insertion of plant aquaporins. *Sci. Rep.* **2012**, *2*, 1–4.
52. Wang, H.; Chung, T.S.; Tong, Y.W. Study on water transport through a mechanically robust Aquaporin Z biomimetic membrane. *J. Membr. Sci.* **2013**, *445*, 47–52.
53. Wang, H.; Chung, T.S.; Tong, Y.W.; Jeyaseelan, K.; Armugam, A.; Chen, Z.; Hong, M.; Meier, W. Highly Permeable and Selective Pore-Spanning Biomimetic Membrane Embedded with Aquaporin Z. *Small* **2012**, *8*, 1185–1190.
54. Zhong, P.S.; Chung, T.S.; Jeyaseelan, K.; Armugam, A. Aquaporin-embedded biomimetic membranes for nanofiltration. *J. Membr. Sci.* **2012**, *407–408*, 27–33.
55. De Vocht, C.; Ranquin, A.; Willaert, R.; Van Ginderachter, J.A.; Vanhaecke, T.; Rogiers, V.; Versées, W.; Van Gelder, P.; Steyaert, J. Assessment of stability, toxicity and immunogenicity of new polymeric nanoreactors for use in enzyme replacement therapy of MNGIE. *J. Control. Release* **2009**, *137*, 246–254.
56. Grzelakowski, M.; Cherenet, M.F.; Shen, Y.x.; Kumar, M. A framework for accurate evaluation of the promise of aquaporin based biomimetic membranes. *J. Membr. Sci.* **2015**, pp. 1–32.
57. Grzelakowski, M.; Onaca, O.; Rigler, P.; Kumar, M.; Meier, W. Immobilized Protein-Polymer Nanoreactors. *Small* **2009**, *5*, 2545–2548.
58. Ihle, S.; Onaca, O.; Rigler, P.; Hauer, B.; Rodríguez-Ropero, F.; Fioroni, M.; Schwaneberg, U. Nanocompartments with a pH release system based on an engineered OmpF channel protein. *Soft Matter* **2011**, *7*, 532–539.

59. Tanner, P.; Balasubramanian, V.; Palivan, C.G. Aiding Nature's Organelles: Artificial Peroxisomes Play Their Role. *Nano Lett.* **2013**, *13*, 2875–2883.
60. Tanner, P.; Onaca, O.; Balasubramanian, V.; Meier, W.; Palivan, C.G. Enzymatic Cascade Reactions inside Polymeric Nanocontainers: A Means to Combat Oxidative Stress. *Chem. Eur. J.* **2011**, *17*, 4552–4560.
61. Kowal, J.Ł.; Kowal, J.K.; Wu, D.; Stahlberg, H.; Palivan, C.G.; Meier, W.P. Functional surface engineering by nucleotide-modulated potassium channel insertion into polymer membranes attached to solid supports. *Biomaterials* **2014**, *35*, 7286–7294.
62. Winterhalter, M.; Hilty, C.; Bezrukov, S.M.; Nardin, C.; Meier, W.; Fournier, D. Controlling membrane permeability with bacterial porins: Application to encapsulated enzymes. *Talanta* **2001**, *55*, 965–971.
63. Xie, W.; He, F.; Wang, B.; Chung, T.S.; Jeyaseelan, K.; Armugam, A.; Tong, Y.W. An aquaporin-based vesicle-embedded polymeric membrane for low energy water filtration. *J. Mater. Chem. A* **2013**, *1*, 7592–7600.
64. Heinisch, T.; Langowska, K.; Tanner, P.; Reymond, J.L.; Meier, W.; Palivan, C.; Ward, T.R. Fluorescence-Based Assay for the Optimization of the Activity of Artificial Transfer Hydrogenase within a Biocompatible Compartment. *ChemCatChem* **2013**, *5*, 720–723.
65. Broz, P.; Driamov, S.; Ziegler, J.; Ben-Haim, N.; Marsch, S.; Meier, W.; Hunziker, P. Toward Intelligent Nanosize Bioreactors: A pH-Switchable, Channel-Equipped, Functional Polymer Nanocontainer. *Nano Lett.* **2006**, *6*, 2349–2353.
66. Langowska, K.; Palivan, C.G.; Meier, W. Polymer nanoreactors shown to produce and release antibiotics locally. *Chem. Commun.* **2013**, *49*, 128–130.
67. Graff, A.; Sauer, M.; Meier, W. Virus-assisted loading of polymer nanocontainer. *Proc. Natl. Acad. Sci. USA* **2002**, *99*, 5064–5068.
68. Ranquin, A.; Versées, W.; Meier, W.; Steyaert, J.; Van Gelder, P. Therapeutic Nanoreactors: Combining Chemistry and Biology in a Novel Triblock Copolymer Drug Delivery System. *Nano Lett.* **2005**, *5*, 2220–2224.
69. Sauer, M.; Haefele, T.; Graff, A.; Nardin, C.; Meier, W. Ion-carrier controlled precipitation of calcium phosphate in giant ABA triblock copolymer vesicles. *Chem. Commun.* **2001**, *7*, 2452–2453.
70. Haefele, T.; Kita-Tokarczyk, K.; Meier, W. Phase Behavior of Mixed Langmuir Monolayers from Amphiphilic Block Copolymers and an Antimicrobial Peptide. *Langmuir* **2006**, *22*, 1164–1172.
71. Nallani, M.; Benito, S.; Onaca, O.; Graff, A.; Lindemann, M.; Winterhalter, M.; Meier, W.; Schwaneberg, U. A nanocompartment system (Synthosome) designed for biotechnological applications. *J. Biotechnol.* **2006**, *123*, 50–59.
72. Nallani, M. A Novel Nanocompartment System Named Synthosome for Biotechnological Applications. Ph.D. Thesis, Universität Bremen, Bremen, Germany, 2005.
73. Onaca, O. Functionalized polymer vesicles and interactions with Polymyxin B and derivates. Ph.D. Thesis, Universität Bremen, Bremen, Germany, 2007.
74. Graff, A. Insertion of Membrane Proteins in Artificial Polymer Membranes. Ph.D. Thesis, Universität Basel, Basel, Switzerland, 2006.

75. Meier, W.; Nardin, C.; Winterhalter, M. Reconstitution of channel proteins in (polymerized) ABA triblock copolymer membranes. *Angew. Chem. Int. Ed.* **2000**, *39*, 4599–4602.
76. Nardin, C.; Widmer, J.; Winterhalter, M.; Meier, W. Amphiphilic block copolymer nanocontainers as bioreactors. *Eur. Phys. J. E* **2001**, *4*, 403–410.
77. Duong, P.H.H.; Chung, T.S.; Jeyaseelan, K.; Armugam, A.; Chen, Z.; Yang, J.; Hong, M. Planar biomimetic aquaporin-incorporated triblock copolymer membranes on porous alumina supports for nanofiltration. *J. Membr. Sci.* **2012**, *409-410*, 34–43.
78. Choi, H.J.; Lee, H.; Montemagno, C.D. Toward hybrid proteo-polymeric vesicles generating a photoinduced proton gradient for biofuel cells. *Nanotechnology* **2005**, *16*, 1589–1597.
79. Lee, H.; Ho, D.; Kuo, K.; Montemagno, C.D. Vectorial insertion of bacteriorhodopsin for directed orientation assays in various polymeric biomembranes. *Polymer* **2006**, *47*, 2935–2941.
80. Choi, H.J.; Germain, J. Effects of different reconstitution procedures on membrane protein activities in proteopolymersomes. *Nanotechnology* **2006**, *17*, 1825–1830.
81. Choi, H.J.; Montemagno, C.D. Biosynthesis within a bubble architecture. *Nanotechnology* **2006**, *17*, 2198–2202.
82. Choi, H.J.; Montemagno, C. Light-Driven Hybrid Bioreactor Based on Protein-Incorporated Polymer Vesicles. *IEEE Trans. Nanotechnol.* **2007**, *6*, 171–176.
83. Dobrunz, D.; Toma, A.C.; Tanner, P.; Pfohl, T.; Palivan, C.G. Polymer Nanoreactors with Dual Functionality: Simultaneous Detoxification of Peroxynitrite and Oxygen Transport. *Langmuir* **2012**, *28*, 15889–15899.
84. Thoma, J.; Belegrinou, S.; Rossbach, P.; Grzelakowski, M.; Kita-Tokarczyk, K.; Meier, W. Membrane protein distribution in composite polymer-lipid thin films. *Chem. Commun.* **2012**, *48*, 8811–8813.
85. Onaca, O.; Sarkar, P.; Roccatano, D.; Friedrich, T.; Hauer, B.; Grzelakowski, M.; Güven, A.; Fioroni, M.; Schwaneberg, U. Functionalized Nanocompartments (Synthosomes) with a Reduction-Triggered Release System. *Angew. Chem. Int. Ed.* **2008**, *47*, 7029–7031.
86. Ho, D.; Chu, B.; Lee, H.; Montemagno, C. Protein-driven energy transduction across polymeric biomembranes. *Nanotechnology* **2004**, doi:10.1088/0957-4484/15/8/038.
87. Ho, D.; Chu, B.; Lee, H.; Brooks, E.K.; Kuo, K.; Montemagno, C.D. Fabrication of biomolecule–copolymer hybrid nanovesicles as energy conversion systems. *Nanotechnology* **2005**, *16*, 3120–3132.
88. Xi, J.Z.; Ho, D.; Chu, B.; Montemagno, C.D. Lessons Learned from Engineering Biologically Active Hybrid Nano/Micro Devices. *Adv. Funct. Mater.* **2005**, *15*, 1233–1240.
89. Ho, D.; Chu, B.; Schmidt, J.J.; Brooks, E.K.; Montemagno, C.D. Hybrid Protein-Polymer Biomimetic Membranes. *IEEE Trans. Nanotechnol.* **2004**, *3*, 256–263.
90. Habel, J. *Functional and Chemical Characterization of Vesicular Diblock Copolymer Bilayers with Aquaporin Included*; Technical Report; Aquaporin A/S, Copenhagen, Denmark, 2011.
91. Espina, M. Barrier Properties of Biomimetic Membranes. Master Thesis, Danish Technical University (DTU), Kgs. Lyngby, Denmark, 2012.
92. Nallani, M.; Andreasson-Ochsner, M.; Tan, C.W.D.; Sinner, E.K.; Wisantoso, Y.; Geifman-Shochat, S.; Hunziker, W. Proteopolymersomes: *In vitro* production of a membrane protein in polymersome membranes. *Biointerfaces* **2011**, *6*, 153–157.

93. Bomholt, J. Human Aquaporins—From *in vivo* detection to industrial scale production. Ph.D. Thesis, University Copenhagen, Copenhagen, Denmark, 2014.
94. Zhang, X.; Fu, W.; Palivan, C.G.; Meier, W. Natural channel protein inserts and functions in a completely artificial, solid-supported bilayer membrane. *Sci. Rep.* **2013**, *3*, doi:10.1038/srep02196.
95. Dorn, J.; Belegrinou, S.; Kreiter, M.; Sinner, E.K.; Meier, W. Planar Block Copolymer Membranes by Vesicle Spreading. *Macromol. Biosci.* **2011**, *11*, 514–525.
96. Vijayan, K.; Discher, D.E.; Lal, J.; Janmey, P.; Goulian, M. Interactions of Membrane-Active Peptides with Thick, Neutral, Nonzwitterionic Bilayers. *J. Phys. Chem. B* **2005**, *109*, 14356–14364.
97. Toughrai, S. Functional Surfaces through Biomimetic block Copolymer Membranes. Ph.D. Thesis, Universität Basel, Basel, Switzerland, 2014.
98. Amado, E.; Schöps, R.; Brandt, W.; Kressler, J. Spontaneous Formation of Giant Bioactive Protein-Block Copolymer Vesicles in Water. *ACS Macro Lett.* **2012**, *1*, 1016–1019.
99. Noor, M.; Dworeck, T.; Schenk, A.; Shinde, P.; Fioroni, M.; Schwaneberg, U. Polymersome surface decoration by an EGFP fusion protein employing Cecropin A as peptide "anchor". *J. Biotechnol.* **2012**, *157*, 31–37.
100. Kuang, L.; Fernandes, D.A.; O'Halloran, M.; Zheng, W.; Jiang, Y.; Ladizhansky, V.; Brown, L.S.; Liang, H. "Frozen" Block Copolymer Nanomembranes with Light-Driven Proton Pumping Performance. *ACS Nano* **2014**, *8*, 537–545.
101. Hua, D.; Kuang, L.; Liang, H. Self-Directed Reconstitution of Proteorhodopsin with Amphiphilic Block Copolymers Induces the Formation of Hierarchically Ordered Proteopolymer Membrane Arrays. *J. Am. Chem. Soc.* **2011**, *133*, 2354–2357.
102. Kuang, L.; Olson, T.L.; Lin, S.; Flores, M.; Jiang, Y.; Zheng, W.; Williams, J.C.; Allen, J.P.; Liang, H. Interface for Light-Driven Electron Transfer by Photosynthetic Complexes across Block Copolymer Membranes. *J. Phys. Chem. Lett.* **2014**, *5*, 787–791.
103. Ibata, K.; Takimoto, S.; Morisaku, T.; Miyawaki, A.; Yasui, M. Analysis of Aquaporin-Mediated Diffusional Water Permeability byCoherent Anti-Stokes Raman Scattering Microscopy. *Biophys. J.* **2011**, *101*, 2277–2283.
104. Mamonov, A.B.; Coalson, R.D.; Zeidel, M.L.; Mathai, J.C. Water and Deuterium Oxide Permeability through Aquaporin 1: MD Predictions and Experimental Verification. *J. Gen. Physiol.* **2007**, *130*, 111–116.
105. Itel, F.; Al-Samir, S.; Oberg, F.; Chami, M.; Kumar, M.; Supuran, C.T.; Deen, P.M.T.; Meier, W.; Hedfalk, K.; Gros, G.; Endeward, V. CO2 permeability of cell membranes is regulated by membrane cholesterol and protein gas channels. *FASEB J.* **2012**, *26*, 5182–5191.
106. GFP-Lifetime. Available online: http://www.iss.com/ (accessed on 7 July 2015).
107. Choi, H.J.; Montemagno, C. Recent Progress in Advanced Nanobiological Materials for Energy and Environmental Applications. *Materials* **2013**, *6*, 5821–5856.
108. Pendergast, M.M.; Hoek, E.M.V. A review of water treatment membrane nanotechnologies. *Energy Environ. Sci.* **2011**, *4*, 1946–1971.
109. Aquaporin Home Page. Available online: www.aquaporin.dk (accessed on 6 July 2015).
110. MEMBAQ Home Page. Available online: www.membaq.eu (accessed on 6 July 2015).

111. Montemagno, C.; Schmidt, J.; Tozzi, S. Biomimetic Membranes. Patent WO 2004/011600, 5 February 2004.
112. Hansen, J.S.; Perry, M.; Vogel, J.; Vissing, T.; Hansen, C.R.; Geschke, O.; Emnéus, J.; Hélix-Nielsen, C. Development of an automation technique for the establishment of functional lipid bilayer arrays. *J. Micromech. Microeng.* **2009**, *19*, doi:10.1088/0960-1317/19/2/025014.
113. Hansen, J.S. Development of supported biomimetic membranes for insertion of aquaporin protein water channels for novel water filtration applications. Ph.D. Thesis, Danish Technical University, Kgs. Lyngby, Denmark, 2010.
114. Rein, C.; Pszon-Bartosz, K.; Stibius, K.B.; Bjørnholm, T.; Hélix-Nielsen, C. Free-Standing Biomimetic Polymer Membrane Imaged with Atomic Force Microscopy. *Langmuir* **2011**, *27*, 499–503.
115. Ibragimova, S.; Stibius, K.; Szewczykowski, P.; Perry, M.; Bohr, H.; Hélix-Nielsen, C. Hydrogels for *in situ* encapsulation of biomimetic membrane arrays. *Polym. Adv. Technol.* **2010**, *23*, 182–189.
116. Perry, M.; Hansenz, J.; Stibius, K. Surface Modifications of Support Partitions for Stabilizing Biomimetic Membrane Arrays. *J. Membr. Sci. Technol.* **2011**, doi:10.4172/2155-9589.S1-001.
117. Rein, C. Stabilization and characterization of 2D and 3D biomimetic membranes. Ph.D. thesis, University of Copenhagen, Copenhagen, Denmark, 2011.
118. Aquaporin A/S. Biomimetic Membranes and Uses Thereof. Patent WO 2010/146365, 23 December 2010.
119. Aquaporin A/S. Membrane for Filtering of Water. Patent WO 2006/122566, 23 November 2006.
120. Aquaporin A/S. Biomimetic Water Membrane Comprising Aquaporins Used in the Production of Salinity Power. Patent WO 2007/033675, 29 March 2007.
121. Aquaporin A/S. Scaffold for Composite Biomimetic Membrane. Patent WO 2009/074155, 18 June 2009.
122. Aquaporin A/S. Assays Relating to Biomimetic Membranes and Their Uses. Patent WO 2010/146366, 23 December 2010.
123. Montemagno, C.; Aquaz; Danfoss. Nanofabricated Membrane Using Polymerized Proteoliposomes. Patent WO 2010/091078, 12 August 2010.
124. Wang, H.; Chung, T.S.; Tong, Y.W.; Meier, W.; Chen, Z.; Hong, M.; Jeyaseelan, K.; Armugam, A. Preparation and characterization of pore-suspending biomimetic membranes embedded with Aquaporin Z on carboxylated polyethylene glycol polymer cushion. *Soft Matter* **2011**, *7*, 7274.
125. Sun, G.; Zhou, H.; Li, Y.; Jeyaseelan, K.; Armugam, A.; Chung, T.S. A novel method of AquaporinZ incorporation via binary-lipid Langmuir monolayers. *Colloids Surf. B: Biointerfaces* **2012**, *89*, 283–288.
126. Kaufman, Y.; Grinberg, S.; Linder, C.; Heldman, E.; Gilron, J.; Freger, V. Fusion of Bolaamphiphile Micelles: A Method to Prepare Stable Supported Biomimetic Membranes. *Langmuir* **2013**, *29*, 1152–1161.
127. Li, X.; Wang, R.; Wicaksana, F.; Zhao, Y.; Tang, C.Y.; Torres, J.; Fane, A.G. Fusion behaviour of aquaporin Z incorporated proteoliposomes investigated by quartz crystal microbalance with dissipation (QCM-D). *Colloids Surf. B: Biointerfaces* **2013**, *111*, 446–452.

128. Kaufman, Y.; Berman, A. Supported lipid bilayer membranes for water purification by reverse osmosis. *Langmuir* **2010**, *26*, 7388–7395.
129. Freger, V.; Kaufman, Y. Biomimetic Membranes, Their Production and Uses Thereof in Water Purification. Patent US 2011/0084026, 14 April 2011.
130. Li, X.; Wang, R.; Tang, C.Y.; Vararattanavech, A.; Zhao, Y.; Torres, J.; Fane, A.G. Preparation of supported lipid membranes for aquaporin Z incorporation. *Colloids Surf. B: Biointerfaces* **2012**, *94*, 333–340.
131. Aquaporin AS.; NTU. Aquaporin Based Thin Film Composite Membranes. Patent WO 2013/043118, 28 March 2013.
132. Aquaporin AS. Systems for Water Extraction. Patent WO 2014/128293, 28 August 2014.
133. Zhao, Y.; Vararattanavech, A.; Li, X.; Hélix-Nielsen, C.; Vissing, T.; Torres, J.; Wang, R.; Fane, A.G.; Tang, C.Y. Effects of Proteoliposome Composition and Draw Solution Types on Separation Performance of Aquaporin-Based Proteoliposomes: Implications for Seawater Desalination Using Aquaporin-Based Biomimetic Membranes. *Environ. Sci. Technol.* **2013**, *5*, 1496–1503.
134. Li, X.; Wang, R.; Wicaksana, F.; Tang, C.Y.; Torres, J.; Fane, A.G. Preparation of high performance nanofiltration (NF) membranes incorporated with aquaporin Z. *J. Membr. Sci.* **2014**, *450*, 181–188.
135. Tanner, P. Design and Development of Protein-Polymer Assemblies to Engineer Artificial organelles. Ph.D. Thesis, Universität Basel, Basel, Switzerland, 2013.
136. Pawar, P.V.; Gohil, S.V.; Jain, J.P.; Kumar, N. Functionalized polymersomes for biomedical applications. *Polym. Chem.* **2013**, *4*, 3160–3176.
137. Jesorka, A.; Orwar, O. Liposomes: Technologies and Analytical Applications. *Annu. Rev. Anal. Chem.* **2008**, *1*, 801–832.
138. Montemagno, C. Biomimetic membrane formed from a vesicle-thread conjugate. Patent WO 2010/040353, 15 April 2010.
139. Sun, G.; Chung, T.S.; Jeyaseelan, K.; Armugam, A. Stabilization and immobilization of aquaporin reconstituted lipid vesicles for water purification. *Colloids Surf. B: Biointerfaces* **2012**, *102*, 466–471.
140. Kaufman, Y.; Grinberg, S.; Linder, C.; Heldman, E.; Gilron, J.; Shen, Y.X.; Kumar, M.; Lammertink, R.G.H.; Freger, V. Towards supported bolaamphiphile membranes for water filtration: Roles of lipid and substrate. *J. Membr. Sci.* **2014**, *457*, 50–61.
141. Sun, G.; Chung, T.S.; Chen, N.; Lu, X.; Zhao, Q. Highly permeable aquaporin-embedded biomimetic membranes featuring a magnetic-aided approach. *RSC Adv.* **2013**, *3*, 9178–9184.
142. Wang, M.; Wang, Z.; Wang, X.; Wang, S.; Ding, W.; Gao, C. Layer-by-Layer Assembly of Aquaporin Z-Incorporated Biomimetic Membranes for Water Purification. *Environ. Sci. Technol.* **2015**, *49*, 3761–3768.
143. Shen, Y.x.; Saboe, P.O.; Sines, I.T.; Erbakan, M.; Kumar, M. Biomimetic membranes: A review. *J. Membr. Sci.* **2014**, *454*, 359–381.
144. Thomas, J.A.; McGaughey, A.J.H. Reassessing Fast Water Transport through Carbon Nanotubes. *Nano Lett.* **2008**, *8*, 2788–2793.

145. Holt, J.; Park, H.; Wang, Y.; Stadermann, M.; Artyukhin, A.; Grigoropoulos, C.; Noy, A.; Bakajin, O. Fast Mass Transport Through Sub-2-Nanometer Carbon Nanotubes. *Science* **2006**, *312*, 1034–1037.
146. Fei, Z.; Zhao, D.; Geldbach, T.J.; Scopelliti, R.; Dyson, P.J.; Antonijevic, S.; Bodenhausen, G. A Synthetic Zwitterionic Water Channel: Characterization in the Solid State by X-ray Crystallography and NMR Spectroscopy. *Angew. Chem. Int. Ed.* **2005**, *44*, 5720–5725.
147. Percec, V.; Dulcey, A.E.; Balagurusamy, V.S.K.; Miura, Y.; Smidrkal, J.; Peterca, M.; Nummelin, S.; Edlund, U.; Hudson, S.D.; Heiney, P.A.; Duan, H.; Magonov, S.N.; Vinogradov, S.A. Self-assembly of amphiphilic dendritic dipeptides into helical pores. *Nature* **2004**, *430*, 764–768.
148. Barboiu, M. Artificial Water Channels. *Angew. Chem. Int. Ed.* **2012**, *51*, 11674–11676.
149. Zhou, X.; Liu, G.; Yamato, K.; Shen, Y.; Cheng, R.; Wei, X.; Bai, W.; Gao, Y.; Li, H.; Liu, Y.; *et al*. Self-assembling subnanometer pores with unusual mass-transport properties. *Nat. Commun.* **2012**, *3*, doi:10.1038/ncomms1949.
150. Alsvik, I.; Hägg, M.B. Pressure Retarded Osmosis and Forward Osmosis Membranes: Materials and Methods. *Polymers* **2013**, *5*, 303–327.
151. Wittbecker, E.L.; Morgan, P.W. Interfacial polycondensation. I. *J. Polym. Sci.* **1959**, *40*, 289–297.
152. Ghosh, A.K.; Jeong, B.H.; Huang, X.; Hoek, E.M.V. Impacts of reaction and curing conditions on polyamide composite reverse osmosis membrane properties. *J. Membr. Sci.* **2008**, *311*, 34–45.
153. Dalwani, M.; Zheng, J.; Hempenius, M.; Raaijmakers, M.J.T.; Doherty, C.M.; Hill, A.J.; Wessling, M.; Benes, N.E. Ultra-thin hybrid polyhedral silsesquioxane-polyamide films with potentially unlimited 2D dimensions. *J. Mater. Chem.* **2012**, *22*, 14835–14838.
154. Habel, J.; Ogbonna, A.; Skaarup, N.; Schulte, L.; Almdal, K.; Hélix-Nielsen, C. How molecular internal-geometric parameters affect PB-PEO polymersome size in aqueous solution. *Phys. Chem. Chem. Phys.* **2015**, To be submitted.
155. PB-FTIR-Spectrum. Available online: http://webbook.nist.gov/cgi/cbook.cgi?ID=B6002924 Mask=80 (accessed on 6 July 2015).
156. PEO-FTIR-Spectrum. Available online: http://webbook.nist.gov/cgi/cbook.cgi?ID=B6002924 Mask=80 (accessed on 6 July 2015).
157. Germic, L.; Ebert, K.; Bouma, R.H.B.; Borneman, Z.; Mulder, M.H.V.; Strathmann, H. Characterization of polyacrylonitrile ultrafiltration membranes. *J. Membr. Sci.* **1997**, *132*, 131–145.
158. Lee, K.P.; Zheng, J.; Bargeman, G.; Kemperman, A.J.B.; Benes, N.E. pH stable thin film composite polyamine nanofiltration membranes by interfacial polymerisation. *J. Membr. Sci.* **2015**, *478*, 75–84.

8.3 Appendix III: Accepted manuscript of Paper 2

Selecting analytical tools for characterization of polymersomes in aqueous solution

Joachim Habel, Anayo Ogbonna, Nanna Larsen, Solène Cherré, Søren Kynde, Søren Roi Midtgaard Koji Kinoshita, Simon Krabbe, Grethe Vestergaard Jensen, Kristoffer Almdal, Claus Hélix-Nielsen

Accepted manuscript to RSC Advances

doi: 10.1039/c5ra16403f

The Department of Environmental Engineering (DTU Environment) conducts science-based engineering research within four sections:
Water Resources Engineering, Urban Water Engineering,
Residual Resource Engineering and Environmental Chemistry & Microbiology.

The department dates back to 1865, when Ludvig August Colding, the founder of the department, gave the first lecture on sanitary engineering as response to the cholera epidemics in Copenhagen in the late 1800s.

DTU Environment
Department of Environmental Engineering
Technical University of Denmark

Miljoevej, building 113
2800 Kgs. Lyngby
Denmark

Phone: +45 4525 1600
Fax: +45 4593 2850
e-mail: info@env.dtu.dk
www.env.dtu.dk